

## CHAPTER 5

# **RESULTS AND DISCUSSION**

⚡ Abbreviations Used in Chapter No. 5

<b>Results &amp; Discussion</b>	<b>A SEM</b>	1. TiN 2. ZrN 3. ZrTiN
	<b>B XRD</b>	1. TiN 2. ZrN 3. ZrTiN
	<b>C Corrosion</b>	1. TiN (a) 1N H <sub>2</sub> SO <sub>4</sub> 2. ZrN (b) 3.5%NaCl 3. ZrTiN (c) 0.1N HCl (d) 11pH Na <sub>2</sub> SO <sub>4</sub>
		(P) Potentiodynamic (B) Bode's plot (S) SEM (E) EDX analysis
	<b>D. Wear</b>	1. TiN (a) 1.5μ 2. ZrN (b) 2.0μ 3. ZrTiN (c) 2.5μ (d) 3.0μ (e) 4.0μ

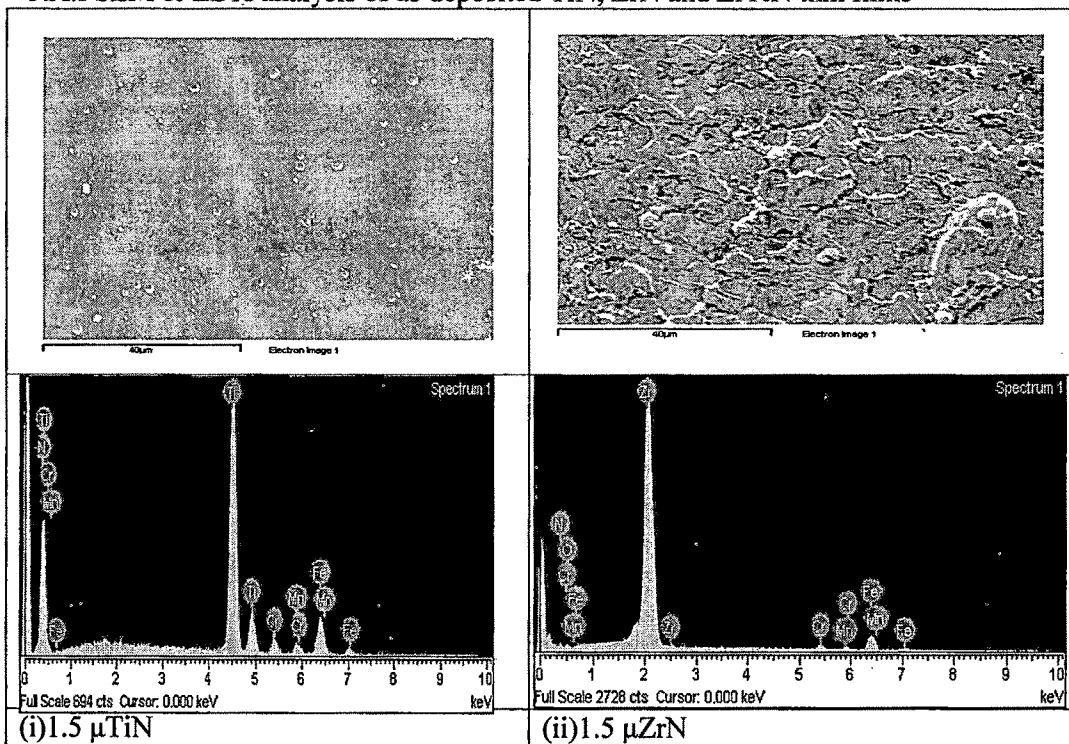
## CHAPTER 5

### RESULTS & DISCUSSION

The microstructure and properties of Thin films vary with different deposition techniques and processing parameters. The Thin films of TiN, ZrN and ZrTiN of varying thickness were prepared by Cathode arc evaporation PVD technique at Multiarc (I) ltd. Umargoan. Film thickness was chosen as the controlling parameter and single-variable experiments were conducted. The resulting coatings were characterized using the following techniques: Scanning Electron microscope (Hitachi 3400 and Joel 5610), Cu K $\alpha$  X-ray diffraction analysis (Philips PHILIPS PANalytica Xpert pro diffractometer), Potentiodynamic test for corrosion resistance(EG & G PARC 273 and Gamry potentiostat( reference 600) ), Pin on disc (Model TR-20,DUCOM-Banglore)for Wear resistance measurement. The surface morphological and chemical changes before and after corrosion and wear were measured in terms of SEM and EDX analysis.

#### 5. A SEM CHARACTERISATION

##### 5.A.I SEM & EDX analysis of as deposited TiN, ZrN and ZrTiN thin films



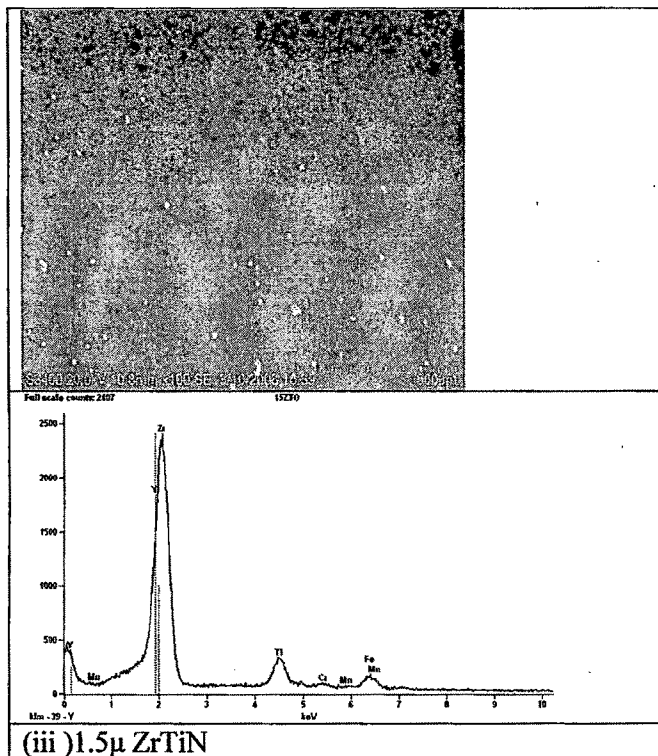


Fig. 5.A I SEM and EDX analysis of as deposited TiN, ZrN and ZrTiN thin films without corrosion and wear

In Fig 5.I, SEM and EDX analysis indicates the presence of Ti and N, Zr and N and Zr, Ti and N in the coatings of (i)TiN, (ii)ZrN and (iii)ZrTiN ,thus confirming their chemical composition.

#### 5. A.1 SEM Microstructure of TiN thin Films of varying thickness

The SEM micrograph fig 5.A.1.1 indicates the presence of macroparticles. One of the main disadvantages in using the cathodic arc process is the formation and subsequent incorporation of macroparticles in the growing coating. Large number of coarse macroparticles is observed in 1.5 $\mu$  and 2.0 $\mu$  TiN (Fig 5.A.1.1 a, b). However quantity and size of macroparticles reduces as thickness of coating is increased

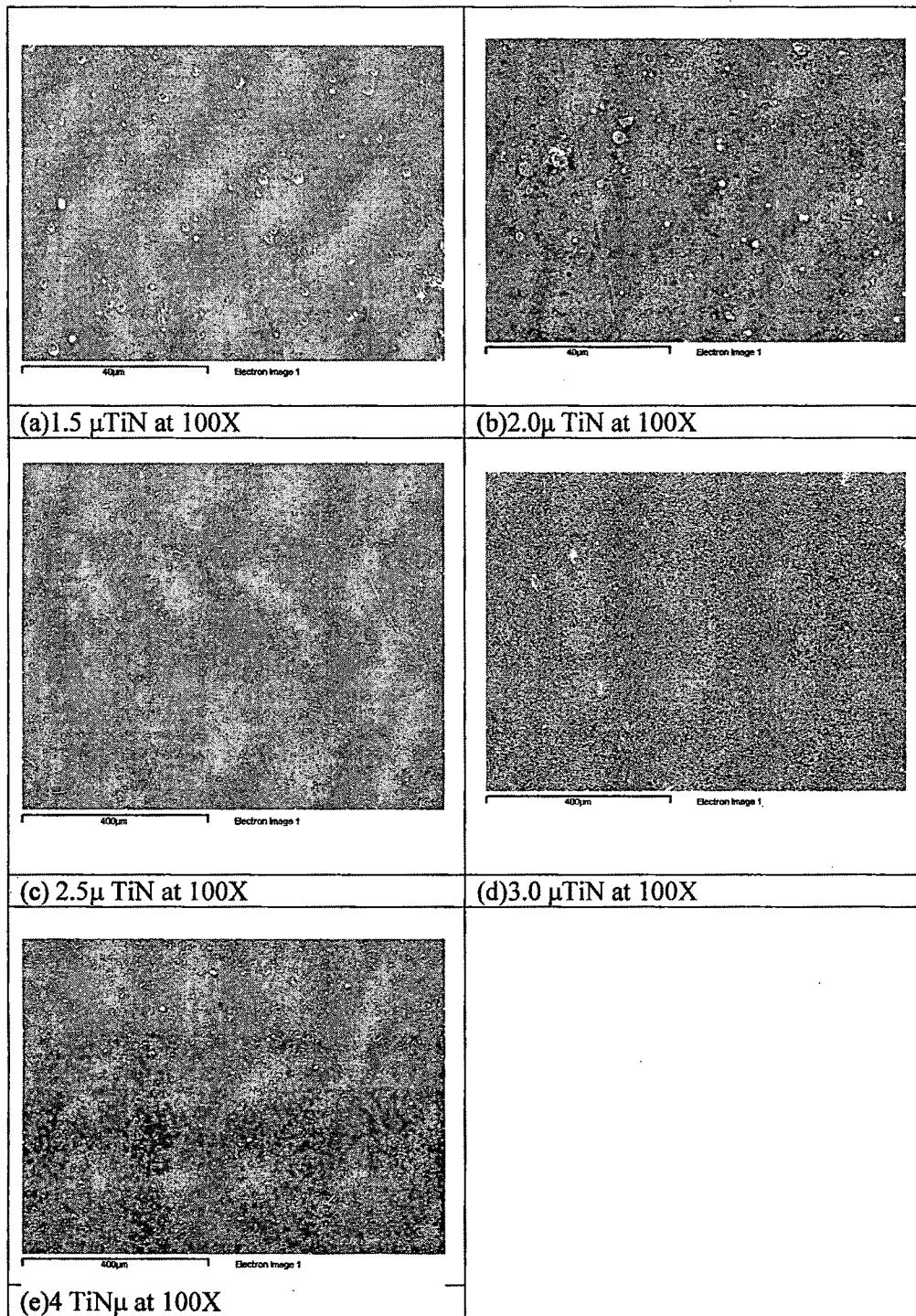


Fig 5.A.1.1 SEM Microstructure of TiN thin Films of Varying thickness

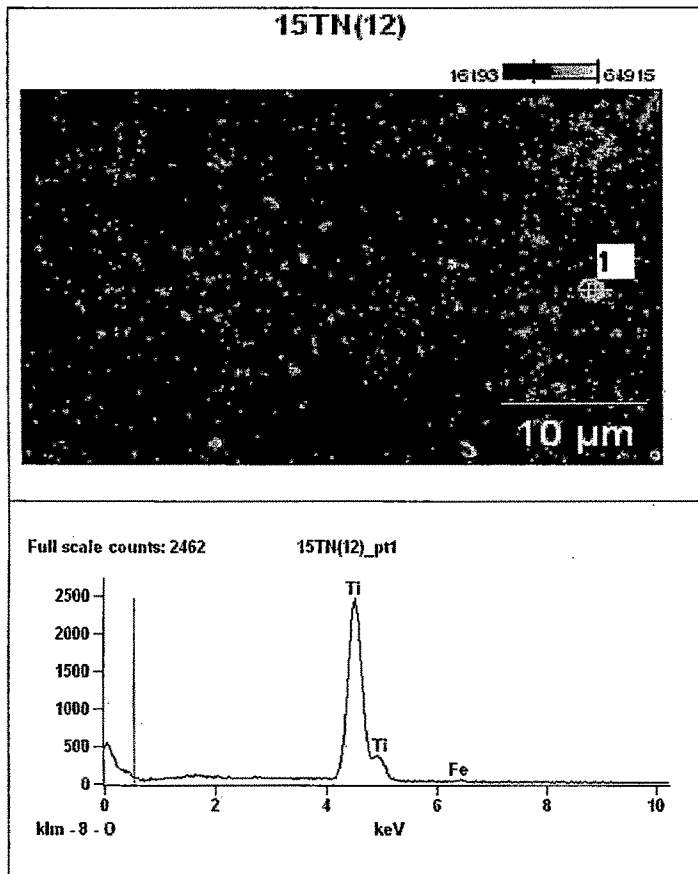


Fig 5.A.1.2 EDX analysis of macroparticle in 1.5μ TiN

The EDX analysis in fig 5.A.1.2 at the point indicates that the macroparticle is composed of Ti. It is generally considered that these macroparticles are harmful to the properties of the TiN coating deposited by arc ion plating. [1] However, the presence of the macroparticles in the TiN- substrate interface may be useful to the adhesion of TiN coating to the substrate. The presence of macroparticles in the TiN coating is favorable for the release of internal stresses, because the Ti macro-particle has a much higher plasticity than the TiN phase. [2-4]

**5. A. 2 SEM Microstructure of ZrN thin Films of varying thickness**

In the Fig 5.A.2.1 (a) Coarse macrodroplets are observed on the surface of 1.5 $\mu$  ZrN. However as the thickness of coating increases the quantity of macrodroplets decreases fig 5.A.2.1 (d)

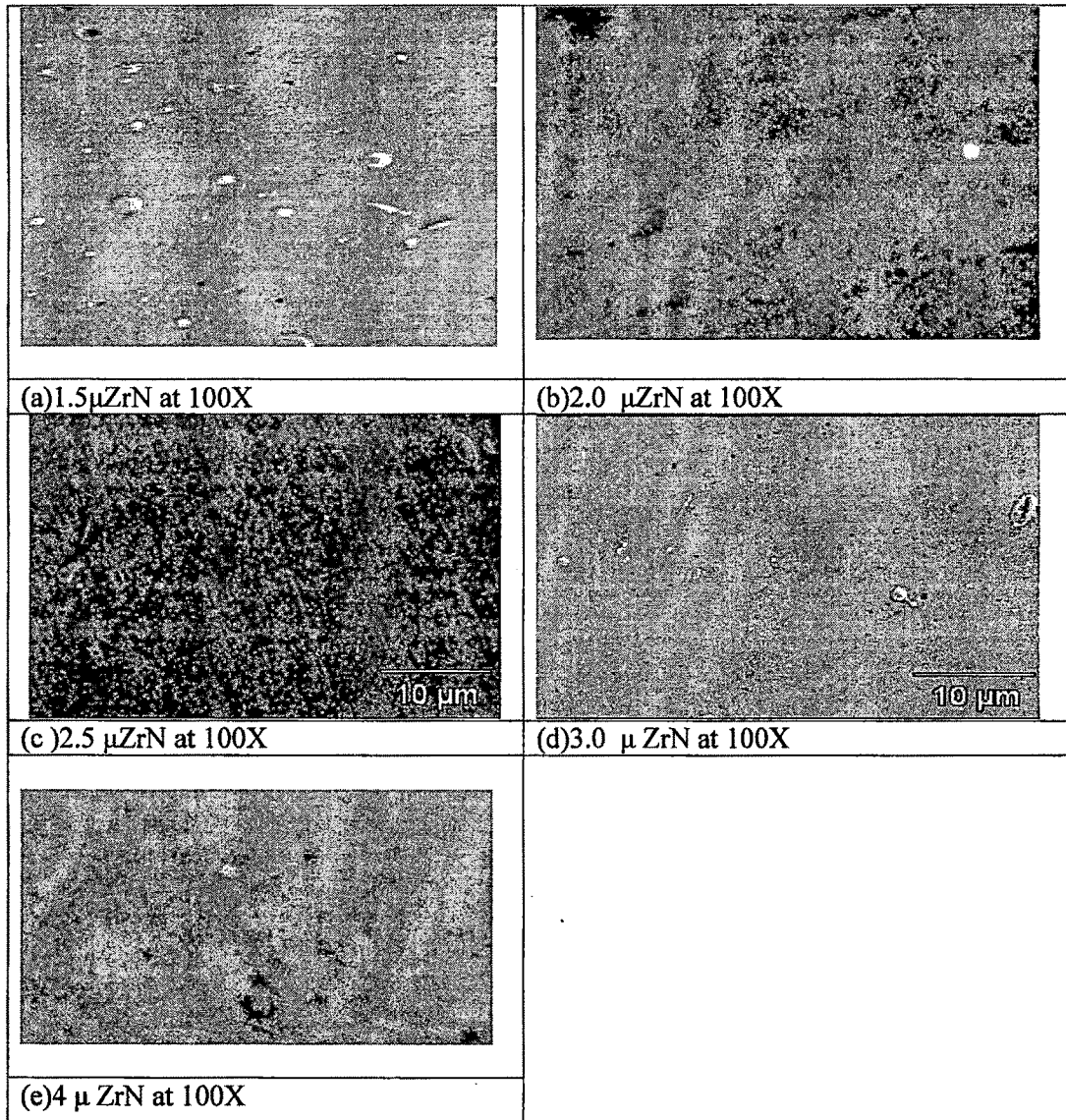


Fig 5.A.2.1 SEM Microstructure of ZrN thin Films of Varying thickness

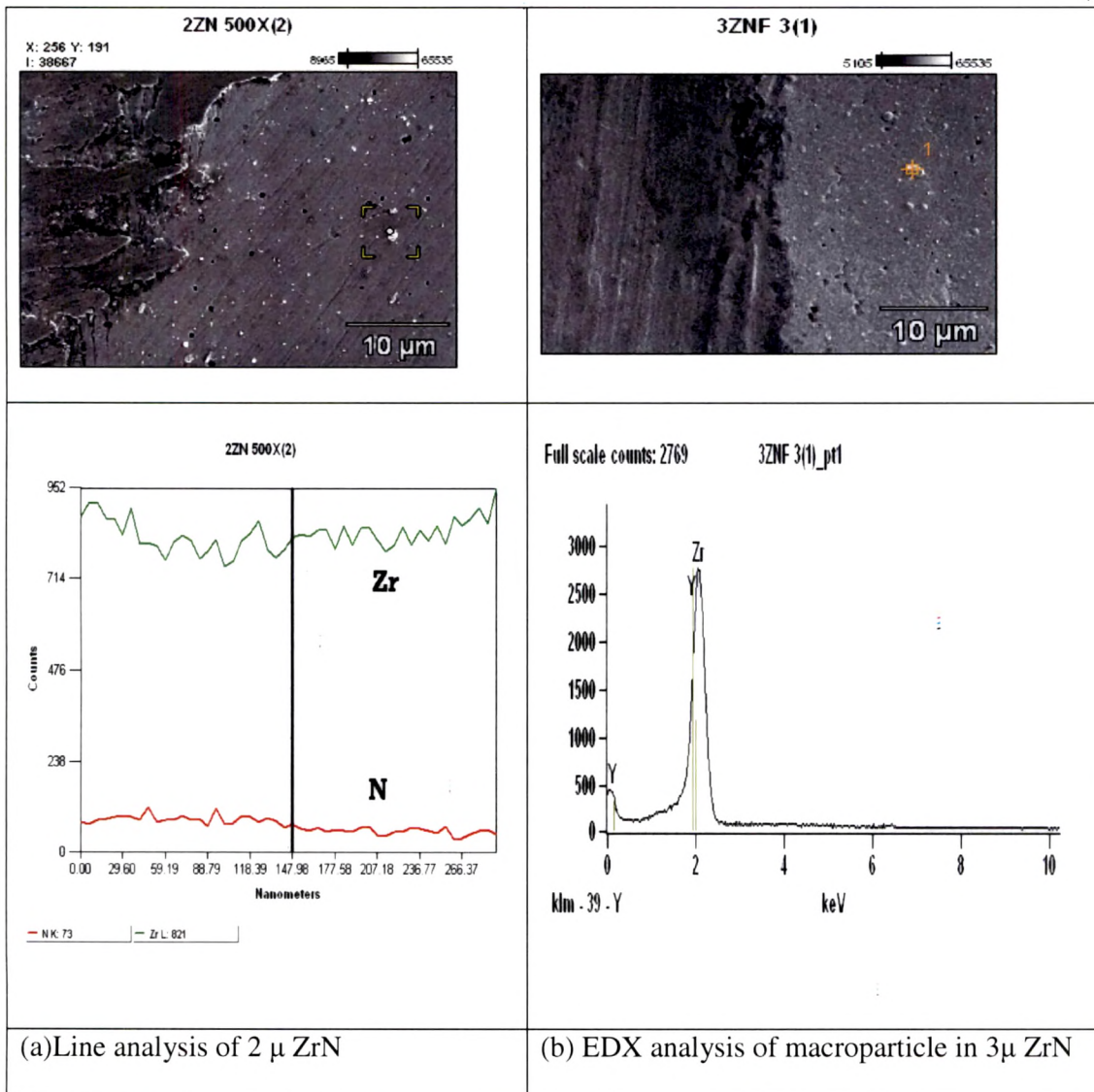


Fig 5.A.2.2 Compositional analysis of 2.0 μ ZrN (a) Line analysis (b) Macroparticle

The Fig 5.A.2.2 indicates EDX analysis. The line analysis indicates the presence of Zr and N whereas point analysis indicates that the macroparticle is composed of Zr. Since the mass of Ti atoms is almost half of the Zr, there is a greater loss of kinetic energy of Ti atoms by collision than those of the Zr, generating a coating of coarse columnar grains that would have many voids and other structural defects that can absorb oxygen. [5]

### 5. A. 3 SEM Microstructure of ZrTiN thin Films of varying thickness

The Fig 5.A.3.1 indicates Coarse macrodroplets on the surface of 1.5  $\mu$  ZrTiN .However as the thickness of coating increases the quantity of macrodroplets decreases 5.A.3.1 (d)

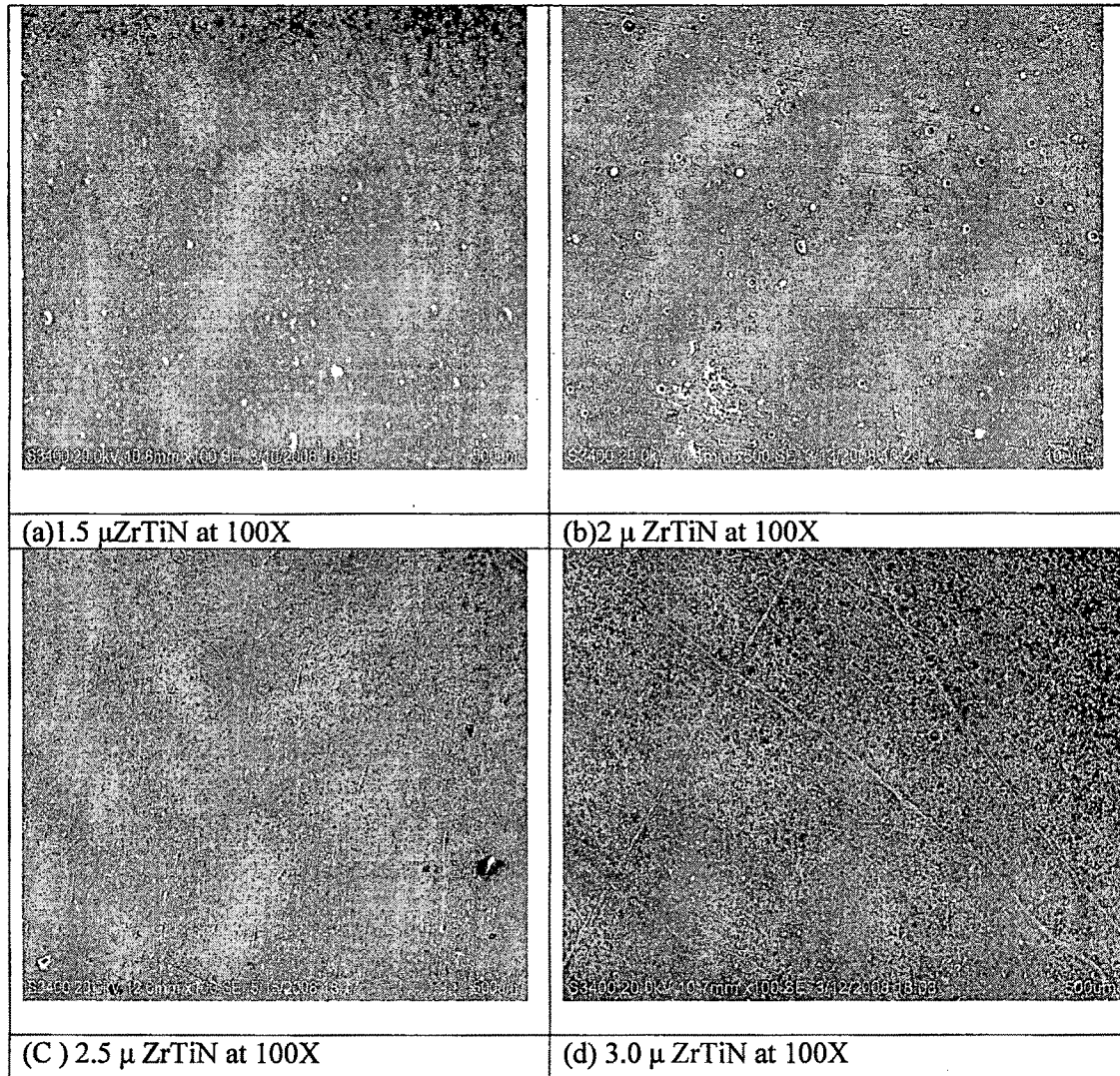


Fig 5.A.3.1 SEM Microstructure of ZrTiN thin Films of Varying thickness

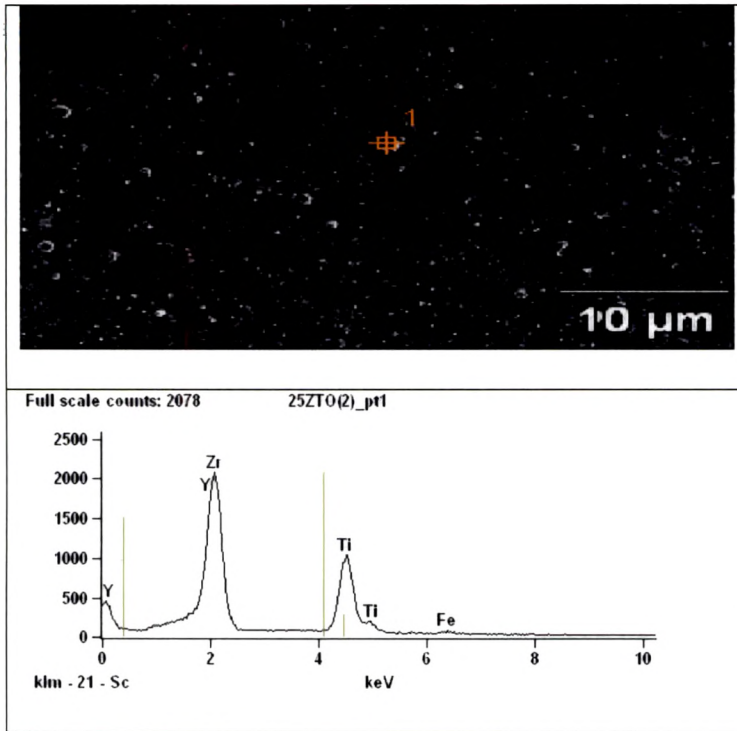
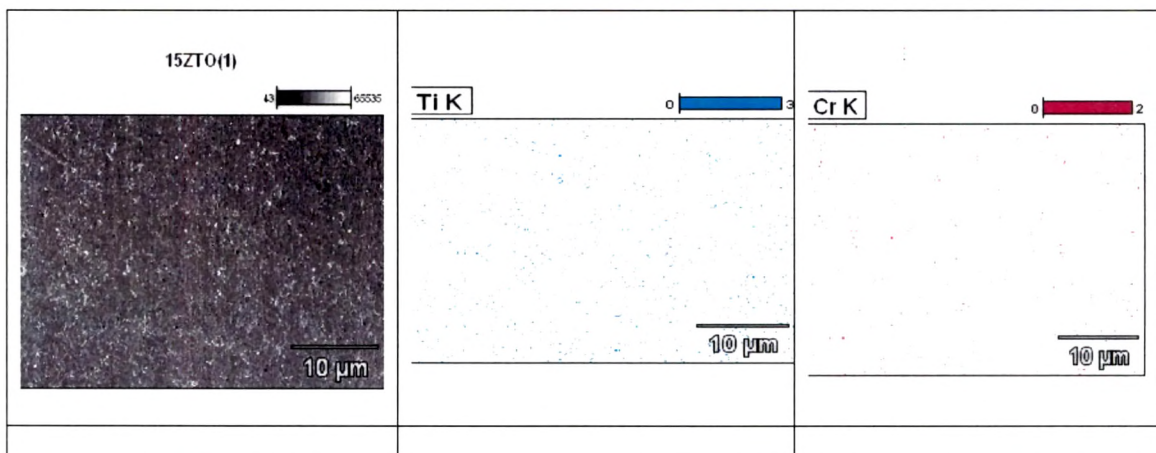


Fig 5.A.3.2 EDX analysis of macroparticle in 2.5μm ZrTiN

The Fig 5.A.3.2 indicates EDX analysis at the point indicates that the macroparticle is composed of Zr and Ti both. It seems that under thermodynamic conditions prevailing in Cathode arc evaporation(CAE) macroparticles must be forming solid solution between Zr and Ti metal.



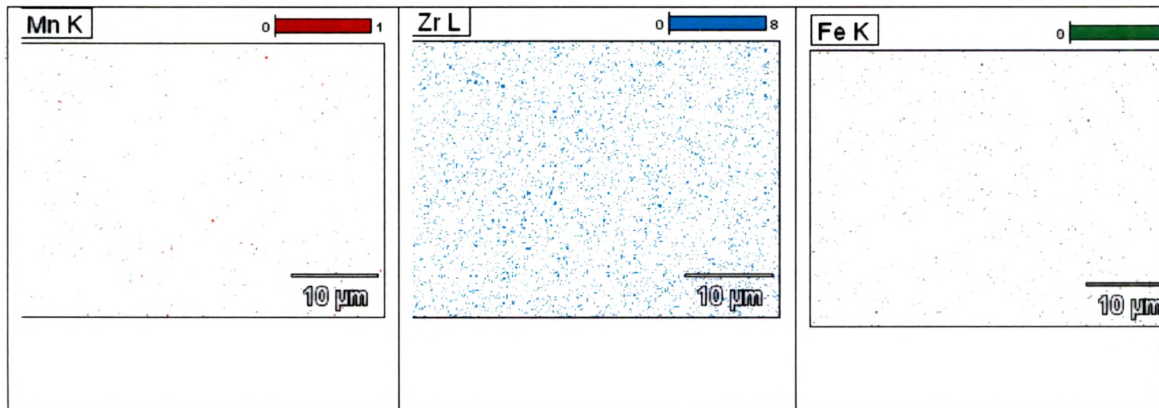


Fig 5.A.3 3 SEM micrograph with EDX mapping of Ti, Cr, Mn, Zr and Fe

The Fig 5.A.3 3 indicates that the atomic concentration of Ti and Zr depended on the background pressure, though cathode currents were initially set to obtain equal fluxes of Ti and Zr ions, while at all pressures the concentration of Zr is higher, the dominance of Zr at higher pressure is even stronger. This behavior may possibly be explained by deflection of the ions. The lighter Ti ion is more affected by the background gas nitrogen pressure than the heavier Zr ion, resulting in a larger scattering of the Ti ions. [5] Due to the same reason the peak intensity of Ti in fig 5.A.I. (iii) is less than Zr. [6]

The number of macro-particles per square centimeter was significantly higher in the TiN and  $Ti_xZr_yN$  than ZrN, probably owing to the lower melting point of the titanium target material. [7]

As illustrated in the cross-section SEM of all the micrograph above deposited TiN/ZrN/ZrTiN films have a dense and compact microstructure which is attributed to the energetic metal ion bombardment during the deposition process. Voids and columnar structure are not observed in the SEM micrograph. However, macroparticles (as typical CAE by-products) are clearly visible on the film surface. These are Ti, Zr or Zr+Ti droplets ejected from localized molten pools on hot cathode surfaces. These micron sized particles are embedded in film synthesized by the CAE process. For applications of these films where a fine surface finish is required, these macroparticles are not desirable and an additional particle filtering mechanism is required. [8]

## 5. B XRD CHARACTERISATION

XRD can be roughly separated into two categories: low angle ( $2\theta \leq 15$ ) and high-angle ( $2\theta \geq 15$ ) XRD. The distinction is made because low-angle XRD results from the reflection of X-rays off the interfaces between layers, while high-angle XRD results from diffraction of X-rays of individual atomic planes in the super lattice. Thus, low-angle XRD is not affected by the crystalline quality within each layer. [9]

In order to minimize the structural analysis to only the first 1–2  $\mu\text{m}$  of the coatings, Glancing angle X-ray diffraction (GAXRD) should be carried out the incidence angle should be chosen as  $3^\circ$  to eliminate the overlap of the substrate peaks with the peaks of the coatings.[10,11]

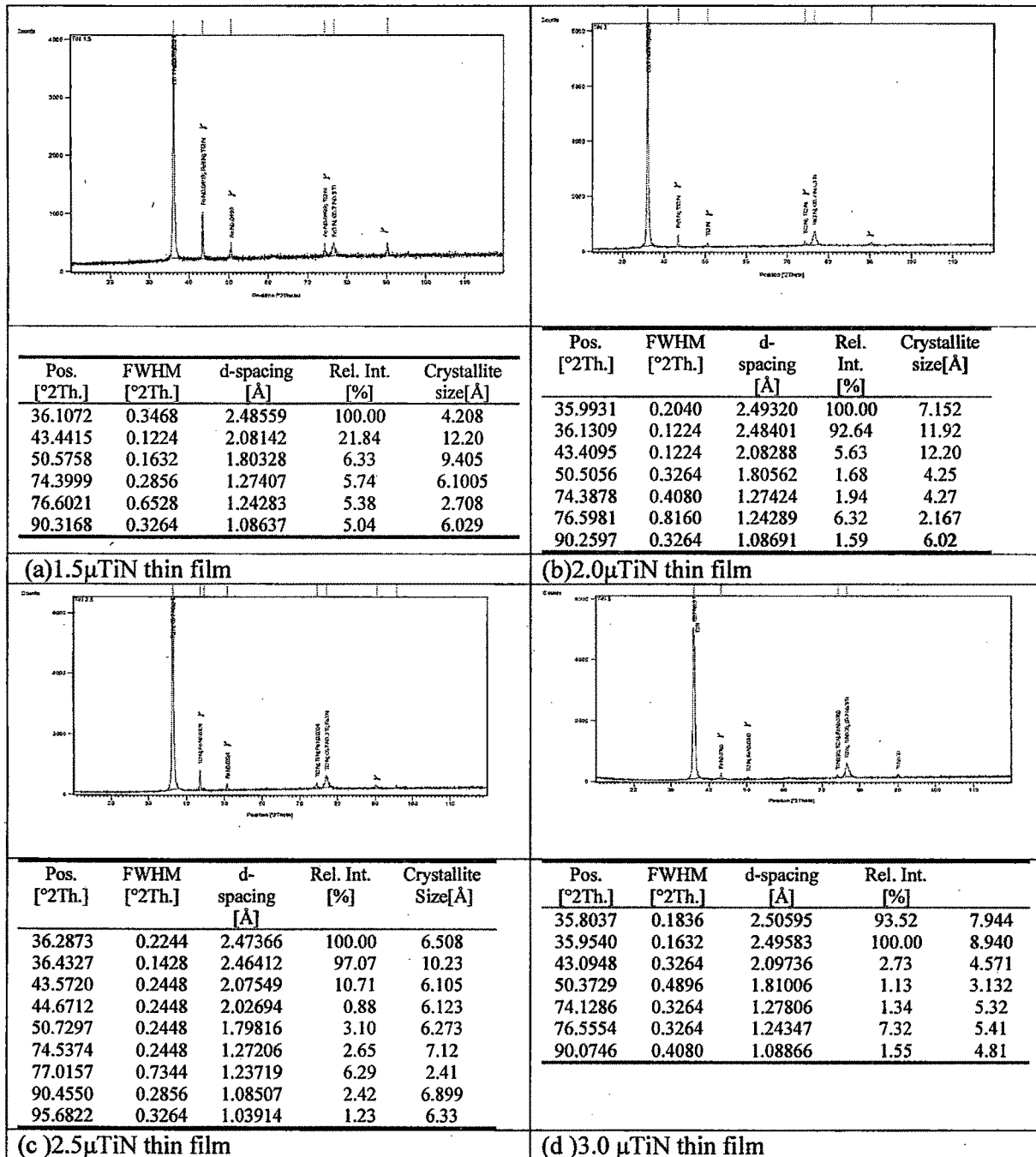
According to Henry J. Ramos et al for deposition of ZrN thin films, showed that the ZrN peak locations from sample to sample of varying thickness are consistent with each other and agree with the data that has been reported for ZrN films. The relative intensities of the peaks from this study show some variation from sample to sample and do not necessarily match the random powder relative peak intensities from JCPDS file data. The reason for this is that there is very likely a preferred orientation of the ZrN grains in the films compared to random orientation in the JCPDS (2-0956 for ZrN) powder. Considering the above statement, matching up to two decimals is considered. [12]

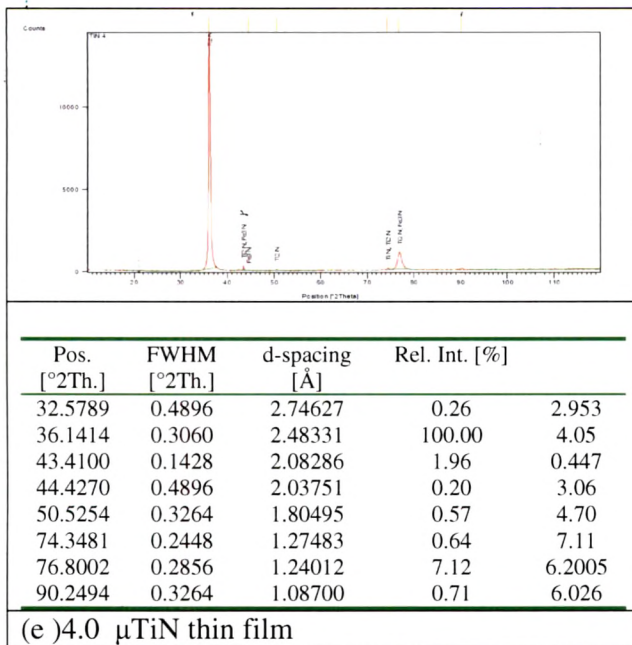
The Films prepared by physical vapour deposition (PVD) techniques are, in general, nonstoichiometric. [13]

### 5.B.1 XRD Charactersation of Ti-N thin films

X-ray diffraction (XRD) analysis was performed to study micro structural changes and new phases formation induced by increasing thickness of TiN thin films.

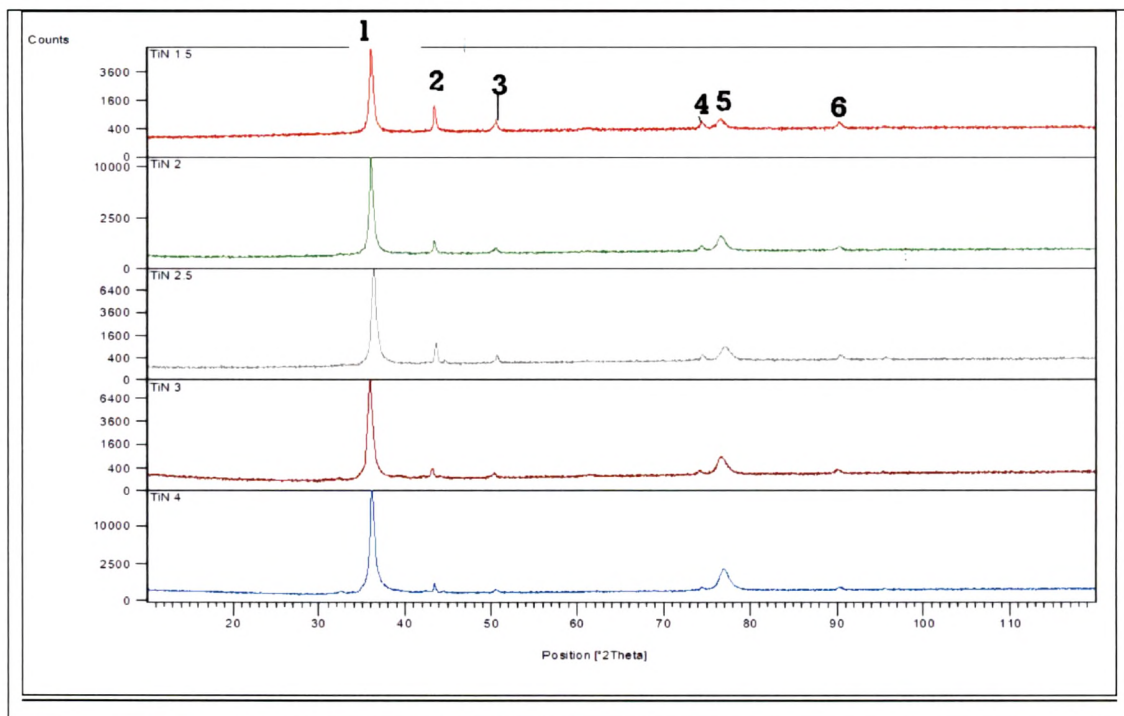
Fig 5.B.1 (i) shows the diffractograms obtained for TiN thin films of varying thickness indicating composition, phases and relative intensity at different thickness.





5. B.1 (i) Diffractograms of Ti-N thin films at different thickness

The above diffractograms.5.B.1 (i) indicates presence of  $Ti_2N$  instead of TiN. As stated by G.L.N. Reddy et al [13], the Films prepared by (PVD) techniques are, in general, nonstoichiometric .Intense peak of  $\gamma$  Fe is obtained in 5. B.1 (i) (a)



1	Ti <sub>2</sub> N
2	γFe
3	γ Fe
4	γ Fe/TiN <sub>0.9</sub>
5	Ti <sub>2</sub> N
6	γ Fe

Fig 5. B.1. (ii) Combined XRD spectra of TiN thin film of varying thickness

The Fig 5. B. 1 (ii) shows combined diffraction patterns of Ti-N at different thickness (1.5, 2.0, 2.5, 3.0 and 4.0 μ) Peaks corresponding to the Ti<sub>2</sub>N and γ Fe are observed. All the peaks corresponding to Ti<sub>2</sub>N formation showed the greatest intensity and it was predominant. This means that the phases in the coating did not alter with the coating thickness. The peak corresponding to γ Fe (Peak2 & Peak 3) are from the stainless steel substrate, the height of Fe diffraction peaks rapidly decreases with the increase of the thickness of TiN coating, indicating the complete coverage of the coating. At Peak (4) in addition to Ti<sub>2</sub>N, small peak corresponding to TiN<sub>0.9</sub> is obtained, therefore composition of the coating is not purely Ti<sub>2</sub>N, consequently in all the experimental studies instead of Ti<sub>2</sub>N, Ti-N is considered. With the increase in thickness the peak broadening (Peak 5) is observed. These peak broadening phenomena, in general, result from both diminution of grain size and residual stress induced in the crystal lattice [12] or may be due to insertion of free N atoms in the crystals and therefore to a non-uniform lattice distance with spread interference peaks. [14] Stoichiometric titanium nitride (TiN) is one of the most important technological coating materials, not only because of its excellent tribological properties but also due to a good chemical stability. It is used in a wide range of applications, which vary from a protective material for machine parts and cutting tools to diffusion barriers in semiconductor technology. [15]

Titanium nitride crystallizes in the B1 NaCl structure and exists as a solid solution containing nitrogen in the range 37.5-50 % at. as shown in figure (fig. 5.B.1.(iii))[16]

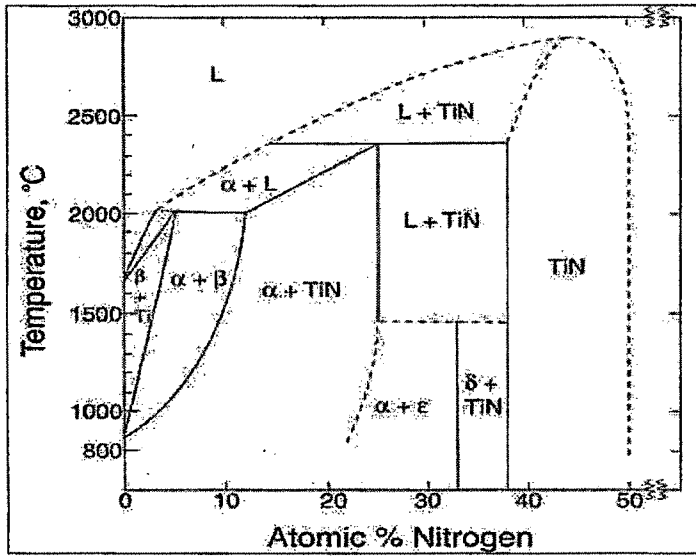


Fig 5. B. 1. (iii) Equilibrium phase diagram of Ti-N binary system

The titanium–nitrogen phase diagram is complex, but basically Ti crystal is said to be an ‘interstitial’ crystal where N atoms fit into the gaps of the Ti structure. This structure evolves from hexagonal  $\alpha$ -Ti, to face-centred-cubic  $\delta$ TiN, the N atoms being into octahedral sites of the Ti lattice as the amount of nitrogen is increased, the  $\alpha$ -Ti lattice is able to accept small amounts of nitrogen at octahedral sites but since PVD is a thermodynamically non-equilibrium process, the  $\alpha$ -Ti lattice may be forced to accept more nitrogen atoms. Due to hindered mobility of the deposited particles therefore an oversaturated metastable solution of nitrogen in titanium is formed for the lower N contents. [15] Since  $N_2$  is the reactive gas, its quantity in the deposition chamber is of major importance. [16,17]

From the Ti-N phase diagram, it is clear that in addition to TiN a second Ti-N phase can be formed:  $Ti_2N$  ( $\epsilon$  phase). The two phases have different crystal structures: TiN is cubic (face-centered cubic) and  $Ti_2N$  is tetragonal. In contrast with the TiN phase, which can be formed over a rather broad nitrogen concentration range (at  $500^\circ\text{C}$  from less than 30 at.% N up to 50 at.% N),  $Ti_2N$  has a well-defined nitrogen concentration of 25 at.%.

From this it follows that only for a well-defined Ti/N ratio can monophasic  $Ti_2N$  be deposited. Therefore PVD of a monophasic  $Ti_2N$  coating demands stringent control of the influx of titanium and nitrogen atoms and ions. [18, 20]

To further investigate the conditions under which  $Ti_2N$  has formed in present case and considering the results obtained by L.A Roacha[15] for different nitrogen flow and its effect is considered

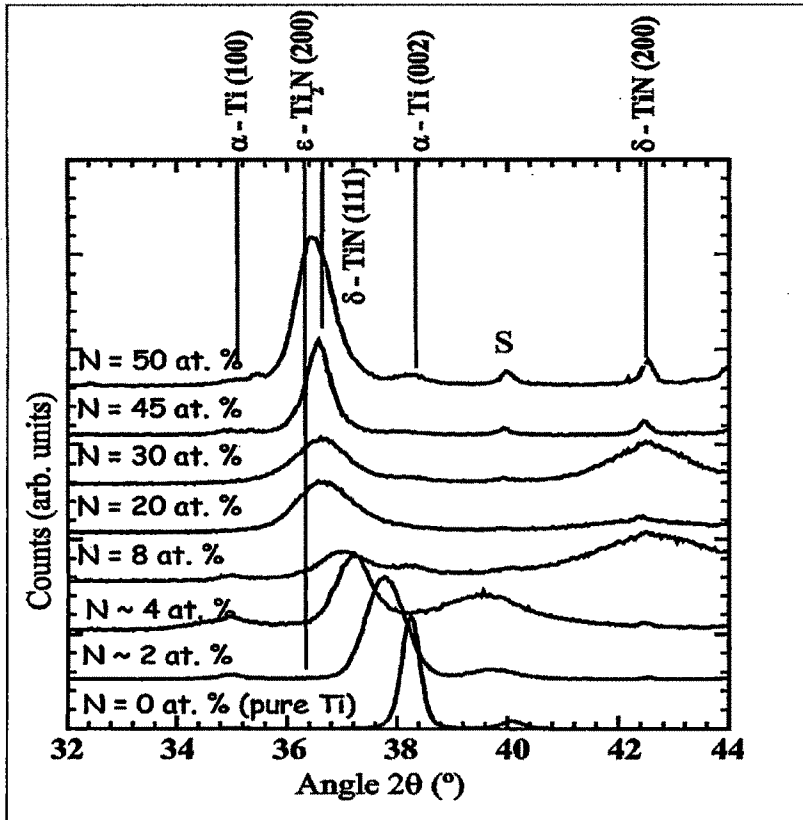


Fig 5. B. 1. (iv) Evolution of the XRD patterns of  $TiN_x$  films as a function of nitrogen contents. S corresponds to the diffraction lines of the substrate.

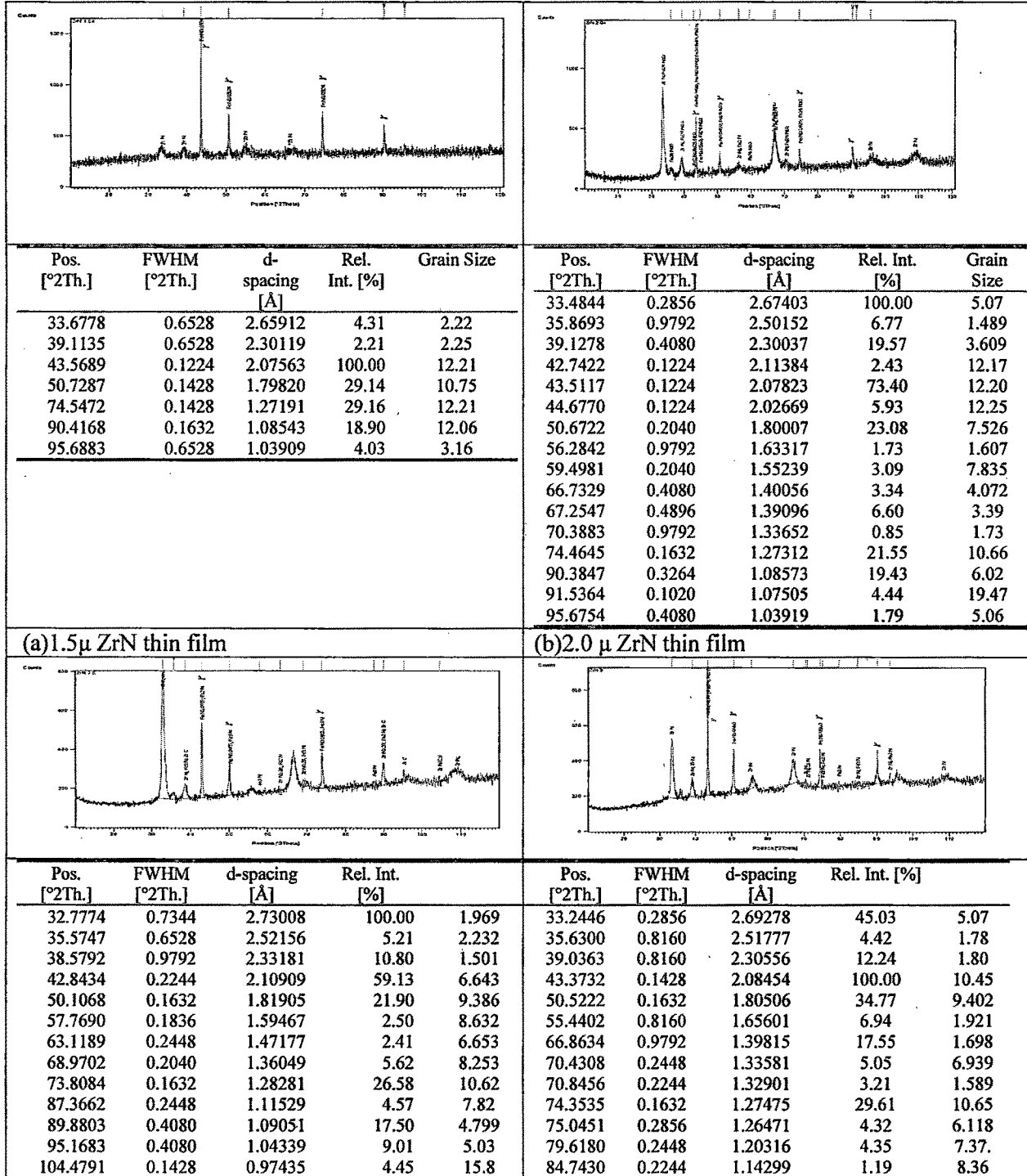
The investigation of  $TiN_x$  films by [15] deposited by different PVD techniques shows that increasing nitrogen flows and then the gas pressure during the deposition process leads to gradually higher nitrogen contents in the films. A closer look to the XRD diffraction patterns reveals the development of the hexagonal  $\alpha$ -Ti phase with strong [002] orientation for low nitrogen contents. (Fig. 5.B.1. (iv)) The diffraction peaks are progressively shifted towards lower diffraction angles as the N content increases. For nitrogen contents of 20 and 30 at.%, the  $\epsilon$ -  $Ti_2N$  phase appears with a [200] orientation. Furthermore, although it does not seem clearly visible, the  $\delta$ -TiN phase might be already

developing. The broad diffraction lines do not allow concluding unambiguously concerning the exact nature of the crystalline compounds present whereas the phase diagram predicts only the  $\epsilon$   $\text{Ti}_2\text{N}$  phase as well as the  $\alpha$ -Ti but with diffraction peaks shifted to lower diffraction angles due to nitrogen insertion. With further increasing the nitrogen content, the  $\delta$ -TiN phase becomes dominant. [15, 19]

Hard coatings like TiN normally contain a high degree of internal (usually compressive in-plane) stress owing to lattice distortion and thermal mismatch effects; it is, therefore, difficult to produce single-layer TiN coatings thicker than 6–7  $\mu\text{m}$ , high stress values present in the coatings e.g. stress values up to 10 GPa have been reported for TiN coatings. When the coating thickness increases the critical compressive stress needed to delaminate the coating decreases. Lower stresses present in  $\text{Ti}_2\text{N}$  coatings, can be deposited with thicknesses up to tens of micrometres without encountering adhesion problems on typical substrate materials employed. [18,21,22]

### 5.B.2 XRD Charactersation of ZrN thin films

Fig 5. B.2 (i) shows the diffractograms obtained for ZrN thin films of varying thickness indicating composition, phases and relative intensity at different thickness.



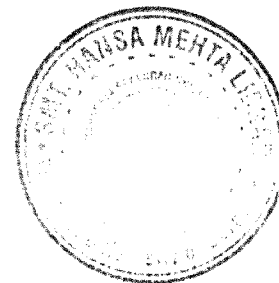
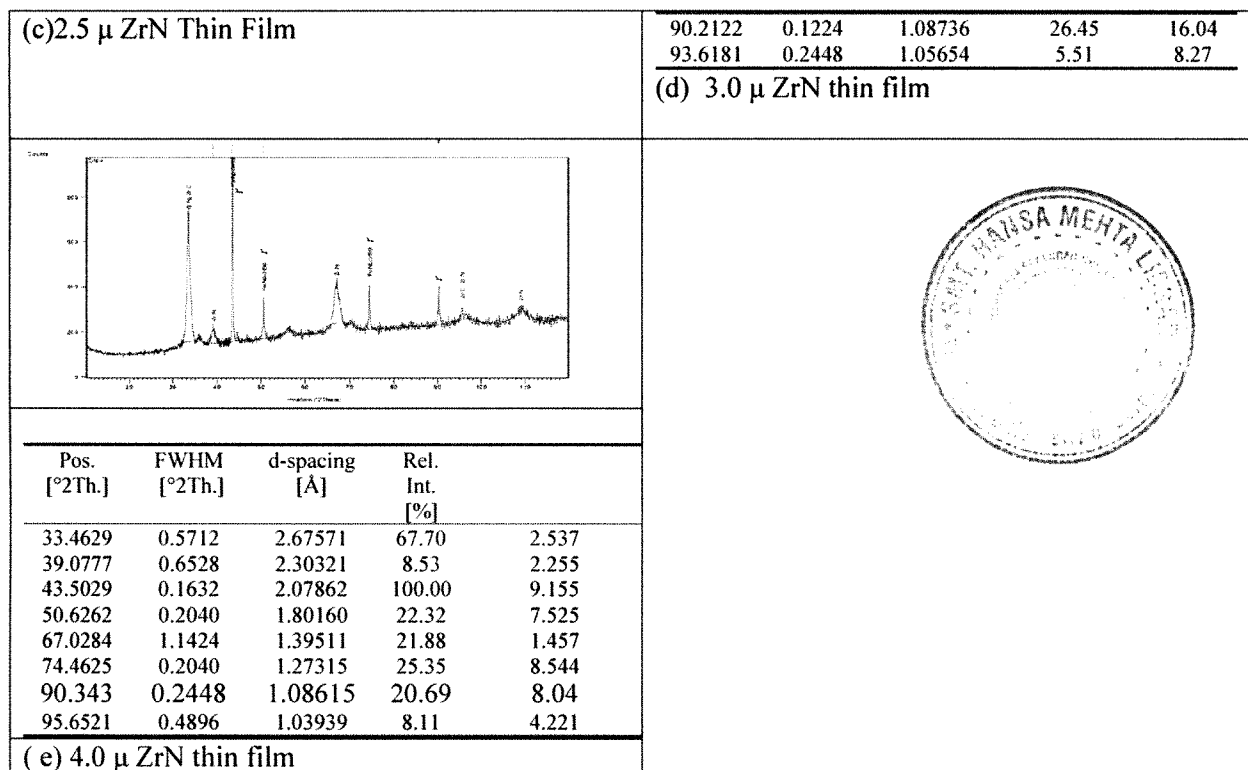
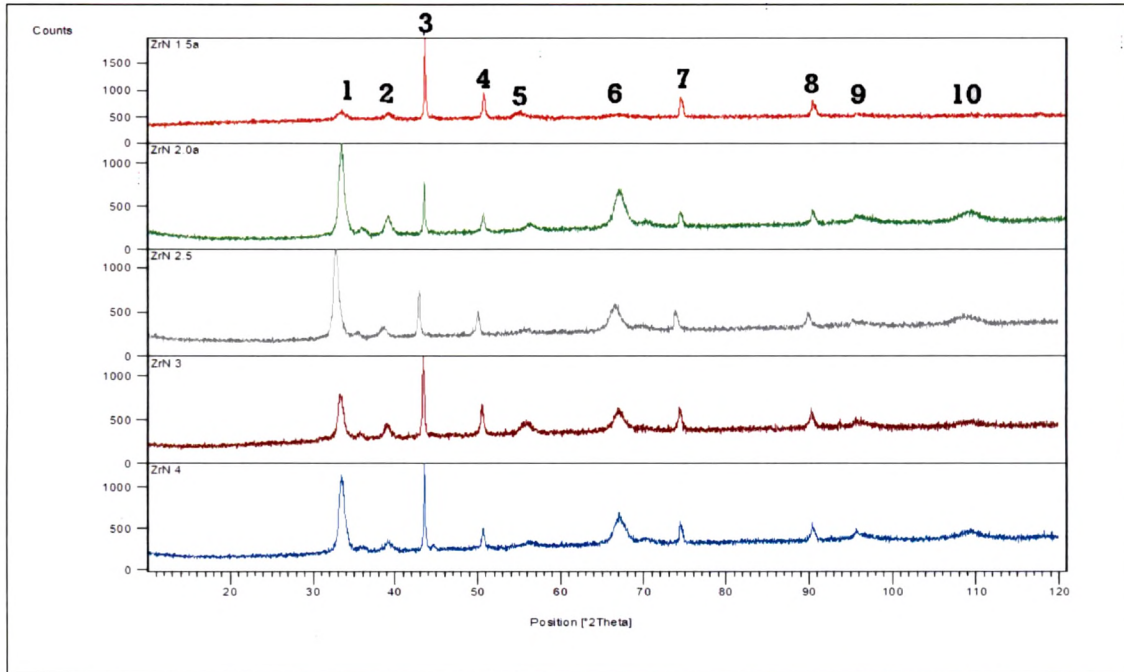


Fig. 5. B.2 (i) Diffractograms of ZrN at different thickness

As indicated in Fig 5.B.2 (i), at low thickness ( $1.5\mu$  ZrN), high intensity peak of  $\gamma$ Fe is obtained indicating incomplete coverage of coating. The intensity and grain size of  $\gamma$ Fe varies according to thickness. High intensity peak of  $\gamma$ Fe is observed for  $3\mu$  ZrN and  $4\mu$  ZrN, however the size is smaller than  $1.5\mu$  ZrN. The peak corresponds to 100% in case of  $2\mu$  ZrN and  $2.5\mu$  ZrN is at  $2\theta=33.33$  which shows ZrN (111). Comparatively less intense peak is observed for  $2\theta=39.11$  (200) ZrN. Further peaks at  $2\theta = 104.479$  &  $2\theta= 66.86$  corresponds to (420) and (311) planes respectively are obtained. XRD revealed the variation in grain size of various phases with increase in thickness. [23]



1	ZrN (111)
2	ZrN(200)
3	$\gamma$ Fe
4	$\gamma$ Fe
5	ZrN(220)
6	ZrN(311)
7	$\gamma$ Fe
8	$\gamma$ Fe
9	ZrN(331)
10	ZrN(420)

Fig 5. B. 2 (ii) Combined XRD spectra of ZrN thin film of varying thickness.

As indicated in fig 5. B. 2 (ii), the ZrN phase with varying direction is observed. However maximum number of planes with different orientation is observed in 2  $\mu$ , 2.5 $\mu$  and 3  $\mu$  ZrN thin films. The intense peak of ZrN(111) and ZrN(200) is observed in 2  $\mu$  ZrN and 2.5  $\mu$  ZrN. The substrate bias voltage is influence the texture of ZrN – generally the texture changed from (111) to (220) and (200) with increasing  $|V_{bias}|$  .indicating change in  $V_{bias}$  during deposition, may have occurred in the present case. Increase in bias voltage increases residual stress, dislocation density and defect density, crystallographic structure in the coatings [24-27,33-35]

In present investigation stoichiometric ZrN thin films of varying composition is obtained. However orientation of these planes cannot be obtained. Hence considering the XRD spectra obtained by V.N Zhitomirsky [27] (fig 5.B.2.(iii)) et al wherein by using the triple cathode vacuum arc deposition apparatus, substrate sample ISO -K25 XRD spectra of ZrN with different orientation was obtained, substrate temp 400<sup>o</sup> C and substrate bias of 0V.

The XRD show the presence of single distinct peaks at  $2\theta=33.96$  and  $2\theta =39.35$  corresponding to the (1 1 1) and (2 0 0) reflections of ZrN, respectively. [27]

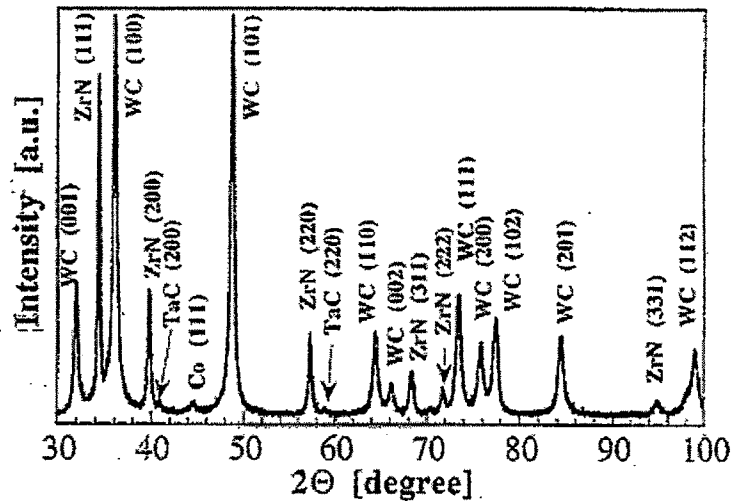


Fig 5.B.2 (iii) XRD spectrum of ZrN coating on cemented carbide substrate ( $T_s=400$  C  
v bias=0v)

In the present case it can be seen that a single phase of ZrN films was formed after deposition on the substrate. The ZrN films present a preferential crystalline orientation following the [1 1 1] axis. This (111) texture appears when a critical level of internal stress is present in the coating since this tends to minimize the stress. [28] ZrN has a higher negative free energy of formation than TiN, hence ZrN seemed to form itself more easily than TiN. H. Jiménez, E. Restrepo, A. Devia [29] studied the influence of substrate temperature ( $T_s$ ) during the ZrN films growth process on 304 stainless steel samples, using a repetitive pulsed arc plasma assisted technique, on parameters such as grain size, micro strain, lattice parameter, crystallite size and morphology. The values of

the  $T_s$  were 50°C, 100°C, 140°C, 170°C, 200°C, 230°C and 260°C. The conditions for film deposition were vacuum of  $10^{-5}$  mbar, nitrogen as working gas at a pressure of 3mbar and a voltage of 270V. These researchers suggest that the preferential orientation is determined by the competition between two thermodynamic parameters, the free surface energy and the strain energy. They stated that for low thickness, the film presents a preferential orientation corresponding to the one with the lowest surface energy. This argument is based on the high quantity of broken bonds. When the thickness is increased, the strain energy begins to increase while the surface energy does not vary with the thickness of the film. At low substrate deposition temperatures, the mobility of adatoms on the surface is low and therefore textures, even in thick films, are determined in the early stages of deposition where nucleation plays the most dominant role in determining the film structure. Further as mentioned, Walton [29] predicted that low  $T_s$  or high rates of deposition favored the alignment of the material closest to packed planes being then deposited parallel to the surface. Therefore, for the case of F.C.C. materials, (ZrN is F.C.C) the preferred texture for low substrate deposition temperatures involves (111) planes being parallel to the surface since the (111) planes are the most densely packed planes in F.C.C. C. Mendibide et al[28] also stated that (111) texture appears when a critical level of internal stress is present in the coating since this orientation tends to minimize the stress.[28,29]

According to H. Jiménez et al[29] at higher temperature(200<sup>o</sup> C) the preferential crystallographic orientation changes from (111) to (200), it appears that the surface energy is greater than the strain energy, making the total energy of the (200) plane lower than the one for the (111) plane. [21]

Also as suggested by J.V Ramana et al [30] with increase in nitrogen partial pressure ZrN coatings prepared by reactive arc deposition, exhibited anomalous (200) rather than (111) preferred growth orientation. Thus process parameter like substrate temperature and nitrogen partial pressure determines the orientation in ZrN thin films. [30]

As indicated by M.M. Larijani et al [31] although (2 0 0) planes are thermodynamically the most stable planes with the minimum surface energy, the growth parameters and conditions in ion beam sputtering method privilege dynamically the domination of the

(1 1 1) plane with faster growth rate, In this case also the preferable orientation is ZrN(111) instead of ZrN(200) for all the thickness.[31]

However D.F. Arias, Y.C. Arango, A. Devia preferential direction for ZrN was (2 0 0) and it is not (1 1 1). [5]

ZrN thin films were deposited by Cheng-Shi Chen et al[32] on Si(1 0 0) substrates using a high purity (99.5%) Zr target by dc magnetron sputtering. Substrate temperature and substrate bias was varied also  $T_s$  was increased to 92, 97 and  $117^{\circ}\text{C}$  for the substrate biases of  $V_b=0, -45$  and  $50$  V, respectively. The elastic modulus was determined from the load–displacement data obtained by the nanoindentation using a Berkovich tip. The elastic modulus is a measure of the stiffness of a material. It is anisotropic in nature and thus sample orientation dependent. The elastic modulus increased rapidly with increasing the substrate bias from 166.4 GPa at  $V_b= -45$  V to 196.3 GPa at  $V_b=20$  V. As shown in fig. 5. B. 2. (iii) both (111) and (200) peaks coexist. Intense peak of ZrN (111) is obtained at 20V whereas as weaker peak is obtained at -45V suggesting that the elastic modulus of ZrN (111) planes might be larger than ZrN that of (200) planes. Further macro stress at different bias was derived indicating stress of -0.186, -0.322 and -1.8 GPa for the ZrN films deposited at  $V_b= -45, -20,$  and  $20$  V, respectively (At +20 V  $\text{Zr}_2\text{N}$  is present).Fig 5.B.2.(iii) indicates that coexistence of both ZrN(111) and ZrN(200) contribute to high macro stress within the coating.

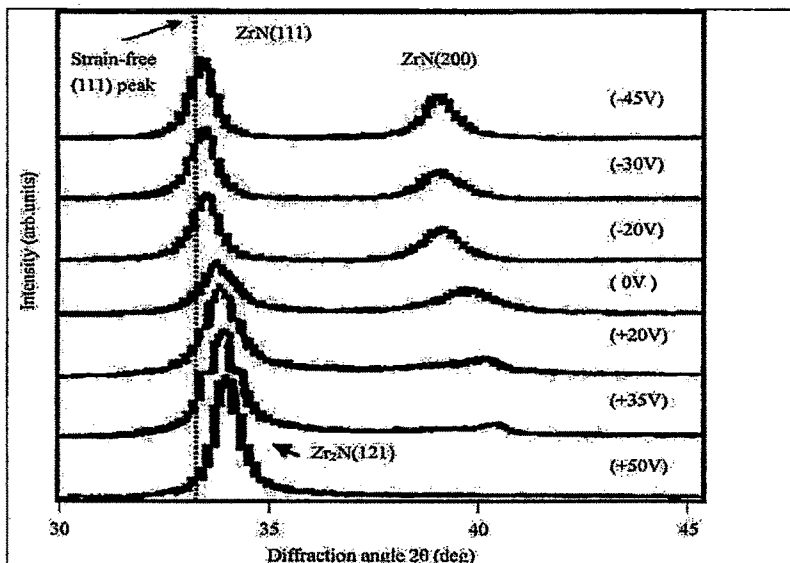


Fig. 5.B.2.(iv) XRD patterns of the ZrN films deposited on Si at various substrate biases.

In present studies for  $2\mu$  ZrN and  $2.5\mu$  ZrN, peak intensity of ZrN(111) and ZrN(200) is high indicating high macro stress within the coating.

### 5. B. 3 XRD characterisation of Zr-Ti- N thin films

Fig 5.B.3 (i) shows the diffractograms obtained for ZrN thin films of varying thickness indicating composition, phases and relative intensity at different thickness

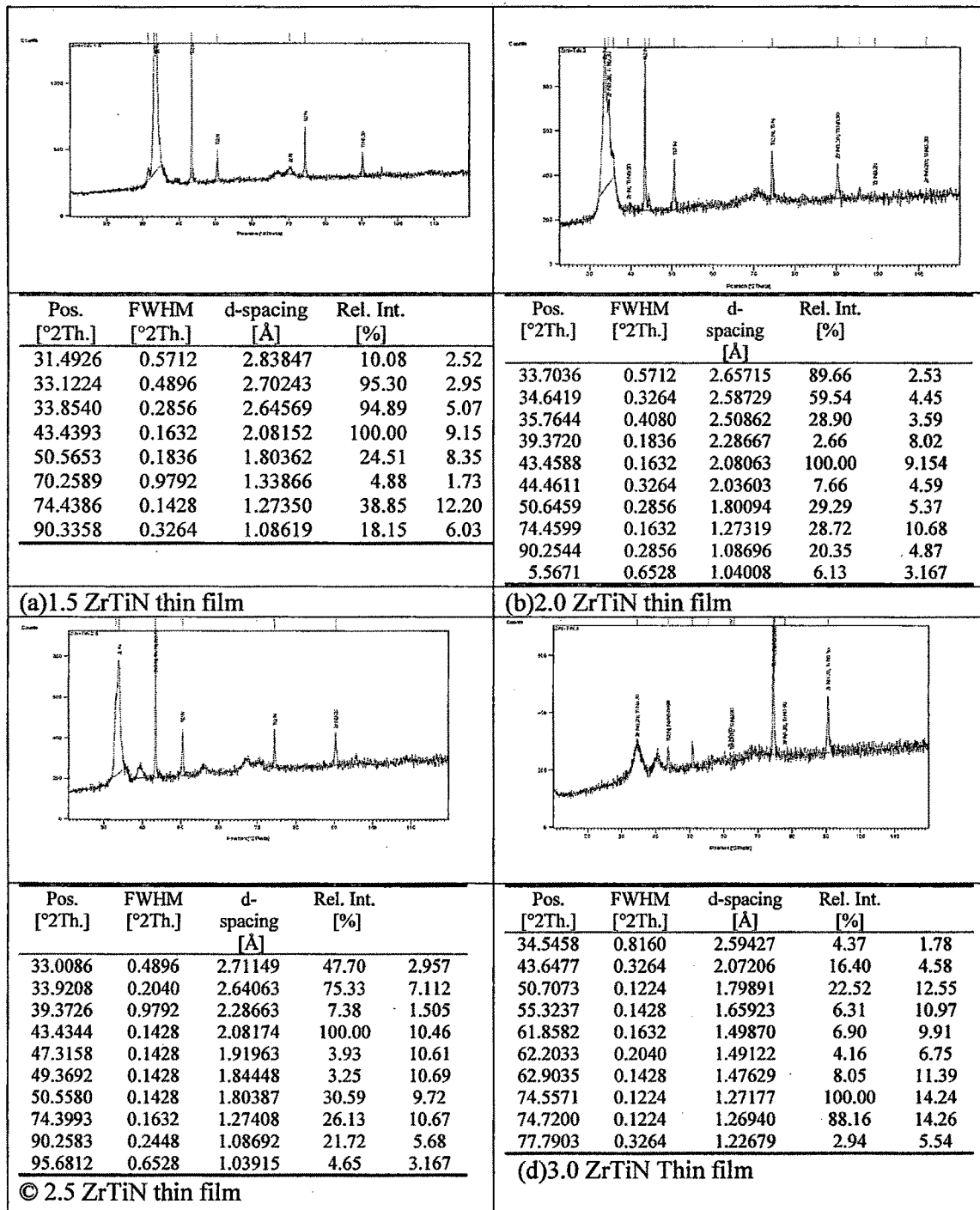


Fig.5. B. 3.(i) Diffractograms of ZrTiN at different thickness

In vacuum arc deposition of nitride coatings, the process parameters, and especially the ratio of the arc current to the nitrogen pressure determine the composition and the structure of the coating.[6]Fig 5.B.3 (i) indicates that two separate phases corresponding to ZrN and Ti<sub>2</sub>N and ZrN<sub>0.3</sub>, TiN<sub>0.3</sub> is formed. The peak corresponding to substrate is also observed.

At low thickness (1.5μ ZrTiN), (5.B.3.(i) (a)) high intensity peak of γ Fe is obtained indicating incomplete coverage of coating. The intensity and grain size of γ Fe varies according to thickness.

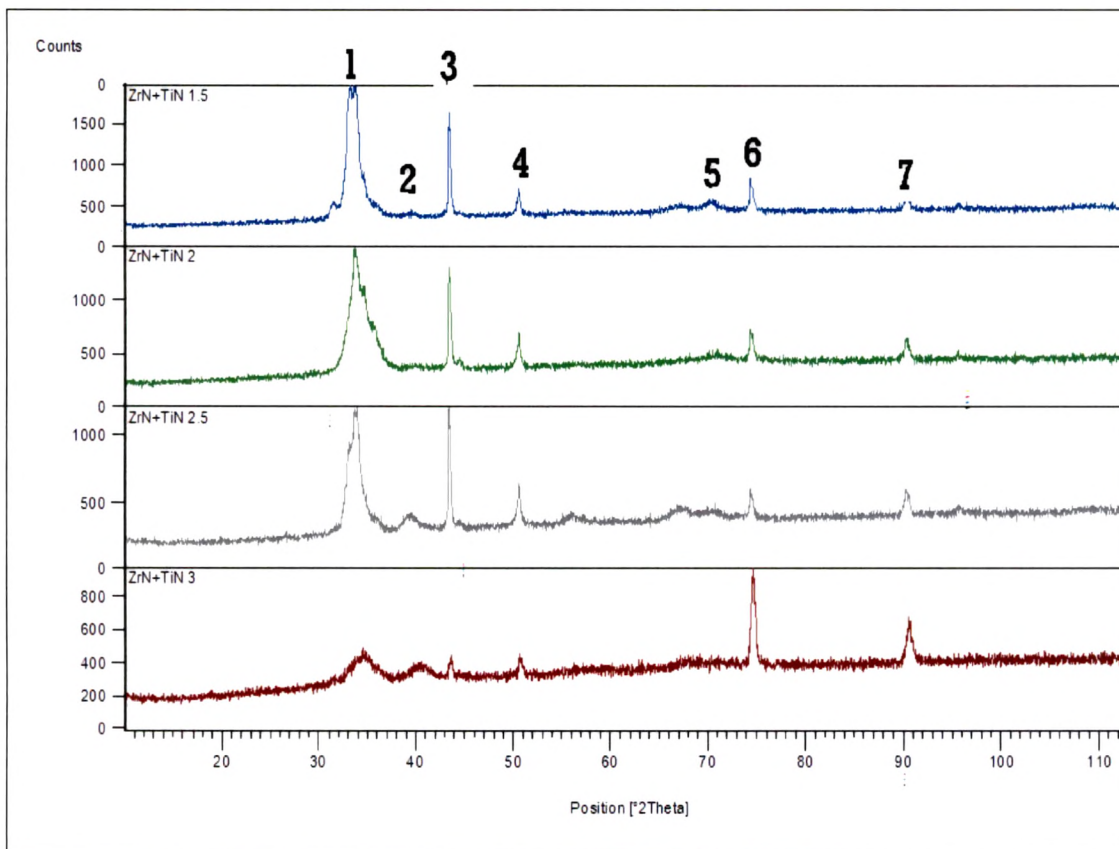


Fig 5.B.3.(ii) Combined XRD spectra of ZrTiN thin film of varying thickness.

1	ZrN (111)
2	ZrN(200)
3	γFe
4	γFe
5	ZrN(220)
6	Ti <sub>2</sub> N
7	ZrN <sub>0.3</sub> ,TiN <sub>0.3</sub>

On comparing the orientation of various phases in Fig 5.B.3. (ii), for thickness of 2.5 $\mu$  and 3 $\mu$  ZrTiN intense peak corresponding to ZrN(200) is observed. In case of 3  $\mu$  ZrTiN peak corresponding to  $\gamma$  Fe is less intense than other coatings. As revealed by XRD intense peak corresponding to Ti<sub>2</sub>N is obtained in 3  $\mu$  ZrTiN. The peak corresponding to formation of Ti<sub>2</sub>N and ZrN<sub>0.3</sub>,TiN<sub>0.3</sub> is highest in 3 $\mu$  ZrTiN.

As observed by I. Grimberg et al [6]Ti–Zr–N coatings deposited using a triple-cathode vacuum arc deposition apparatus and substrate samples were ISO-K25 cemented carbide bars (5 $\times$ 6 $\times$ 20 mm), having a composition of 90% WC, 8% Co, 1.8% TaC, and 0.2% NbC. The coatings were deposited at three different nitrogen pressures –0.67, 1.33 and 2 Pa. The XRD spectra at all three pressures indicate that a (Ti,Zr)N solid solution was formed. A solid solution of (Ti,Zr)N, with single FCC structure and no evidence of phase separation, was formed for multicomponent Ti–Zr–N coatings.[33-38]

However in present case we obtained separate phase of ZrN and Ti<sub>2</sub>N. This may be due to formation of Ti<sub>2</sub>N instead of TiN which has tetragonal crystal structure different than FCC ZrN structure lattice parameter and tetragonal structure. and this does not fulfill the criteria for formation of solid solutions according to Hume rothery rules.

On comparing the orientation of various phases in Fig 5.B.3.(ii),for all thickness, peak 7 consisting of ZrN<sub>0.3</sub>,TiN<sub>0.3</sub> correspond to same peak (90.2544) indicating either solid solution may form or two phases may coexist on same plane.

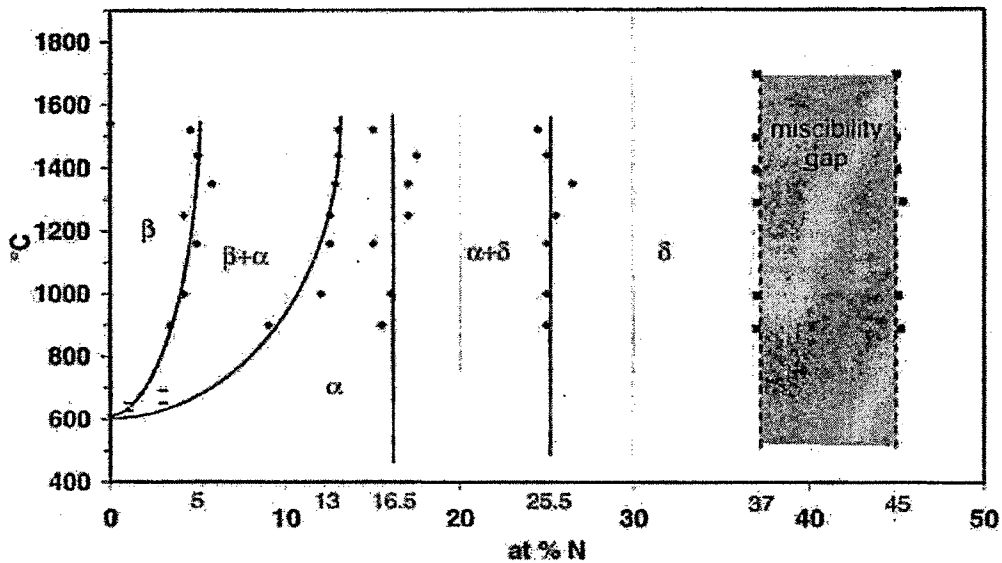


Fig 5.B.3.(iii) Partial experimental (Ti<sub>0.5</sub>Zr<sub>0.5</sub>)-N phase diagram: (♦) These results, (—) dilatometric results (■) nitride decomposition study [29]

The partial pseudobinary phase diagram, Fig 5.B.3.(iii) plotted by E. Etchessahar et al [34] taking dilatometric and calorimetric results and concluded that the δ-(Ti Zr)N nitride (cubic NaCl type structure) exists in a large nitrogen composition range. The lower limit of this non-stoichiometric nitride is found to be 25.5 at.% N, that is to say lower than the limit observed for the δ ZrN nitride (35 at.%). No subnitride was found in this pseudo binary (Ti<sub>0.5</sub>Zr<sub>0.5</sub>)-N diagram.[34] Hence in this case ZrN<sub>0.3</sub>,TiN<sub>0.3</sub> must have formed solid solution.

## 5. C Corrosion Behaviour Thin Films in Various Environment

The corrosion behaviour of the coating-substrate systems can be characterized by current density-potential measurement [39]. Electrochemical experiments proved to be good test for studying the resistance and compactness of coatings. [40]

### 5.C.1 CORROSION BEHAVIOUR OF Ti-N THIN FILMS

#### 5. C1. (a) Corrosion Behaviour of Ti-N in 1N 1NH<sub>2</sub>SO<sub>4</sub>

The corrosion behaviour of Ti-N coatings of varying thickness was measured by potentiodynamic corrosion tests in 1N H<sub>2</sub>SO<sub>4</sub> solution.

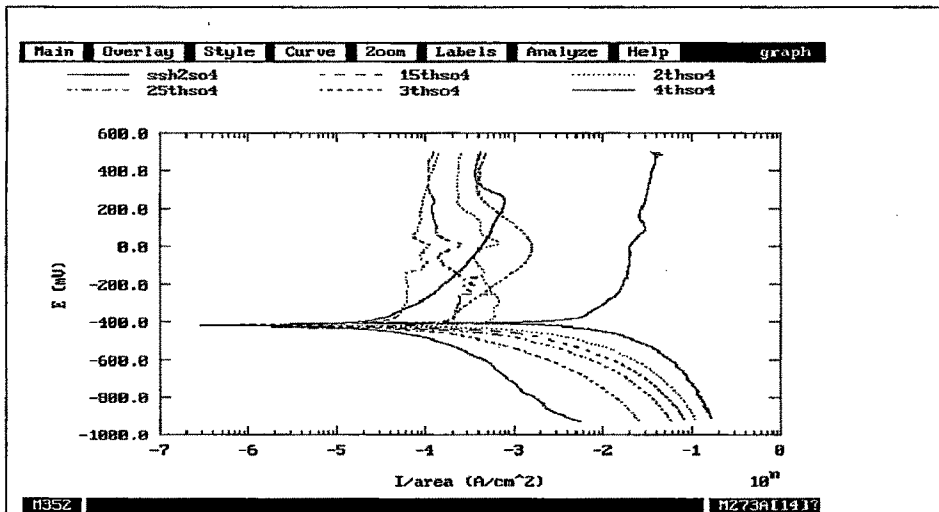


Fig 5.C.1.(a)(P) Potentiodynamic corrosion test of S.S substrate & Ti-N thin films of varying thickness in 1N H<sub>2</sub>SO<sub>4</sub>

1N H <sub>2</sub> SO <sub>4</sub>	E <sub>corr</sub> (mV)	I <sub>corr</sub> (μA/cm <sup>2</sup> )	Protective efficiency, P <sub>i</sub> (%)
S.S	-408	31.05 mA/cm <sup>2</sup>	
1.5μ TiN	-422.2	696.7	97.75
2μ TiN	-421.4	1.540	99.99
2.5μ TiN	-427.3	454.8	98.54
3μ TiN	-417.6	123.2	99.61
4 μ TiN	-420.6	102.0	99.68

Table C.1.(a) Values of corrosion potential (E<sub>corr</sub>) corrosion current density (I<sub>corr</sub>) and protective efficiency for all Ti-N specimens in 1N H<sub>2</sub>SO<sub>4</sub>

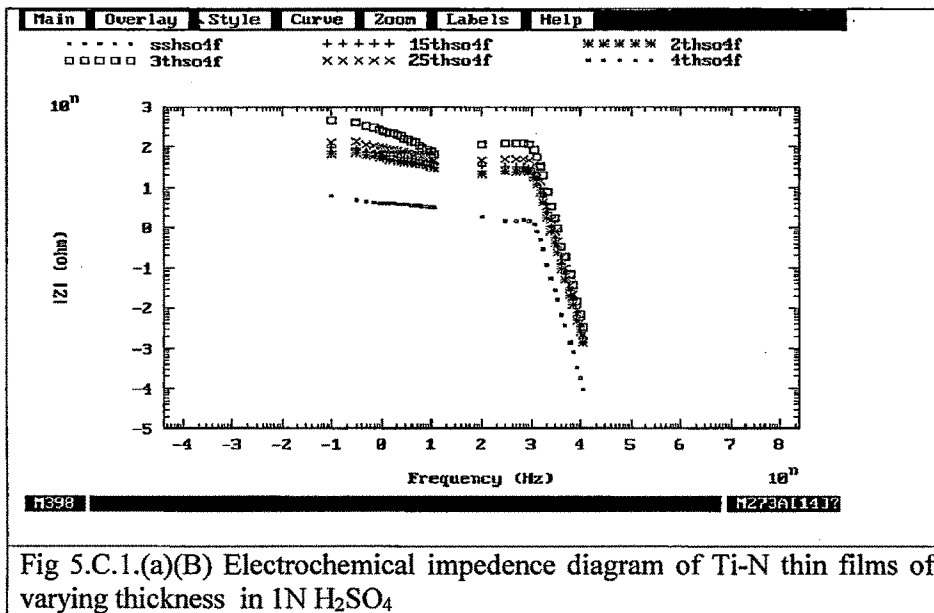


Fig 5.C.1.(a)(B) Electrochemical impedance diagram of Ti-N thin films of varying thickness in 1N H<sub>2</sub>SO<sub>4</sub>

The Tafel plots obtained for steel substrate and Ti-N coating of varying thickness in 1N H<sub>2</sub>SO<sub>4</sub> shown in fig 5.C.1.(a)(P) the electrochemical parameters (corrosion current, corrosion potential and % porosity) calculated from polarization curves are summarized in Table C.1. (a)

The corrosion potential of the steel substrate is about -0.408 V. Each sample's open circuit potential is approximately in the same position. The corrosion potential ( $E_{corr}$ ) of the coated specimens are only slightly away from that of stainless steel, within 25 mV, which indicates that the corrosion of the Ti-N coated-specimens are mainly from the dissolution of the metal substrate and not from the Ti-N film. Since corrosion potential is a thermodynamic property of the substrate material the variation of  $E_{corr}$  is not supposed to be far away from that of bare steel. [41, 42]

The corrosion current density ( $i_{corr}$ ) is an important parameter to evaluate the kinetics of corrosion reactions and is normally proportional to the corrosion current density measured via polarization. The lower the  $i_{corr}$ , the lower corrosion rate the sample has.[43] In the above test the  $i_{corr}$  value obtained is always less than bare Stainless steel substrate indicating protection to the substrate. Lowest  $i_{corr}$  and hence highest corrosion resistance is observed in 2 $\mu$  Ti-N thin films. During the anodic scan, the passive currents are reduced in the case all Ti-N coatings (Fig 5.C.1.(a)(P)) indicating the good protection

efficiency of the coating not only in the corrosion potential domain but also in the passivity potential domain. [44] All the coating exhibit “passive like” behaviour. It is well known that the corrosion resistance of materials or coatings has a close relationship to their passivity maintaining low current densities in the polarization curves. The smaller the passivity density in the passive range, the better the corrosion resistance. Passivity maintaining current density is a current density at which it remains stable as the electric potential increases within a certain potential zone. It is evident that, from the polarization response of Ti-N, from  $-400\text{mV}$  to  $+400\text{mV}$  passivity is maintained. [45]

As suggested by Fengqun Lang et al the polarization response of TiN thin film, with the thickness range  $6\text{-}30\ \mu$  successfully deposited on A3 steel by arc ion plating AIP at a lower temperature in  $1\text{N H}_2\text{SO}_4$  from  $-0.6$  to  $1.3\ \text{V}$ , features several sequential processes, including a cathode evolution of  $\text{H}_2$ , passivation due to TiN, slow dissolution of the macro particles existing in the area near the surface of TiN coating, and a mild dissolution of TiN coating.[2] However this sequence may or may not occur in this coatings, since the composition is  $\text{Ti}_2\text{N}$  for all thickness as indicated in XRD (Fig. 5.B.1(ii)) instead of TiN. The results of XRD Fig. 5.B.1(i) shows presence of  $\text{Ti}_2\text{N}$  instead of TiN as indicated by Roacha et al films are characterized by columnar growth and films containing nitrogen in excess seems to present denser structures than the stoichiometric film. Further the amount of pitting is strongly influenced by the amount of nitrogen in the film, or, in other words, appears to be proportional to the  $i_{\text{corr}}$ , hence in present case, with under stoichiometric thin film, the corrosion behaviour seems to be inferior than conventional TiN coating.[15] However further results are to be confirmed by carrying out Polarisation tests with stoichiometric TiN thin films and in same test conditions.

As shown in the figure 5.C.1.(a)(P), polarization curves in passivation area have a horizontal peak for  $1.5$ ,  $2.0$  and  $2.5\ \mu$  Ti-N. Existence of this peak is related to the formation of secondary phase such as  $\gamma\text{Fe}$  (revealed by XRD Fig. 5.B.1(ii)) for which the corrosion current is higher than matrix phase. When more than one metallic phase is present in alloy, its polarization behavior will be the volume average sum of the behavior of each phase that leads to the presence of the horizontal peak in the passive region. [46] The width of this peak can indicate the activity or amount of secondary phase in matrix.

The intensity of peak corresponding to  $\gamma$ Fe is highest in case of XRD of 1.5  $\mu$  Ti-N (Fig 5.B.1. (i) (a)) hence the width of horizontal peak in Fig 5.C.1.(a)(P) is maximum for 1.5 $\mu$ Ti-N.

EIS gives information regarding corrosion potential and polarization resistance during the immersion of a system in a corrosive medium and hence ongoing corrosion reaction processes as well as additional information about the coating/solution interface and substrate/solution interface.[47]

The Bode plot 5.C.1.(a)(B) for the coated alloy before defect formation has three distinguishable time-dependent processes. The time constant at high frequencies is related to the capacitive response of the film. The resistive plateau at  $10^2$ – $10^3$ Hz represents the pore resistance of film. The relaxation process at about 1–10 Hz is attributed to the capacitance of the intermediate oxide layer present at the metal/coating interface. The resistance of such interlayer, which is situated at lower frequencies, is very important from the corrosion protection standpoint, since it is the last barrier for the corrosive species before reaching the metal surface. The third time constant is weakly defined at lowest frequencies and is related to the corrosion activity. In the fig.5.C.1.(a)(B), at high frequency the impedance value of coating of all thickness is same, indicating same capacitive response of all coatings. However at low frequency there is variation in impedance value. The highest impedance value is observed for 3 $\mu$  Ti-N and there is decrease in the impedance for lower thickness at low frequencies. [48]

A higher impedance values when compared uncoated sample is evidence of superior corrosion resistance. A fast drop of impedance at low frequencies is observed in 2 $\mu$  Ti-N compared to 3 $\mu$  Ti-N and is related to the breakdown of the film and the corrosion activity started on the naked metal surface.

In the low and middle frequency ranges, the Bode impedance diagram (5.C.1.(a)(B)) for coated samples display a linear slope of about -1 as frequency decreases. This is the characteristic response of a capacitive behaviour (high corrosion resistance) of a compact passive film, observed over nearly the whole measurement frequency range for Ti-N films of all thickness. Similar behaviour was observed for Ti and Ti rich layers by E. Ariza and L.A. Rocha et al. [49]

SEM studies were carried out to determine morphology of coating after typical anodic polarization tests in 1N H<sub>2</sub>SO<sub>4</sub>

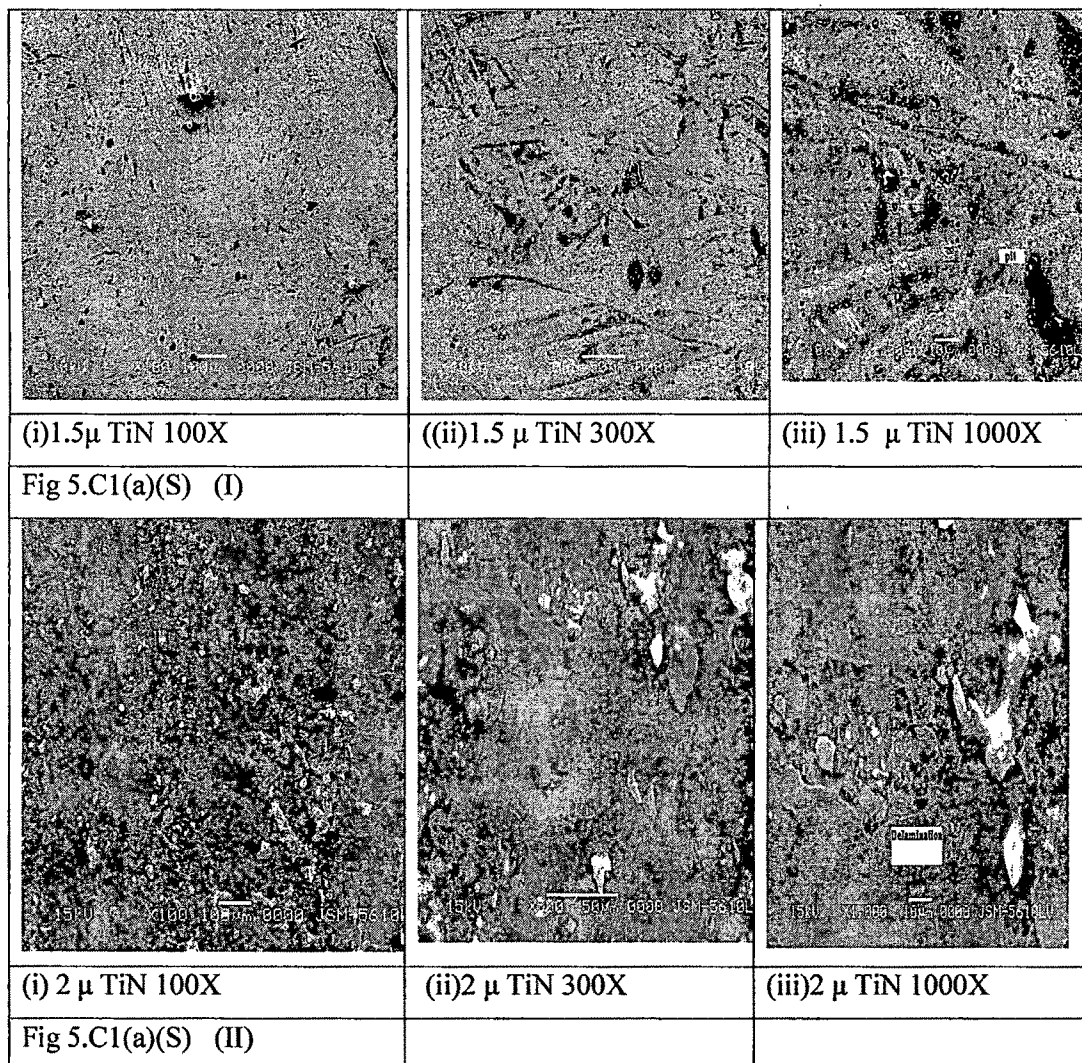


Fig 5.C.1.(a)(S) Typical SEM morphologies of the (I) 1.5 μ Ti-N and (II) 2.0 μ Ti-N coating which had been subjected to the anodic polarization tests 1N H<sub>2</sub>SO<sub>4</sub> solution

As displayed in SEM micrograph of Ti-N (Fig 5.A.1(i)) large number of coarse macroparticles is observed in 1.5 μ Ti-N coating. When 1.5 μ Ti-N coating is subjected to corrosion in 1N H<sub>2</sub>SO<sub>4</sub> solution, as observed in fig 5.C.1. (a)(S)(I) no clear corrosion pit

was found on the surface of the 1.5  $\mu$  Ti-N coating and there were only traces of the macroparticles after they peeled off from the TiN coating. However, from fig. 5.C.1.(a)(S) (II) a large number of quite large corrosion pits in the Ti-N coating of 2  $\mu$  thickness were observed. The decrease of the corrosion resistance of the TiN coating of 2  $\mu$ , compared with the Ti-N coatings of 1.5  $\mu$  may be due to the increased total number of the defects in the Ti-N coating. [2]

As experimented by L.A. Rocha et al [15] TiN Coating of varying nitrogen content were deposited on steel substrate. In their studies they concluded that coating thickness by itself is unable to explain the corrosion behaviour of the films. The graph shown therein reveals that films presenting the noblest behaviour (for 50, 52 and 55 at. % N) was the thinner ones. Therefore, microstructure is likely to play an important role on the definition of the corrosion behaviour of the films.

In 2 $\mu$  Ti-N coating a spherical depressed pits at the center is observed at high magnification for Fig 5.C.1.(a)(S)(II)(iii). The coating has a pinhole and the cracked skin is seen in the surroundings. These pinholes and cracks could provide a direct path for the corrosive medium entering the substrate, leading to total destruction of the coating on the surface. In addition, various tiny pits are also observed on the Ti-N surface. Similar morphology of the corroded TiN coating was observed by V.K. William et al [50] Hong Liang et al observed SEM photomicrograph of the surface morphology of the Ti, Fe, C. film after pitting corrosion. As the Ti, Fe, C. film was not textured; the corrosion rates in different directions are identical. Consequently pits were of circular shape. In this case also for 2 $\mu$  Ti-N circular pit is observed indicating that Ti-N thin film is not textured. Delamination of coatings near the pit was observed [51]

The compositional analysis of coatings after potentiodynamic test was done using EDX attached to SEM.

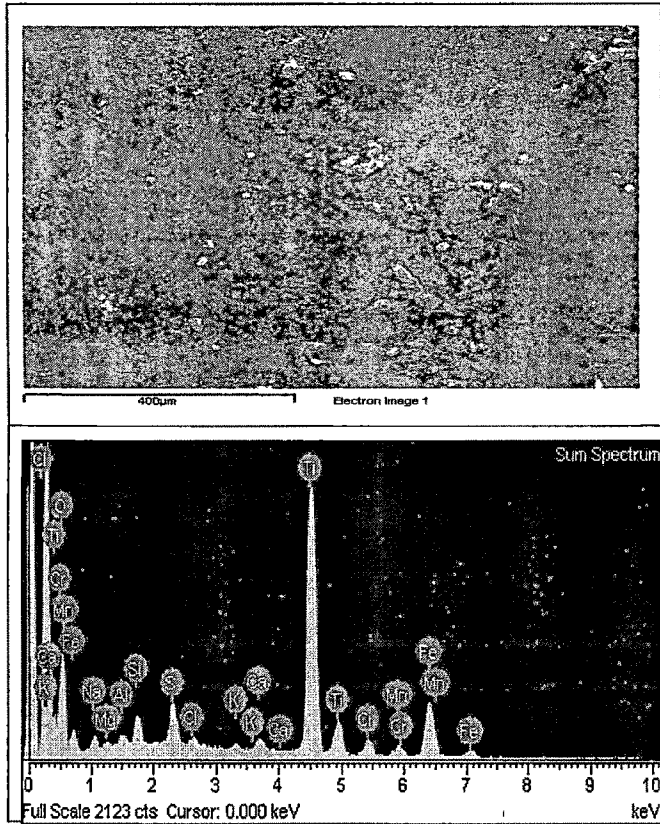


Fig 5.C.1.(a)(E)The EDX analysis of 1.5 $\mu$  Ti-N thin film subjected to potentiodynamic test in 1N H<sub>2</sub>SO<sub>4</sub>

The Fig 5.C.1.(a)(E) indicates the large peak of Ti, and small peaks of Fe, ,Mn. indicating less intense corrosive attack. The coating system shows few very small and shallow pits.

### 5. C.1. (b) Corrosion Behaviour of Ti-N in 3.5%NaCl

The corrosion behaviour of Ti-N coatings of varying thickness was measured by potentiodynamic corrosion tests in 3.5% NaCl solution.

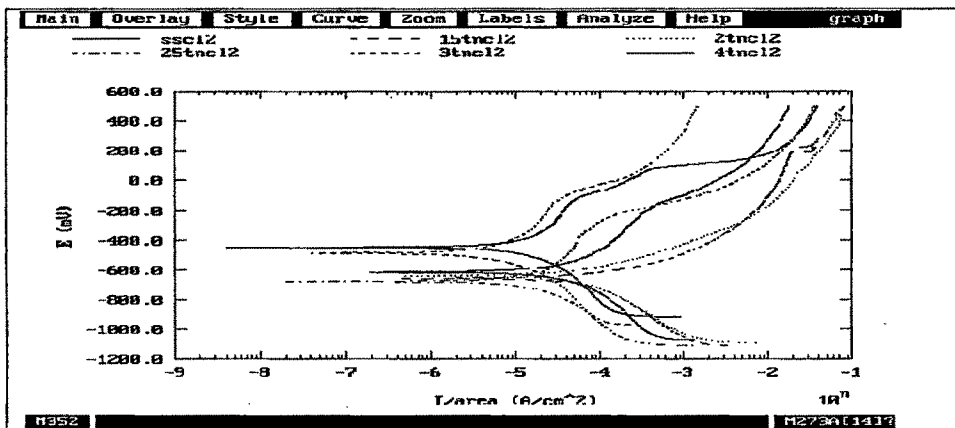


Fig 5.C.1.(b)(P) Potentiodynamic corrosion test of S.S substrate & Ti-N thin films of varying thickness in 3.5%NaCl

3.5%NaCl	$E_{corr}$ (mV)	$I_{corr}$ ( $\mu\text{A}/\text{cm}^2$ )	Protective efficiency, % $P_i$
Substrate S.S	-446.9	101.9	
1.5 $\mu$ TiN	-658.0	94.38	7.37
2.0 $\mu$ TiN	-640.0	56.13	45
2.5 $\mu$ TiN	-677.4	81.22	20.3
3.0 $\mu$ TiN	-487.3	20.35	80
4.0 $\mu$ TiN	-614.6	95.33	6.5

Table C.1.(b) Values of corrosion potential ( $E_{corr}$ ) corrosion current density ( $I_{corr}$ ) and protective efficiency for all Ti-N specimens in 3.5%NaCl

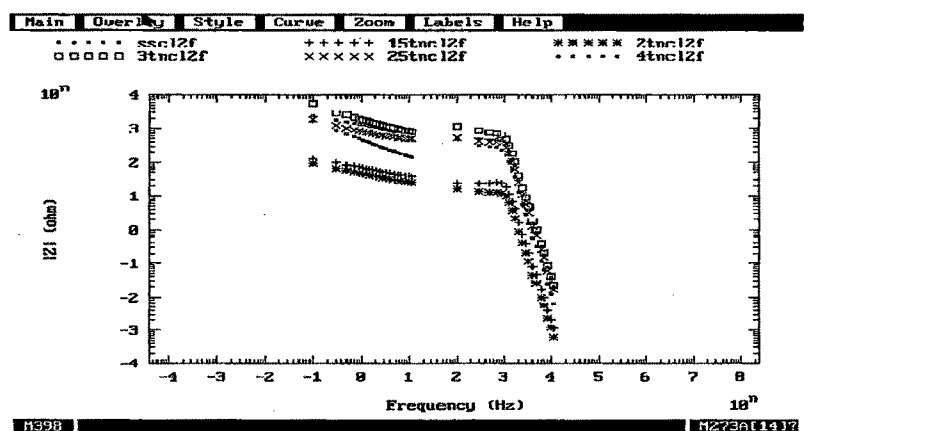


Fig 5.C.1.(b)(B) Electrochemical impedance diagram of Ti-N thin films of varying thickness in 3.5%NaCl

The Tafel plots obtained for steel substrate and Ti-N coating of varying thickness in 3.5%NaCl are shown in Fig 5.C.1.(b)(P) The electrochemical parameters (corrosion current, corrosion potential and % porosity ) calculated from polarization curves are summarized in Table C.1.(b).

The corrosion potential of the steel substrate is about  $-0.449$  V. Large variation in  $E_{\text{corr}}$  of substrate & coatings is observed. The corrosion potential of coated sample is at lower value than  $E_{\text{corr}}$  of the steel without a coating because the thin coating, having a high porosity, causes an electrochemical heterogeneity of the surface contacting the electrolyte. This heterogeneity is the reason for physico-chemical instability of the substrate coating system in an aggressive environment. [52]

The corrosion current density is used as an important parameter to evaluate the kinetics of corrosion reactions. Corrosion protection is normally inversely proportional to the corrosion current density ( $i_0$ ) measured via polarization. In this case, where PVD coatings are chemically not reactive, the corrosion current density indicates pores in the coatings, where the electrochemical reaction of the substrate takes place. Although  $E_{\text{corr}}$  value is high the  $i_{\text{corr}}$  for coatings of all the thickness is lower than substrate.[11] indicating corrosion protection of substrate. Lowest  $i_{\text{corr}}$  and hence highest corrosion resistance was observed in  $3\mu$  Ti-N thin films.

All the coating except  $3.0\mu$  and  $4.0\mu$  Ti-N did not performed better than uncoated samples. Film thickness is an effective barrier against the diffusion of the corrosive environment. As the coatings grow thicker, the chance of having the pinholes that directly connect the atmosphere and the substrate is lowered. [53]As per Fig 5.C1.(b) (P), the  $3\mu$  TiN coating exhibited passivation characteristics at suitable anodic potentials (200mV) and showed the most positive breakdown potential, the widest passive region and the smallest minimum passive current density ( $i_{\text{pass}}$ ). All the coatings showed some passive character at a certain anodic potentials, but the breakdown potential was lower and the minimum passive current density was larger than that of the  $3\mu$  Ti-N coating Although  $E_{\text{corr}}$  of all the coatings is higher, than uncoated sample may be due to large amount of porosity as indicated in table and consequently galvanic corrosion between the stainless steel and TiN coating,  $i_{\text{corr}}$  is always lower than uncoated sample. Similar

behaviour was observed by T. Savisalo et al where they used duplex nitriding-PVD CrN/NbN super lattice coating in 3%NaCl system [54]

The icorr and hence porosity of coating, generally decreases with increase in the thickness but at the same time strains increase, causing the peeling off of the film from the substrate. So, the effectiveness of the corrosion protectiveness by a Ti-N coating is determined by its continuity and its good adhesion to the substrate. The latter depends on the production conditions. [52]

Ti-N coating for all the thickness showed poor corrosion resistance in 3.5%NaCl and the protective properties were completely lost above 200 mV, as indicated by the high current densities recorded and displayed in Fig 5.C.1.(b)(P). Similar behaviour for TiN coating was observed by M. Herranen et al deposited by triode ion plating with high plasma density in a Balzers BAI 640R equipment steel on ASP2030. However, direct comparison cannot be made as film deposition technique, composition, thickness and substrate was different and the testing was done in 0.05 M H<sub>2</sub>SO<sub>4</sub>. [55]

The Figures 5.C.1.(b)(B) show representative electrochemical impedance diagrams obtained in Ti-N thin films of varying thickness in 3.5 % NaCl. As it can be seen,

3 $\mu$  Ti-N has the higher impedance values when compared with the Ti-N of different thickness. At high-frequency the process is related to the coating/ solution interface and represents the dielectric characteristic of the PVD coating, whereas the low-frequency process is associated with the substrate/solution interface and represents the corrosion process with the stainless steel in the pores. At high frequency the impedance value of 1.5 $\mu$  and 2  $\mu$  Ti-N coating is of two orders lower than 3  $\mu$  Ti-N. At the low frequency, the peak height of 1.5 $\mu$  and 2 $\mu$  Ti-N decreases and it is found less than even stainless steel substrate. This is indicative of large number of pores in the coatings and aggressive nature of chloride ion in NaCl solution. [48]

SEM studies were carried out to determine morphology of coating after typical anodic polarization tests 3.5%NaCl

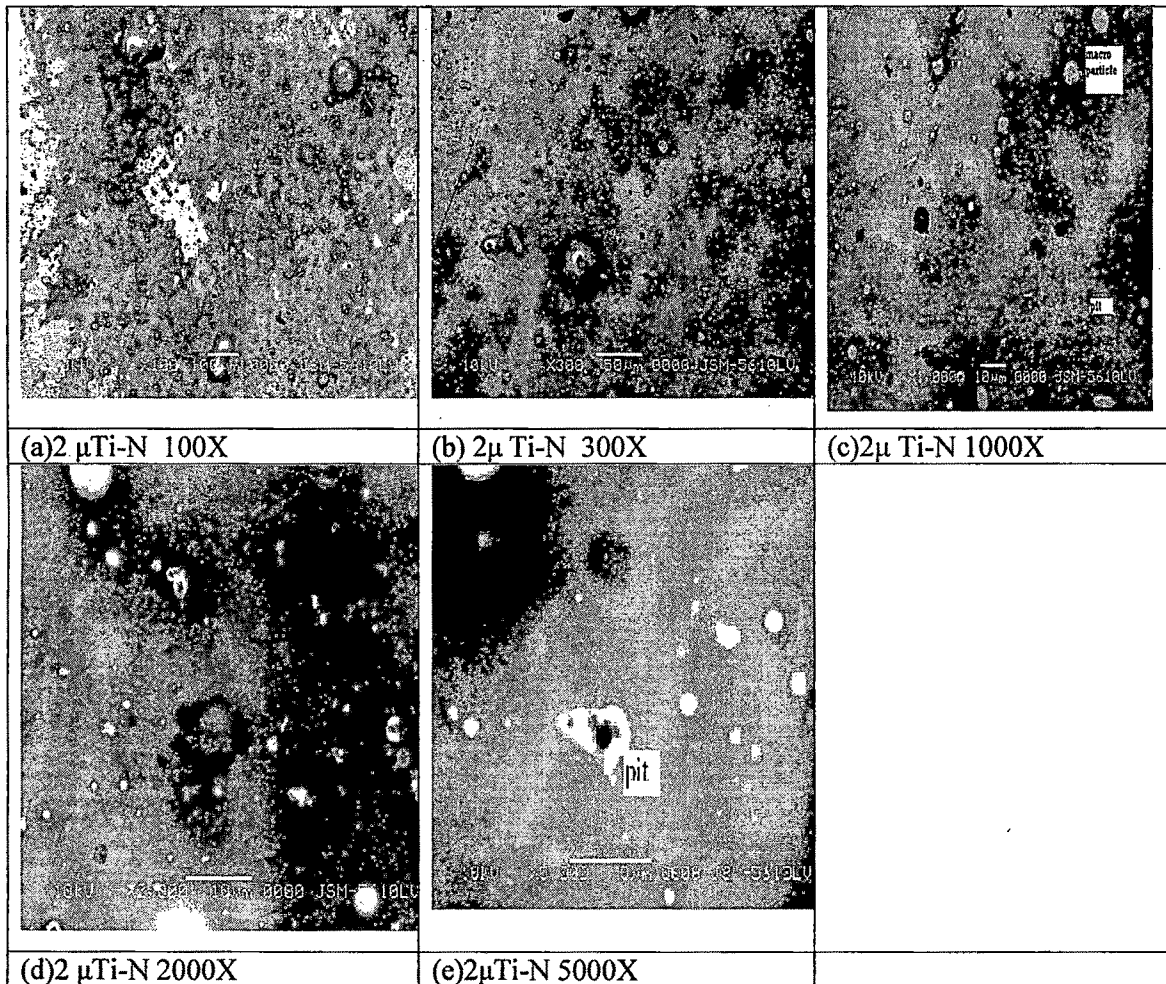


Fig 5.C.1.(b)(S) Typical SEM morphologies of the 2.0 μ TiN coating s which had been subjected to the anodic polarization tests 3.5%NaCl at different magnification.

The SEM micrograph Fig 5.C.1.(b)(S) indicates that the extent of pitting observed in 2μ Ti-N in 3.5%NaCl was low. At low magnification (Fig 5.C.1.(b)(S)(a & b)) it appears as a general uniform corrosion, however at high magnification (Fig 5.C.1.(b)(S)(e)) small pits were observed.

The EDX analysis for carried out for compositional analysis on the surface of coating after potentiodynamic test in 3.5% NaCl .

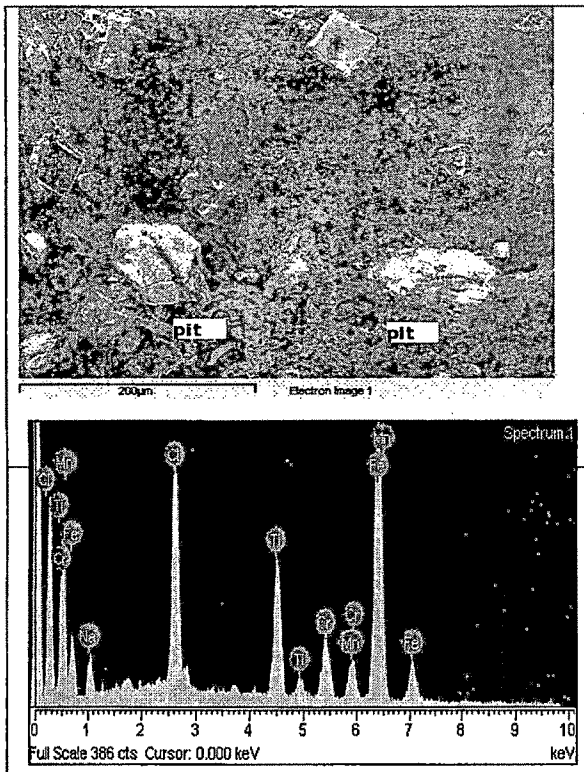


Fig 5.C.1.(b)(E) EDX profile of 2 $\mu$  TiN in 3.5%NaCl

The EDX analysis for carried out for compositional analysis on the surface of coating after potentiodynamic test in 3.5% NaCl. The EDX analysis Fig 5.C.1.(b)(E) indicates the intense peak of Ti and large peaks of Fe, Mn. The coating system shows few very small and shallow pits of other constituents.

Surface images and chemical analysis of 2 $\mu$  Ti-N coated alloys after corrosion tests were given in Fig 5.C.1.(b)(E). When the SEM image was examined, it was seen that the coating layer was broken from the substrate as large pieces, causing removal of the larger pieces. The formation of the coating defects is very much difficult to avoid totally. Consequently, when subjected to a corrosive atmosphere, coated materials will form galvanic cells at the defects near the interface since ceramic coatings are electrochemically more stable than most substrate materials, once aggressive ions such as chloride penetrate the coating through these small channels, driven by capillary forces, the exposed area will begin to experience anodic dissolution, which will usually extend laterally along the interface between the coating and the substrate. Finally the pits formed linked up each other, causing removal of the entire coating by flaking. [56, 66, 67]

### 5. C.1. (c) Corrosion Behaviour of Ti-N in 0.1N HCl

The corrosion behaviour of Ti-N coatings of varying thickness was measured by potentiodynamic corrosion tests in 0.1N HCl solution.

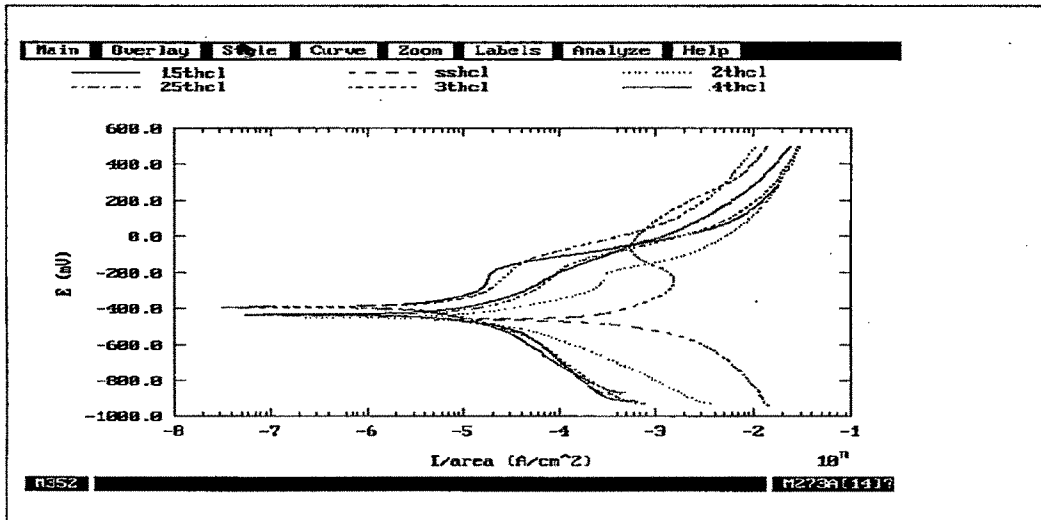


Fig 5.C.1.(c)(P) Potentiodynamic corrosion test of S.S substrate & Ti-N thin films of varying thickness in 0.1NHCl

0.1NHCl	$E_{corr}$ (mV)	$I_{corr}$ ( $\mu\text{A}/\text{cm}^2$ )	Protective efficiency, $P_i$ (%)
S.S	-460.6	1.827 mA/cm <sup>2</sup>	
1.5 $\mu$ TiN	-391.5	17.93	99.01
2.0 $\mu$ TiN	-450.4	27.79	98.48
2.5 $\mu$ TiN	-439.1	29.67	98.38
3.0 $\mu$ TiN	-392.0	18.51	98.99
4.0 $\mu$ TiN	-433.4	19.16	98.96

Table C.1.(c) Values of corrosion potential ( $E_{corr}$ ) corrosion current density ( $I_{corr}$ ) and protective efficiency for all Ti-N specimens in 0.1N HCl.

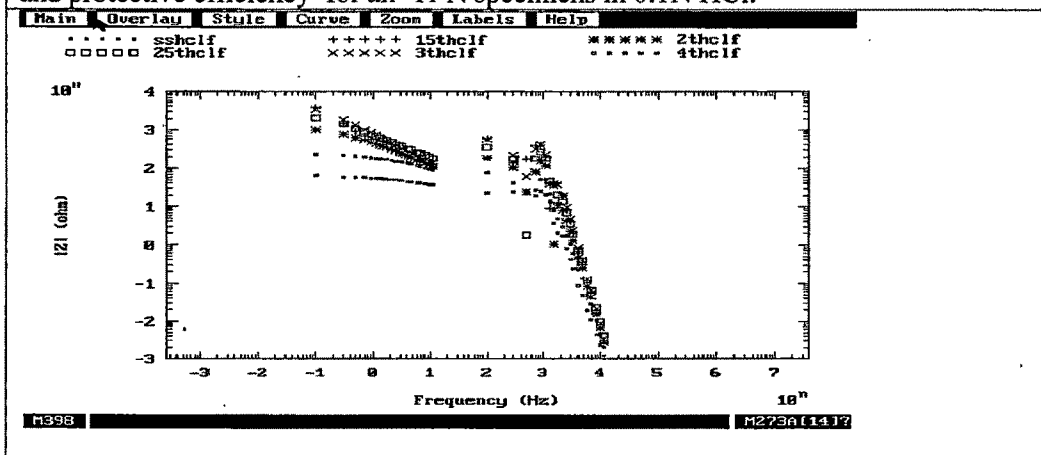


Fig 5.C.1.(b)(B) Electrochemical impedance diagram of Ti-N thin films of varying thickness.

The Tafel plots obtained for steel substrate, and Ti-N coating of varying thickness in 0.1N HCl are shown in Fig 5.C.1.(c)(P). The electrochemical parameters (corrosion current, corrosion potential and % porosity) calculated from polarization curves are summarized in Table C.1.(c)

The corrosion potential of the steel substrate is about  $-0.460$  V. The comparison between the corrosion potential  $E_{corr}$  for coated and uncoated steel (Table C.1.(c)) revealed that with coated steel, the corrosion potential is nobler than the uncoated steel. This means that the Ti-N coatings shifts the corrosion potential to more positive potential values and consequently protects 316 SS from corrosion to a different extent. In acid solution, rapid corrosion of steel coated with Ti-N takes place at pores and pinholes in the coating substrate are easily passivated. [55]

As already mentioned, the lower the  $i_{corr}$ , the lower corrosion rate the sample is. In Fig 5.C.1.(c)(P), all the coated samples, the  $i_{corr}$  is two or three orders of magnitude lower than that of the substrate, revealing an improved corrosion resistance of the film. From the corresponding curve, the anodic current density for  $2 \mu$  Ti-N and  $4 \mu$  Ti-N changes a little with potential increasing from  $-200$  mV to the breakthrough potential  $+150$  mV. In this interval, the passive layer protects specimen surface from dissolving. While, anodic current density increases dramatically with potential over  $200$  mV, probably due to a pitting corrosion mechanism initiated at the local defects of the film.[43]The formation of pit can be further confirmed by considering the curve in cathodic region. In cathodic polarization one can see that the coated samples starts at a current lower than the stainless steel, but near the corrosion potential the coated sample current increases until it becomes almost equal to that of stainless steel . This phenomenon can be explained by pitting of the coatings at defect sites. [57]

In the anodic region the current density of all the coatings is higher than the substrate. The corrosion current density is often used as an important parameter to evaluate the kinetics of corrosion reactions. Corrosion protection is normally inversely proportional to the corrosion current density ( $i_o$ ) measured via polarization.[47] In this case, where PVD coatings are chemically not reactive, the corrosion current density indicates pores in the coatings, where the electrochemical reaction of the substrate takes place. Although

icorr value is low, the current in anodic region for all the thickness is higher than Stainless steel.( Fig 5.C.1.(c)(P))

Corrosion behavior under open-circuit condition was investigated in more detail using EIS. Technique Two relaxation processes are associated with the EIS response: the high-frequency relaxation process is related to the coating/ solution interface and represents the dielectric characteristic of the PVD coating, whereas the low-frequency process is associated with the substrate/solution interface and represents the corrosion process with the stainless -steel in the pores. In Fig 5.C.1.(b)(B) high impedance at high frequency of all the coatings indicates that the capacitive property of film is good, however in the lower frequency range the disturbance is observed in impedance value this may be due to the fact that the coating may not be able to resist the penetration of chloride ion through pores till the substrate.[47]In frequency range of 1 Hz to 0.1Hz the difference in impedance value of 3  $\mu$  Ti-N and uncoated substrate is of two order of magnitude. The sequence of corrosion resistance is in agreement with that obtained from Potentiodynamic polarization measurements.

Compositional analysis of the surface after potentiodynamic test was investigated using EDX attached to SEM

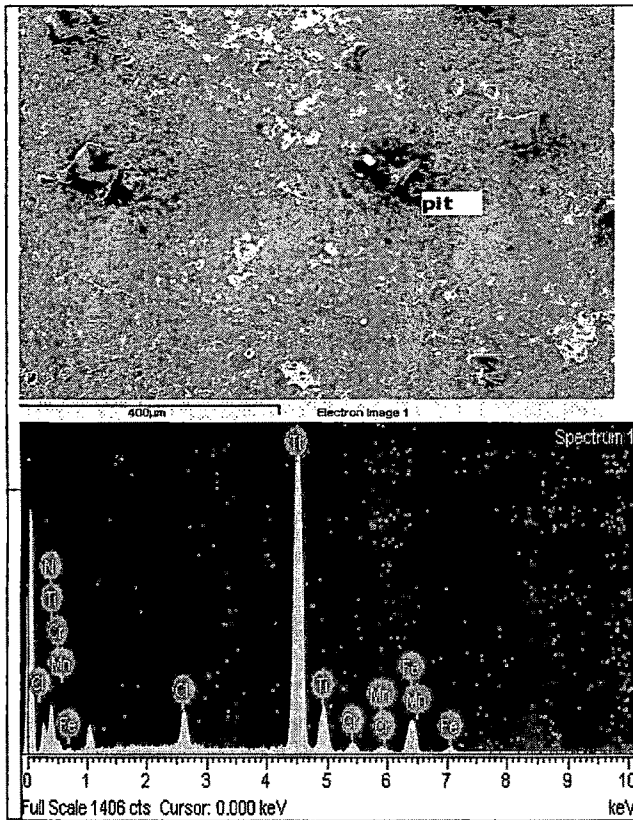


Fig 5.C.1.(c)(E)The EDX analysis of 2 $\mu$  Ti-N thin film subjected to potentiodynamic test in 0.1 N HCl .

The EDX analysis Fig 5.C.1.(c) (E) indicates large number of corrosion pits in the 2 $\mu$  Ti-N coating was observed. Although intense peak of Ti is observed, localized attack as pitting might have occurred. This indicates that the 2  $\mu$  Ti-N coating of is too thin to inhibit the aggressive action of corrosion media with the presence of physical defects running through the Ti-N coating

### 5. C 1 (d) Corrosion Behaviour of Ti-N in 11pH Na<sub>2</sub>SO<sub>4</sub>

The corrosion behaviour of Ti-N coatings of varying thickness was measured by potentiodynamic corrosion tests in 11pH Na<sub>2</sub>SO<sub>4</sub> solution.

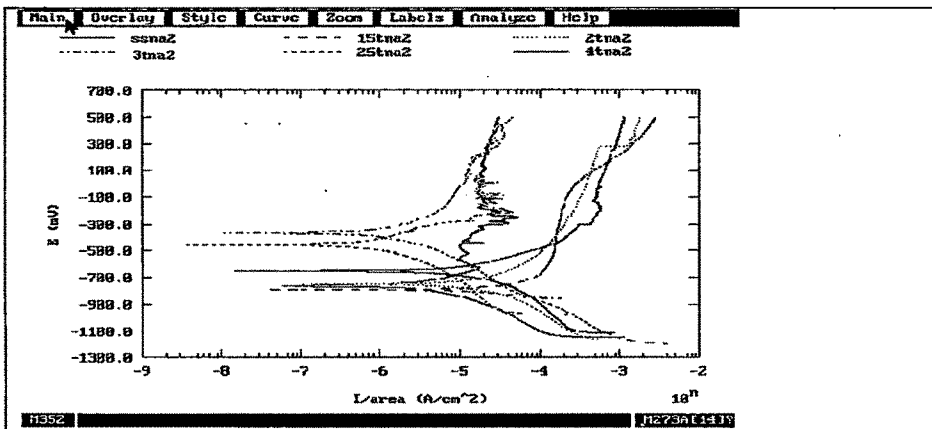


Fig 5.C.1. (d)(P) Potentiodynamic corrosion test of S.S substrate & Ti-N thin films of varying thickness in 11pH Na<sub>2</sub>SO<sub>4</sub>

11pH Na <sub>2</sub> SO <sub>4</sub>	E <sub>corr</sub> (mV)	I <sub>corr</sub> (μA/cm <sup>2</sup> )	Protective efficiency, P <sub>i</sub> (%)
S.S	-725.6	30.99	
1.5μ TiN	-791.4	34.97	
2.0μ TiN	-750.8	41.05	
2.5μ TiN	-484.9	11.12	64.11
3.0μ TiN	-367.5	2.536	91.81
4.0 μ TiN	-694.4	13.19	57.43

Table C.1.(d) Values of corrosion potential (E<sub>corr</sub>) corrosion current density (I<sub>corr</sub>) and protective efficiency for all Ti-N specimens. 11pH Na<sub>2</sub>SO<sub>4</sub>

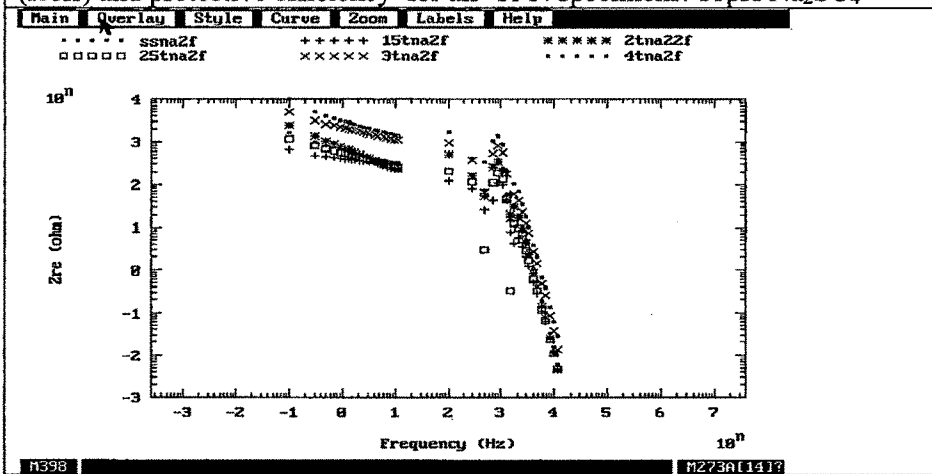


Fig 5.C.1.(d)(B) Electrochemical impedance diagram of Ti-N thin films of varying thickness. 11pH Na<sub>2</sub>SO<sub>4</sub>

The Tafel plots obtained for steel substrate and Ti-N coating of varying thickness in 11pH Na<sub>2</sub>SO<sub>4</sub> are shown in Fig 5.C.1.(d)(P). The electrochemical parameters (corrosion current, corrosion potential and % porosity) calculated from polarization curves are summarized in Table C.1. (d).

The corrosion potential of the steel substrate is about -0.725 V. The comparison between the corrosion potential  $E_{corr}$  for coated and uncoated steel (Table C 1 (d)) revealed that with 2.5 $\mu$  Ti-N, 3  $\mu$  Ti-N and 4  $\mu$  Ti-N coated steel, the corrosion potential is nobler than the uncoated steel . This means that the Ti-N coatings shifts the corrosion potential to more positive potential values and consequently protects 316 SS from corrosion to a different extent where as  $E_{corr}$  for 1.5  $\mu$  Ti-N and 2  $\mu$  Ti-N is slightly higher than substrate, correspondingly  $i_{corr}$  is also higher than S.S. this may be because of strong increase in through pin hole defect density for thin coatings.

As the film grows thicker, there is a lesser likelihood for the film to have pinholes interconnecting with one another from the top surface to the bottom surface adjacent to the underlying metal that needs protection. As a result, the corroding medium would encounter more resistance during its penetration or diffusion through the film to the metal substrate. [44,45,49,53,58]The 2.5,3.0 and 4.0 $\mu$  Ti-N coatings exhibit passive like behaviour i.e. less increase in current with increase in potential. Oscillations are observed for 4 $\mu$  Ti-N in -700mV to +100mV indicating region of incomplete passivity. [2]

According to Bode's plot, Fig 5.C.1.(b)(B) the difference in impedance value of all the coatings at high frequency is less and at low frequency the difference is of one order magnitude. Discontinuity is observed in middle frequency range indicating pore resistance of film to the penetration of sulphate ions in alkaline environment is poor.

Compositional analysis of the surface after corrosion was investigated using EDX attached to SEM

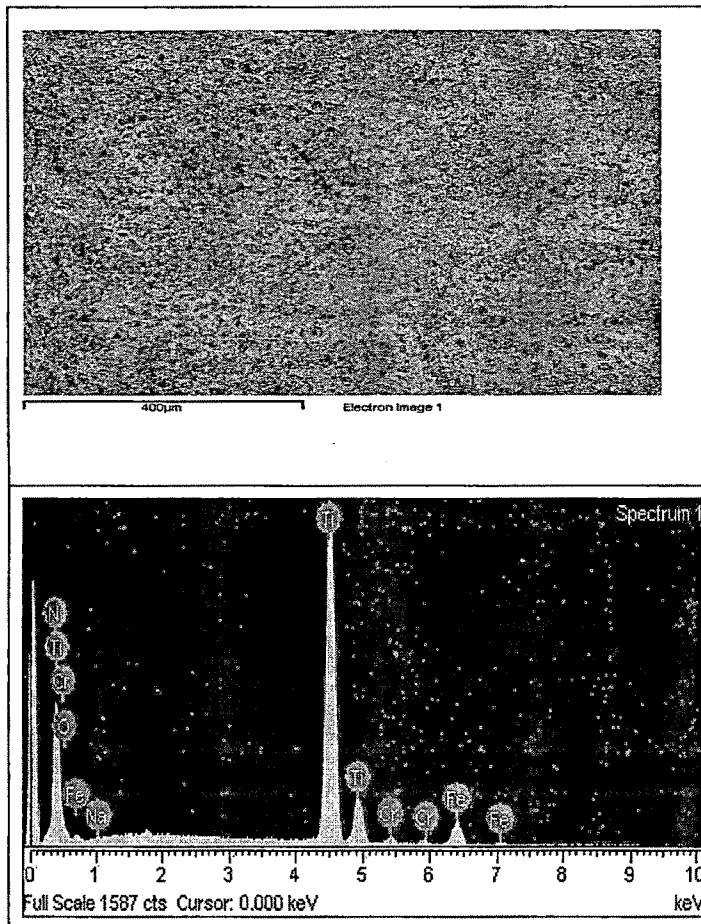


Fig 5. C 1(d) (E) The EDX analysis of 2 $\mu$  Ti-N thin film subjected to potentiodynamic test in 11pH Na<sub>2</sub>SO<sub>4</sub>

The Fig 5.C.1.(d)(E) indicates intense peak of Ti and Nitrogen and very small peak of Fe, Mn indicating that coating is intact.

#### **General discussion on Behaviour of Ti-N thin Film in different Environment**

The main limitation of ceramic coatings (deposited by Cathode arc evaporation technique) for improving the corrosion resistance of stainless steel is the presence of structural defects in the films. These defects permit the electrolyte to reach the substrate, accelerating the corrosion rate. Imperfections in the coatings and imperfections in the substrate surface can both generate these defects [57]

The formation of pinholes in PVD coated thin films is nearly impossible to avoid. This is due to the fact that the coated surfaces are always non-uniform and because the coating tends to start to grow in a non-uniform manner. Various growth models have been developed to describe the growth process. A general feature of these is that, after the original nucleation stage, the growth takes place in isolated islands which then grow together, after leaving voids between them. The general growth morphology of the coatings is typically columnar. Although various techniques can be used to minimize the number of pinholes, they cannot usually be totally eliminated. They occur commonly in all kinds of coatings and on all kinds of substrates [40]

Transition metal nitrides are inert to the chemical attacks. However, the PVD coatings contain cracks, pinholes and pores, which allow the corrosive media to enter the substrate, thus degrading the corrosion behavior of the coating/substrate System [46]. In spite of their excellent mechanical and tribological properties, their corrosion resistance has always been conditioned by the presence of structural defects such as pores, pinholes and cracks that appear during application. [58, 59]

The effect of the TiN porosity varies in the different solutions and depends on the electrochemical behaviour of the substrate in those solutions [60]

As mentioned by W Precht et al with the percentage increase in porosity, the corrosion protection decreased. [50,61] K. A Pischow et al mentioned that the corrosion performance of PVD TiN coatings is strongly affected by porosity, which can cause local and rapid corrosion of the base metal. Aromaa et al have used corrosion current to calculate porosity during investigations of three commercial TiN coating but concluded that it seems to be difficult to find any simple correlation between porosity and corrosion behaviour. [62]

As suggested by Guosong Wu et al for electron beam deposited metal oxide TiO<sub>2</sub> or Al<sub>2</sub>O<sub>3</sub> thin films on AZ31 magnesium alloy, porosity in their calculation was higher than the expected value. In fact, small structural defects e.g. pinholes, pores, or cracks, are inevitable in coatings. Every defect allows corrosion medium to contact substrate surface and leads to formation of a galvanic cell and pitting corrosion starts. With increasing time the domain of defects will be enlarged and the quantity will be also increased. Due to the high chemical reactivity of magnesium, the speed of galvanic reaction in the defect is

especially high. In order to eliminate the influence of the factor as above, Konyashin suggested that the high scan rate should be chosen and used the rate of 20 mV /sec in their experiment. [63] Compared with their study, the rate used in this study is much lower. Therefore, the data calculated by the formula used does not exactly represent the porosity of the initial surface. Thus the effect of the scan rate on the porosity measurement of TiN thin films is to be considered.

Hard coatings like TiN normally contain a high degree of internal (usually compressive in-plane) stress owing to lattice distortion and thermal mismatch effects; it is, therefore, difficult to produce single-layer TiN coatings thicker than 6–7  $\mu$ , without encountering adhesion problems on typical substrate materials employed. [21]

Since hydrogen evolution takes place during scan at iron surface in pores the coating substrate adhesion plays important role in potentiodynamic test.[69].In present investigation the XRD results indicates the presence of Ti<sub>2</sub>N instead of TiN for all the thickness of coating. As stated by C. Quaezhaegens et al due to the remarkably lower stresses present in Ti<sub>2</sub>N coatings, they can be deposited with thicknesses up to tens of micrometers. [18]

As stated by Ellina Lunarska et al [64], it could be concluded that chloride ions are more aggressive than sulfate ions for stainless steel. It can be said that the presence of chloride ions in the solution affects the passivity of stainless steel substrate more negatively than that of sulfate ions

The general shape of the potentiodynamic curves in the presence of Cl<sup>-</sup> ions (3.5%NaCl & 0.1N HCl) is characterized for localized corrosion and breakdown of passivity. It is well known that Cl<sup>-</sup> ions are aggressive enough to attack steel and initiate pitting. The passivity domains became shorter in acidic solution in comparison with that in sulphate solution .The effect of chloride ion is more aggressive in HCl compared to NaCl as the bonding in HCl is ionic and hence even when small potential is applied, its dissociation occurs whereas that in case of NaCl bonding is covalent resulting in better stability. However evolution of hydrogen decreases the in homogeneity in the corrosion behaviour depicted by difference in E<sub>corr</sub> values of coating and substrate in 3.5% NaCl,

11pH Na<sub>2</sub>SO<sub>4</sub> and 0.1N HCl and 1N H<sub>2</sub>SO<sub>4</sub> .[44]

### 5. C.1.P Potentiodynamic behaviour of Ti-N thin film in various environment

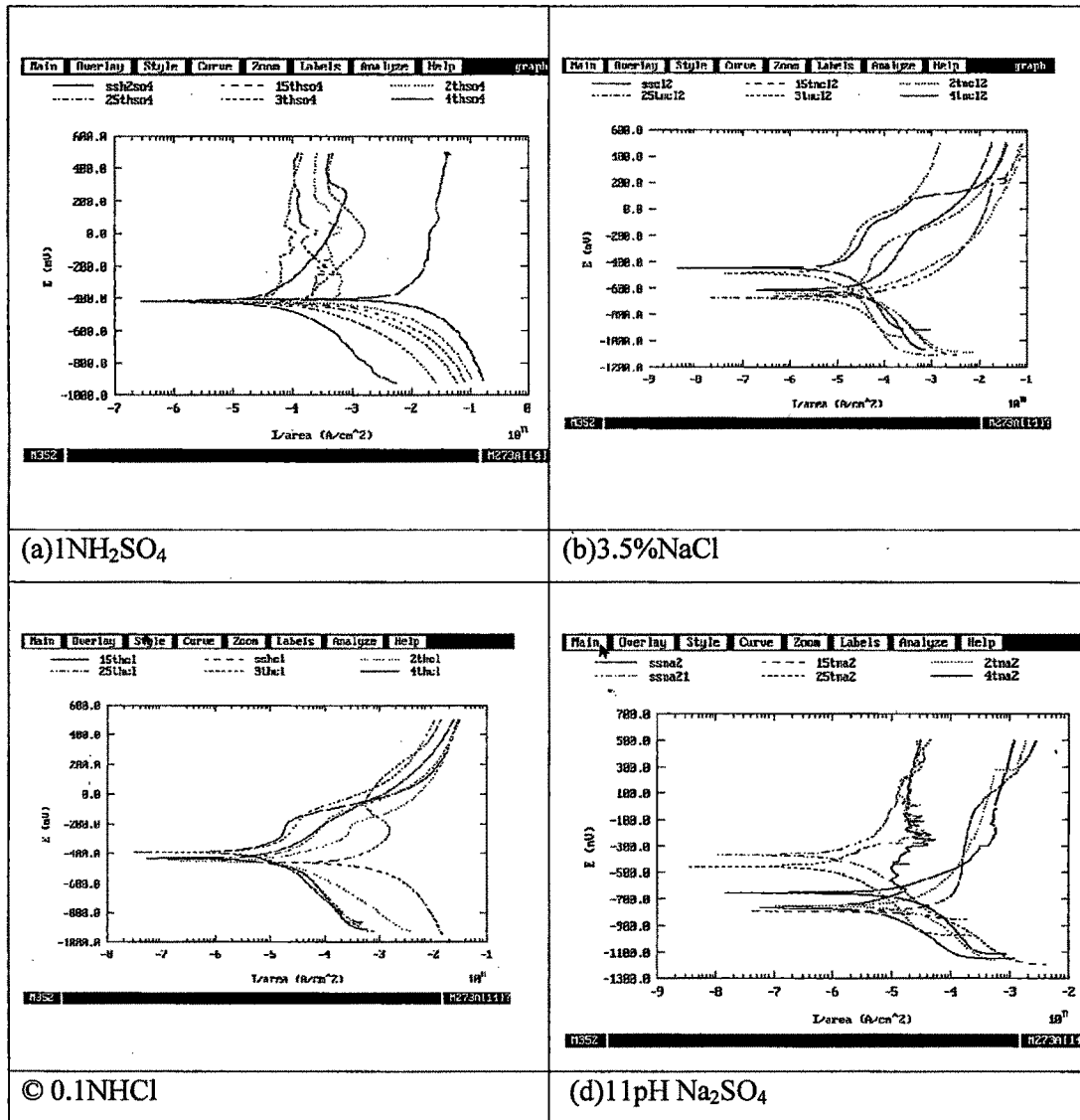


Fig 5.C.1.P (a,b,c,d) potentiodynamic Corrosion behaviour of Ti-N thin film in various environment.

As indicated in diagram 5.C.1.P (a,b,c,d), good corrosion protection is observed in case of sulphate containing ions than chloride ions. The current value in anodic region for all the thickness is higher in 0.1N HCl than 3.5% NaCl. Potentiodynamic curve indicates that chances of pitting corrosion is more in 0.1N HCl than 3.5% NaCl solution.

### 5.C.1.B Electrochemical impedance behavior of Ti-N thin films in various environment

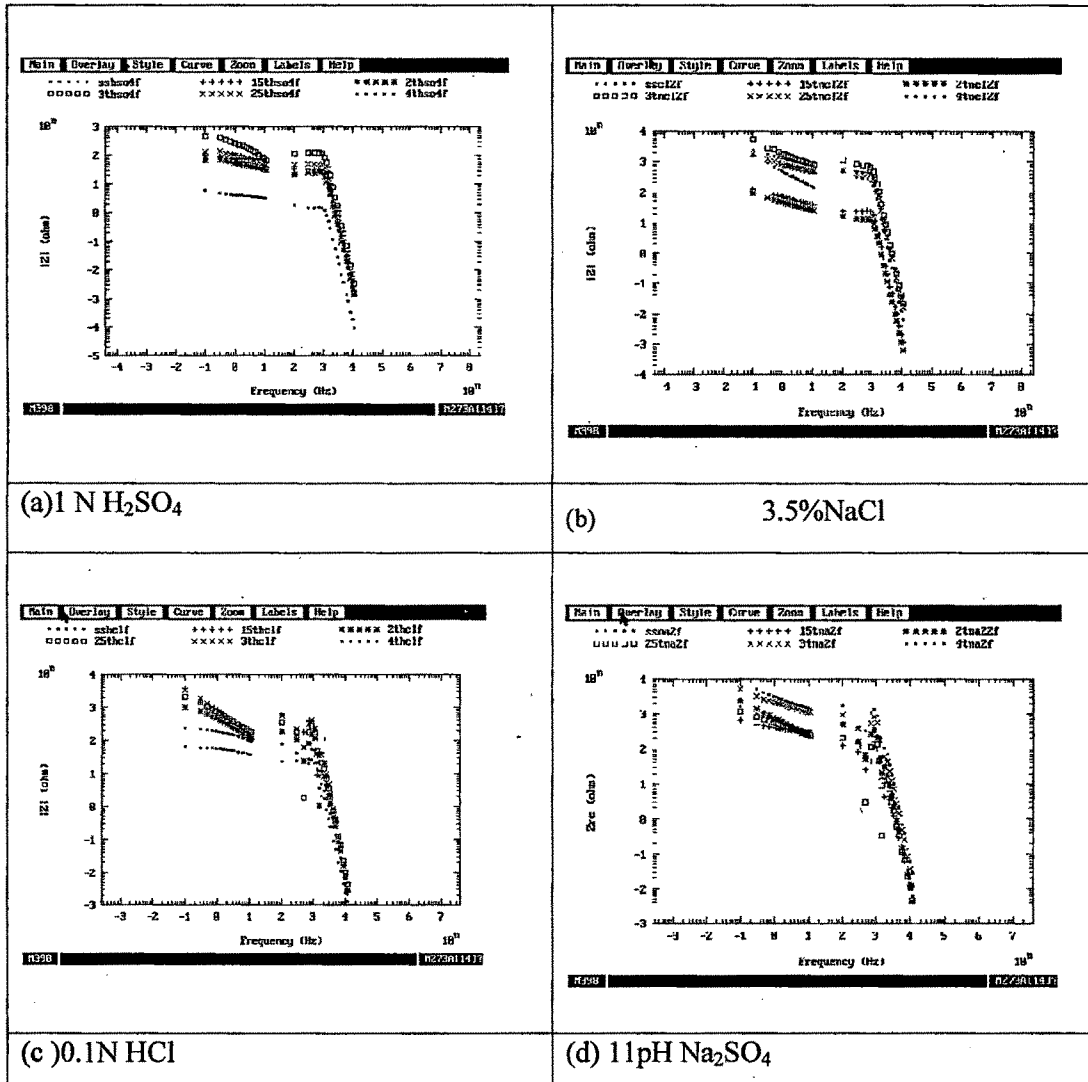


Fig 5. C.1.B (a,b,c,d) Impedence behaviour of Ti-N thin film in various environment

The impedance diagram indicates that in case of 0.1N HCl disturbance is observed in impedance Vs frequency curve Fig 5. C.1.B (c) indicative of pitting corrosion, where as in case of 11pH  $Na_2SO_4$  it may be due to incomplete passivity of coating Fig 5. C.1.B(d). At high frequency difference in impedance is less for Fig 5. C.1.B (c) (0.1N HCl) and Fig 5. C.1.B (d) (11pH  $Na_2SO_4$ ) indicating similar capacitive response of all thickness.

## 5. C.2 CORROSION BEHAVIOUR OF ZrN IN VARIOUS ENVIORNMENT

### 5. C 2 (a) Corrosion Behaviour of ZrN in 1NH<sub>2</sub>SO<sub>4</sub>

The corrosion behaviour of ZrN coatings of varying thickness was measured by potentiodynamic corrosion tests in 1N H<sub>2</sub>SO<sub>4</sub> solution.

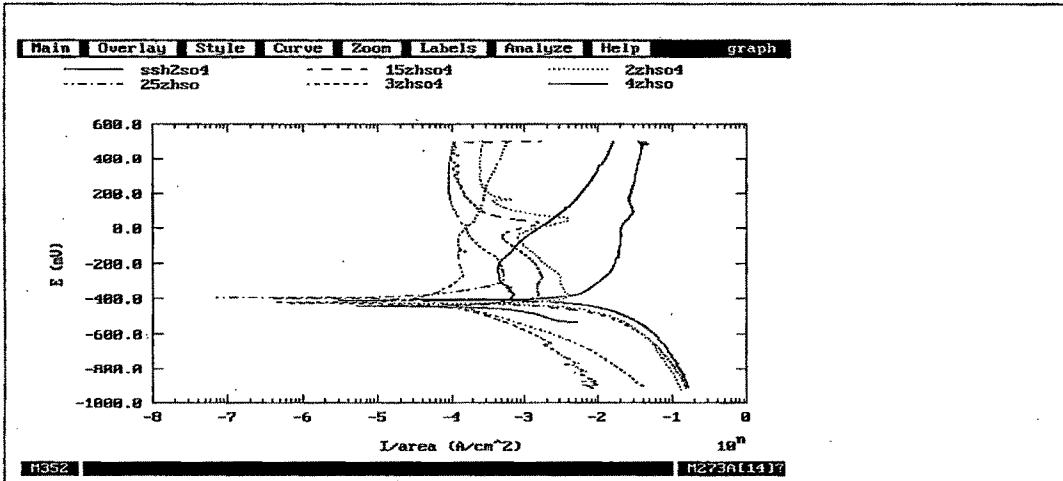


Fig 5.C.2.(a)(P) Potentiodynamic corrosion test of S.S substrate & ZrN thin films of varying thickness 1N H<sub>2</sub>SO<sub>4</sub> solution

1N H <sub>2</sub> SO <sub>4</sub>	E <sub>corr</sub> (mV)	I <sub>corr</sub> (μA/cm <sup>2</sup> )	Protective efficiency, P <sub>i</sub> (%)
S.S	-408	31.05 mA/cm <sup>2</sup>	
1.5 μ ZrN	-427.4	3.768 mA/cm <sup>2</sup>	88%
2.0 μ ZrN	-429.0	68.23 mA/cm <sup>2</sup>	
2.5 μ ZrN	-396.0	52.84	99.82
3.0 μ ZrN	-422.1	145.1	99.54
4.0 μ ZrN	-442.1	1.767 mA/cm <sup>2</sup>	94.4

Table C.2.(a) Values of corrosion potential (E<sub>corr</sub>) corrosion current density (I<sub>corr</sub>) and protective efficiency for all ZrN specimens. 1N H<sub>2</sub>SO<sub>4</sub> solution

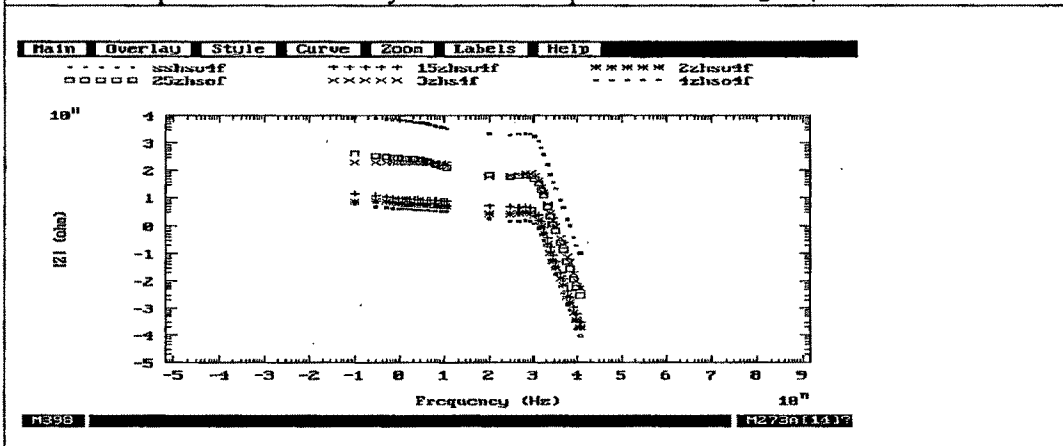


Fig 5.C.2.(a)(B) Electrochemical impedance diagram of ZrN thin films of varying thickness 1N H<sub>2</sub>SO<sub>4</sub> solution

The Tafel plots obtained for steel substrate, and ZrN coating of varying thickness in 1N H<sub>2</sub>SO<sub>4</sub> are shown in Fig 5.C.2.(a)(P) . The electrochemical parameters (corrosion current and corrosion potential and % porosity) calculated from polarization curves are summarized in Table C.2.(a).

The corrosion potential of the steel substrate is about  $-0.408$  V. Each sample's open circuit potential is approximately in the same position. The corrosion potentials ( $E_{corr}$ ) of the coated specimens are only slightly away from that of stainless steel, within 25 mV, which indicates that the corrosion of the ZrN coated-specimens are mainly from the dissolution of the metal substrate and not from the ZrN film. Since corrosion potential is a thermodynamic property of the substrate material the variation of  $E_{corr}$  is not supposed to be far away from that of bare steel. [41, 42]

The corrosion current density ( $i_{corr}$ ) is an important parameter to evaluate the kinetics of corrosion reactions, normally proportional to the corrosion current density measured via polarization. The lower the  $i_{corr}$ , the lower corrosion rate the sample is. In the present test the  $i_{corr}$  value obtained is always less than bare Stainless steel substrate [43]except for 2 $\mu$  ZrN may be due to high internal stresses within the coating.

The Bode plot Fig 5.C.2.(a)(B) for the coated alloy before defect formation has three distinguishable time-dependent processes. The time constant at high frequencies is related to the capacitive response of the film. The resistive plateau at  $10^2$ – $10^3$ Hz represents the pore resistance of film. The relaxation process at about 1–10 Hz is attributed to the capacitance of the intermediate oxide layer present at the metal/coating interface. The resistance of interlayer, which is situated at lower frequencies, is very important from the corrosion protection standpoint, since it is the last barrier for the corrosive species before reaching the metal surface. The third time constant is weakly defined at lowest frequencies and is related to the corrosion activity. The difference in impedance of two orders is observed in case of uncoated and 4  $\mu$  ZrN thin film at high frequency and at low frequency indicating good capacitive and resistive property of films. [48]

A higher impedance values when compared uncoated sample is evidence of superior corrosion resistance. A fast drop of impedance at low and high frequencies is observed in 2.5  $\mu$  ZrN compared to 4  $\mu$  ZrN and 2.5  $\mu$  ZrN and 1.5  $\mu$  ZrN indicating decrease in protective properties of coating with decrease in thickness. [53]

In the low and middle frequency ranges, the Bode impedance diagram Fig 5.C.2.(a)(B) for coated samples display a linear slope of about -1 as frequency decreases. This is the characteristic response of a capacitive behaviour (high corrosion resistance) of a compact passive film, observed over nearly the whole measurement frequency range for ZrN. Similar behavior was observed for Ti and Ti rich layers by E. Ariza et al [48]

As indicated in Fig 5.C.2.(a)(P), 4 $\mu$  ZrN coating did not exhibit the best corrosion resistance although it had largest impedance shown in Fig 5.C.2.(a)(B). According to the phenomenon in the experiment, it can be explained that the coating was severely attacked under the increasing potential. Similar behavior was observed by Guosong Wu et al [63] for electron beam evaporation upper metal oxide thin films on AZ31 magnesium alloy with TiO<sub>2</sub> or Al<sub>2</sub>O<sub>3</sub> as donors.

The compositional analysis of coatings after potentiodynamic test was done using EDX attached to SEM.

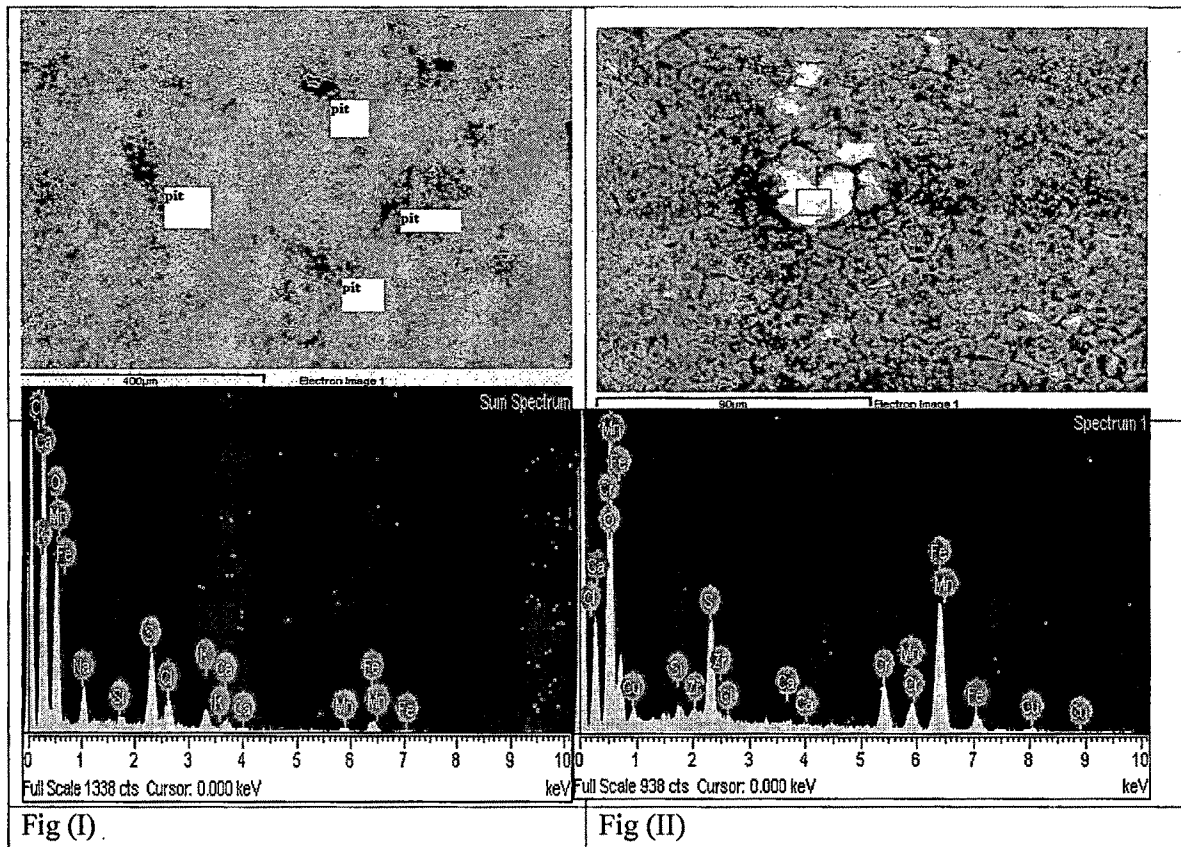


Fig 5.C.2.(a)(E)The EDX analysis of 2µ ZrN (I) corroded sample and (II)small region in corroded sample in 1N H<sub>2</sub>SO<sub>4</sub>

The SEM and EDX analysis Fig 5.C.2.(a)(E) (I) shows large number of corrosion pits in the 2µ ZrN coating This indicates that the 2µ ZrN coating is too thin to inhibit the aggressive action of corrosion media with the presence of physical defects running through the coating. The intense and small peaks of Fe and Mn are observed.

As seen in SEM micrograph in Fig 5.C.2.(a)(E) (II) after potentiodynamic test some micro-cracks were formed and complete removal of coating in certain region have occurred. PVD coatings are always under the compressive residual stress. The thermal expansion coefficient of ZrN is  $7.24 \times 10^{-6}$  while that for S.S is  $10.4 \times 10^{-6}$ . This difference in thermal expansion might give rise to compressive stresses in the films when samples are cooled down after deposition. Under the synergetic effect of compressive residual stresses and thermal stresses cracks are formed on 2µ ZrN coating when subjected to potentiodynamic test. Hovsepien et al. notified that the deposition of PVD coatings nearly

always results in generating compressive stress state in the coatings and stress-corrosion cracking will be promoted in an aggressive environment, resulting in severe corrosion failure. As indicated in XRD diagram 5.B.2.(i) (b) for 2 $\mu$  ZrN coexistence of both ZrN(111) and ZrN(200) contribute to high macro stress within the coating, .The present potentiodynamic test supports the above result.[60,65]

### 5. C.2 (b) Corrosion Behaviour of ZrN in 3.5%NaCl

The corrosion behaviour of ZrN coatings of varying thickness was measured by potentiodynamic corrosion tests in 3.5%NaCl solution.

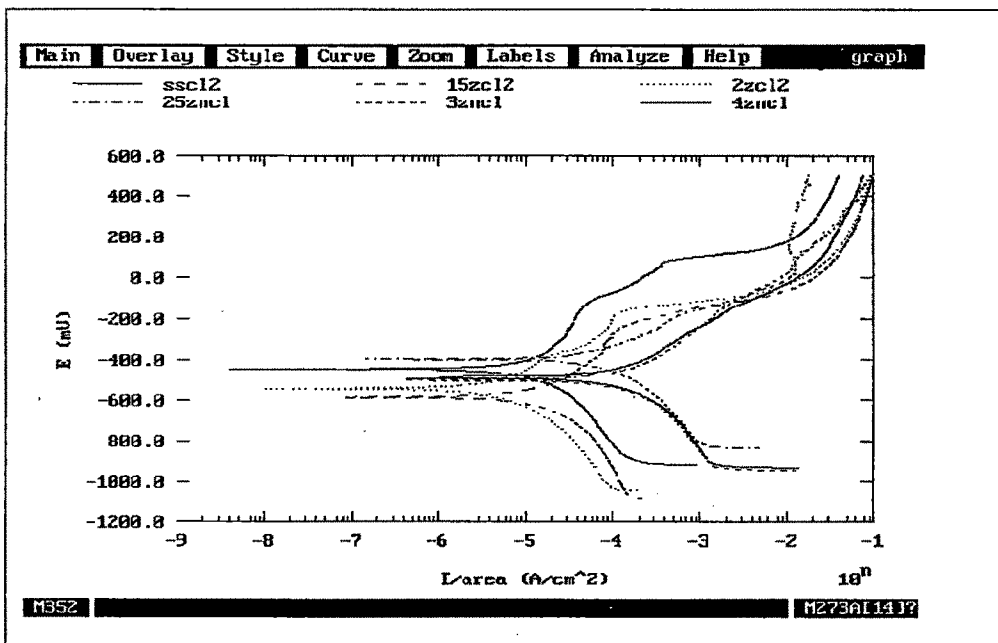
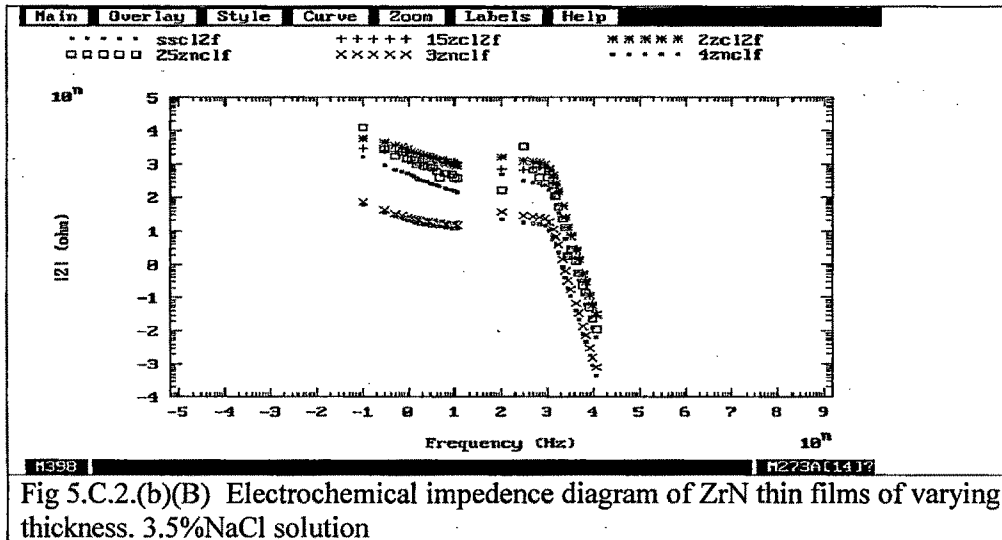


Fig 5.C.2.(b)(P) Potentiodynamic corrosion test of S.S substrate &ZrN thin films of varying thickness 3.5%NaCl solution

3.5%NaCl	$E_{corr}$ (mV)	$I_{corr}$ ( $\mu$ A/cm <sup>2</sup> )	Protective efficiency, $P_i$ (%)
S.S	-446.9	101.9	
1.5 $\mu$ ZrN	-585.9	50.27	51.8
2.0 $\mu$ ZrN	-545.6	6.366	93.75
2.5 $\mu$ ZrN	-397.8	97.21	5.00
3.0 $\mu$ ZrN	-502.8	158.9	
4.0 $\mu$ ZrN	-492.3	67.73	33.6

Table C.2. (b) Values of corrosion potential ( $E_{corr}$ ) corrosion current density ( $I_{corr}$ ) and protective efficiency for all ZrN specimens. 3.5%NaCl solution



The Tafel plots obtained for steel substrate, and ZrN coating of varying thickness in 3.5%NaCl are shown in Fig 5.C.2.(b)(P). The electrochemical parameters (corrosion current, corrosion potential and % porosity) calculated from polarization curves are summarized in Table C.2. (b)

The corrosion potential of the steel substrate is about  $-0.446\text{V}$ . The corrosion potential of coated samples has a lower value than  $E_{\text{corr}}$  of the steel without a coating because the thin coating, having a high porosity, causes an electrochemical heterogeneity of the surface contacting the electrolyte. This heterogeneity is the reason for a physico-chemical instability of the substrate coating system in an aggressive environment. [52]

The corrosion current density ( $i_{\text{corr}}$ ) is an important parameter to evaluate the kinetics of corrosion reactions, normally proportional to the corrosion current density measured via polarization. The lower the  $i_{\text{corr}}$ , the lower corrosion rate the sample is. In the present test the  $i_{\text{corr}}$  value obtained is less than bare Stainless steel substrate. The  $i_{\text{corr}}$  values of all the coatings in the anodic region are higher than stainless steel except  $2\ \mu\text{m}$  ZrN is lower than stainless steel indicating protection of substrate. [43]

As observed in Polarisation curve, in cathodic polarization region the coated samples starts at a current lower than the stainless steel, but near the corrosion potential the coated sample current increases until it becomes almost equal to that of stainless steel. This phenomenon can be explained by pitting of the coatings at defect sites. [57]

As indicated in Bode's plot fig 5.C.2.(b)(B) the difference in the impedance of 3 $\mu$  ZrN and 2 $\mu$  ZrN is less at high frequency whereas at low frequency difference is more indicating although both the coatings are having similar capacitive property, however 2 $\mu$  ZrN has better corrosion resistance property than 3 $\mu$  ZrN, this may be due to increased number of defects in 3 $\mu$  ZrN. [48]

SEM studies were carried out to determine morphology of coating after typical anodic polarization tests in 3.5%NaCl

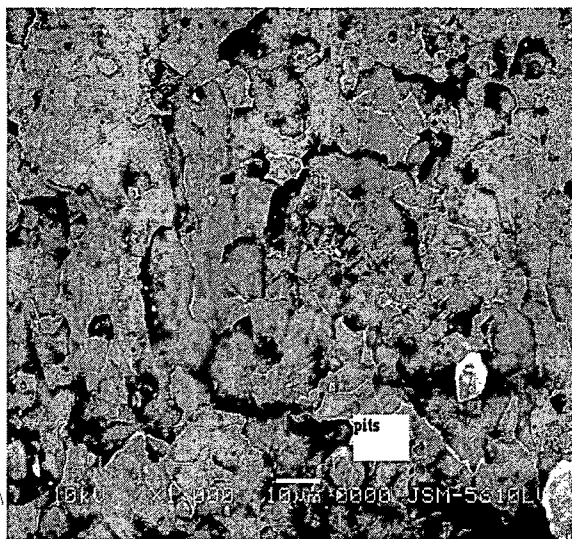


Fig 5.C.2.(b)(S) Typical morphologies of the 2.0  $\mu$  ZrN coatings which had been subjected to the anodic polarization test in 3.5%NaCl

Surface image of the 2.0  $\mu$  ZrN coated alloy after corrosion tests is shown in Fig 5.C.2.(b)(S). When the SEM image was examined, it was seen that the coating layer was broken from the substrate as large pieces, causing removal of the larger pieces. The formation of the coating defects is very much difficult to avoid totally. Consequently, when subjected to a corrosive atmosphere, coated materials will form galvanic cells at the defects near the interface since ceramic coatings are electrochemically more stable than most substrate materials. Once aggressive ions such as chlorides penetrate the coating through these small channels, driven by capillary forces, the exposed area will begin to experience anodic dissolution, which will usually extend laterally along the interface between the coating and the substrate. Finally the pits to be formed linked up each other,

causing removal of the entire coating by flaking. The coating defects e.g., pores, pinholes, cracks, observed at the SEM images before corrosion tests lead the electrolyte to reach to the substrate and contribute to developing of the corrosion.[60,66,67]

The compositional analysis of coatings after potentiodynamic test was done using EDX attached to SEM.

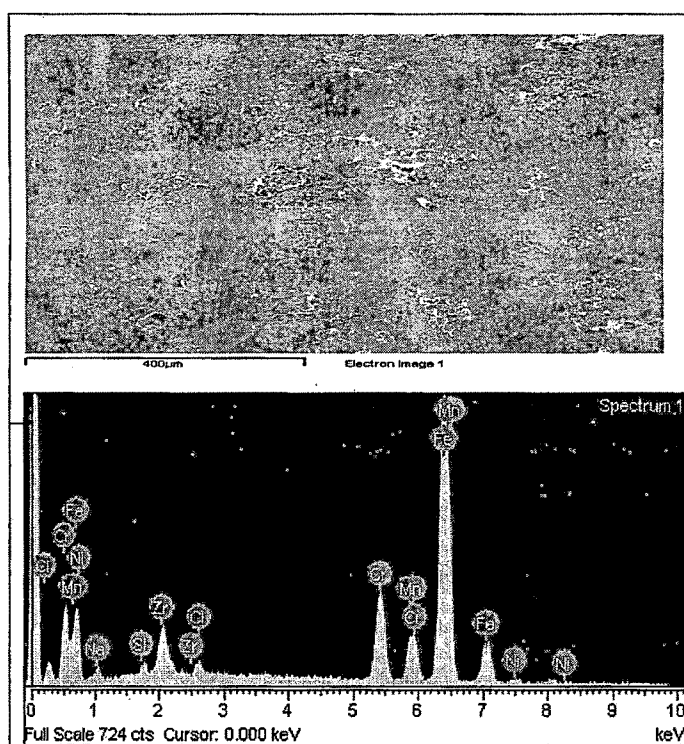


Fig 5.C.2.(b)(E)The EDX analysis of 2 $\mu$  ZrN thin film subjected to potentiodynamic test in 3.5%NaCl

As indicated in Fig 5.C.2.(b)(E)intense peak of iron and less intense peak of Zr is observed indicating removal of coating.

### 5. C. 2 (c) Corrosion behaviour of ZrN in 0.1N HCl

The corrosion behaviour of ZrN coatings of varying thickness was measured by potentiodynamic corrosion tests in 0.1N HCl solution.

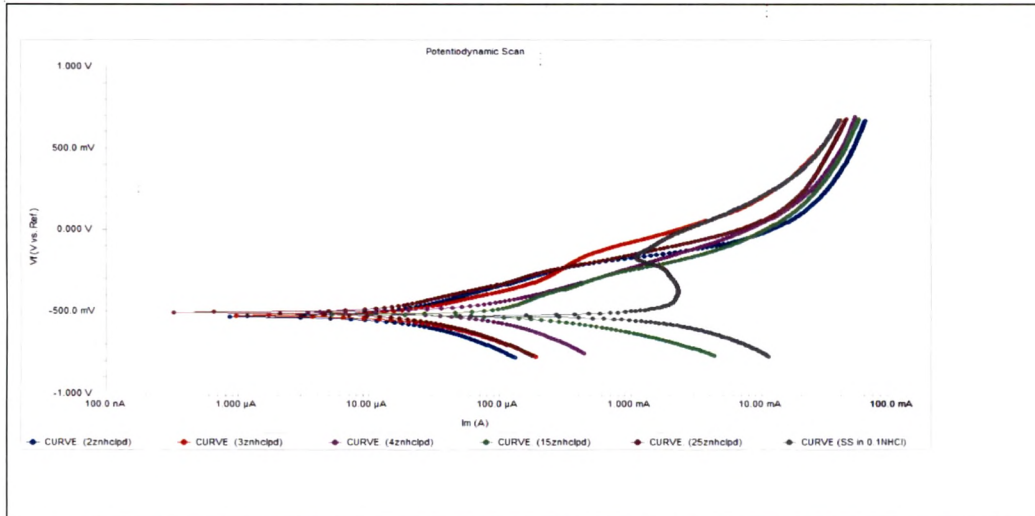


Fig 5.C.2.(c)(P) Potentiodynamic corrosion test of S.S substrate & ZrN thin films of varying thickness in 0.1NHCl

0.1NHCl	$E_{corr}$ (mV)	$I_{corr}$ ( $\mu\text{A}/\text{cm}^2$ )	Protective efficiency, $P_i$ (%)
S.S	-528	3.574 mA/cm <sup>2</sup>	
1.5 $\mu$ ZrN	-520.6	244.6	93.17
2.0 $\mu$ ZrN	-530	240.0	93.32
2.5 $\mu$ ZrN	-532	132	96.3
3.0 $\mu$ ZrN	-527	80.70	97.74
4.0 $\mu$ ZrN	-506	136.0	96.20

Table C.2(c) Values of corrosion potential ( $E_{corr}$ ) corrosion current density ( $I_{corr}$ ) and protective efficiency for all ZrN specimens in 0.1N HCl

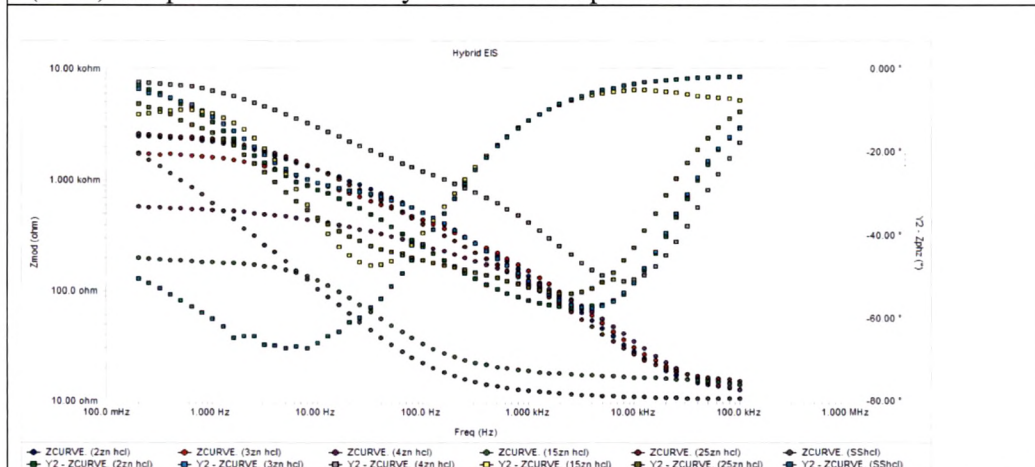


Fig 5.C.2.(c)(B) Electrochemical impedance diagram of ZrN thin films of varying thickness.

The Tafel plots obtained for steel substrate, and ZrN coating of varying thickness in 0.1N HCl are shown in Fig 5.C.2.(c)(P). The electrochemical parameters (corrosion current, corrosion potential and % porosity) calculated from polarization curves are summarized in Table C.2.(c)

The corrosion potential of the steel substrate is about  $-0.528\text{V}$ . The corrosion potentials ( $E_{\text{corr}}$ ) of the coated specimens are only slightly away from that of stainless steel, within 25 mV, which indicates that the corrosion of the TiN coated-specimens are mainly from the dissolution of the metal substrate and not from the TiN film. Since corrosion potential is a thermodynamic property of the substrate material the variation of  $E_{\text{corr}}$  is not supposed to be far away from that of bare steel. [41,42]

The corrosion current density ( $i_{\text{corr}}$ ) is an important parameter to evaluate the kinetics of corrosion reactions normally proportional to the corrosion current density measured via polarization. The lower the  $i_{\text{corr}}$ , the lower corrosion rate the sample is. In the present test the  $i_{\text{corr}}$  value obtained for all the thickness is always less than bare Stainless steel substrate indicating protection of substrate. [43]

As observed in Polarisation curve, in cathodic polarization region the coated samples starts at a current lower than the stainless steel, but near the corrosion potential the coated sample current increases until it becomes almost equal to that of stainless steel. This phenomenon can be explained by pitting of the coatings at defect sites. [57] From the polarisation curve, the anodic current density for 1.5 $\mu$ , 2  $\mu$ , 2.5  $\mu$  and 4 $\mu$  ZrN changes a little with potential increasing from -200 mV to the breakthrough potential +100 mV. In this interval, the passive layer protects specimen surface from dissolving. While, anodic current density increases dramatically with potential over 100 mV, probably due to a pitting corrosion mechanism initiated at the local defects of the film. [43]

As indicated in Bode's plot Fig 5.C.2.(c)(B) at high frequency the impedance value of all the coating is almost same and higher than uncoated S.S. In the medium frequency range i.e 10 Hz to 1000 Hz, 3  $\mu$  ZrN has higher impedance value of all. However at very low frequency highest impedance is obtained for 1.5  $\mu$  and 4  $\mu$  ZrN.

The results that can be inferred are that in medium frequency range the resistance to corrosion in 3 $\mu$  ZrN is high it may be due to formation of dielectric film. However

further decrease in the frequency and increase in passage of time, the unexposed pinholes and pores come in contact with corrosive media and results in lower impedance value

SEM studies were carried out to determine morphology of coating after typical anodic polarization tests in 0.1N HCl.

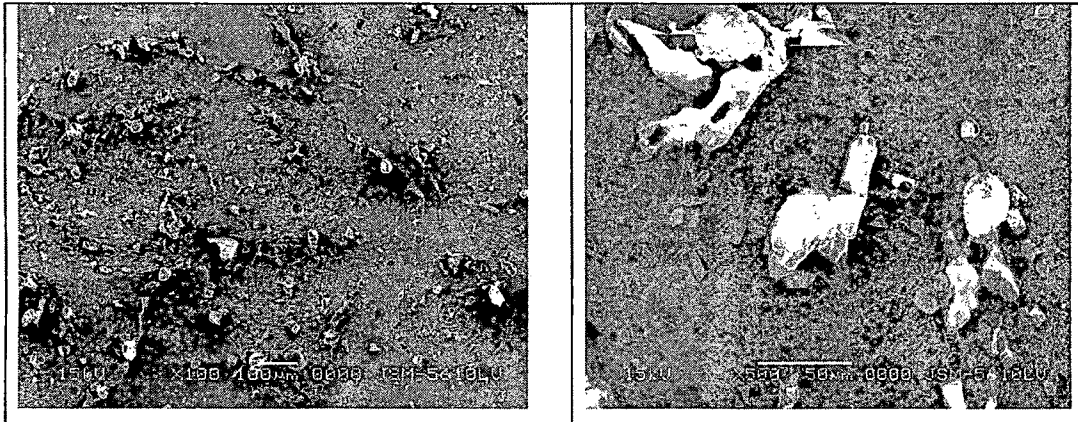


Fig 5.C.2.(c)(S) Typical SEM morphologies of the 3.0  $\mu$  ZrN at (a) 100X and (b) 500X coating which had been subjected to the anodic polarization tests 0.1N HCl

As indicated in Fig 5.C.2.(c)(S) (a) No sign of pitting corrosion is observed for the coating of 3 $\mu$  ZrN. However at high magnification (b) Corrosion products are obtained on the surface of coating. The SEM is in support for the good corrosion resistance of 3 $\mu$ ZrN in 0.1N HCl.

The compositional analysis of coatings after potentiodynamic test was done using EDX attached to SEM.

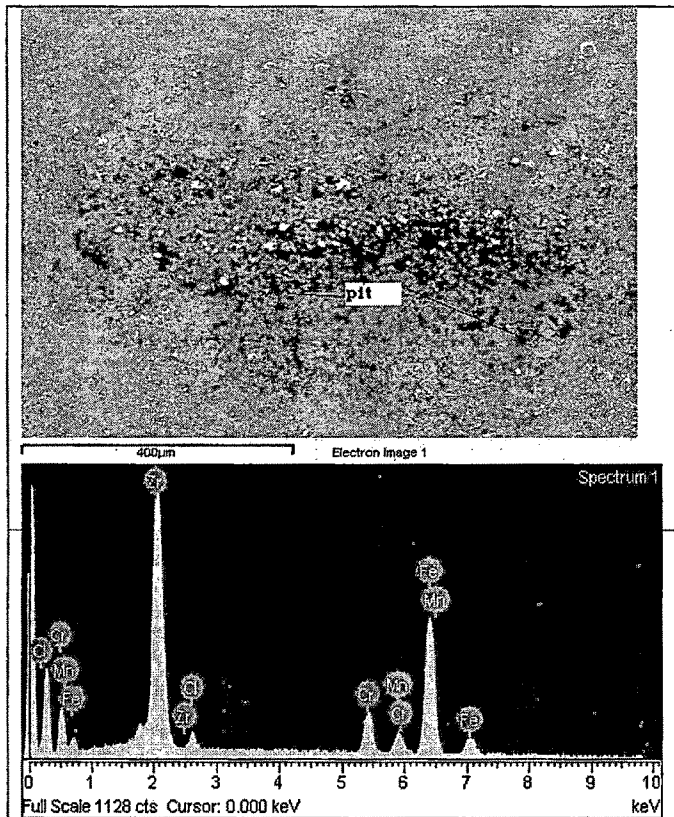


Fig 5.C.2.(c)(E)The EDX analysis of 1.5  $\mu$  ZrN thin film subjected to potentiodynamic test in 0.1 N HCl

In the Fig 5.C.2(c)(E) the EDX indicates the intense peak of Zr, and less intense peaks of Fe, Mn. The coating system at 100X shows few very small and shallow pits

### 5.C 2 (d) Corrosion Behaviour of ZrN in 11pH Na<sub>2</sub>SO<sub>4</sub>

The corrosion behaviour of ZrN coatings of varying thickness was measured by potentiodynamic corrosion tests in 11pH Na<sub>2</sub>SO<sub>4</sub> solution.

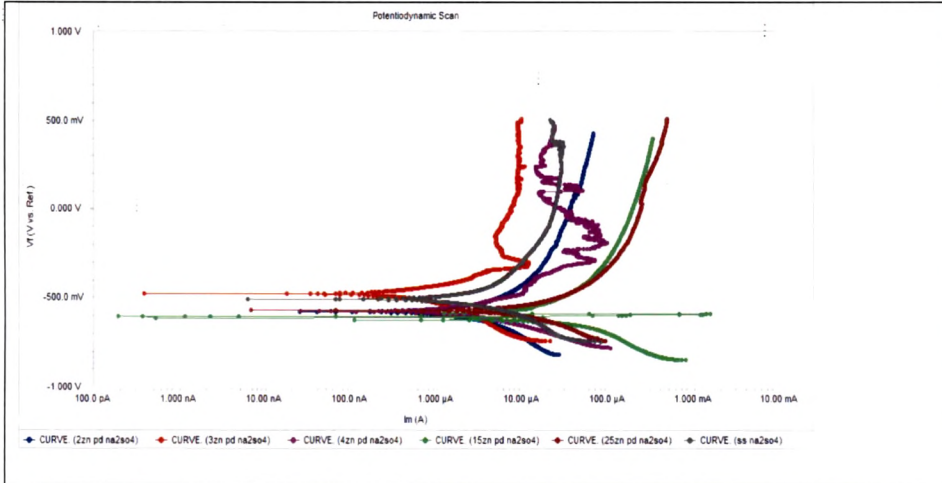


Fig 5.C.2.(d)(P) Potentiodynamic corrosion test of S.S substrate & ZrN thin films of varying thickness in 11pH Na<sub>2</sub>SO<sub>4</sub>

11pHNa2SO4	E <sub>corr</sub> (mV)	I <sub>corr</sub> (μA/cm <sup>2</sup> )	Protective efficiency, P <sub>i</sub> (%)
S.S	-508	5.970	
1.5μ ZrN	-603.5	2.792	53.3
2μ ZrN	-578	16.60	
2.5μ ZrN	-571.1	8.241	
3μ ZrN	-480.0	663nA/ cm <sup>2</sup>	99.99
4 μ ZrN	-576.1	2.309	61.32

Table C.2.(d) Values of corrosion potential (E<sub>corr</sub>) corrosion current density (I<sub>corr</sub>) and protective efficiency for all ZrN specimens in 11pH Na<sub>2</sub>SO<sub>4</sub>

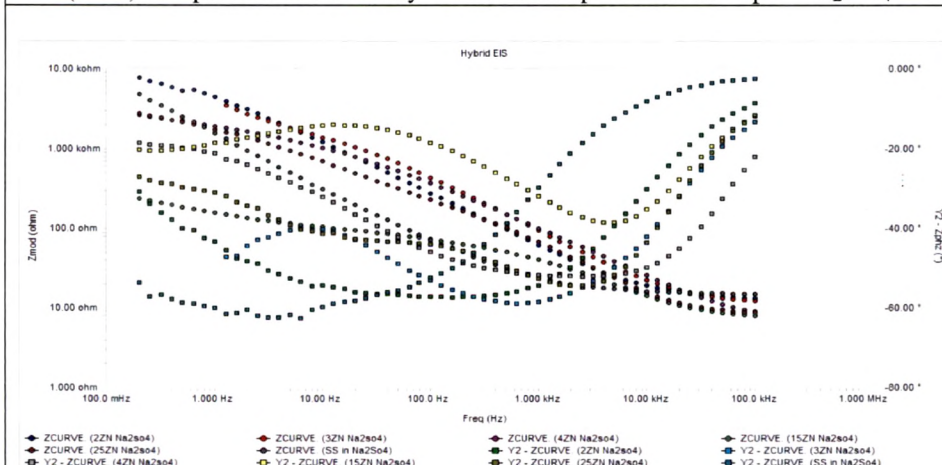


Fig 5.C.2.(d)(B) Electrochemical impedance diagram of ZrN thin films of varying thickness in 11pH Na<sub>2</sub>SO<sub>4</sub>

The Tafel plots obtained for steel substrate and ZrN coating of varying thickness in 11pH  $\text{Na}_2\text{SO}_4$  are shown in Fig 5.C.2.(d)(P). The electrochemical parameters (corrosion current, corrosion potential and % porosity) calculated from polarization curves are summarized in Table C.2.(d).

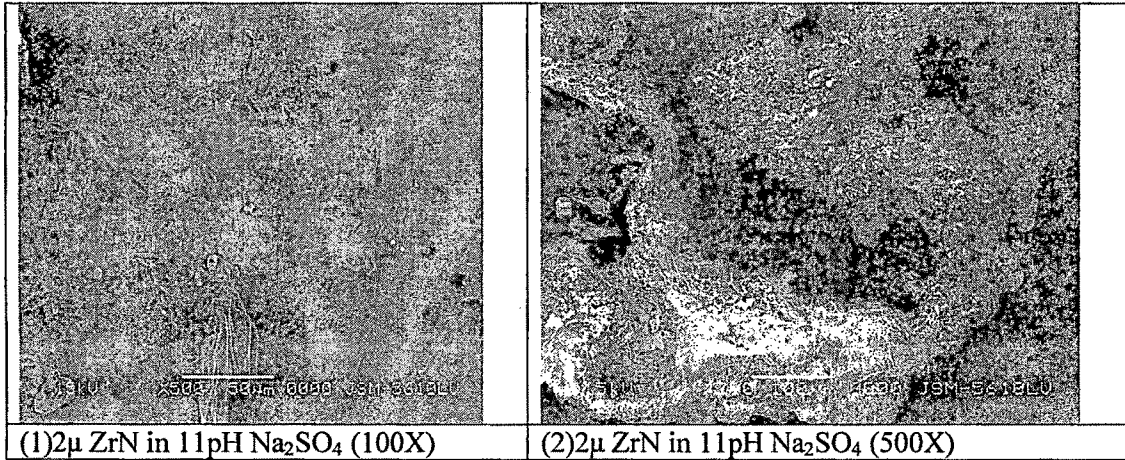
The corrosion potential of the steel substrate is about  $-0.508\text{V}$ . The corrosion potential of coated samples has a lower value than  $E_{\text{corr}}$  of the steel without a coating because the thin coating, having a high porosity, causes an electrochemical heterogeneity of the surface contacting the electrolyte. This heterogeneity is the reason for physico-chemical instability of the substrate coating system in an aggressive environment. [52]

It is well known that, the corrosion current density ( $i_{\text{corr}}$ ) is an important parameter to evaluate the kinetics of corrosion reactions, normally proportional to the corrosion current density measured via polarization. The lower the  $i_{\text{corr}}$ , the lower corrosion rate the sample is. In the present test the  $i_{\text{corr}}$  value obtained is less than bare Stainless steel substrate for  $1.5\mu$ ,  $3\mu$  and  $4\mu$  ZrN whereas  $i_{\text{corr}}$  for  $2.0\mu$  and  $2.5\mu$  ZrN is more than steel indicating very poor corrosion resistance of coating. For all the E values the value of I(current) is always less for  $3\mu$  ZrN than uncoated steel indicating its good corrosion resistance. The  $i_{\text{corr}}$  values of all the coatings except  $3\mu$  ZrN in the anodic region is higher than stainless steel.[43]

All the coatings exhibit passive like behaviour i.e. less increase in current with increase in potential. Oscillations are observed in  $4\mu$  ZrN  $-400\text{mV}$  to  $200\text{mV}$  indicating region of incomplete passivity.[40]

At high frequency the impedance value of all the coating is almost same .The initial capacitive behaviour of coating is high, indicating that the environment used for corrosion is not severe. Sudden deflection in curve to low impedance value is observed in medium frequency range for  $1.5\mu$  ZrN and the impedance of  $1.5\mu$  ZrN at low frequency is less than stainless steel. Results indicate that thickness of  $1.5\mu$  ZrN is insufficient for corrosion protection.

SEM studies were carried out to determine morphology of coating after typical anodic polarization tests in 11pH Na<sub>2</sub>SO<sub>4</sub>



(1) 2μ ZrN in 11pH Na<sub>2</sub>SO<sub>4</sub> (100X)

(2) 2μ ZrN in 11pH Na<sub>2</sub>SO<sub>4</sub> (500X)

Fig 5.C.2.(d)(S) Typical morphologies of the 2.0 μ ZrN coatings which had been subjected to the anodic polarization tests in 11pH Na<sub>2</sub>SO<sub>4</sub> at (1) 100X and (2) 500X

Fig 5.C.2.(d)(S)(1) indicates corrosion products are observed on the surface. Higher magnification (2) indicates the mild attack on the surface of coating.

The compositional analysis of coatings after potentiodynamic test was done using EDX attached to SEM

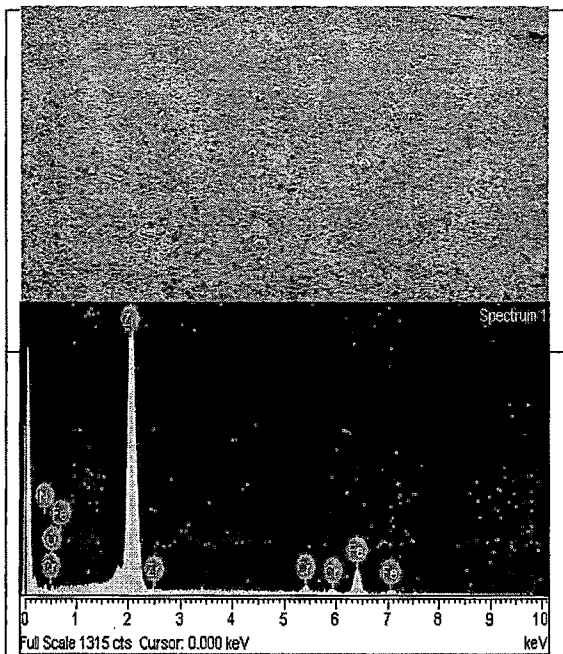
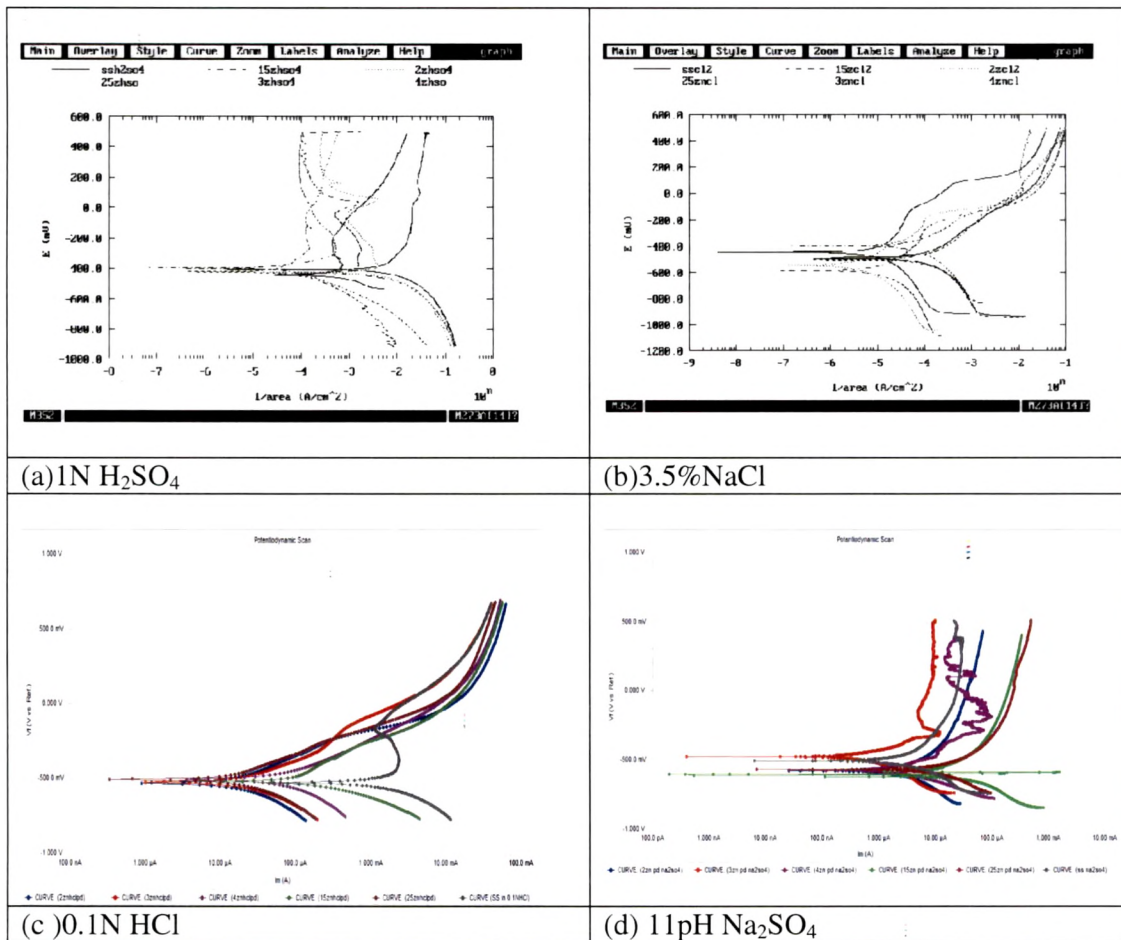


Fig 5.C.2.(d)(E) The EDX analysis of 2μ ZrN thin film subjected to potentiodynamic test in 11pH Na<sub>2</sub>SO<sub>4</sub>

The EDX analysis in Fig 5.C.2.(d)(E) indicates the large peak of Zr and small peaks of Fe, Mn. This indicates uniform and mild corrosion on the surface of coating.

**General Discussion on behaviour of ZrN thin films in different environment.**

**5. C.2.P Potentiodynamic behaviour of ZrN thin film in various environment**

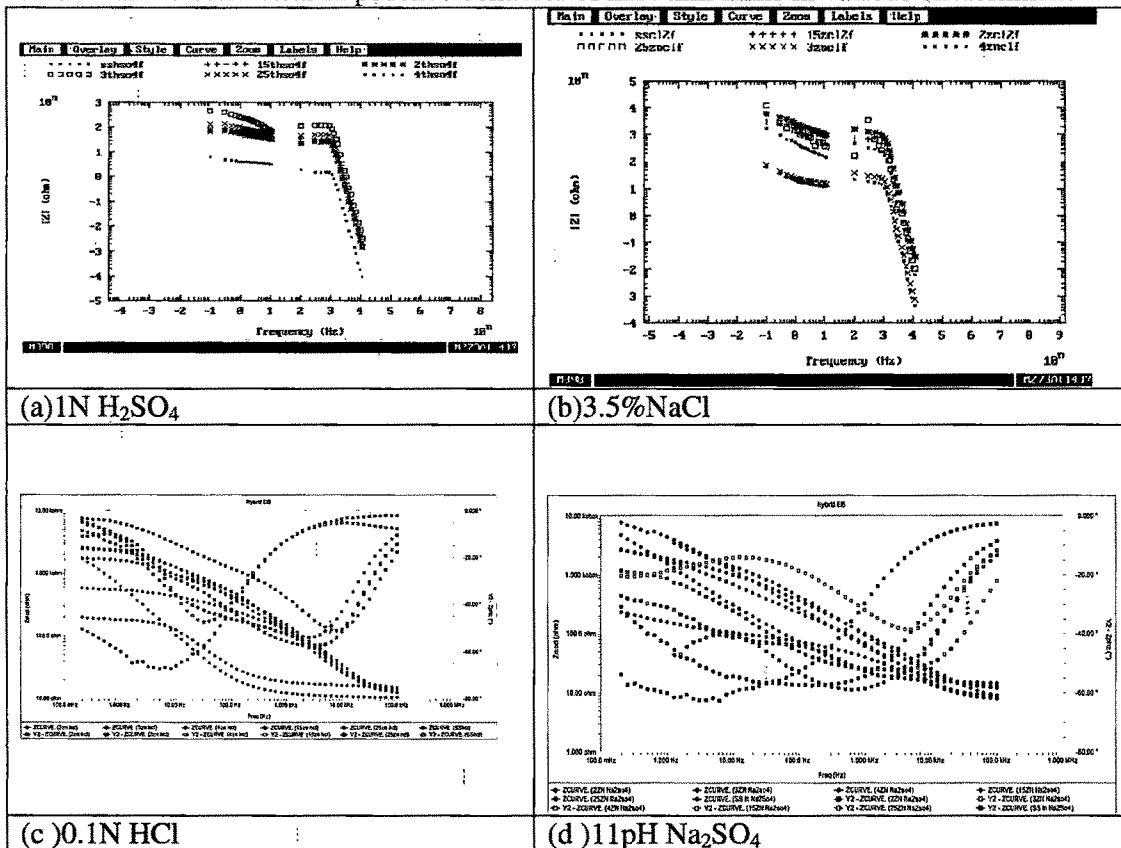


5.C.2.P (a,b,c,d) Behaviour of ZrN thin films in Various Environment after potentiodynamic test

Considering E-log I behaviour of ZrN coating of various thickness in various environment one tend to conclude that corrosion behaviour is strongly dependent on the environment to which it is subjected to. Highest corrosion resistance is observed in case of 1N H<sub>2</sub>SO<sub>4</sub> (5.C.2.P (a)) and 3.5%NaCl (5.C.2.P (a)) where as inferior behaviour is observed for 11pH Na<sub>2</sub>SO<sub>4</sub> and 0.1NHCl

The Ecorr in case of 11pH Na<sub>2</sub>SO<sub>4</sub> (5.C.2(d)) shifted to lower Ecorr and higher current density value than 1N H<sub>2</sub>SO<sub>4</sub>, whereas in case of 3.5% NaCl (5.C.2.P (b)) and 0.1N HCl (5.C.2.P (c)) displayed same Ecorr value however domain of anodic current density is higher in 0.1N HCl.

### 5. C. 2 Electrochemical impedance behavior of ZrN thin films in various environment



### 5.C.2.B(a,b,c,d) Behaviour of ZrN thin films in Various Environment after Electrochemical impedance spectroscopy test

For 1N H<sub>2</sub>SO<sub>4</sub> fig. 5.C.2.B(a) and 3.5%NaCl fig. 5.C.2.B(b), the variation in the impedance value at high frequency is observed whereas in case of 0.1N HCl and 11pH Na<sub>2</sub>SO<sub>4</sub> the variation at high frequency is very low indicating similar capacitive property of all the coated and uncoated samples. However in all the cases variation in impedance value at low frequency is observed.



### 5.C.3 CORROSION BEHAVIOUR OF ZrTiN THIN FILMS

As revealed by XRD results, the ZrTiN thin films consist of three phases, Ti<sub>2</sub>N, ZrN and  $\gamma$ Fe proportion of each changes as per thickness of coating. Presence of two or more phases in the coating results in the different corrosion behaviour compared to single phase obtained in Ti-N or Zr-N coatings. As discussed in XRD of ZrN, in case of 2.5 $\mu$  ZrTiN intense peak of both ZrN (111) and ZrN (200) is present indicating this coating is under highest stress.

#### 5. C .3 (a) Corrosion behaviour of ZrTiN thin films in 1N H<sub>2</sub>SO<sub>4</sub>

The corrosion behaviour of ZrTiN coatings of varying thickness was measured by potentiodynamic corrosion tests in 1N H<sub>2</sub>SO<sub>4</sub> solution.

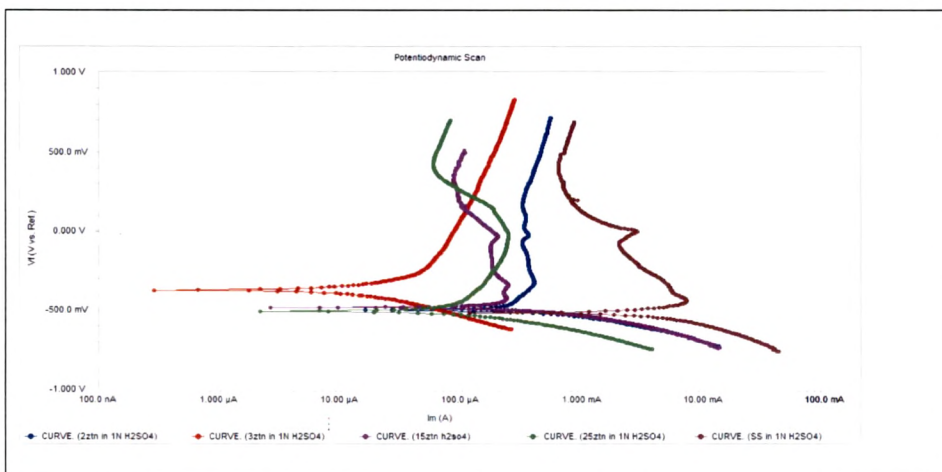


Fig 5.C.3.(a)(P) Potentiodynamic corrosion test of S.S substrate & ZrTiN thin films of varying thickness in 1N H<sub>2</sub>SO<sub>4</sub> solution

1N H <sub>2</sub> SO <sub>4</sub>	E <sub>corr</sub> (mV)	I <sub>corr</sub> ( $\mu$ A/cm <sup>2</sup> )	Protective efficiency, P <sub>i</sub> (%)
S.S	-516.3	55.47 mA/cm <sup>2</sup>	
1.5 $\mu$ ZrTiN	-482.2	1.948 mA/cm <sup>2</sup>	96.5
2.0 $\mu$ ZrTiN	-499.6	503.7	99.09
2.5 $\mu$ ZrTiN	-507.2	164.4	99.7
3.0 $\mu$ ZrTiN	-370.0	32.50	99.94

Table.C.3.(a) Values of corrosion potential (E<sub>corr</sub>) corrosion current density (I<sub>corr</sub>) and protective efficiency for all ZrTiN specimens in 1N H<sub>2</sub>SO<sub>4</sub> solution.

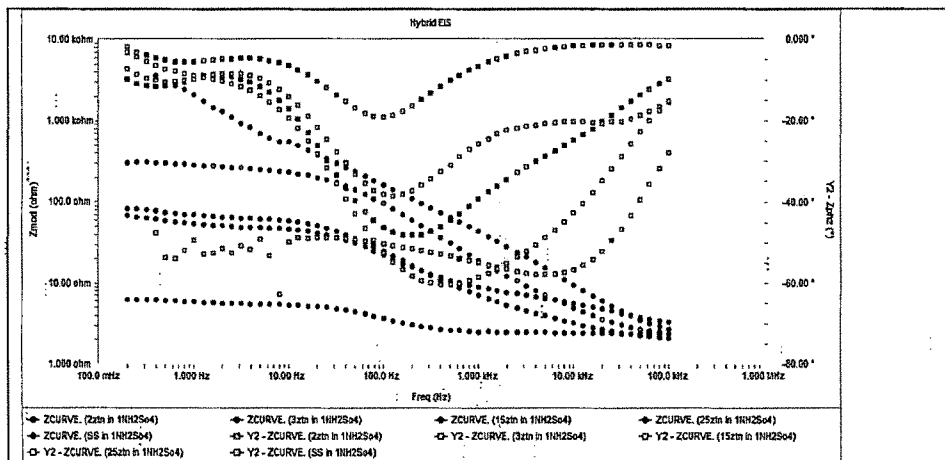


Fig 5.C.3.(a)(B) Electrochemical impedance diagram of ZrTiN thin films of varying thickness in 1N H<sub>2</sub>SO<sub>4</sub> solution

The Tafel plots obtained for steel substrate and ZrTiN coating of varying thickness in 1N H<sub>2</sub>SO<sub>4</sub> are shown in Fig 5.C.3.(a)(P). The electrochemical parameters (corrosion current, corrosion potential and % porosity) calculated from polarization curves are summarized in Table C.3. (a).

The corrosion potential of the steel substrate is about -516 mV. The E<sub>corr</sub> of single layer coated samples, when compared to the substrate, shows a shift towards the positive side. The positive shift of E<sub>corr</sub> (-516.3 to -482.2 V for 1.5 μm ZrTiN, for example) indicates better corrosion resistance of the ZrTiN coatings. The corrosion potential and the corrosion current for various single layer coatings along with the steel substrate are given in Table C.3.(a).

It is known that transition metal nitrides are inert to the chemical attacks. However, the PVD coatings contain cracks, pinholes and pores, which allow the corrosive media to enter the substrate, thus degrading the corrosion behavior of the coating/substrate system. Moreover, as the film grows thicker, there is a lesser likelihood for the film to have pinholes interconnecting with one another from the top surface to the bottom surface adjacent to the underlying metal that needs protection. As a result, the corroding medium would encounter more resistance during its penetration or diffusion through the film to the metal substrate. From Table C.1.(a) it is seen that the corrosion resistance of lesser thickness ZrTiN is inferior than 3 μm ZrTiN because of strong increase in pin hole defect density for thin coatings. [45,50,58]

As observed in Polarisation curve, in cathodic polarization region the coated samples starts at a current lower than the stainless steel, but near the corrosion potential the coated sample current increases until it becomes almost equal to that of stainless steel . This phenomenon can be explained by pitting of the coatings at defect sites. [21] All coated samples except 2.5  $\mu$  ZrTiN showed “passive like” anodic behaviour. Since the corrosion is localized at the defect locations and the coating remains passive the anodic current density can be related to the active substrate area. At an anodic potential of +500 mV vs. SCE, 1.5  $\mu$  ZrTiN has almost 3 orders of magnitude smaller corrosion current density of substrate and almost 2 orders of magnitude smaller corrosion current density for 2.0 $\mu$  ZrTiN and 2.5 $\mu$  ZrTiN.

The porosity decreases with increasing the thickness but at the same time strains increase, causing the peeling off of the film from the substrate. So, the effectiveness of the corrosion protectiveness by a ZrTiN coating is determined by its continuity and its good adhesion to the substrate. The latter depends on the production conditions. [52]

Polarization curves in passivation area have a horizontal peak as shown in Fig.5.C.3.(a) for S.S, 1.5 and 2.0 $\mu$  ZrTiN. Existence of this peak is related to the formation of secondary phase such as  $\gamma$ Fe (revealed by XRD Fig. 5.B.3.i) for which the corrosion current is higher than matrix phase. When more than one metallic phase is present in alloy, its polarization behavior will be the volume average sum of the behavior of each phase that leads to the presence of the horizontal peak in the passive region. The width of this peak can indicate the activity or amount of secondary phase in matrix. [46]

The Bode plot Fig 5.C.3.(a)(B) for the coated alloy before defect formation ,time constant at high frequencies is related to the capacitive response of the film. The resistive plateau at  $10^2$ – $10^3$ Hz represents the pore resistance of film. The relaxation process at about 1–10 Hz is attributed to the capacitance of the intermediate layer present at the metal/coating interface. The resistance of such interlayer, which is situated at lower frequencies, is very important from the corrosion protection standpoint, since it is the last barrier for the corrosive species before reaching the metal surface. The third time constant is weakly defined at lowest frequencies and is related to the corrosion activity. At high frequency the capacitive response of all the coatings is same, however at low frequency when presence of pore is detrimental the impedance behaviour changes and highest impedance

is obtained for 3 $\mu$  ZrTiN. This is in agreement with best corrosion properties obtained for 3 $\mu$  ZrTiN under potentiodynamic test. [48]

SEM studies were carried out to determine morphology of coating after typical anodic polarization tests in 1N H<sub>2</sub>SO<sub>4</sub>

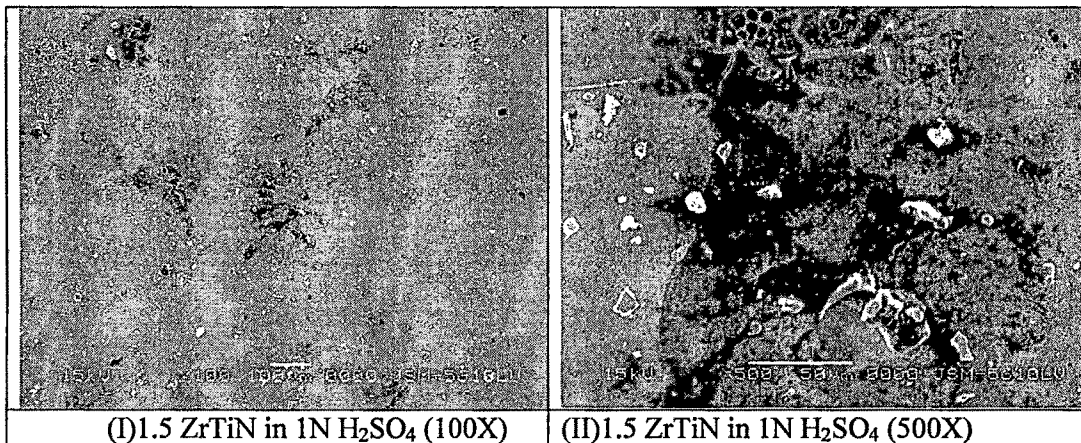


Fig 5.C.3.(a)(S) Typical SEM morphologies of the 1.5  $\mu$  ZrTiN coating which had been subjected to the anodic polarization tests 1N H<sub>2</sub>SO<sub>4</sub> solution at (I)(100X) and (II) (500X)

SEM micrograph Fig 5.C.3.(a)(S)(I) indicates uniform corrosion on the surface of the coating. At Higher magnification Fig 5.C.3.(a)(S)(II) pits are observed. However pits are not deep and the substrate is not observed indicating less severe attack.

The compositional analysis of coatings after potentiodynamic test was done using EDX attached to SEM

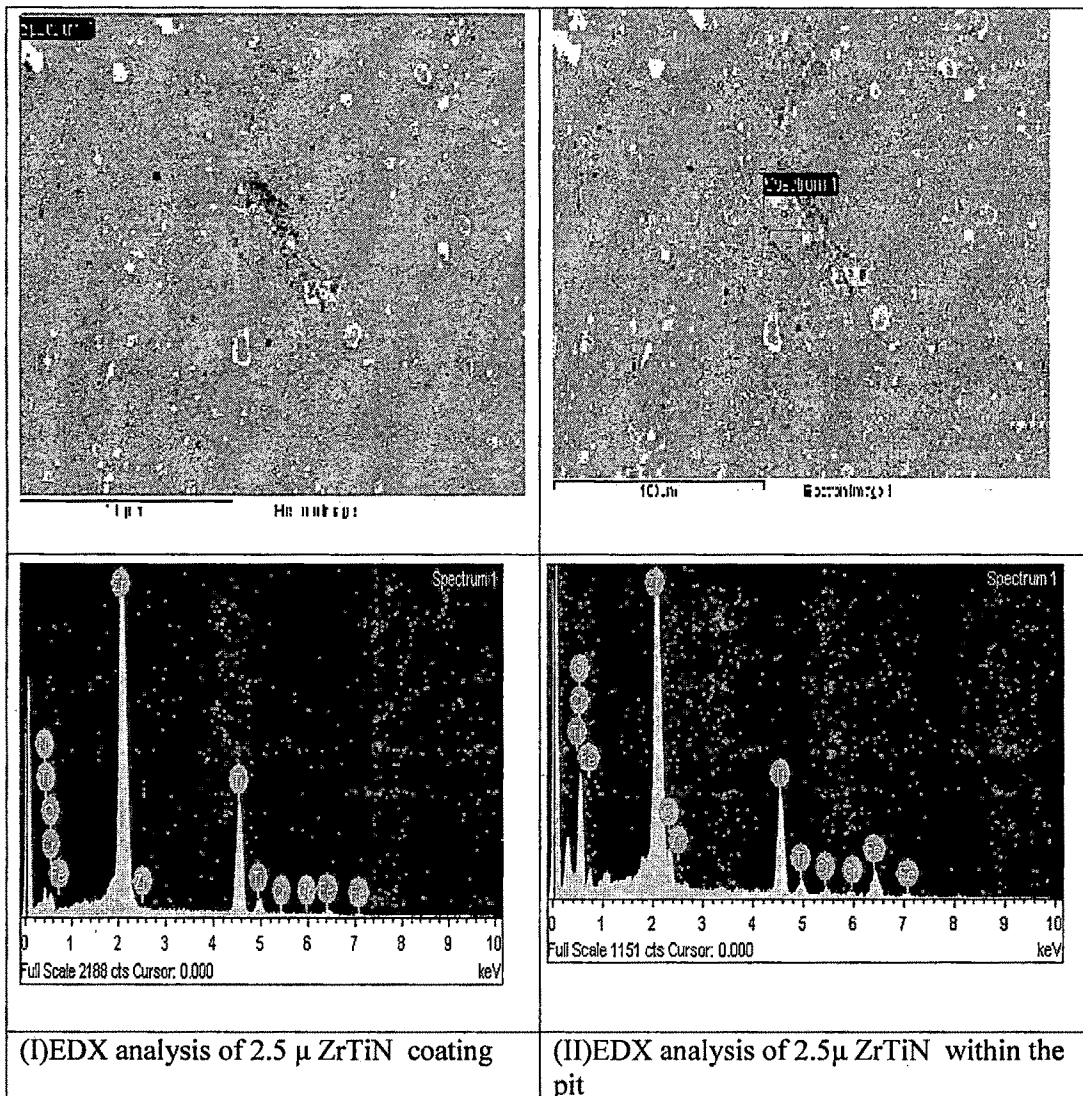


Fig 5.C.3.(a)(E)The EDX analysis of 2.5μ ZrTiN thin film subjected to potentiodynamic test in 1NH<sub>2</sub>SO<sub>4</sub> (I) corroded region (II) within the pit

The EDX analysis Fig 5.C.3.(a)(E) (I) indicates the large peak of Zr and small peak of Ti. The EDX analysis is very similar to that obtained without corrosion (5.A.I.(iii)).EDX analysis within the pit Fig 5.C.3.(a)(E) (II) indicate that both Zr and Ti are present indicates that complete removal of coating has not occurred and pits formed are superficial.

### 5.C 3. (b) Corrosion behaviour of ZrTiN thin films in 3.5% NaCl

The corrosion behaviour of ZrTiN coatings of varying thickness was measured by potentiodynamic corrosion tests in 3.5%NaCl solution.

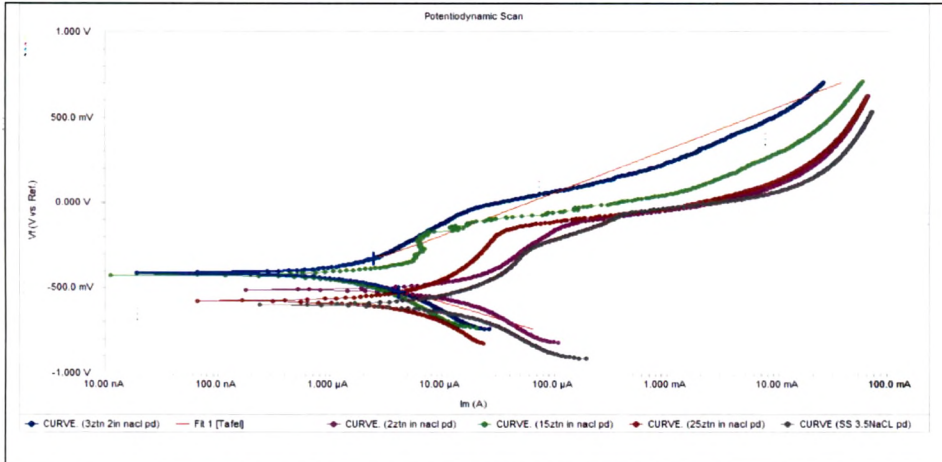


Fig 5.C.3.(b)(P) Potentiodynamic corrosion test of S.S substrate & ZrTiN thin films of varying thickness in 3.5%NaCl solution.

3.5% NaCl	$E_{corr}$ (mV)	$I_{corr}$ ( $\mu\text{A}/\text{cm}^2$ )	Protective efficiency, $P_i$ (%)
S.S	-599.3	63.79	
1.5 $\mu$ ZrTiN	-612.3	79.23	
2.0 $\mu$ ZrTiN	-511.8	14.52	77.3
2.5 $\mu$ ZrTiN	-578.0	22.90	64.2
3.0 $\mu$ ZrTiN	-508.1	5.062	92.1

Table C.3.(b) Values of corrosion potential ( $E_{corr}$ ) corrosion current density ( $I_{corr}$ ) and protective efficiency for all ZrTiN specimens. in 3.5%NaCl solution.

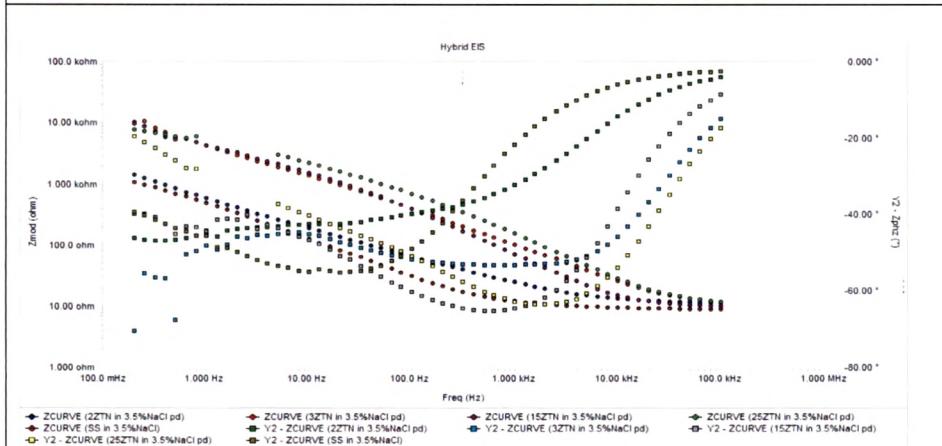


Fig 5.C.3.(b)(B) Electrochemical impedance diagram of Zr-Ti-N thin films of varying thickness. in 3.5%NaCl solution.

The Tafel plots obtained for steel substrate, and ZrN coating of varying thickness in 3.5%NaCl are shown in Fig 5.C.3.(b)(P). The electrochemical parameters (corrosion current, corrosion potential and % porosity ) calculated from polarization curves are summarized in Table C.3.(b).

The corrosion potential of the steel substrate is about  $-0.599$  V. The corrosion potential of coated samples has a lower value than  $E_{\text{corr}}$  of the steel without a coating because the thin coating, having a high porosity, causes an electrochemical heterogeneity of the surface contacting the electrolyte. This heterogeneity is the reason for a physico-chemical instability of the substrate coating system in an aggressive environment. [52]

Polarisation curves shows a lower corrosion current for  $3\mu$  ZrTiN than for all other thickness and stainless steel. The curve for  $3\mu$  ZrTiN and all other thickness have a similar shape but consistently lower anodic dissolution. A comparison between coatings suggests some improved corrosion resistance was offered by  $3\mu$  ZrTiN. However protection offered is broadly similar. [41, 42]

The corrosion current density ( $i_{\text{corr}}$ ) is an important parameter to evaluate the kinetics of corrosion reactions normally proportional to the corrosion current density measured via polarization. The lower the  $i_{\text{corr}}$ , the lower corrosion rate the sample is. In the present test the  $i_{\text{corr}}$  value obtained is less than bare Stainless steel substrate. The  $i_{\text{corr}}$  values of all the coatings in the anodic region is higher than stainless steel except at high E value,  $i_{\text{corr}}$  of  $2\mu$  ZrTiN is lower than stainless steel.[43]

As observed in Polarisation curve, in cathodic polarization region the coated samples starts at a current lower than the stainless steel, but near the corrosion potential the coated sample current increases until it becomes almost equal to that of stainless steel . This phenomenon can be explained by pitting of the coatings at defect sites.[57]From the potentiodynamic curve, the anodic current density for all coatings except  $3\mu$  ZrTiN changes a little with potential increasing from  $-200$  mV to the breakthrough potential  $+200$  mV. In this interval, the passive layer protects specimen surface from dissolving. While, anodic current density increases dramatically with potential over  $200$  mV, probably due to a pitting corrosion mechanism initiated at the local defects of the film. Also discontinuity is observed in  $1.5\mu$  ZrTiN coating. [43]

However, the overall corrosion process is dominated by locally active dissolution, which occurred as the substrate was exposed via coating porosity [47]

As discussed by Tamilaevi, R. et al [68] EIS data for the Ti-6Al-4V alloy in saline solution at different impressed potential ( $E_{corr}, 0\text{mV(SCE)}$  and  $+500\text{mV(SCE)}$ ). The bode plot exhibits two time constants at all impressed potential, as evidenced by the appearance of two distinct frequency regions. The time constant in high frequency part arises from the uncompensated ohmic resistance due to electrolytic solution. However in low frequency part the phase angle  $\theta$  decreased almost linearly to a constant value of approximately  $-40^\circ$ , suggesting occurrence of the diffusion process in the solid phase at the substrate/electrolyte interface.

As indicated in fig 5.C.3.(b)(B) at high frequency the capacitive behaviour of all the coatings is same. However at low frequency wherein at low frequency resistive behaviour of coating is important, the difference in impedance between  $3\ \mu\text{ ZrTiN}$  and  $2\ \mu\text{ ZrTiN}$  is more. Discontinuity is observed in  $2.5\ \mu\text{ ZrTiN}$ . This may be due to highly stressed structure of coating. The impedance value is of the order of one magnitude higher than uncoated substrate at lower frequency, indicating good corrosion resistance behaviour of coatings.

SEM studies were carried out to determine morphology of coating after typical anodic polarization tests in 3.5%NaCl

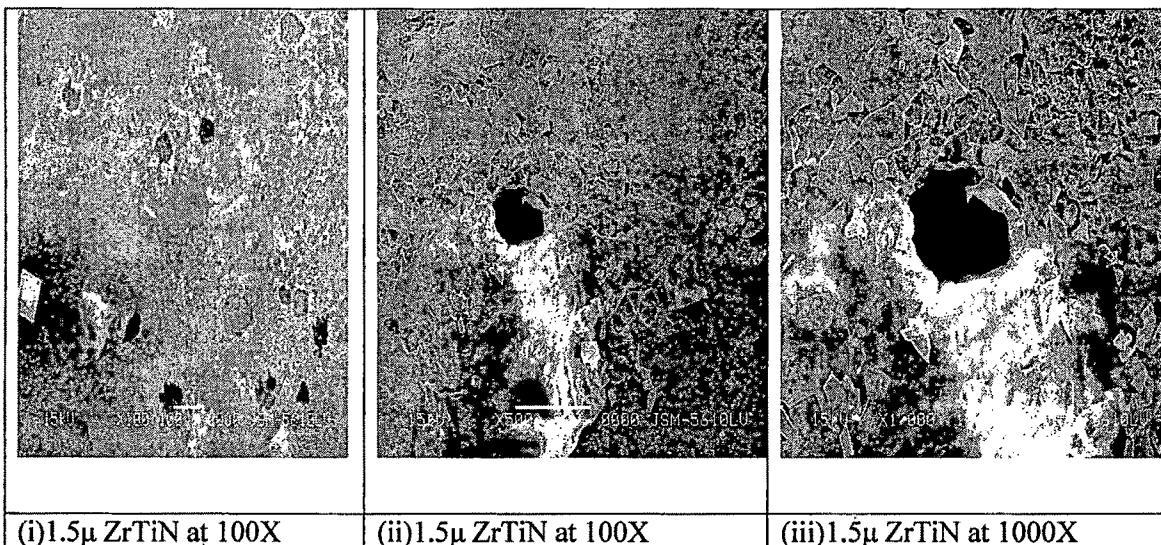


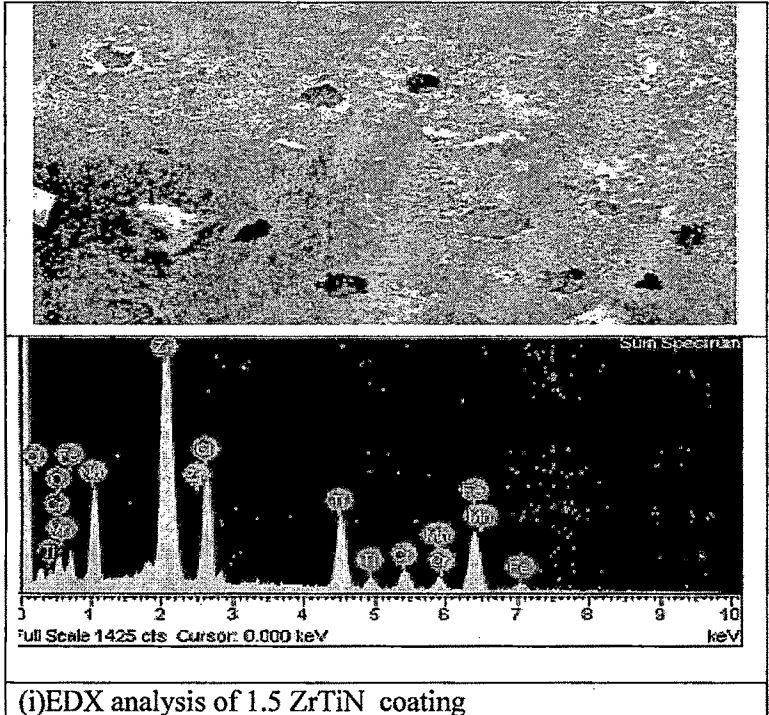
Fig 5.C.3.(b)(S) Typical morphologies of the  $1.5\ \mu\text{ Zr TiN}$  coatings which had been subjected to the anodic polarization tests 3.5%NaCl

As shown in Fig 5.C.3.(b)(S) (i) At low magnification large number of pits can be seen. The number of pits covering the corrosive area is many. The depth of the pits in the corroded surface of the coating system is shallow and is further confirmed by the EDX analysis results. The iron peaks measured in the bottom of a pit in the corroded coating system are very weak. ( Fig 5.C.3. (b)( E) (i)).

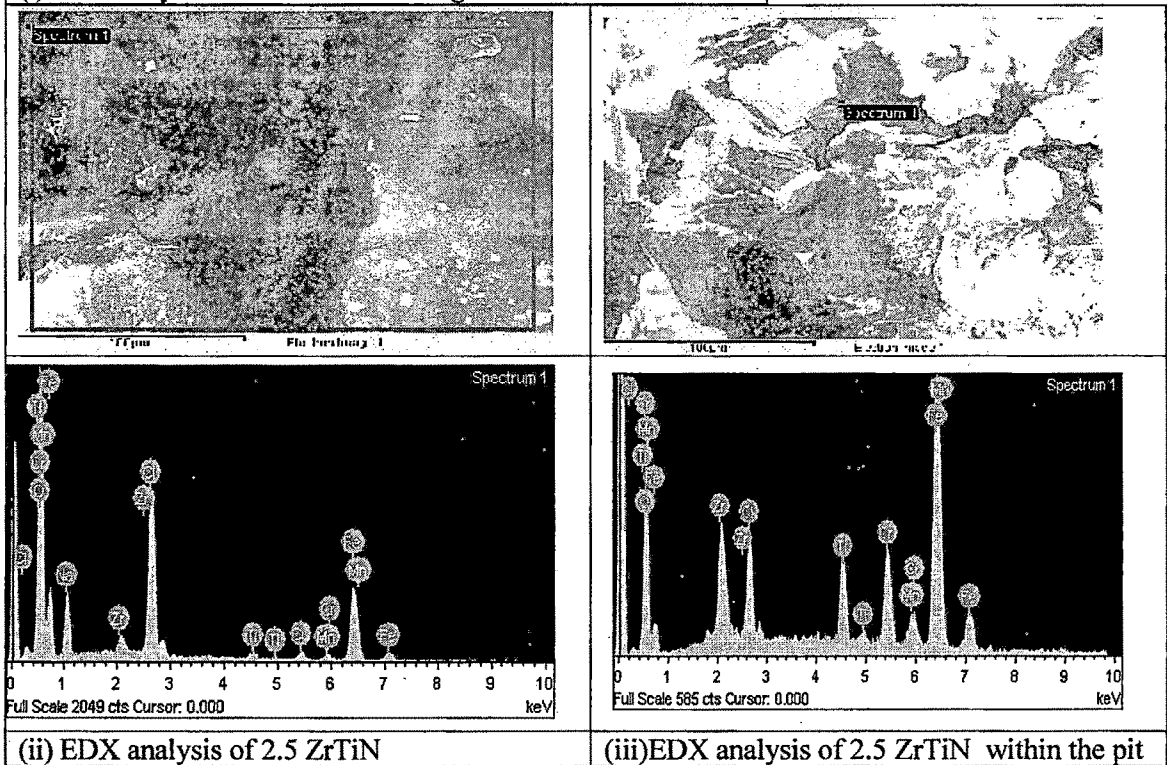
Surface images of 1.5 $\mu$  ZrTiN coated alloys after corrosion tests at high magnification is given in Fig 5.C.3.(b)(S) (iii). When the SEM images were examined, it was seen that the coating layer was broken from the substrate as large pieces, causing removal of the larger pieces. The formation of the coating defects is very much difficult to avoid totally. Consequently, when subjected to a corrosive atmosphere, coated materials will form galvanic cells at the defects near the interface. Since ceramic coatings are electrochemically more stable than most substrate materials, once aggressive ions such as chloride penetrate the coating through these small channels, driven by capillary forces, the exposed area will begin to experience anodic dissolution, which will usually extend laterally along the interface between the coating and the substrate. Finally the pits to be formed linked up each other, causing removal of the entire coating by flaking [38]. The coating defects e.g., pores, pinholes, cracks, observed at the SEM images before corrosion tests lead the electrolyte to reach to the substrate and contribute to developing of the corrosion. Similar behaviour was observed by when TiN was deposited on AZ91 alloy magnesium alloys by cathodic arc PVD technique. [60]

Micrographic evidence shows that localized pitting or crevice corrosion initiates at surface defects. These are metallic droplets or associated growth defects and arise during the initial arc-cleaning stage. It is suggested that, in a coating with high internal stresses, areas adjacent to such defects are more prone to cracking, after corrosion has commenced. Such behaviour is quite typical of internally stressed coatings where corrosion can initiate microcracks or pits which then grow as microscopic cracks. [59]

The compositional analysis of coatings after potentiodynamic test was done using EDX attached to SEM



(i)EDX analysis of 1.5 ZrTiN coating



(ii) EDX analysis of 2.5 ZrTiN

(iii)EDX analysis of 2.5 ZrTiN within the pit

Fig 5.C 3(b)(E)The EDX analysis of (i) 1. 5 $\mu$  ZrTiN & (ii)2.5 $\mu$  ZrTiN overall on the surface and (iii) 2.5 $\mu$  ZrTiN within the pit of thin film subjected to potentiodynamic test in 3.5%NaCl

EDX analysis Fig 5.C.3.(b)(E)(ii) of the coating indicates that intense peak of Zr and smaller peak of Ti is observed. EDX analysis within the pit Fig 5.C.3.(b)(E)(iii) indicates that both Zr and Ti are present in addition to intense iron peak indicates incomplete removal of coating .

### 5.C. 3 (c) Corrosion behaviour of ZrTiN thin films 0.1N HCl

The corrosion behaviour of ZrTiN coatings of varying thickness was measured by potentiodynamic corrosion tests in 0.1N HCl solution.

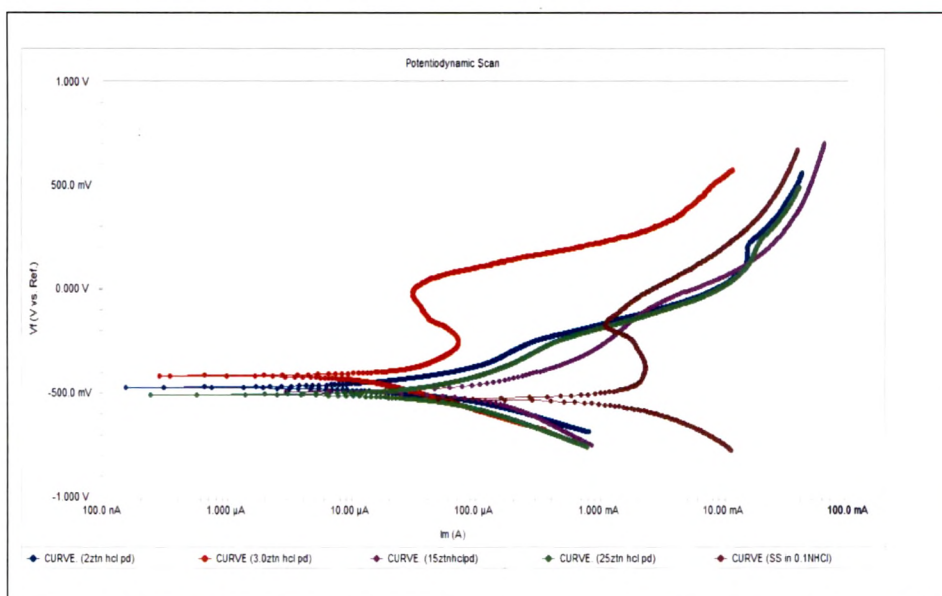


Fig 5.C.3(c)(P) Potentiodynamic corrosion test of S.S substrate & ZrTiN thin films of varying thickness in 0.1N HCl solution

0.1N HCl	$E_{corr}$ (mV)	$I_{corr}$ ( $\mu A/cm^2$ )	Protective efficiency, $P_i$ (%)
S.S	-528.8	3.574 mA/cm <sup>2</sup>	
1.5 $\mu$ ZrTiN	-495.0	136	96.2
2 $\mu$ ZrTiN	-472.2	13.87	99.6
2.5 $\mu$ ZrTiN	-507.2	66.20	98.2
3 $\mu$ ZrTiN	-416.2	92.14	97.5

Table C.3.(c) Values of corrosion potential ( $E_{corr}$ ) corrosion current density ( $I_{corr}$ ) and protective efficiency for all ZrTiN specimens. in 0.1N HCl solution

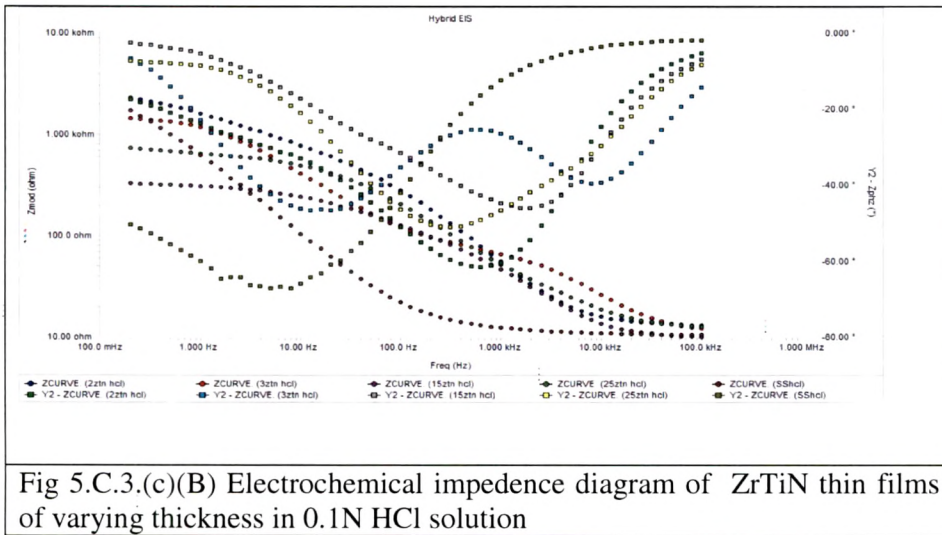


Fig 5.C.3.(c)(B) Electrochemical impedance diagram of ZrTiN thin films of varying thickness in 0.1N HCl solution

The Tafel plots obtained for steel substrate, and ZrTiN coating of varying thickness in 0.1N HCl are shown in Fig 5.C 3 (c)(P). The electrochemical parameters (corrosion current, corrosion potential and % porosity ) calculated from polarization curves are summarized in Table C.3.(c).

The corrosion potential of the steel substrate is about  $-0.528$  V. The comparison between the corrosion potential  $E_{corr}$  for coated and uncoated steel (Table C.3.(c)) revealed that with coated steel, the corrosion potential is nobler than the uncoated steel . This means that the ZrTiN coatings shifts the corrosion potential to more positive potential values and consequently protects 316 SS from corrosion to a different extent.

In acid solution, rapid corrosion of steel coated with ZrTiN takes place at pores and pinholes in the coating substrate is easily passivated. [55]

Polarisation curves shows a lower corrosion current for  $3\mu$  ZrTiN than for all other thickness and stainless steel. The curve for  $3\mu$  ZrTiN and all other thickness have a similar shape but consistently lower anodic dissolution. A comparisons between coating suggest some improved corrosion resistance was offered by  $3\mu$  ZrTiN .However protection offered is broadly similar. [41,42]

From the potentiodynamic curve, the anodic current density for 1.5 and  $2\mu$  ZrTiN coatings changes a little with potential increasing from  $-200$  mV to the breakthrough potential  $+100$  mV. In this interval, the passive layer protects specimen surface from dissolving. While, anodic current density increases dramatically with potential over

200 mV, probably due to a pitting corrosion mechanism initiated at the local defects of the film. [43]

EIS is a very effective technique to analyze the various steps involved in an electrochemical reaction by measuring the impedance system response to small ac potential signals over a wide frequency range. It provides a lot of information on the corrosion reactions, the mass transport and the electrical charge transfer, especially the localized corrosion of coating/steel system. The Bode spectra of uncoated and coated samples are presented in. Fig 5.C.3(c)(B). The |Z| values for the ZrTiN coated systems are higher than the SS316 substrate, which demonstrates a better corrosion performance of the coated samples. As for the substrate phase curve, resistive behavior was identified at low frequencies, while capacitive behavior was observed at high frequencies. The curve of  $3\mu$  ZrTiN on SS316, show a 'plateau' behavior at phase angle close to  $30^\circ$ . The surface of  $3\mu$  ZrTiN/SS316 system is expected to a very strong capacitive response as the Zr-Ti-N thin films are electrochemical inert with high dielectric constants. Similar behaviour was observed by Li Li et al [43] for TaN thin films deposited cathodic arc deposition system on 317 S.S

As shown in fig 5.C.3.(c).(B) at high frequency the impedance value of coating of all thickness is same. However at low frequency the difference in the impedance is more, indicating difference in resistive behaviour of coating.

The  $1.5\mu$  ZrN coating did not exhibit the best corrosion resistance Fig 5.C.3(c)(P) although it had largest impedance shown in Fig 5.C.3(c)(B). According to the phenomenon in the experiment, it can be explained that the coating was severely attacked under the increasing potential. Similar behaviour was observed by Guosong Wu [63] for electron beam evaporation upper metal oxide thin films on AZ31 magnesium alloy with  $\text{TiO}_2$  or  $\text{Al}_2\text{O}_3$  as donors.

SEM studies were carried out to determine morphology of coating after typical anodic polarization tests in 0.1N HCl

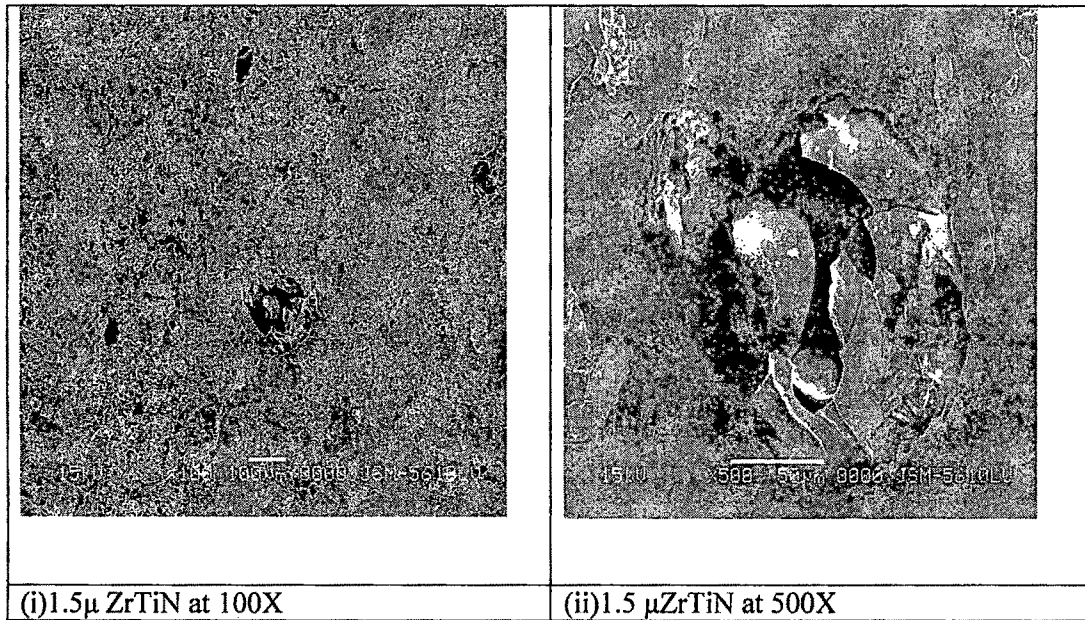


Fig 5.C.3.(c)(S) Typical morphologies of the 1.5 μm Zr TiN coating s which had been subjected to the anodic polarization tests 0.1N HCl at (i) 100X and (ii) 500X).

The SEM micrograph Fig 5.C.3.(c)(S)(i) indicates the small pits on the surface of coating. Fig.5.C.3.(c)(S)(ii) indicate that delamination of coating occurs. However substrate is not observed indicating the superficial damage.

The compositional analysis of coatings after potentiodynamic test was done using EDX attached to SEM

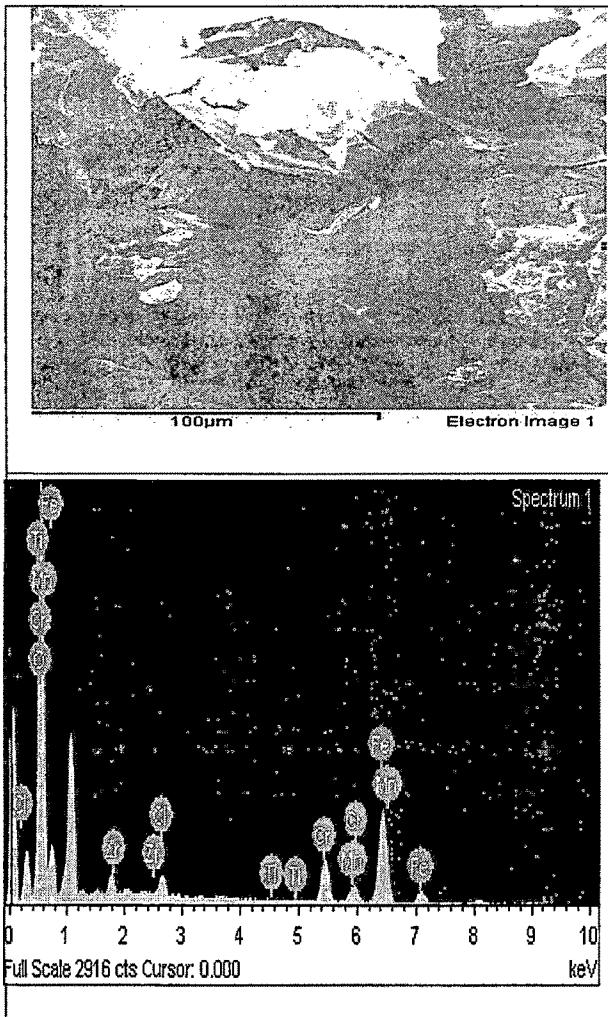


Fig 5.C.3(c)(E)The EDX analysis of 2. 5µ ZrTiN thin film subjected to potentiodynamic test in 0.1N HCl

The EDX analysis at the region near the delamination indicates the removal of coating, since intense peak of iron is observed. Thus additional information about the extent of damage can be obtained by using EDX coupled with SEM.

### 5.C.3 (d) Corrosion behaviour of ZrTiN thin films IN 11pHNaSO<sub>4</sub>

The corrosion behaviour of ZrTiN coatings of varying thickness was measured by potentiodynamic corrosion tests in 11pH Na<sub>2</sub>SO<sub>4</sub> solution.

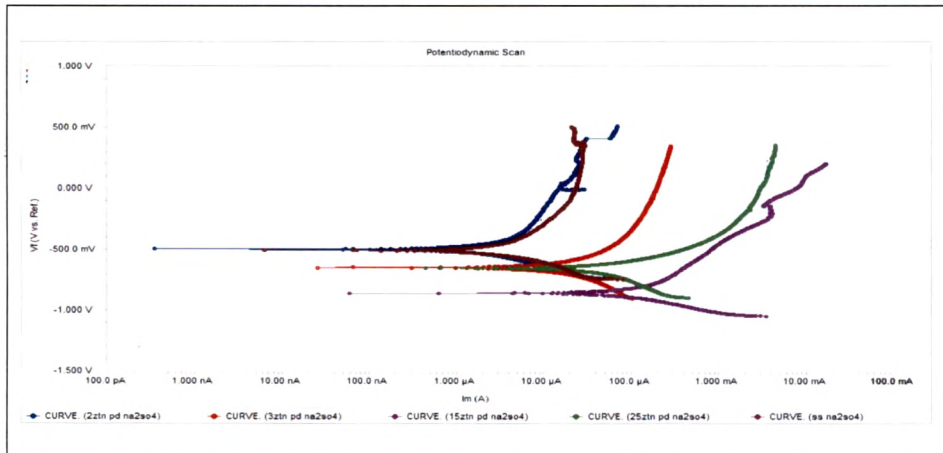


Fig 5.C.3.(d)(P) Potentiodynamic corrosion test of S.S substrate & ZrTiN thin films of varying thickness in 11pH Na<sub>2</sub>SO<sub>4</sub>

11pH Na <sub>2</sub> SO <sub>4</sub>	E <sub>corr</sub> (mV)	I <sub>corr</sub> (µA/cm <sup>2</sup> )	Protective efficiency, P <sub>i</sub> (%)
S.S	-508	5.970	
1.5µ ZrTiN	-858	142.3	
2µ ZrTiN	-496	2.880	52 %
2.5µ ZrTiN	-654	69.00	
3µ ZrTiN	-649	9.310	

Table C.3.(d) Values of corrosion potential (E<sub>corr</sub>) corrosion current density (I<sub>corr</sub>) and protective efficiency for all ZrTiN specimens. in 11pH Na<sub>2</sub>SO<sub>4</sub>

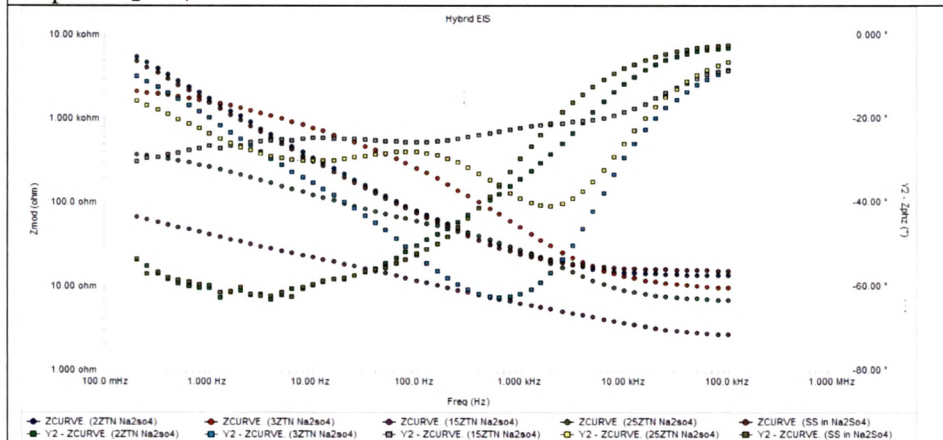


Fig 5.C.3.(d)(B) Electrochemical impedance diagram of ZrTiN thin films of varying thickness. in 11pH Na<sub>2</sub>SO<sub>4</sub>

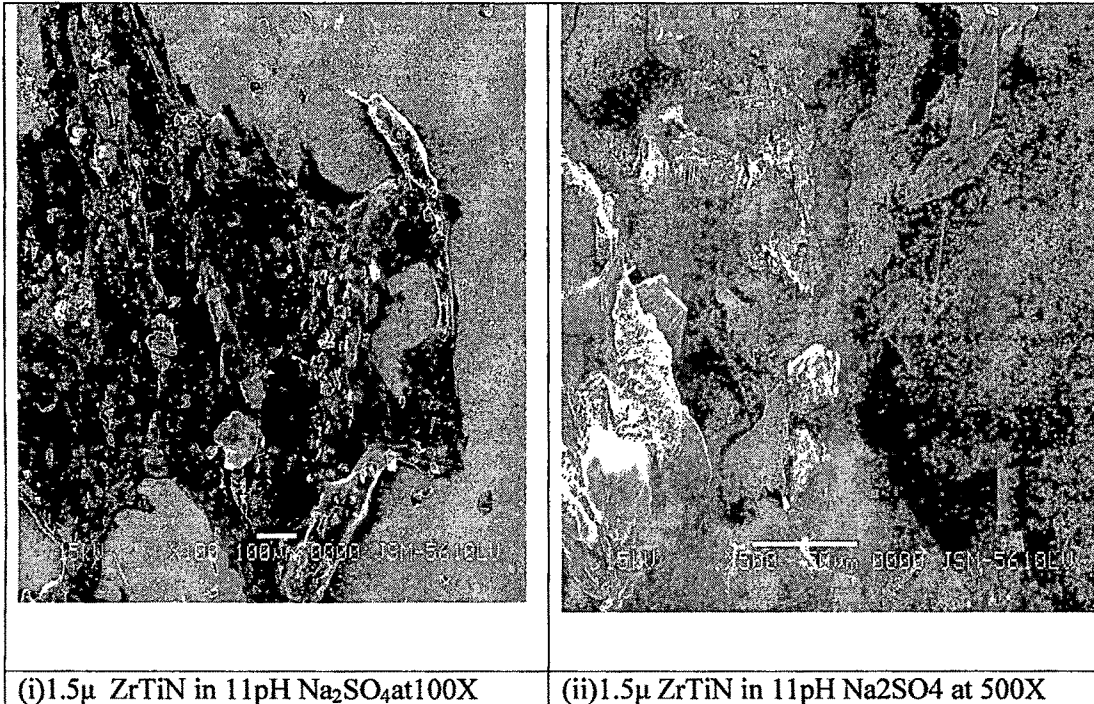
The Tafel plots obtained for steel substrate and ZrTiN coating of varying thickness in 11pH Na<sub>2</sub>SO<sub>4</sub> are shown in Fig 5.C.3.(d)(P) The electrochemical parameters (corrosion current, corrosion potential and % porosity ) calculated from polarization curves are summarized in Table C.3. (d)

The corrosion potential of the steel substrate is about -0.508 V. Large variation in E<sub>corr</sub> of substrate & coatings is observed. The corrosion potential has a lower value than E<sub>corr</sub> of the steel without a coating because the thin coating, having a high porosity, causes an electrochemical heterogeneity of the surface contacting the electrolyte. This heterogeneity is the reason for a physico-chemical instability of the substrate coating system in an aggressive environment. [52]

The corrosion current density is often used as an important parameter to evaluate the kinetics of corrosion reactions. The i<sub>corr</sub> values of all coated samples except 2μ ZrTiN is higher than substrate. This indicates that performance of coating is inferior in given environment. One of the reason for poor performance could be the stainless steel itself is very passive in highly alkaline environment of 11pH Na<sub>2</sub>SO<sub>4</sub> so need for coating is to be excluded..

As indicated in Fig 5.C.3.(d)(B) impedance value of uncoated steel substrate and 1.5μ ZrTiN is of one order inferior to stainless steel substrate. For medium and high range frequency S.S behaves better, however at very low frequency impedance of 2μ ZrTiN is slightly better than S.S. Large variation in impedance is observed at high frequency for all thickness.

SEM studies were carried out to determine morphology of coating after typical anodic polarization tests in 11pH Na<sub>2</sub>SO<sub>4</sub>



(i) 1.5 $\mu$  ZrTiN in 11pH Na<sub>2</sub>SO<sub>4</sub> at 100X      (ii) 1.5 $\mu$  ZrTiN in 11pH Na<sub>2</sub>SO<sub>4</sub> at 500X  
 Fig 5.C.3.(d)(S) Typical morphologies of the 1.5  $\mu$ Zr TiN coating which had been subjected to the anodic polarization tests 11pH Na<sub>2</sub>SO<sub>4</sub>

The SEM micrograph Fig 5.C.3.(d)( S) at low magnification(i) indicates the extent of corrosion on the whole surface .Further investigation at high magnification(ii) indicates presence of pits however the pits does not extent up to the substrate.

The compositional analysis of coatings after potentiodynamic test was done using EDX attached to SEM

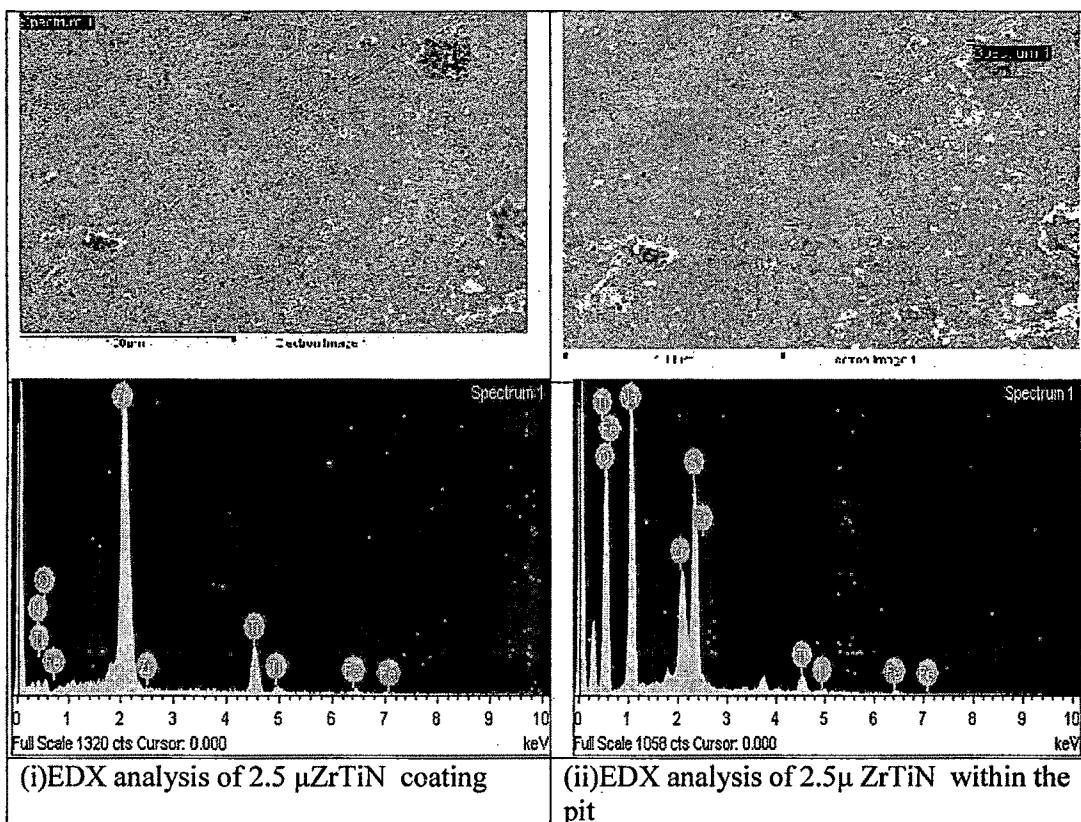


Fig 5.C.3(d)(E)The EDX analysis of 2.5 $\mu$  ZrTiN thin film subjected to potentiodynamic test in 11pH Na<sub>2</sub>SO<sub>4</sub>

EDX analysis in fig Fig 5.C.3.(d)(E)(i) of the coating after anodic polarisation for overall area indicates that intense peak of Zr and smaller peak of Ti. EDX analysis within the pit Fig 5.C.3.(d)(E) (ii) indicates that both Zr and Ti are present but intensity of both the metals is reduced. Also intense peak of sulphur and sodium is observed indicating seepage of sulphate ions to substrate.

### 5.C.3 P Potentiodynamic behaviour of ZrTiN thin film in various environment

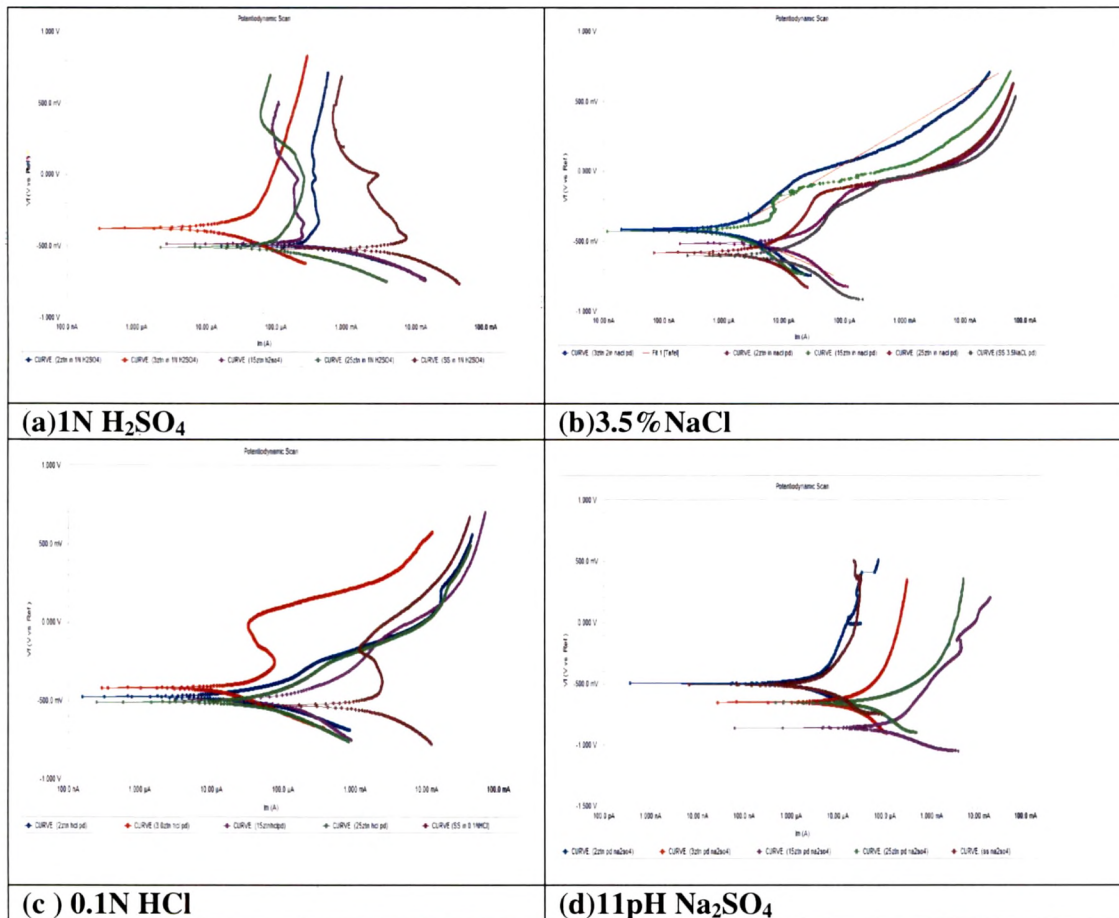


Fig. 5.C.3 P(a,b,c,d)Behaviour of ZrTiN thin films in Various Environment after Electrochemical impedance spectroscopy test

Considering E vs. log I behaviour of ZrTiN coating of various thickness in various environment one tend to conclude that corrosion behaviour is strongly dependent on the environment to which it is subjected to. Highest corrosion resistance is observed in case of 1N H<sub>2</sub>SO<sub>4</sub> (Fig. 5.C.3 P(a)) and 3.5%NaCl (Fig. 5.C.3 P(b)) where as inferior behaviour is observed for 11pH Na<sub>2</sub>SO<sub>4</sub>(Fig. 5.C.3 P(d)) and 0.1N HCl(Fig. 5.C.3 P(c)) The E<sub>corr</sub> in case of 11pH Na<sub>2</sub>SO<sub>4</sub> shifted to lower E<sub>corr</sub> and higher current density value than 1N H<sub>2</sub>SO<sub>4</sub>, whereas in case of 3.5%NaCl and 0.1N HCl both displayed same E<sub>corr</sub> value however domain of anodic current density is higher in 0.1N HCl.

Large variation in the  $E_{corr}$  value for various thickness is observed in case of 11pH  $\text{Na}_2\text{SO}_4$  and 3.5%NaCl indicating influence of sodium ions on corrosion behaviour.

### 5. C .3 B Electrochemical impedance behavior of ZrN thin films in various environment

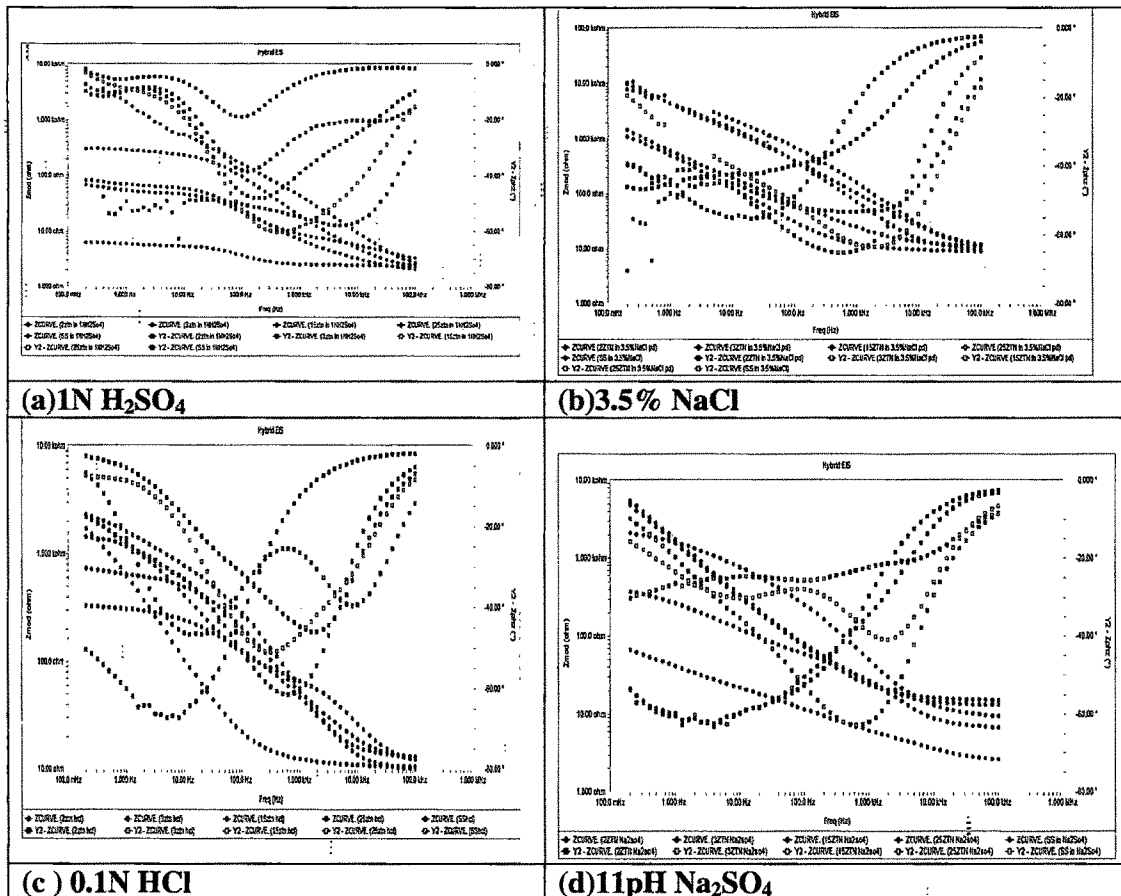


Fig. 5.D.3.B(a,b,c,d) Behavior of ZrTiN thin films in Various Environment after Electrochemical impedance spectroscopy test

Maximum variation in the impedance value at low frequency is observed in case of 1N  $\text{H}_2\text{SO}_4$ (Fig. 5.C.3 B(a)) indicating variation in resistive response of coating. In case of 11pH  $\text{Na}_2\text{SO}_4$ (Fig. 5.C.3 B(d)) at high frequency the variation in impedance value for coating of different thickness is of the one order of magnitude hence variation in capacitive response.

Breaking in impedance curve of 2.5 $\mu$  ZrTiN in 3.5%NaCl indicates the incomplete passivity of coating in that environment(Fig. 5.C.3 B(b))

## 5.D WEAR CHARACTERISATION

A pin-on-disk tribometer was used to evaluate the Wear resistance of as-deposited Ti-N, ZrN and Zr-Ti-N coating of varying thickness. The instrument measured the tangential force between the two contacting surfaces while a normal force of 4Kg was applied. The coefficient of friction was calculated and its value as a function of time was plotted as the tests progressed.

The surface characterization of the worn surfaces after friction and wear tests was conducted using a scanning electron microscope SEM JEOL JSM 5610LV and Hitachi 3400. The accelerating voltage was 15 kV and images were captured using a secondary electron and back scattered electron detector. The working distance was 39 mm. The chemical analysis of debris from the tests was analyzed using EDX attached with SEM.

The wear mechanism varies with composition of coating, thickness of coating and process parameters of film formation. [70]

In the present research work since composition and process parameter for formation of coating is kept constant, thickness of coating plays a major role in determining wear behaviour of coating. Based on the experimental data and the results of microscopic studies the dominant mechanisms responsible for the friction behaviour are evaluated and the role of material transfer is discussed.

PVD coatings produce very hard, low friction surfaces, but due to inherent compressive stresses may be susceptible to coating fracture and delamination under high normal load sliding wear conditions. [11]

The XRD analysis (Fig 5.B.1(ii)) indicates presence of  $Ti_2N$  phase for all thickness. Nodel et al [11] carried out plasma nitriding of TiAlV alloy and confirmed the presence of mixed TiN/ $Ti_2N$  structure. The adhesion of the  $Ti_2N$  film to the substrate is greater than that of the TiN coating, due to the more gradual transition of hardness and elastic modulus across the coating/substrate interface. Any cracking of the coating resulting from substrate deformation is therefore more likely to lead to higher localized coating loss through decohesion and therefore greater mass loss and further deformation of the substrate.

### 5.D.1 WEAR CHARACTERISATION OF Ti-N THIN FILM

#### 5. D.1 (a) Wear Behaviour of 1.5 $\mu$ Ti-N Thin Films:

After the wear tests, the morphologies of each wear scar were observed by scanning electron microscopy (SEM)(HITACHI 3400 and JOEL 5610) Furthermore, the chemical compositions of the micro-zones inside the scars were characterized by energy dispersive X-ray spectrum coupled to SEM

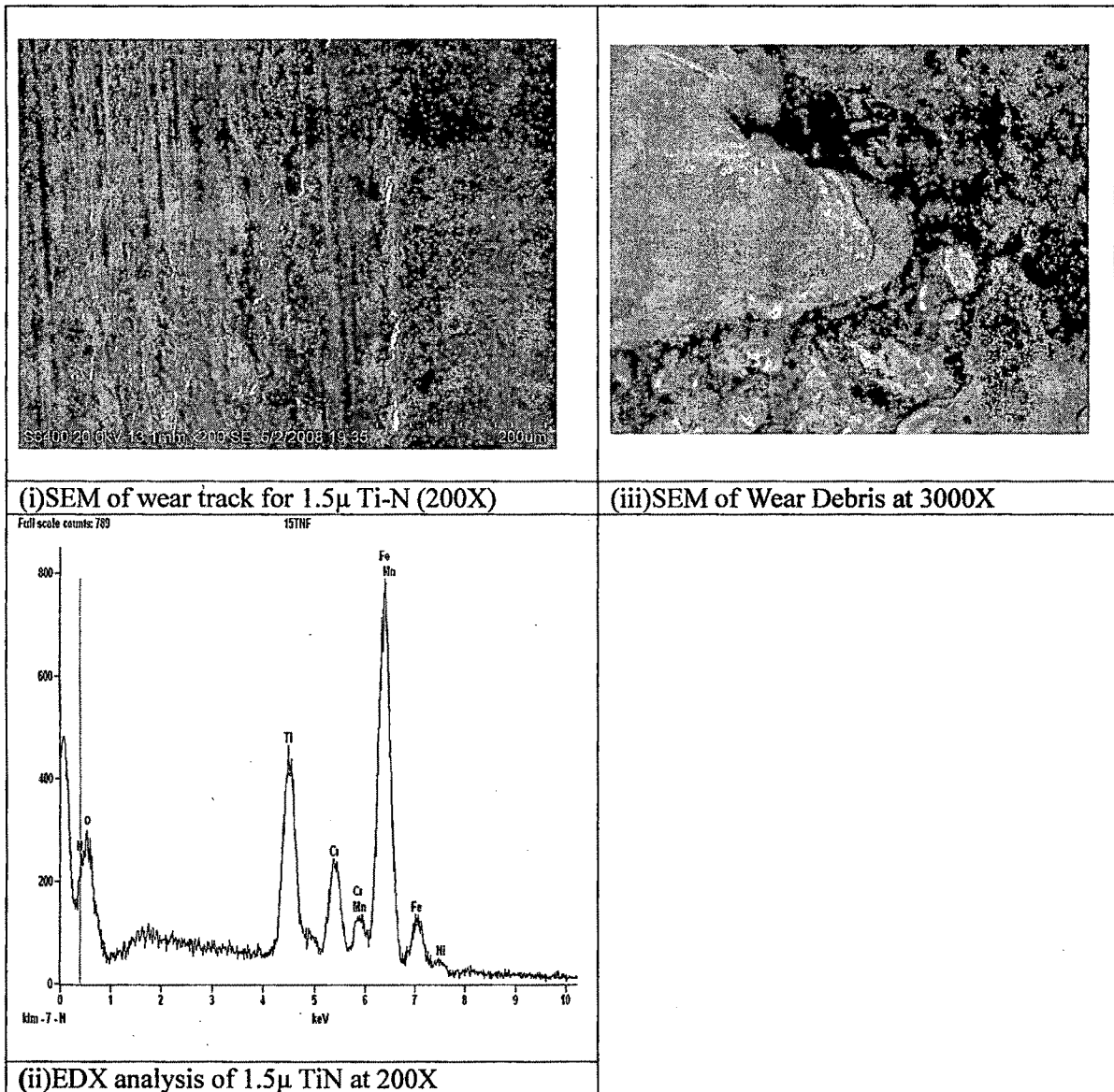
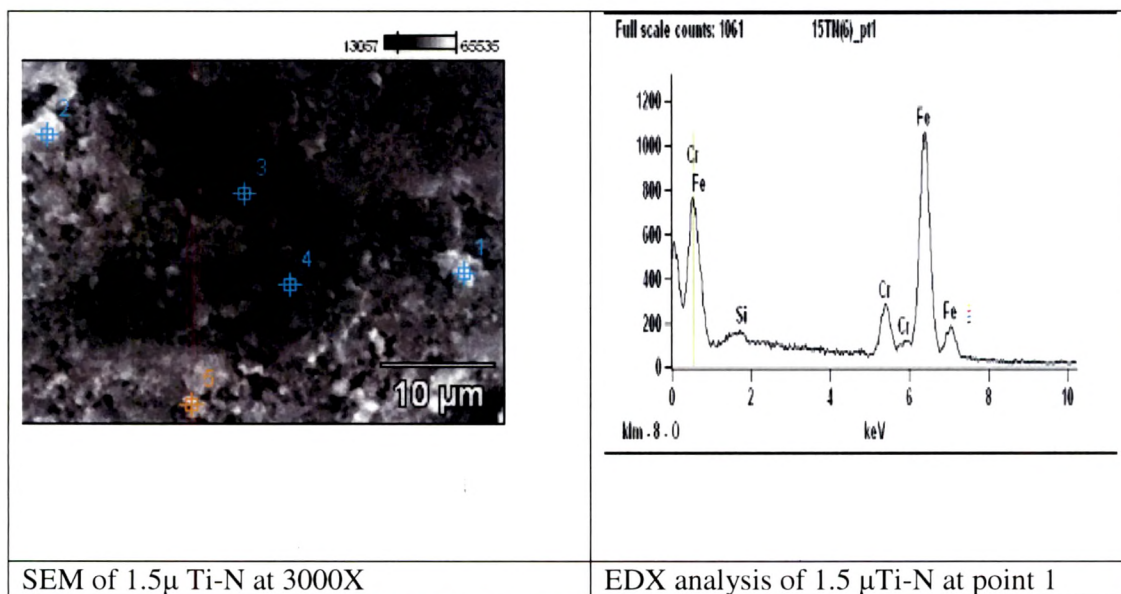


Fig 5. D.1 (a) (I) SEM(i& iii at 200X and 3000X) and EDX analysis(ii at 200X) of 1.5  $\mu$  Ti-N after wear testing

Fig 5. D.1.(a)(I) show the typical profiles of the wear scars of the coatings after ball-on-disc wear test. Fig 5.D.1.(a) (I) (i) shows the shallow ploughing grooves on the surface of specimen. Some pores corresponding to removal of Ti rich macroparticles are observed. EDX analysis (ii) indicates the intense peak of iron and small peak of Ti and oxygen. SEM analysis at high magnification (iii) within the wear track shows flaky and very fine-grained submicron sized wear debris particles. Microgrooves are formed which are associated with crack nucleation on surface, subsequent crack propagation and finally loose particles of large size are trapped and dragged along resulting in formation of macro grooves.[70]Plate shaped particles are observed in wear debris indicative of ploughing wear, nucleation and propagation of subsurface cracks or plastic shear in asperity contact.[71]

The damage pattern indicates that plastic deformation occurred to some extent via ploughing and wedge formation. The results are similar as obtained by [72]

To determine composition of wear debris within the wear track, EDX analysis within the wear track at high magnification was carried out.



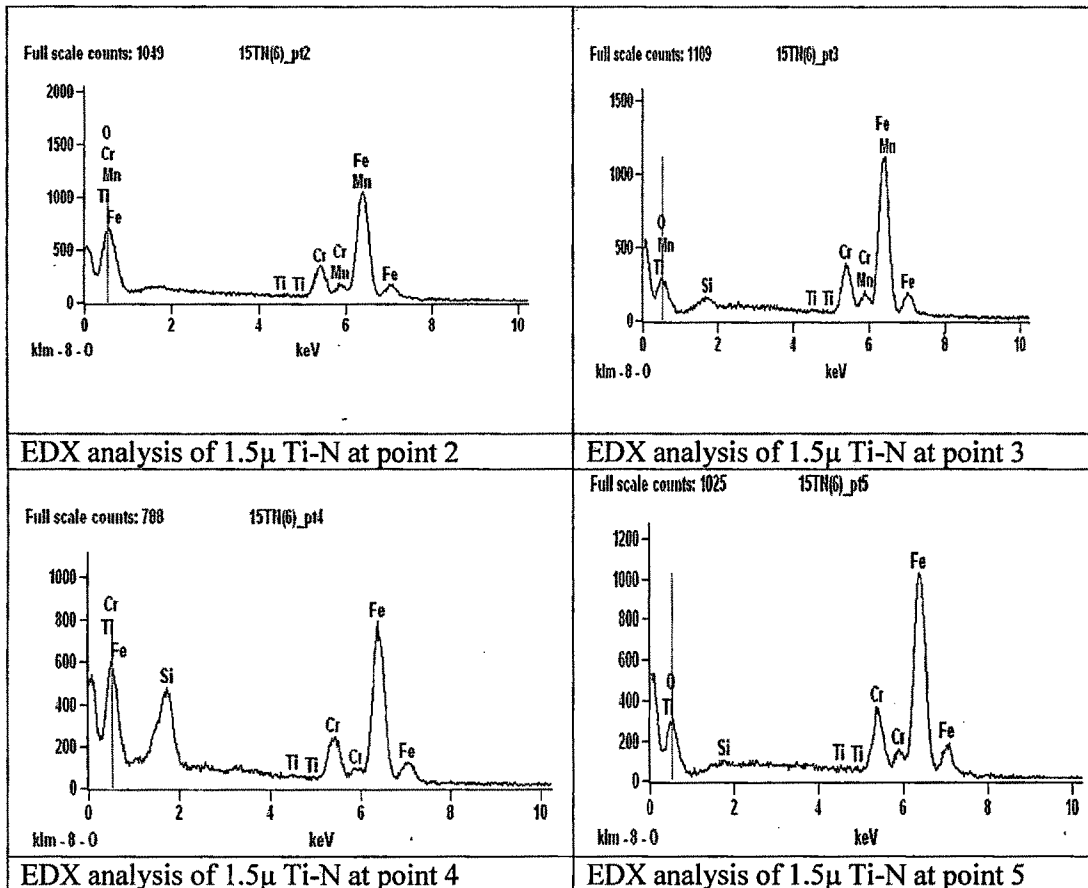


Fig 5.D.1. (a) (II) EDX analysis of Wear Track at various points in 1.5 $\mu$  Ti-N after wear testing.

EDX composition analysis for the coatings at various points as in Fig 5.D.1(a)(II) indicates the presence of Fe, O and Ti species. At point 1 intense Iron peak is observed, point 2, equal proportion of Fe and O is obtained & less intense peak of Ti, at point 3 intense peak of Fe and less intense peak of O is observed, similarly more intense peak of Fe is observed at point 5 compared to 4 i.e., the debris composed mainly of FeO<sub>2</sub> /FeO /TiO<sub>2</sub> or FeTiO<sub>3</sub> compound. The absence of nitrogen in the debris indicated that the generated particles were thoroughly oxidized.

This result showed that the mass transfer from the steel substrate may have happened during the sliding wear test and debris and wear track may have been oxidized during the sliding wear process. Thus the oxidation due to tribo-chemical reaction was the main degradation process. [72, 14]

The friction coefficient values are different for the coatings depending on the time traveled. Fig 5.D.1.(a) (III) shows the friction coefficient of the 1.5  $\mu$  Ti-N coatings with time when sliding against EN24 steel ring.

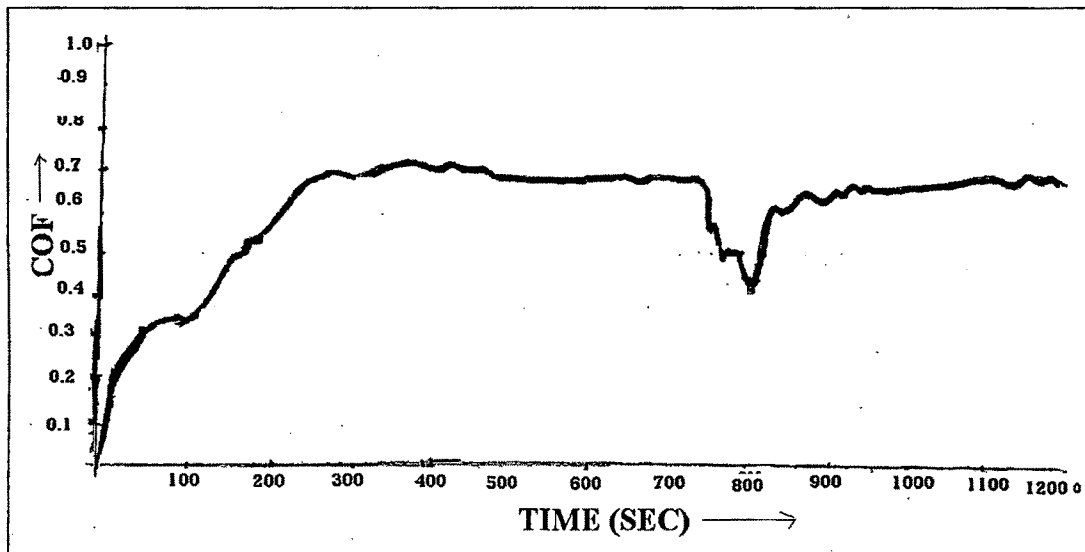


Fig 5. D. 1. (a) (III) variation in COF(Coefficient of friction) with time for 1.5  $\mu$  Ti-N thin film after wear testing.

The increase in COF is equivalent to loss of lubrication layer which promotes localized fracture and wear debris formation. The COF of 1.5 $\mu$  Ti-N coating is 0.600. SEM of original 1.5  $\mu$  Ti-N, Fig 5.A.1 (a) indicates presence of large number of macroparticles.

As indicated by Moulzolf et al [73] initial rapid rise of COF against sliding distance implies that friction mechanism is dominated by formation of wear debris in the interface. A friction value is associated with the removal of macroparticle, decrease is associated with ejection of wear particle (about 800 sec in Fig 5.D.1(a)(III)) and subsequent increase is associated with generation and entrapment of wear particles. [74]

### 5.D.1 (b) Wear Behaviour of 2.0 $\mu$ Ti-N Thin Films

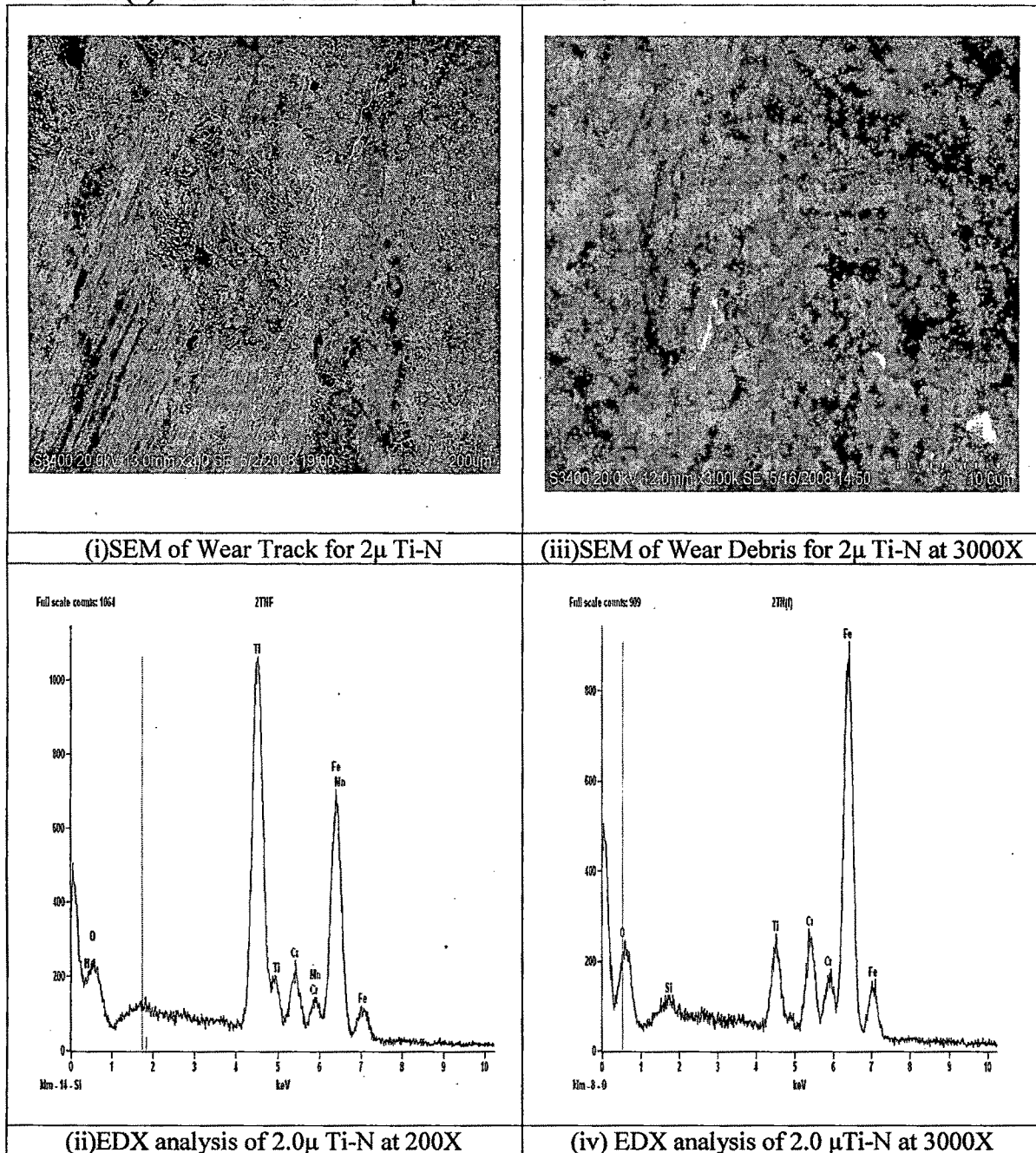


Fig 5.D.1.(b)(I) SEM(i& iii at 200X and 3000X) and EDX analysis(ii & iv at 200X & 3000X) of 2.0  $\mu$  Ti-N after wear testing

The Fig 5.D.1.(b)(I) show the typical profiles of the wear scars of the coatings after ball-on-disc wear test. Fig 5.D.1.(b)(I) (i) shows the accumulation of wear debris near the

interface of coating and wear track. Some pores corresponding to removal of Ti rich macroparticles are observed. EDX analysis (ii) indicates the intense peak of Ti and weak peak of iron and oxygen. SEM analysis at high magnification (iii) within the wear track shows compact and very fine-grained submicron sized wear debris particles. EDX analysis at high magnification indicates intense peak of iron and weak peak of Ti indicating removal of Ti-N coating. Very less quantity of small spherical shape particles are observed in wear track, the reason being, wear particles may not escape from interface to become loose debris and some remain trapped and appear as spherical. The damage pattern indicates that plastic deformation occurred via adhesive wear. [71]

The friction coefficient values are different for the coatings depending on the time traveled. Fig 5.D.1.(b)(II) shows the friction coefficient of the 2.0  $\mu$  Ti-N coatings with the time when sliding against EN24 steel ring.

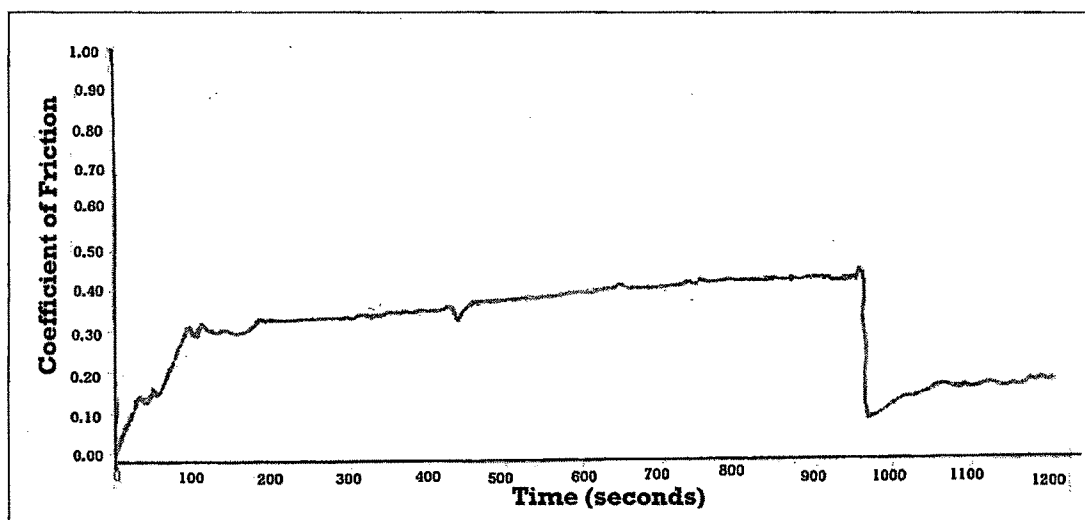


Fig 5.D.1.(b)(II) Variation in COF(Coefficient of friction) with time for 2  $\mu$ Ti-N after wear testing.

The COF of 2 $\mu$  Ti-N coating is 0.325. Less amount of wear debris in the wear track is reflected in terms of low COF. As shown in Fig 5.D.1.(b)(II) the COF values can be related with SEM observations of wear scars on Ti-N coating confirmed that the rise in friction occurred with increasing transfer of debris to the tracks. The wear tracks

corresponding to low COF have very little debris and when COF is high (0.6) debris cover about 80% of wear track.[8]In the present work also high COF in 1.5 $\mu$  Ti-N(0.600) has high amount of debris in the wear track and 2 $\mu$  Ti-N(0.325) has less amount of debris in wear track.[75]

As indicated by Z.P. Huang et al, [76] the curves of friction coefficient vs sliding distance/time for the coatings investigated are characterized by the initial transient state and the steady state. Ploughing actions of the hard asperities of the coating surface and material transfer from the slider to the coating surface play an important role in determining the friction behaviour of the initial transient state and steady state respectively. [83]

The drop in the friction in plastic contacts Fig 5.D.1.(b)(II) (@1100 sec) is associated with ejection of wear particles and a subsequent increase is associated with generation and entrapment of wear particles. [74]

**5.D.1 (c) Wear Behaviour of 2.5 $\mu$  Ti-N Thin Films**

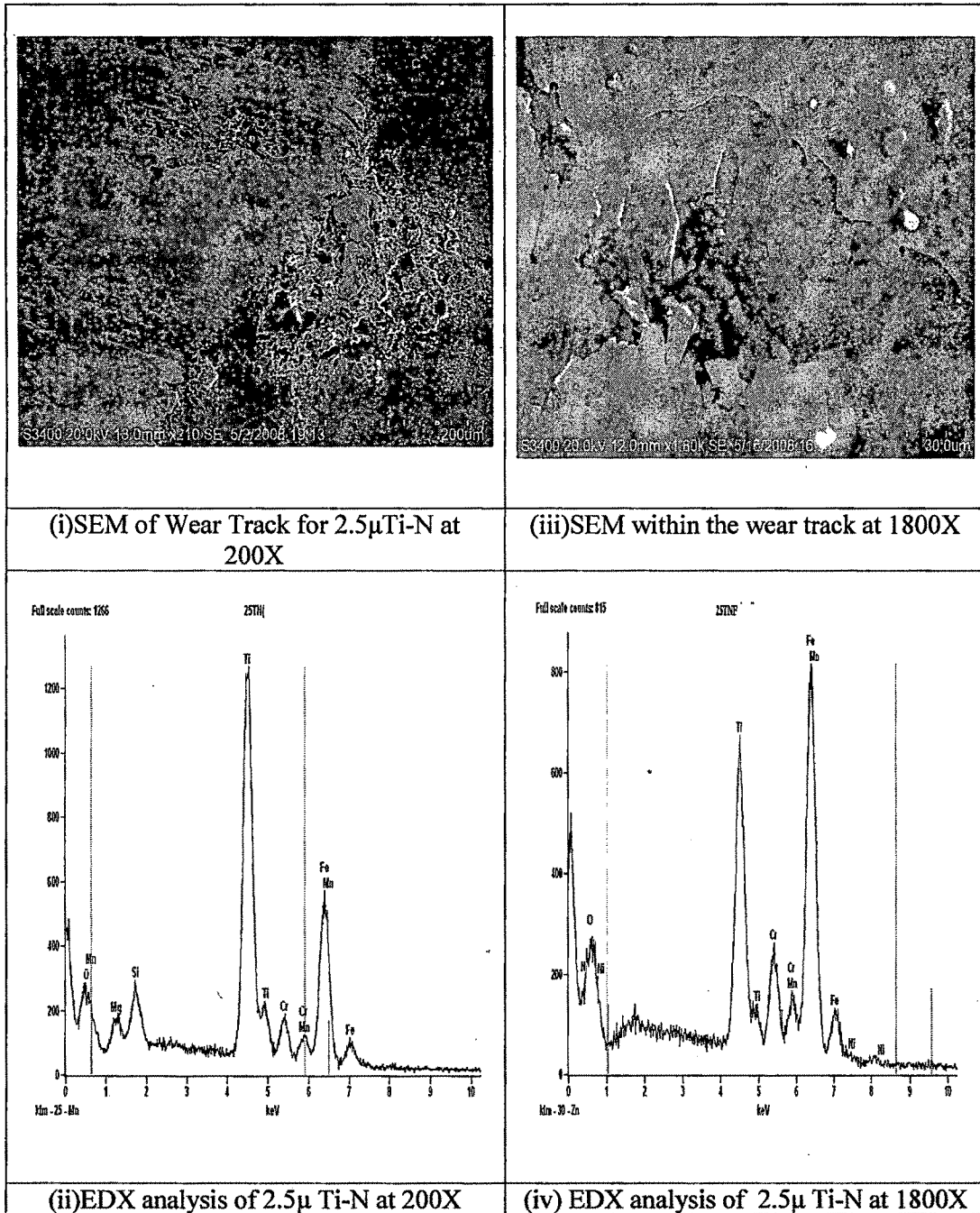


Fig 5.D.1.(c) (I) SEM (i& iii at 200X and 3000X) and EDX analysis (ii & iv at 200X & 3000X) of 2.5 $\mu$  Ti-N after wear testing.

Fig 5.D.1.(c)(I) shows the typical profiles of the wear scars of the coatings after ball-on-disc wear test. Fig 5.D.1.(c)(I) (i) Smooth wear track is observed and wear products are

present at the interface between coating and substrate. EDX analysis (ii) indicates the intense peak of Ti and weak peak of iron and oxygen. SEM analysis at high magnification (iii) indicates that the film worn off only at some locations. Delamination may have originated from either a surface crack or a macroparticle. Similar behaviour is observed by A. Chatterjee et al. [77]. EDX analysis Fig 5.D.1.(c)(I)(iv) at high magnification indicates intense peak of iron and less intense peak of Ti. Slight reduction in intensity of Ti peak at high magnification (within wear track) compared to that at low magnification large coverage area, indicating incomplete removal of coating. Irregular shaped particles are observed within the wear track indicating wear debris are produced by detachment of transferred fragments in adhesive wear and brittle fracture. [71]

The friction coefficient values are different for the coatings depending on the time traveled. Fig 5.D.1.(c)(II) shows the friction coefficient of the 2.5  $\mu$  Ti-N coatings with the time when sliding against EN24 steel ring.

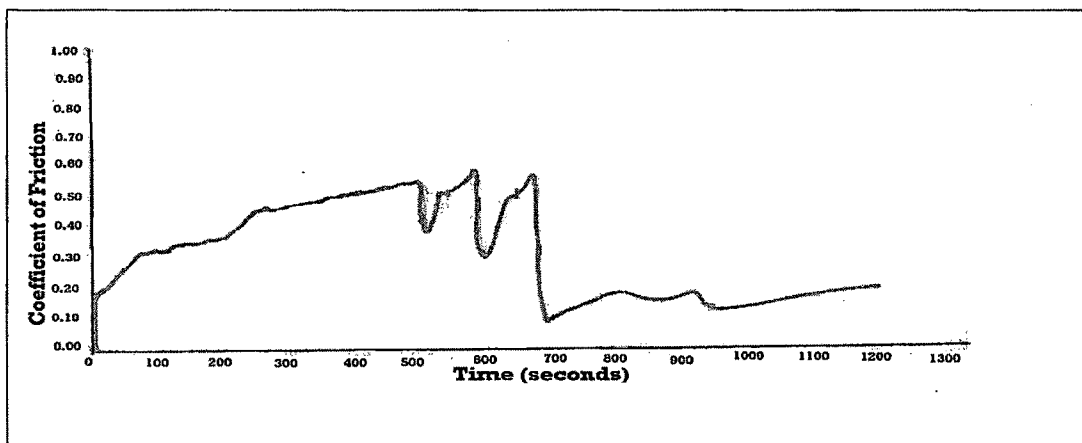


Fig 5.D.1.(c)(II) Variation in COF (Coefficient of friction) with time for 2.5  $\mu$  Ti-N after wear testing.

The COF of 2.5  $\mu$  Ti-N coating is 0.300. COF values can be related with SEM (Fig 5.D.1.(c)(I)(iii)) less amount of wear debris in the wear track is reflected in terms of low COF. The initial increase in COF (Fig 5.D.1.(c)(II)) is associated with ploughing because of roughening and trapped wear particles. The drop in the friction (after 500 sec) about in plastic contacts is associated with ejection of wear particles, and a subsequent increase is associated with generation and entrapment of wear particles. [74]

**5.D.1 (d) Wear Behaviour of 3.0 $\mu$  Ti-N Thin Films**

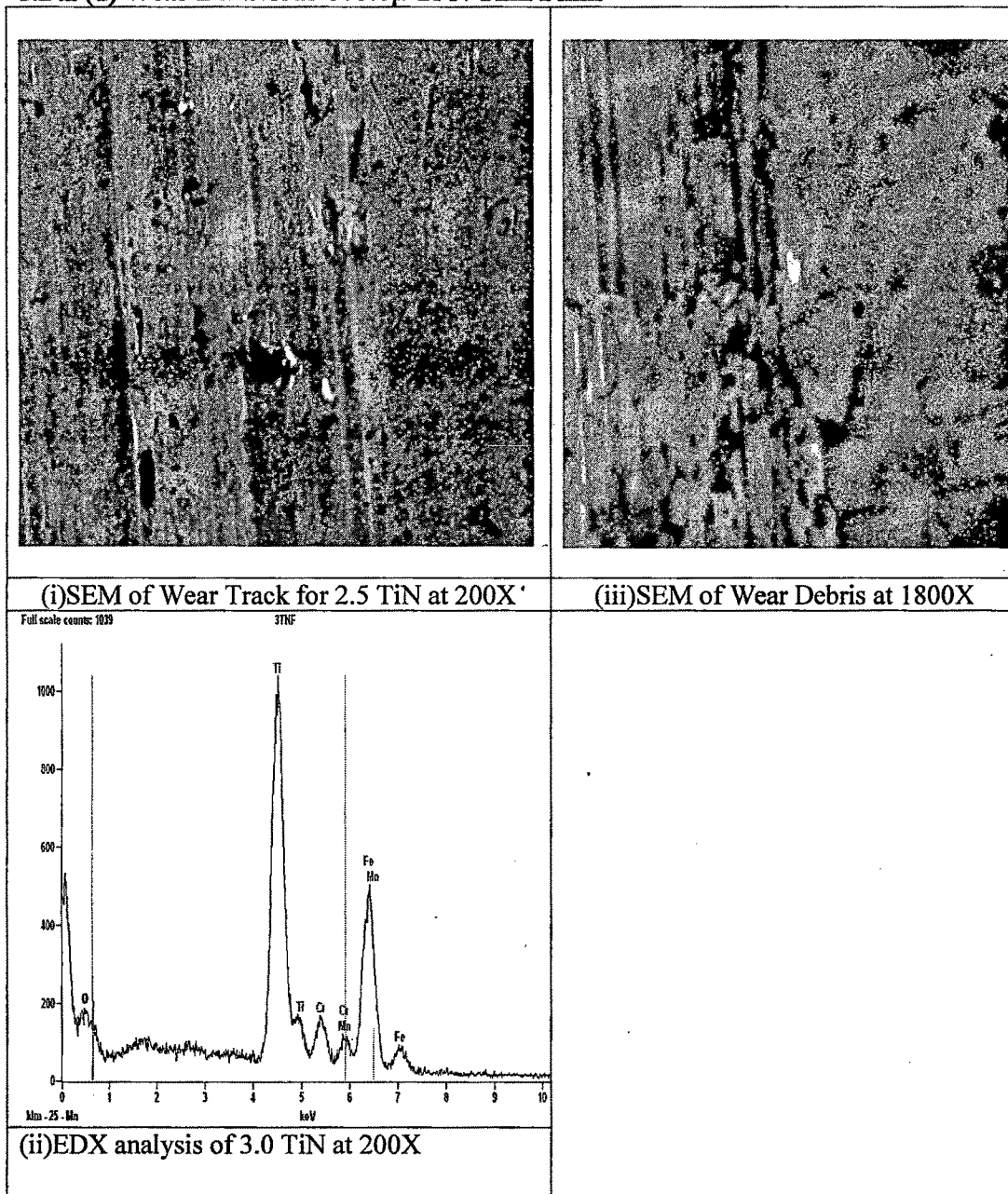


Fig 5.D.1.(d)(I)SEM(i& iii at 200X and 3000X) and EDX analysis(ii at 200X) of 3.0 $\mu$ Ti-N after wear testing.

Fig 5.D.1.(d)(I) show the typical profiles of the wear scars of the coatings after ball-on-disc wear test. Fig 5.D.1.(d)(I) (i) Grooves are observed on the wear track (ii) indicates the intense peak of Ti and weak peak of iron and oxygen indicating that Ti-N coating is

intact. SEM analysis at high magnification (iii) indicates formation of a continuous and thick debris layer covered on the center of wear scar, which was formed during the tribo-oxidation process by repeated grinding and rubbing similar behaviour is observed by J.L. Moa et al [4] for TiAlN coatings were deposited on cemented carbide by the arc-physical vapor deposition. Irregular shaped particles are observed within the wear track indicating wear debris are produced by detachment of transferred fragments in adhesive wear and brittle fracture. [71]

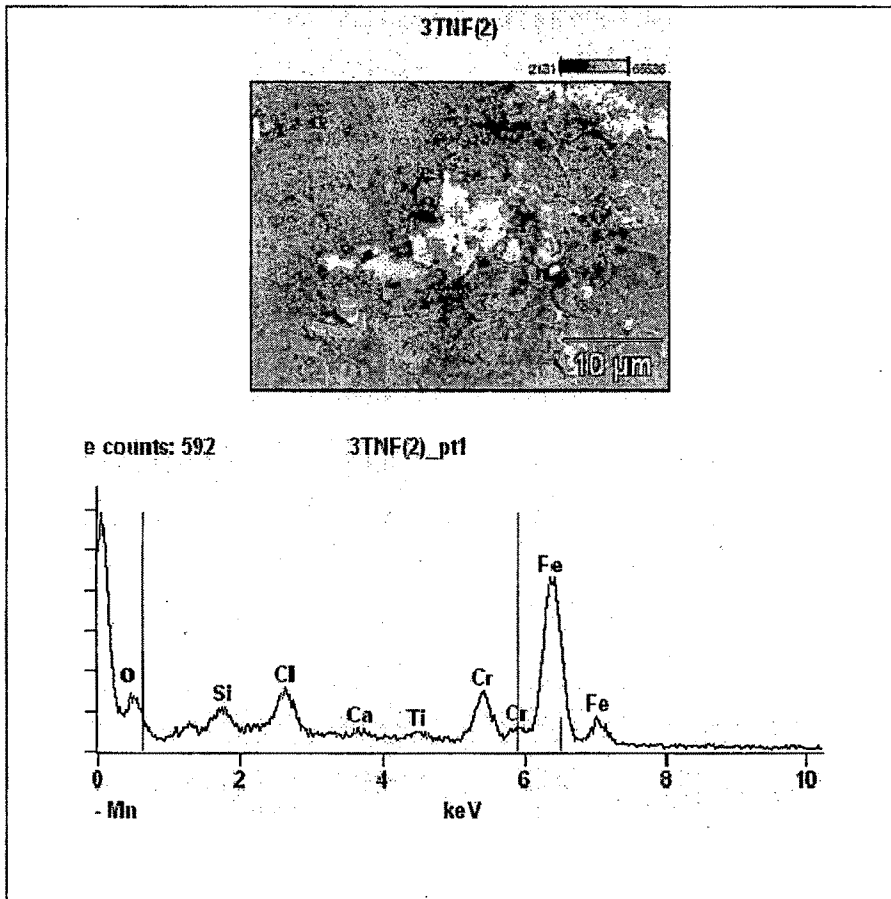


Fig 5. D.1.(d)(II)EDX analysis of particle in wear track of 3 μ Ti-N after wear testing.

As observed by Pranay Asthana et al [78] wear behaviour of boriding heat treatment on pure iron was performed in a solid medium by using commercial EKabor powder and they observed some white particles at the edges of the debris layer indicating the oxidation of pure iron. The white coloring in Fig 5.D.1(d)(II) is due to the electron charge accumulation on the sample surface under the SEM because of conductivity.

Hence white particles in all the SEM indicate presence of FeOx. However the debris formed during sliding wear may contains some amount of TiOx in addition to FeOx [78,79]. Further analysis with more sophisticated instruments like SAD,XPS and TEM are required to confirm the same.

The friction coefficient values are different for the coatings depending on the time traveled. Fig 5.D.1(d)(II) shows the friction coefficient of the 3.0  $\mu$  TiN coatings with time when sliding against EN24 steel ring.

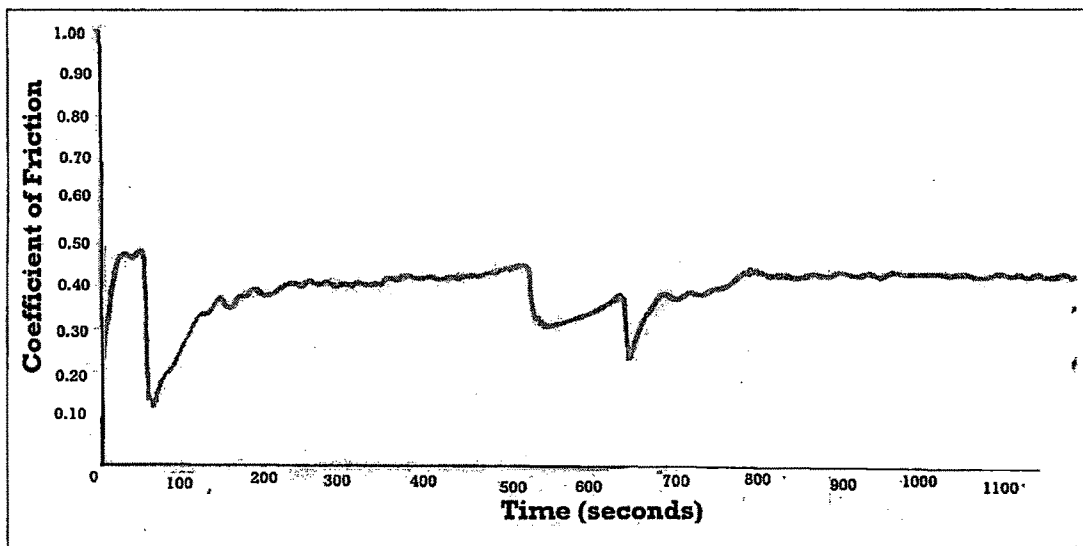


Fig 5.D.1.(d)(II) Variation in COF(Coefficient of friction) with time for 3.0 $\mu$  Ti-N after wear testing

The COF of 3.0  $\mu$  Ti-N coating is 0.321. The initial increase in COF is associated with ploughing because of roughening and trapped wear particles remaining within the wear track. [73]SEM Fig 5 .D.1(d) (iii) and COF values, Fig 5.D.1.(d)(II) can be related the thick and rough debris layer on the wear track causes the COF of Ti-N coating fluctuating during the steady wear stage.[74]

**5.D.1 (e) Wear Behaviour of 4.0 $\mu$  Ti-N Thin Films**

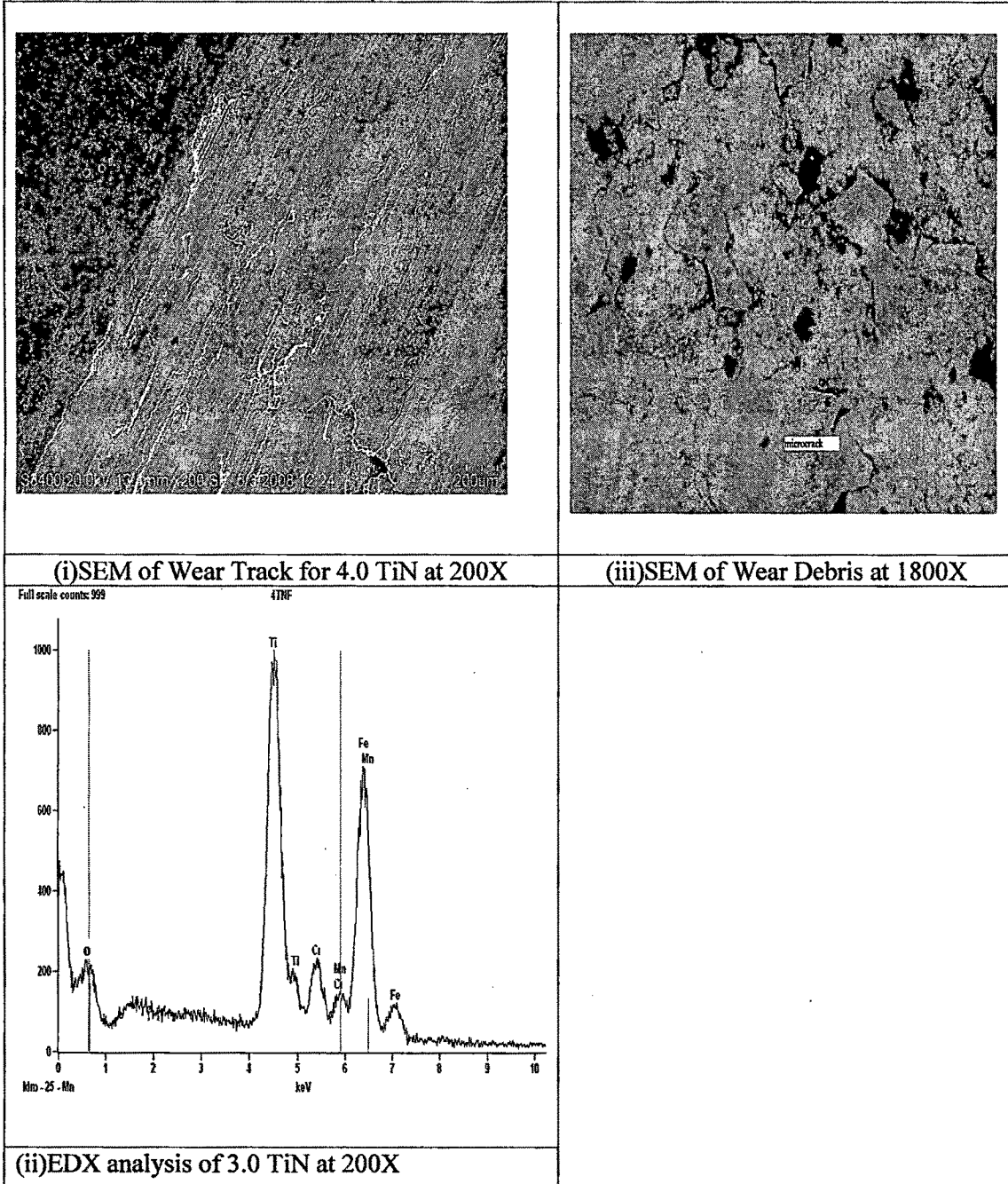


Fig 5.D.1.(e)(I)SEM(i& iii at 200X and 3000X) and EDX analysis(ii at 200X) of 4.0 $\mu$  Ti-N after wear testing.

Fig 5.D.1.(e)(I) show the typical profiles of the wear scars of the coatings after ball-on-disc wear test. Fig 5.D.1.(e)(I) (i) Shallow grooves are observed. There is crack perpendicular to sliding direction within the coating is observed on the wear track.

The explanation for this is when the plastic deformation of substrate is exceeded material causes the formation of micro-cracks, where the intersection of these cracks results in material removal after repeated sliding contacts. SEM micrographs Fig 5.D.1(e)(I) (i) shows the formation of cracks transversal to the sliding direction. Similar results were obtained by [70]. The deep degradation results from a crack propagation perpendicular to the substrate plane, leading to the formation of large debris. [80] (ii) indicates the intense peak of Ti and weak peak of iron and oxygen indicating that Ti-N coating is intact. SEM analysis at high magnification (iii) indicates incomplete removal of coating and absence of the wear debris.

The friction coefficient values are different for the coatings depending on the time traveled. Fig 5.D.1(e)(II) shows the friction coefficient of the 4.0 $\mu$  Ti-N coatings with the time when sliding against EN24 steel ring

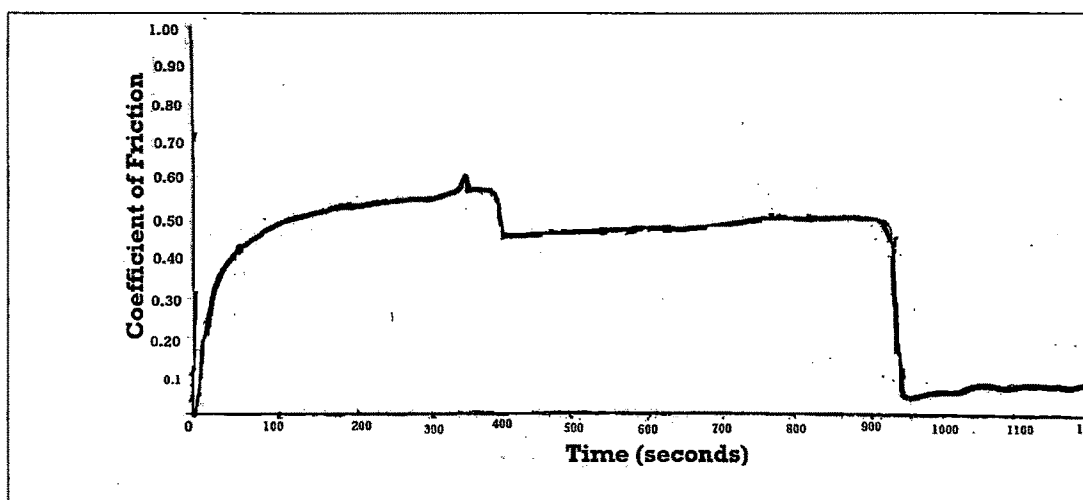


Fig 5.D.1(e)(II) Variation in COF (Coefficient of friction) with time for 4.0 $\mu$  Ti-N after wear testing.

The COF of 4.0 $\mu$  Ti-N coating is 0.284. SEM Fig 5.D.1(e)(I) and COF values can be related. The drop in the coefficient of friction in 4.0 $\mu$  Ti-N ( Fig 5.D.1(e)(II)(iii)) is associated with smoothing of the two hard surfaces experiencing plastic deformation. The absence of adhesive wear and little or no third body interaction result in low friction coefficients similar results were observed by [80,81]

### 5.D.1 Comparison of COF for all thickness of Ti-N Coating

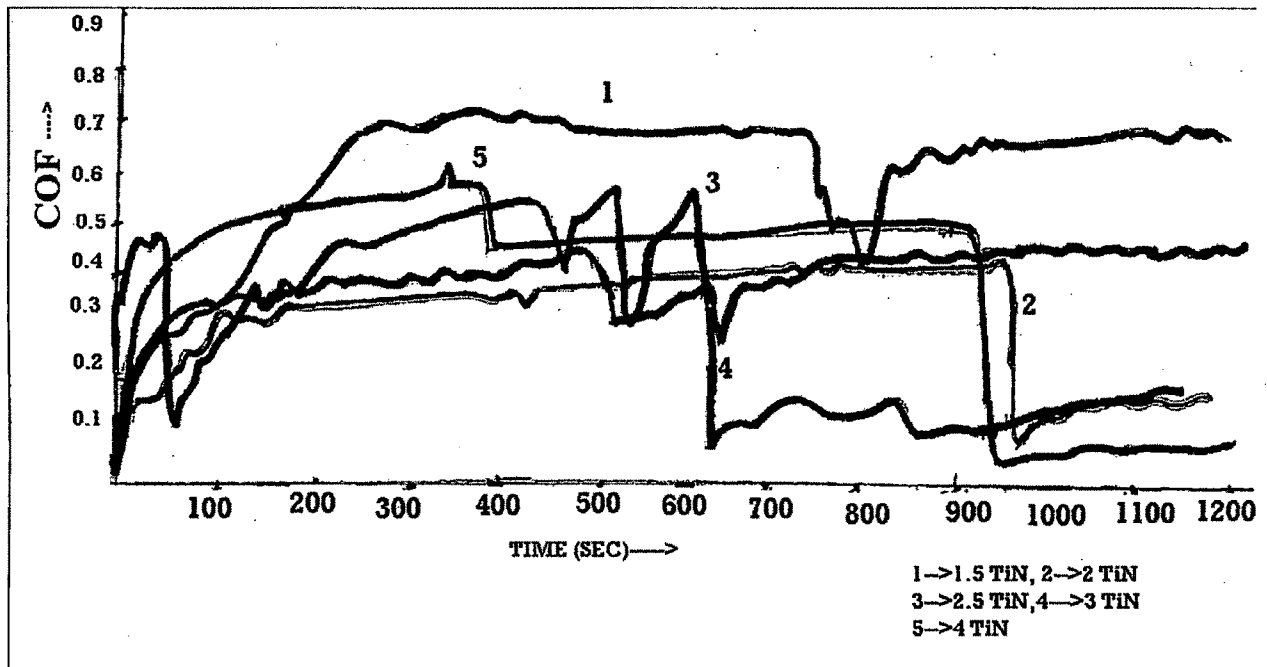


Fig. 5.D.1.(abcde) COF Vs Time for all thickness of Ti-N coating after wear testing.

Increased friction between the contacting bodies not only reduces the mechanical efficiency of tribosystem and increase frictional heating, but also influences distribution of contact stresses in the near surface region. Increasing the friction coefficient of the contacting pair will increase the maximum shear stress and move it towards the surface. Accordingly, it is necessary to study the friction behaviour of various wear-resistant ceramic coatings so as to take appropriate means to reduce friction of the contact pairs.[76]

Typical curves of coefficient of friction vs. Sliding distance and time for all thickness is illustrated in Fig. 5.D.1.(abcde). The changes in wear resistance due to increase in thickness is due to difference in hardness of resultant coating and the adhesive strength between film and substrate. [11]

The initial wear was related to the surface state of the specimen,[2] and microstructure.[82,83] The macroparticles existing on the sample surface played an important role in this stage. All the coatings except 1.5 $\mu$  TiN had similar run-in friction coefficient values. The friction coefficient of 1.5 $\mu$  TiN coating increase rapidly due to the

presence of titanium-rich particles of rounded morphology and these particles have a different distribution over the coatings surface. Metallic titanium adheres to the steel ball, and therefore notably contributes to the increase in the friction coefficient value.[84]

During sliding, changes in the conditions of mating surfaces occur which affect friction and wear properties. After some period, the so-called “run-in,” “break-in” or “wearing-in” period, the friction force generally stabilizes into what is called steady-state sliding.[74] This wearing period is usually taken as the criterion for evaluating the wear resistance of materials. The wider this period, the better the wear resistance.[2] In general, friction is believed to be result from three components: adhesion, ploughing and asperity deformation.

The increase in COF can be attributed to two effects which play in synergetic way .From one side consumption of the protective layer leaves the surface more weak against wear and on other hand debris produced increases COF. [74]

The 1.5 and 2.5  $\mu$  TiN coating exhibited a different debris removing morphology from the 3 $\mu$ TiN coating at the edge of the wear scar. The debris (tribo-chemical products) of the 2.5 $\mu$  & 3 $\mu$  TiN coating was ejected out and accumulated around the edge, while the debris of the 3 $\mu$ TiN coating was difficultly to be ejected out the wear scars. The fluctuation of the COF of 3 $\mu$  TiN coating during the steady wear stage was probably induced by the accumulation of debris on the wear scars and carrying the imposed load caused from debris at the contact interface. [4]

Although COF of 2.0 $\mu$  Ti-N (0.235) thin film is lower than 4.0  $\mu$  TiN(0.284) thin film, the wear resistance of 4.0 TiN is better because of large steady state sliding.

## 5. D.2 WEAR CHARACTERISATION OF ZrN THIN FILMS

### 5. D 2 (a) Wear Behaviour of 1.5 $\mu$ ZrN Thin Films

After the wear tests, the morphologies of each wear scar were observed by scanning electron microscopy(SEM) (HITACHI 3400 and JOEL 5610LV) Furthermore, the chemical compositions of the micro-zones inside the scars were characterized by energy dispersive X-ray spectrum.

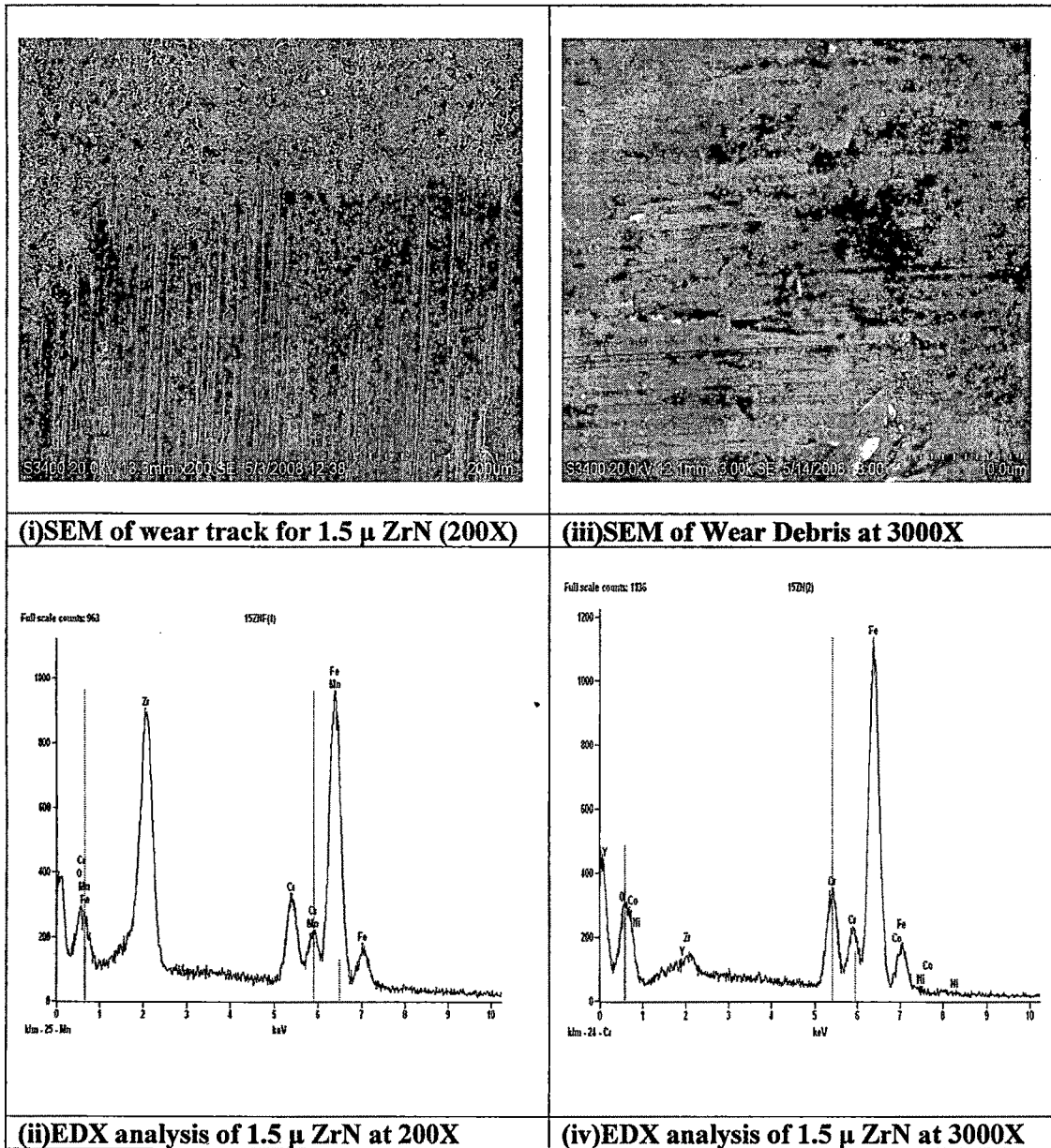


Fig 5.D.2.(a)(I)SEM(i& iii at 200X and 3000X) and EDX analysis(ii & iv at 200X & 3000X ) of 1.5 $\mu$  ZrN after wear testing.

Fig 5. D. 2.(a) (I) show the typical profiles of the wear scars of the coatings after ball-on-disc wear test. Fig 5. D .1.(a)(I) (i) shows a smooth topography, with relatively mild wear exhibiting some micro-abrasion at the wear (ii) indicates the intense peak of Zr and iron, weak peak of oxygen. SEM analysis at high magnification (iii) within the wear track indicates that there are a lot of small cavities on the worn surface, which may be owing to the grain-pullouts of the coatings, no deep mechanical plowing grooves can be observed.[72] However crack is observed on the surface. Under the effect of applied load cracks spread and chipping of large area of total coating may occur. EDX analysis at high magnification shows intense peak of iron and weak peak of Zr indicating removal of ZrN coating.

The damage pattern indicates that plastic deformation occurred via adhesive wear.[71] The friction coefficient values are different for the coatings depending on the time travelled. Fig 5. D. 1.(a)(II). shows the friction coefficient of the 1.5  $\mu$  ZrN coatings with time when sliding against EN24 steel ring.

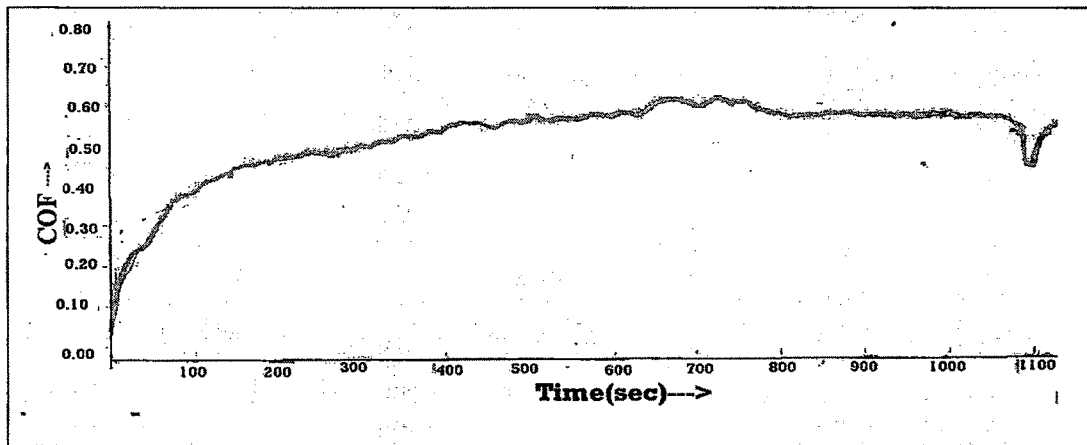


Fig 5.D.2 (a)(II)Variation in Coefficient of friction (COF )with time for 1.5 $\mu$  ZrN after wear testing

The COF of 1.5  $\mu$  ZrN coating is 0.519. Although amount of debris within the wear track is low, the extensive plastic deformation in terms of cracks and flaky particle is observed. Since wear debris are less in case of smooth surfaces involving elastic deformation with dominant adhesive component of friction.( Fig 5.D.2 (a)(II)).[74]

**5.D 2 (b) Wear Behaviour of 2.0  $\mu$  ZrN Thin Films**

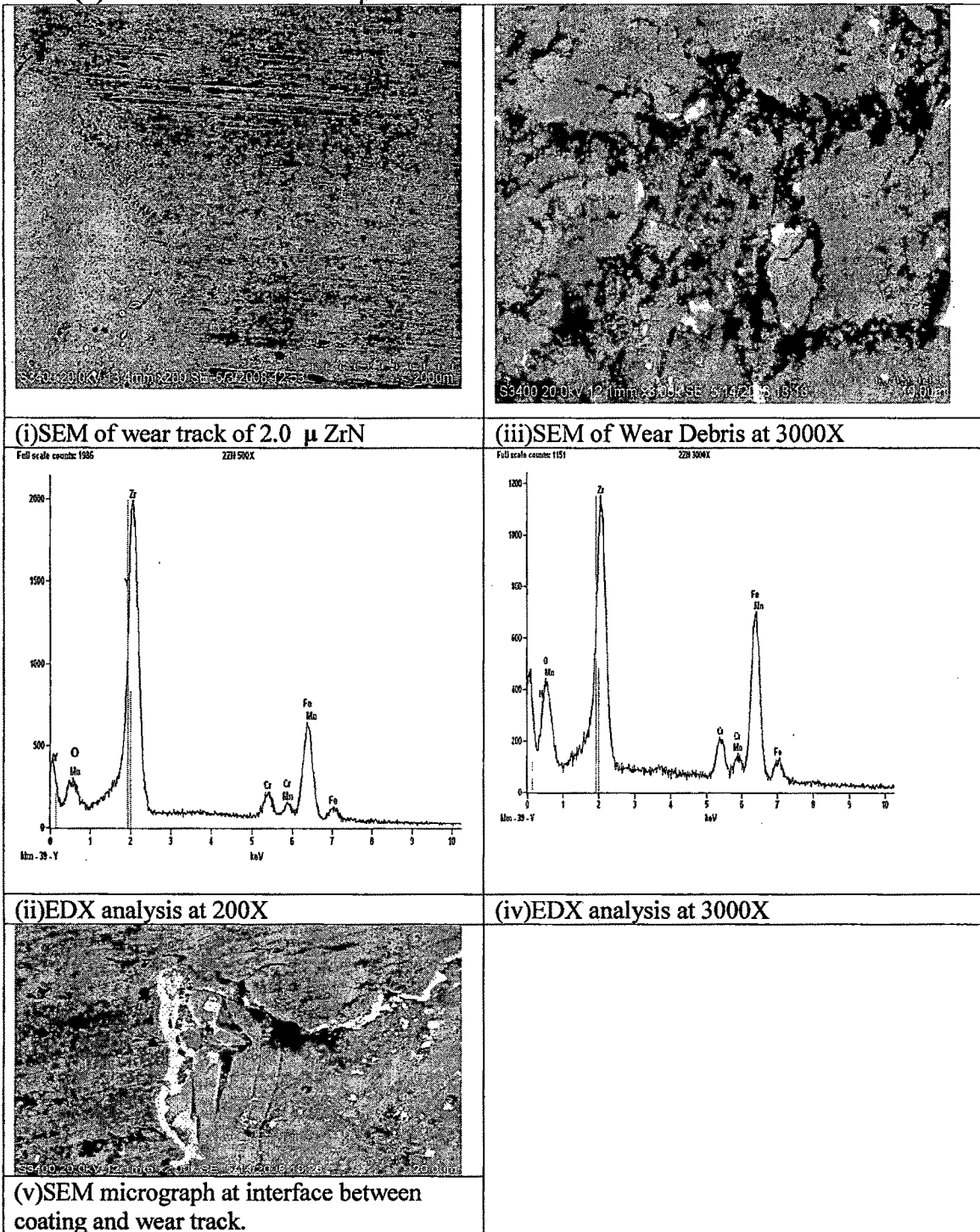


Fig 5. D.2.(b)(I)SEM(i & iii at 200X and 3000X) and EDX analysis(ii & iv at 200X & 3000X ) of 2.0  $\mu$  ZrN, (v) indicates presence of crack at the interface (mag. 2400X)

Fig 5.D.2(b)(I) show the typical profiles of the wear scars of the coatings after ball-on-disc wear test. Fig 5.D.1.(b)(I) (i) shows a smooth topography, with relatively mild wear exhibiting some micro-abrasion at the wear (ii) indicates the intense peak of Zr and weak peak of iron and oxygen. SEM analysis at high magnification (iii) the wear track of 2.0 $\mu$  ZrN coatings revealed a rougher surface and the coating was worn seriously also micro cracks and irregular shaped debris were present. The coating seemed to be very brittle, delaminated completely and the damage is of fractural nature. Similar results were obtained by [75] where in DLC film on alumina substrate using plasma immersion ion deposition PIID process with Cr interlayer, Si was derived from silane SiH<sub>4</sub> for the interlayer within the wear track there were a lot of large irregular shaped debris.

SEM micrographs indicates that cracks have spread and chipping of large area of total coating has occurred.[72] Since wear debris are within the wear track,. EDX analysis at high magnification Fig 5.D.2.(b)(iv) indicates intense peak of Zr. Plate shaped particles are observed in wear debris indicative of ploughing wear followed by repeated loading and unloading fatigue as a result of nucleation and propogation of subsurface cracks or plastic shear in asperity contact.[71] The damage pattern indicates that plastic deformation occurred to some extent via ploughing and wedge formation. The results are similar as obtained by [4] for SEM micrograph at interface between coating and wear track. Fig 5.D.2.(b)(I) (v) indicates brittle type fracture going through compound layer and the coating. Similar behaviour by was observed by T. Savisalo et al where in plasma nitriding processes were carried out prior to the CrN/NbN PVD coating to attain high surface hardness and enhanced load bearing behaviour for S154 and observed brittle type fracture.[82]

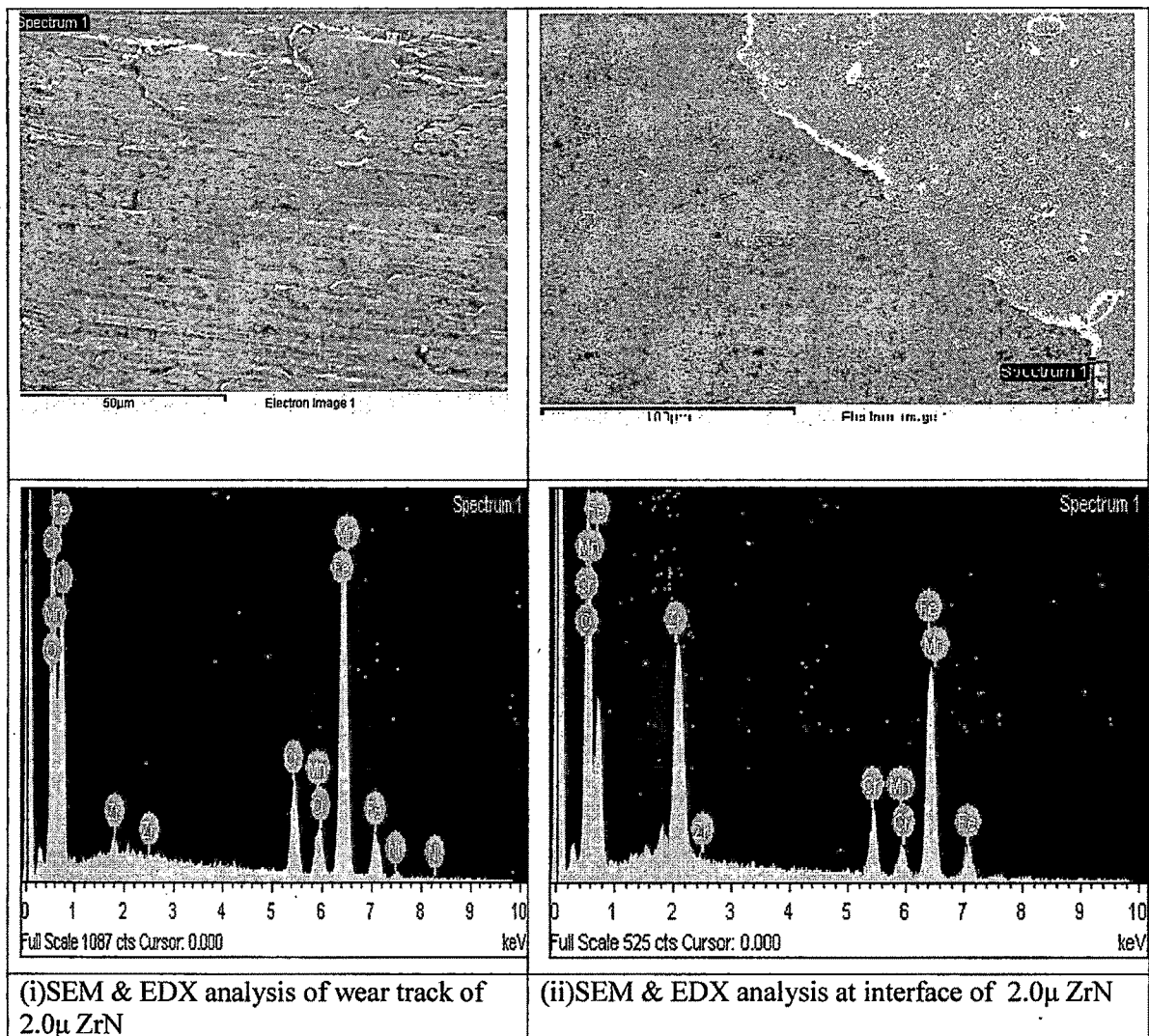


Fig 5 .D.2.(b)(II)SEM and EDX analysis of (i) wear Track and (ii) particle at interface between wear track and coating

The Fig 5.D.2.(b)(II) indicates that the within the wear track complete removal of coating has occurred (absence of Zr peak) while at interface the debris consist of mixed Zr-O-Fe of unknown stiohiometry.

The friction coefficient values are different for the coatings depending on the time traveled. During the wear testing Fig 5.D.2.(b) (III) shows the friction coefficient of the 2.0µ ZrN coatings with time when sliding against EN24 steel ring

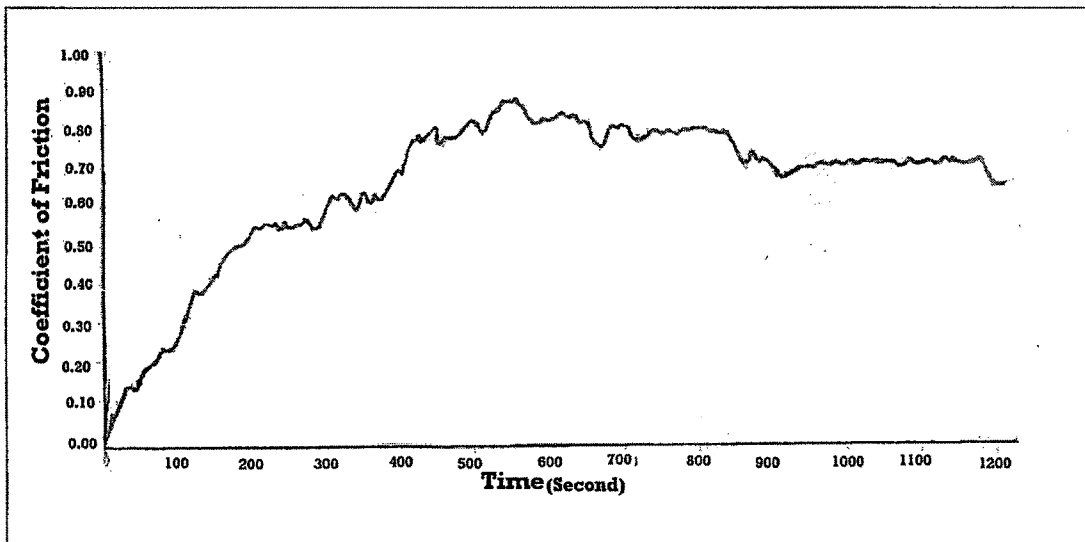


Fig 5.D.2.(b)(II) Variation in COF(Coefficient of friction) with time for 2.0  $\mu$  ZrN thin film after wear testing.

The COF of 2.0  $\mu$  ZrN coating is 0.659. As shown in Fig 5.D.2.(b)(II) The value of COF is very high and high wear is observed in case of 2 $\mu$  ZrN. Continuous increase in COF and small fluctuations are observed. The increase in coefficient are attributed to two effects which play in synergetic way, consumption of the layer leaves surface weak and debris on wear track increases COF. [74] The cohesive failure of the coating, due to the contact pressure applied by the substrate against it, produced an increased amount of debris, and hence an increase in the friction coefficient values at the beginning of the test.[70,78]

**5.D 2 (c) Wear Behaviour of 2.5 $\mu$  ZrN Thin Films**

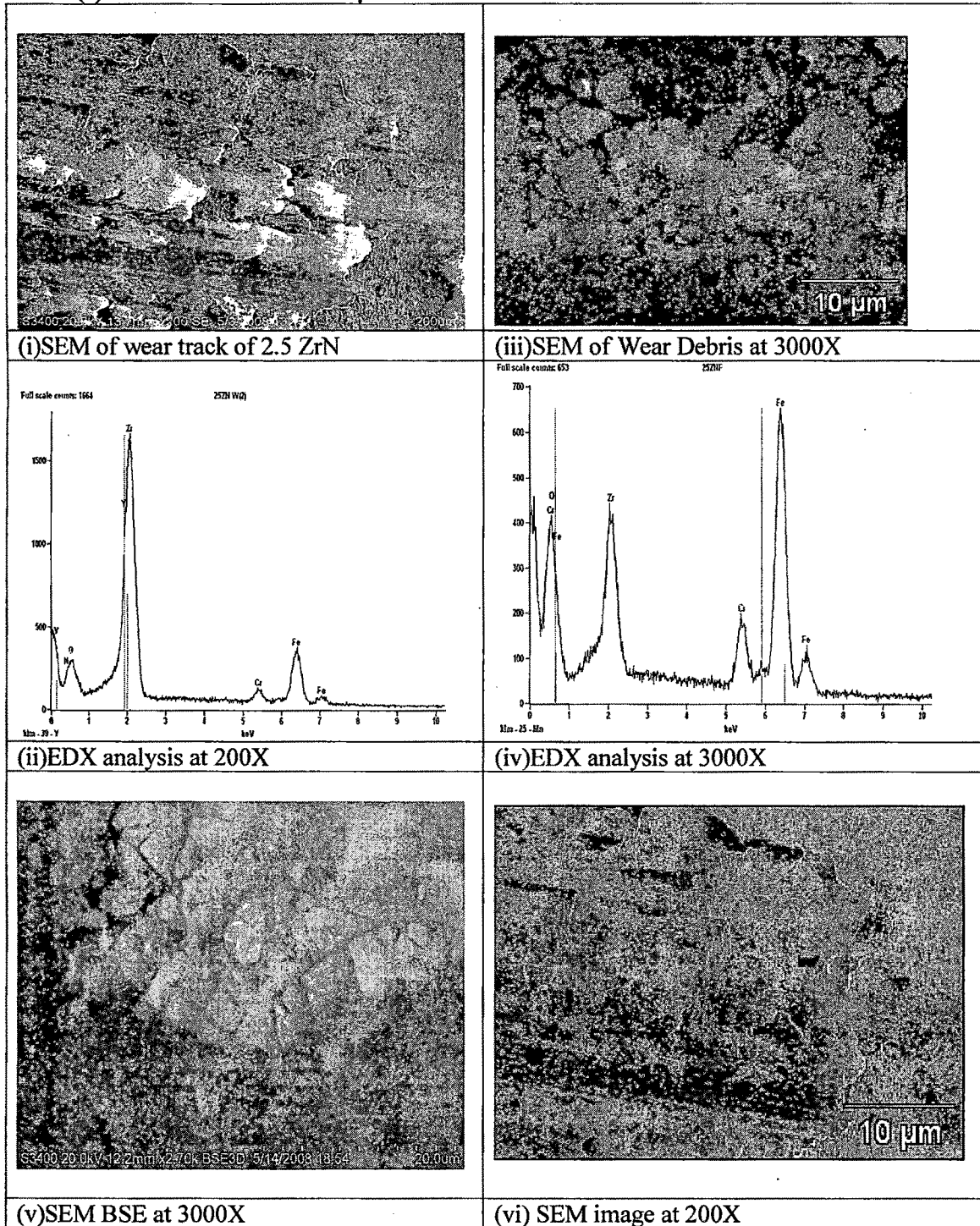


Fig 5.D.2.(c)(I)SEM(i& iii at 200X and 3000X) & EDX analysis(ii & iv at 200X & 3000X ),(v & vi) BSE of the area within the wear track at 3000X and 2000X of 2.5 $\mu$ ZrN

Fig 5.D.2.(c)(I) show the typical profiles of the wear scars of the coatings after ball-on-disc wear test. Fig 5.D.1.(c)(I) (i) shows a some region of smooth topography while in other regions accumulation of wear debris occur near the interface (ii) indicates the intense peak of Zr and weak peak of iron and oxygen. SEM analysis at high magnification (iii) indicates that the wear track of ZrN coatings revealed presence of plate shaped debris. Plate shaped particles are observed in wear debris indicative of ploughing wear followed by repeated loading and unloading fatigue as a result of nucleation and propagation of subsurface cracks or plastic shear in asperity contact.[71] The EDX analysis at high magnification Fig 5.D.2(c)(iv) indicates intense peak of Fe and less intense peak of Zr. Intense peak of Zr indicates that debris are located within the wear track.

A backscattered electron image of the wear scar on the 2.5 $\mu$  ZrN coating(Fig 5.D.2(c)(v)) shows that the coating contains a series of fine micro cracks with a honeycomb structure. The mobility of cracks is mainly governed by the stress field in the films. It is well-established that PVD coatings are subjected to high internal compressive stresses which can reach several GPa. [91] Cracks could also be the result of thermal stress differences between the substrate and the coating upon cooling down from its high deposition temperature. The thermal expansion coefficient of ZrN is  $7.24 \times 10^{-6}$  while that for S.S is  $10.4 \times 10^{-6}$ [65]. This difference in thermal expansion might give rise to compressive stresses in the films when samples are cooled down after deposition. The internal stress is the most important characteristic value for the mechanical loading capacity and the adhesive failure in the coating-substrate interface. Such cracks explain the coating behaviour during both adhesion and wear tests. The cohesive failure of 2.5 $\mu$  ZrN coating due to the contact pressure applied by the substrate against it, produced an increased amount of debris, and hence an increase in the friction coefficient values at the beginning of the test. [79] Similar behaviour was observed by S.J. Bulla et al [84] and Friedrich[89] TiCN coatings on cemented carbide cutting-tool insert substrates deposited by MT CVD. The friction coefficient values are different for the coatings depending on the time traveled. During wear testing fig 5.D.2.(b)(III) shows the friction coefficient of the 2.5  $\mu$  ZrN coatings with time when sliding against EN24 steel ring

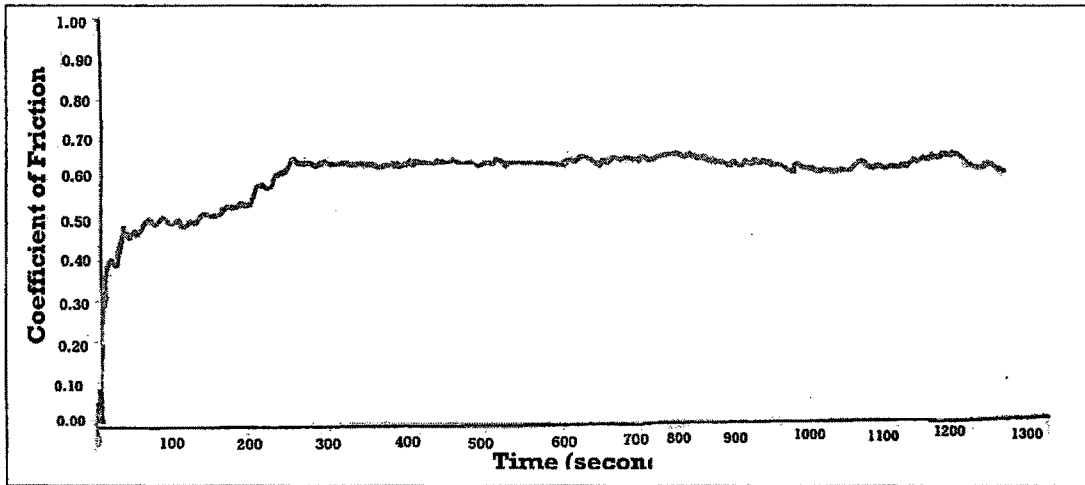


Fig 5.D.2 (c) (II) Variation in COF(Coefficient of friction) with time for 2.5  $\mu$  ZrN after wear testing.

The COF of 2.5 $\mu$  ZrN  $\mu$  coating is 0.616. As shown in Fig 5.D.2.(c)(II) The value of COF is very high and hence high wear is observed in case of 2.5 $\mu$  ZrN. Continuous increase in COF and small fluctuations are observed. The increase in coefficient are attributed to two effects which play in synergetic way, consumption of the layer leaves surface weak and debris on wear track increases COF .[74] The cohesive failure of the coating, due to the contact pressure applied by the substrate against it, produced an increased amount of debris, and hence an increase in the friction coefficient values at the beginning of the test.[84,25]

**5.D 2 (d) Wear Behaviour of 3.0 $\mu$  ZrN Thin Films**

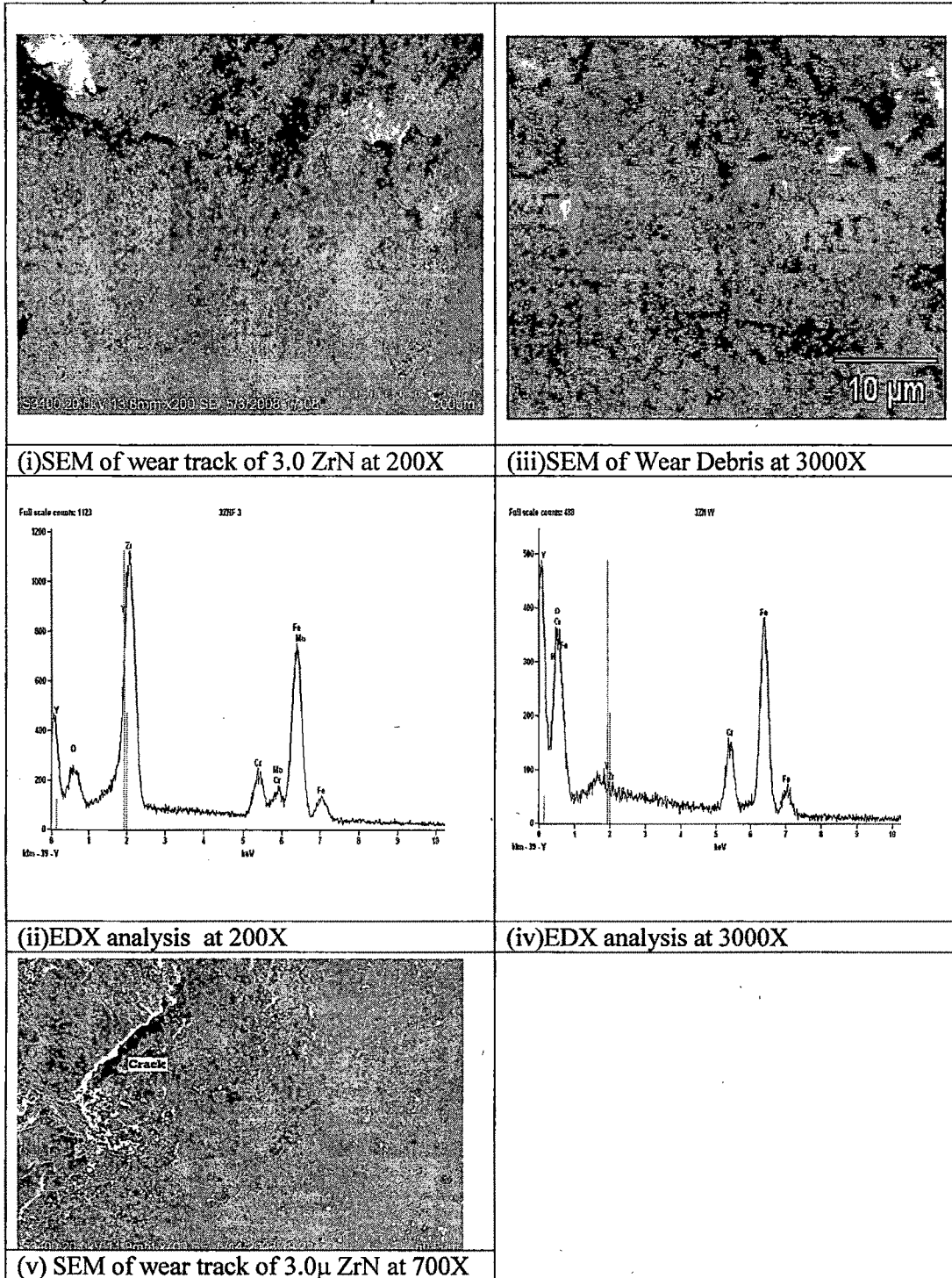


Fig 5.D.2(d)(I)SEM(i& iii at 200X and 3000X) and EDX analysis(ii & iv at 200X & 3000X ) of 3.0  $\mu$  ZrN (v) SEM image at interface at 700X

Fig 5. D.2.(d)(I) show the typical profiles of the wear scars of the coatings after ball-on-disc wear test. Fig 5.D.2.(d)(I) (i) shows a the accumulation of wear debris at the interface between wear track and coating. (ii) indicates the intense peak of Zr and weak peak of iron and oxygen. SEM analysis at high magnification (iii) the wear track of ZrN coatings revealed presence of irregular shaped wear debris of fine size embedded within the track indicating detachment of transferred fragment in adhesive wear and brittle fracture.[71] The EDX analysis at high magnification Fig 5.D.2(c)(iv) indicates intense peak of Fe and weak peak of Zr. Intense peak of oxygen indicating oxidation has occurred. The SEM image ( Fig 5.D.2(d)(v) ) at 700X indicates presence of crack. This may be due to compressive residual stresses within coatings and when subjected to wear testing these stresses are relieved by forming cracks.

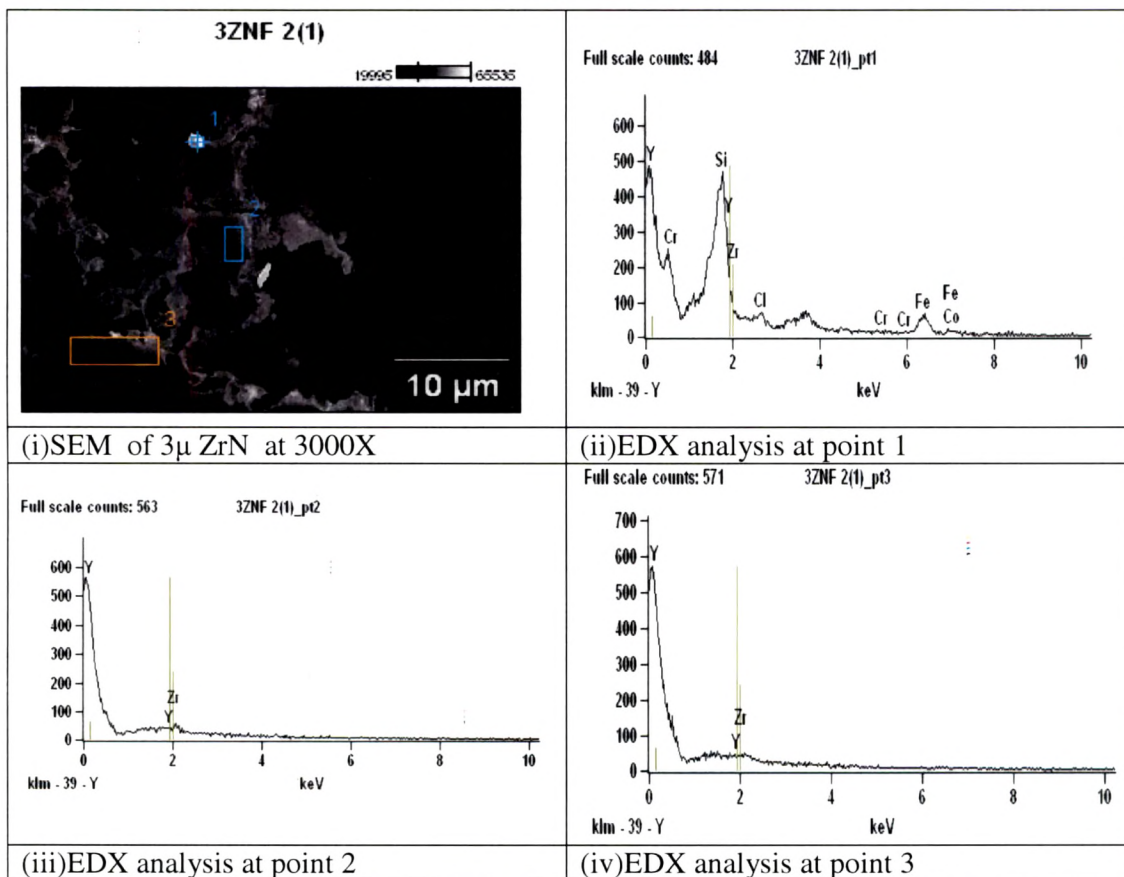


Fig 5.D.2(d)(II)SEM of 3000 and EDX analysis at various point (i,ii and iii) after wear testing.

The Fig 5.D.2.(d)(II) EDX analysis of Wear Track at various points in 3µ ZrN. EDX analysis at various points indicates the presence of Silicon or zirconium at point 1, at

point 2 and 3 peak of yttrium is obtained. Yttrium may have come from the Zirconium target during film deposition.

The friction coefficient values are different for the coatings depending on the time traveled during wear testing. Fig 5.D.2.(b)(III) shows the friction coefficient of the 3.0 $\mu$  ZrN coatings with the time when sliding against EN24 steel ring

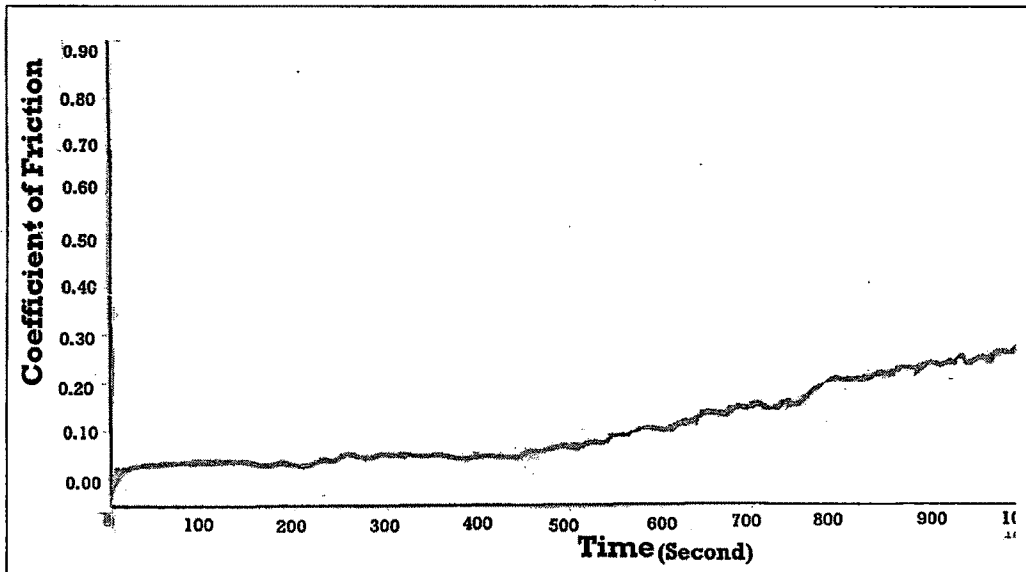


Fig 5.D.2.(d)(III) Variation in COF(Coefficient of friction) with time for 3.0  $\mu$  ZrN after wear testing.

The COF of 3.0  $\mu$  ZrN coating is 0.213. The value of COF is very low. As shown in Fig 5.D.2.(d)(III) continuous increase in COF and small fluctuations are observed. Deep mechanical plowing grooves and large scratched appearance on the substrate after wear test which results in increase in COF. [74]



**5.D 2 (e) Wear Behaviour of 4.0  $\mu$  ZrN Thin Films**

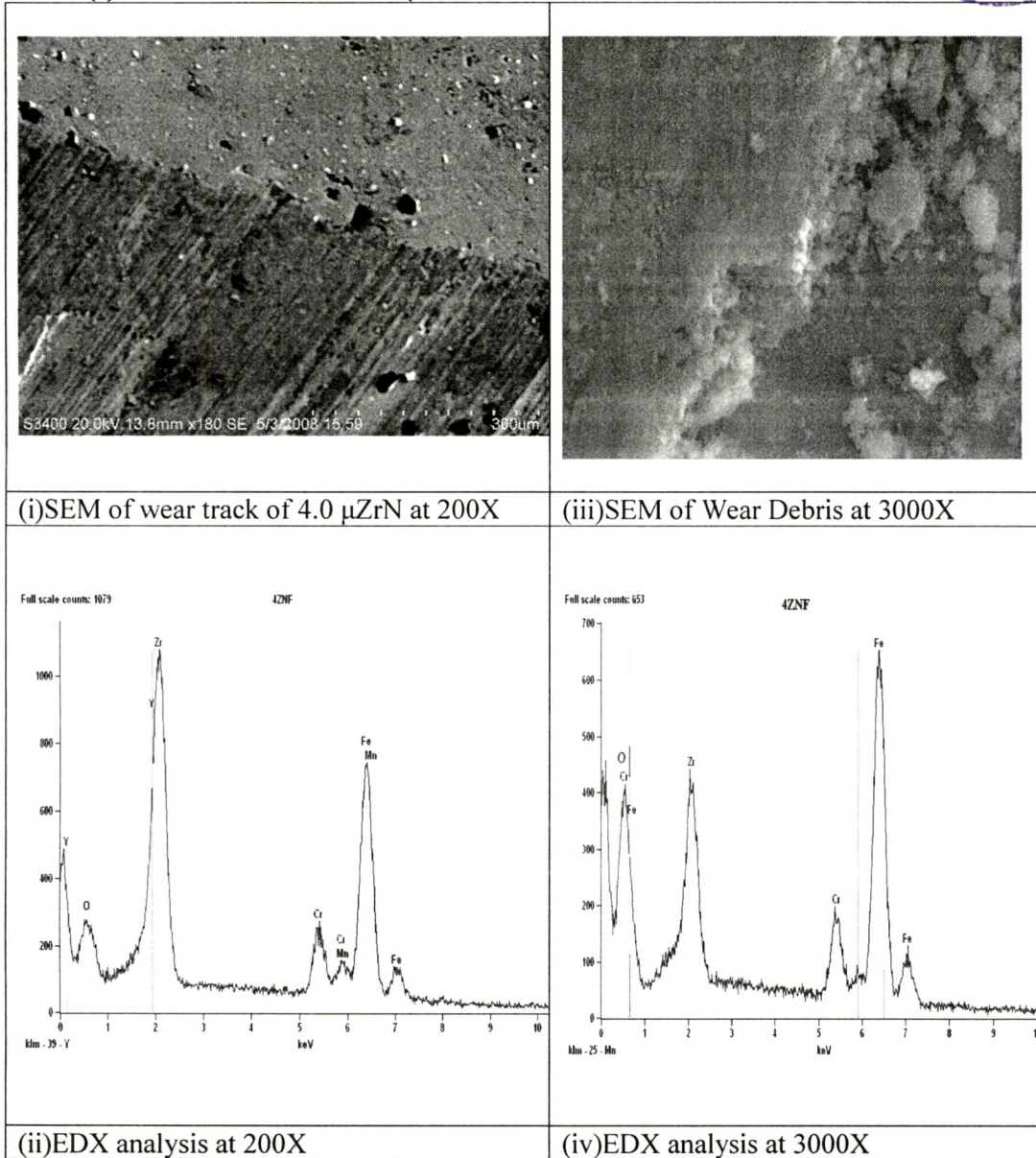


Fig 5.D.2.(e)(I)SEM(i& iii at 200X and 3000X) and EDX analysis(ii & iv at 200X & 3000X ) of 4.0 $\mu$  ZrN

The Fig 5.D. 2.(e)(I) show the typical profiles of the wear scars of the coatings after ball-on-disc wear test. Fig 5.D.1.(e)(I) (i) shows the shallow ploughing grooves on the surface of specimen. EDX analysis (ii) indicates the intense peak of Zr and small peak of Fe and oxygen. SEM analysis at high magnification (iii) within the wear track shows plate shaped particles produced as a result of plouging and nucleation and propogation of

subsurface cracks or plastic shear in asperity contact.[71] Microgrooves are formed which are associated with crack nucleation on surface, subsequent crack propagation and finally loose particles of large size are trapped and dragged along resulting in formation of macrogrooves.[70]EDX analysis at high magnification (iv) indicates intense peak of iron and less intense peak of Zr and oxygen.

The friction coefficient values are different for the coatings depending on the time traveled. Fig 5.D.2(e)(II) shows the friction coefficient of the  $4.0\mu$  ZrN coatings with the sliding distance when sliding against EN24 steel ring

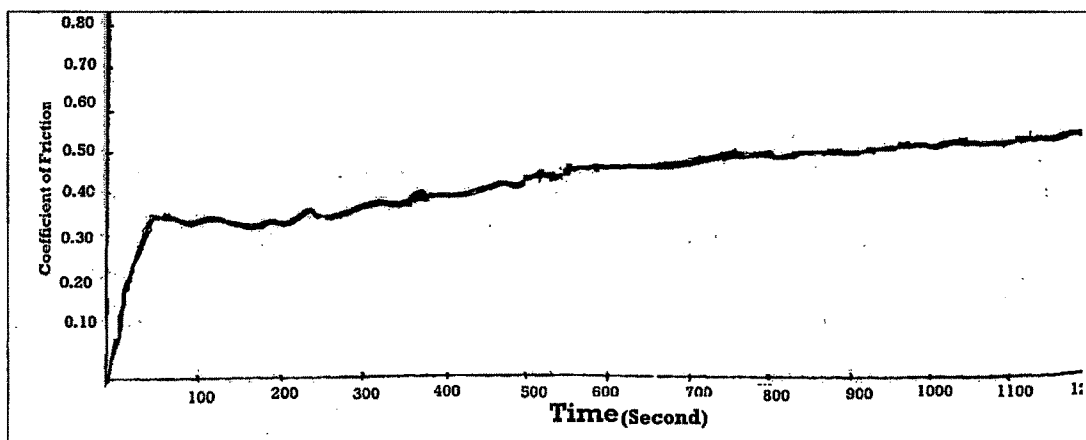
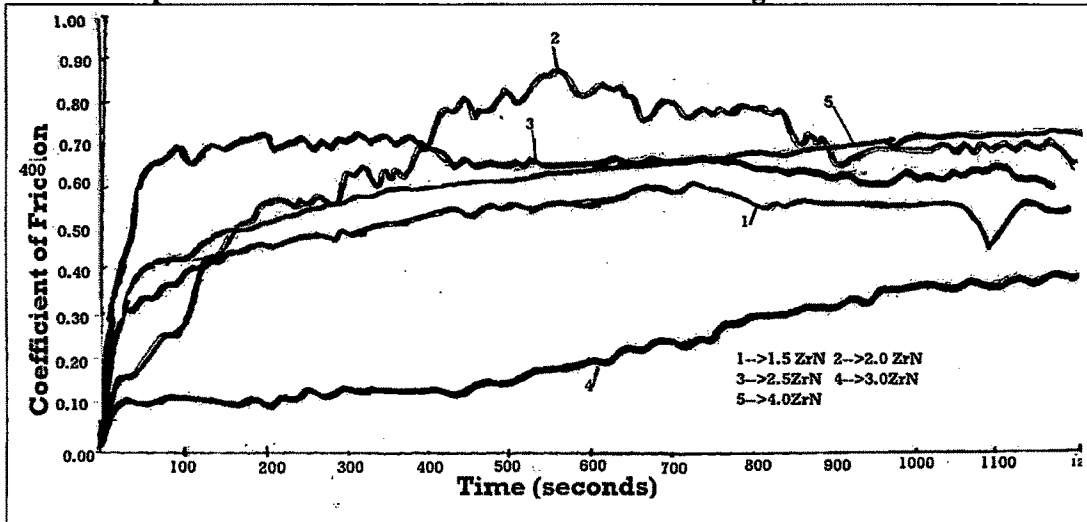


Fig 5.D.2 (e)(II) Variation in COF(Coefficient of friction) with time for  $4.0\mu$  ZrN after wear testing.

The COF of  $4.0\mu$  ZrN coating is 0.489. The value of COF is low. As shown in Fig 5.D.2 (e)(II) The increase is associated with ploughing because of roughening and trapped wear particles. [74]

### 5.D.2 Comparison of COF for all thickness of ZrN Coating



5.D.2.(abcde)COF Vs Time for all thickness of ZrN coating after wear testing.

Typical curves of coefficient of friction vs. Sliding distance and time for all thickness is illustrated in Fig 5.D.2.(abcde).The changes in wear resistance due to increase in thickness is due to difference in hardness of resultant coating and the adhesive strength between film and substrate.

During sliding, changes in the conditions of mating surfaces occur which affect friction and wear properties. After some period, the so-called “run-in,” “break-in” or “wearing-in” period, the friction force generally stabilizes into what is called steady-state sliding. [74] This wearing period is usually taken as the criterion for evaluating the wear.

The internal stresses within the coating contribute to the wear resistance of coating. As indicated in XRD (5.B.2(i)),  $2\ \mu$  and  $2.5\ \mu$  ZrN coating are under high internal stresses due to presence of (200) plane in addition to (111) plane. Hence when these coatings are subjected to sliding test, the quantity of the wear debris produced is large than coatings of other thickness. Hard debris delaminated from the coating layers or the oxides which were formed in the atmosphere are partly entrapped between rubbing surfaces. Friction coefficients are related to the change of the wear debris contour. The three-body rolling wear process enables the friction coefficients in the wear process fluctuating with large amplitudes. Highest COF and hence highest wear was observed for  $2\ \mu$  ZrN. Similar

result was obtained by P.Eh. Hovsepian et al [25] indicating that the increase of the coefficient of friction can be correlated with the increase in the residual stress values in the coatings, which promotes a brittle fracture. This is reflected in terms of large debris in SEM at high magnification.

Although lowest COF is observed in case of  $3\mu$  ZrN (0.213), the COF continuously increase with time and no steady state region was observed. However  $1.5\mu$  ZrN had low COF(0.489) and long and steady wearing period.

#### **5.D .2.1Composition of Wear Debris in Ti-N and ZrN thin Films:**

It is a well known fact that the character of the wear debris (oxides), produced during sliding contact, plays a very crucial role in determining the tribological behavior of sliding system in particular, the chemical nature of these debris particles formed during sliding test (single, complex, stoichiometric, sub-stoichiometric, etc.) may have a significant effect on friction and wear [85,86].In addition micro structural integrity of the coating becomes extremely important. If the coating has a porous microstructure or has internal stresses which are tensile, coating will wear faster.[87]

However, based on our limited surface analytical and structural work in this study, we could not verify the presence and/or absence of such phases within the tribofilms. Attempt has been made to correlate the literature and results obtained to determine composition of wear debris.

As indicated by P. Eh. Hovsepian et al [25] SEM observations and three-dimensional profilometry in their studies they revealed that the ball track morphology produced in the pin-on-disk test depends on the coating constitution and residual stress and is directly related to the wear rate. Lower stressed stoichiometric coatings produce extremely smooth wear tracks, whilst the wear tracks of sub-stoichiometric or coatings deposited at a higher bias voltage, even after short sliding distances, show deep grooving along the wear track and higher wear coefficient. To understand the wear mechanisms involved in dry sliding conditions of the hard ceramic coatings the structure and the composition of the wear debris was further investigated by energy dispersive X-ray analysis EDX., X-ray photoelectron spectroscopy XPS and Raman spectroscopy The investigation by [25] revealed that the wear product released during dry sliding comprises of a mixture of

oxides corresponding to the coating constitution, thus confirming that mainly an oxidative wear mechanism was in force. The oxidative wear may be explained by the high flash temperatures in the asperities an effect magnified by the high contact pressures and low thermal conductivity of the ceramic coatings. Isothermal oxidation experiments in the temperature range of 500<sup>o</sup> and 700<sup>o</sup> C showed oxide phases similar to those found in tribo-testing. However, temperatures of this magnitude not only contribute to fast oxidation but also significantly influence the properties of the formed oxides by increasing the dislocation movement and therefore, the plasticity, or possibly even exceeding the melting point of some oxides. Another interesting result concerns the tribotester itself: is the removal of the wear debris by mechanical brushing during the pin-on-disc test led systematically to a significantly lower coefficient of friction typically,  $\mu=0.18$  to 0.23. This result demonstrates the strong influence of the wear products on the wear behaviour of the tested materials.

S Wilson et al[79]investigated the effects of atmospheric humidity and microstructure of counter face materials on the formation of tribo-layers on TiN coatings. Pin-on-disc sliding wear experiments were conducted on physical vapour deposition (PVD) TiN-coated high speed steel (HSS) discs against HSS, mild steel and A356 Al-15% SiC pin materials. They developed wear mechanism map, representing pin-on-disc dry sliding wear of TiN coatings on HSS (AISI M2 HSS) disc substrates against AISI M2 HSS pins, is shown in Fig. 5.D.1.2

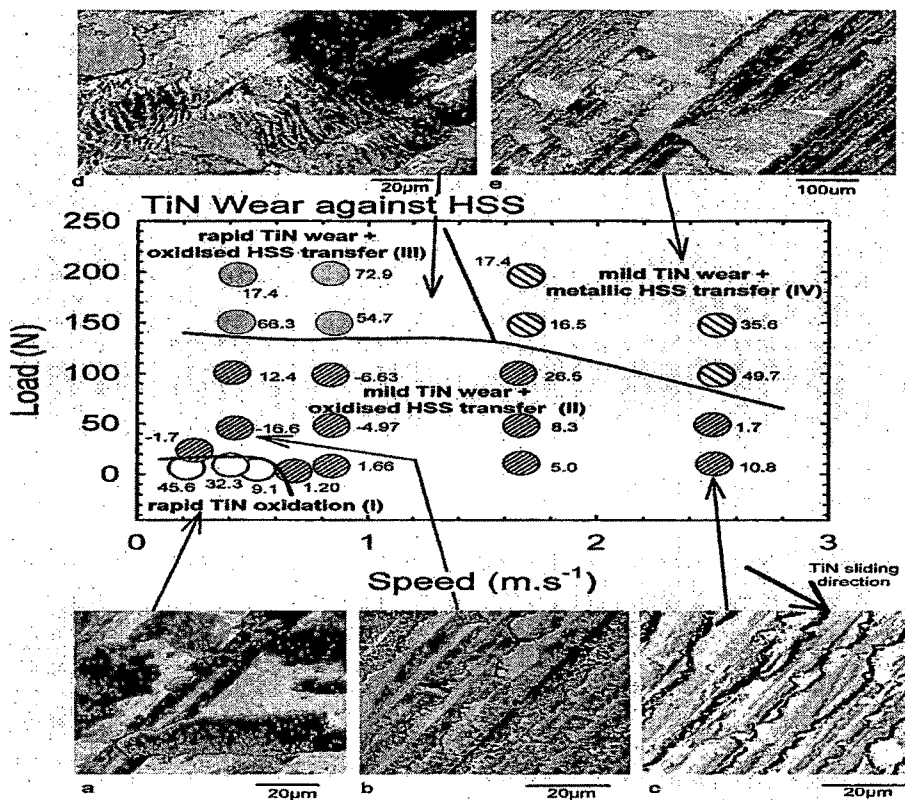


Fig 5.D.1.2. Wear Map for TiN thin films deposited on HSS

Comparing the wear track morphology in Fig 5.D.1.2 and that obtained in present investigation, one tends to conclude that in this case the wear rates matches with Regime II (a & b) (Fig 5.D.1.(d)(I)(i)) and Regime IV (e) (Fig 5. D.1 (a) (I)(iii)). In Regime II slight increases in either load or sliding speed inhibit the tribochemical reaction and introduce a transition to significantly lower TiN wear rates. Increased transfer of Fe-rich oxidized HSS pin material to the TiN results and can contribute to negative wear rates or mass gain. The transferred material is white in appearance under BSE imaging, indicating that it is comprised of the higher atomic number oxidized Fe, W, Mo, V, Cr from the HSS pin with minimal presence of Ti. In the present case EDX analysis of 3µ TiN Fig (5.D.1.(c).(II)) shows white coloured wear debris corresponding to Fe-O. Regime IV indicates the of rapid TiN wear, measurements by thermocouple probe of the HSS pin indicate that the surface sliding temperature,  $T_b$ , reaches a temperature range of 150–200<sup>0</sup> C. Regime IV which is associated with The softening of the HSS pin material, diminishes its ability to remove the coating and mild wear of TiN ensues. This is accompanied by

extensive transfer of heavily deformed Fe from the HSS pin to the TiN surface. The onset of severe wear in the HSS pins correlates approximately with a  $T_b$  of 300<sup>0</sup>C. Thus it can be confirmed that the temperature during the sliding wear of TiN coating ranges from room temperature to 300<sup>0</sup> C.

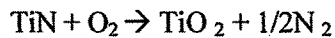
I.L. Singer [75], they performed Friction tests on TiN-coated substrates at low speed (less than 0.1 m/ s) in air. Further optical (Nomarski) and scanning electron microscopy, Auger electron spectroscopy and transmission electron microscopy (TEM) were used to characterize the transfer films and debris generated during sliding against steel and sapphire balls. Friction coefficients of steel against rougher ( $R_a = 60-100$  nm) TiN coatings started and remained relatively high (0.5-0.7) owing to wear and transfer of the steel. Their TEM analysis had identified that the debris to be mainly the ternary FeTiO<sub>3</sub> (ilmenite) and Fe<sub>2</sub>O<sub>3</sub>, (hematite) phase for a steel ball. To further confirm and understand chemical reactions responsible for generation of oxide debris from starting material, quaternary phase diagram (considering reactions between Ti-N & Steel in air) involving four elements (Fe-Ti-N-O) and their compounds was used. The quaternary diagram predicts that three phases for temp @300<sup>0</sup> C should form: Fe<sub>2</sub>O<sub>3</sub>, FeTiO, and TiO<sub>2</sub> These phases, were same as that found by TEM in wear debris..

In the present investigation after compositional analysis intense peaks of Fe, Ti and O were obtained indicating formation of Fe<sub>2</sub>O<sub>3</sub>, FeTiO<sub>3</sub> and TiO<sub>2</sub> may have occurred.

Considering the fact that experimental conditions for wear testing of ZrN & TiN is same and also that TiN and ZrN are thermodynamically stable but are susceptible to oxidation, which can be inferred from their heats of formation of TiN (80 kcal/ mol) and TiO<sub>2</sub> (219 kcal/ mol), and ZrN (87.3 kcal/mol) and ZrO<sub>2</sub> (261.5 kcal/ mol). G.L.N Reddy et al [13] carried out oxidation in dry oxygen or air in the temperature range of 300–1200<sup>0</sup>C. Further as mentioned by [13] due to the gettering nature of Zr, the films may contain O. The solid solubility of O atoms in Zr can be as large as 30 at.% and has a high diffusion rate as well. When annealing was carried out at 350<sup>0</sup> C for 5 hrs the measurements showed that the distribution of N remained nearly identical to that observed in as-deposited films i.e no oxidation has occurred.

However when the annealing was carried out for different duration at 475<sup>0</sup> C oxidation of ZrN results in the formation of monoclinic ZrO<sub>2</sub>.The quantity of ZrO<sub>2</sub> increased progressively with the duration of annealing.[25]

The reactions that occur during oxidation are the formation of oxide layers on top of nitride coatings. The transformation of a nitride to an oxide is accompanied by the evolution of N<sub>2</sub>:



Similar results were obtained by Miloseva et al[88] indicating that when oxidation of ZrN was carried out at 350<sup>0</sup> C complete oxidation of ZrN does not occur and oxynitride layer is formed .Certain amount of nitrogen remains trapped in the uppermost part of the coating. Only with increasing temperature nitrogen is completely removed and pure oxide layer is obtained.[88,89]

The SEM observation of wear tracks obtained in Ti-N indicates that temperature generated during wear testing in present investigation is around 300<sup>0</sup> C. However the dynamic conditions existing in the wear testing formation of Zr-O/Ti-O during the wear test cannot be concluded with confidence. The oxidation of coating not only depends on composition but also on the microstructure of coating which further depends on the processing conditions. A film with an open microstructure absorbed a large amount of oxygen when exposed to air. The coatings consisting of coarse columnar grains should have many voids and other structural defects, which can absorb oxygen. As the working gas pressures are different, the collision rate between sputtered atoms and sputtering gas atoms is different. Since the mass of a Ti atom is almost half of Zr, the energy loss of Ti atoms by collision should be larger than that of Zr. Increasing the loss of kinetic energy of sputtered atoms will promote the coarse columnar (Zone I) structure. Furthermore, it will induce the incorporation of oxygen in the deposition chamber due to the increment in the mean time for arriving at substrate. The oxygen content, which influences in the friction coefficient, depends critically on the microstructure. This effect is more pronounced in the case of the TiN film due to a major presence of oxygen than in the ZrN film. [89-91].Hence in this research work formation of Ti-O may have occurred but formation of Zr-O cannot be said with confidence.

### 5.D.3 WEAR CHARACTERISATION OF ZrTiN THIN FILMS

XRD analysis indicates presence of more than one phase ( $Ti_2N$  and  $ZrN$ )As reported by Hermann A. Jehn[92] presence of multicomponent improves properties of thin film

#### 5.D.3 (a) Wear Behaviour of $1.5\mu$ ZrTiN Thin Films

After the wear tests, the morphologies of each wear scar were observed by scanning electron microscopy (SEM)(HITACHI 3400 and JOEL 5610LV) Furthermore, the chemical compositions of the micro-zones inside the scars were characterized by energy dispersive X-ray spectrum .

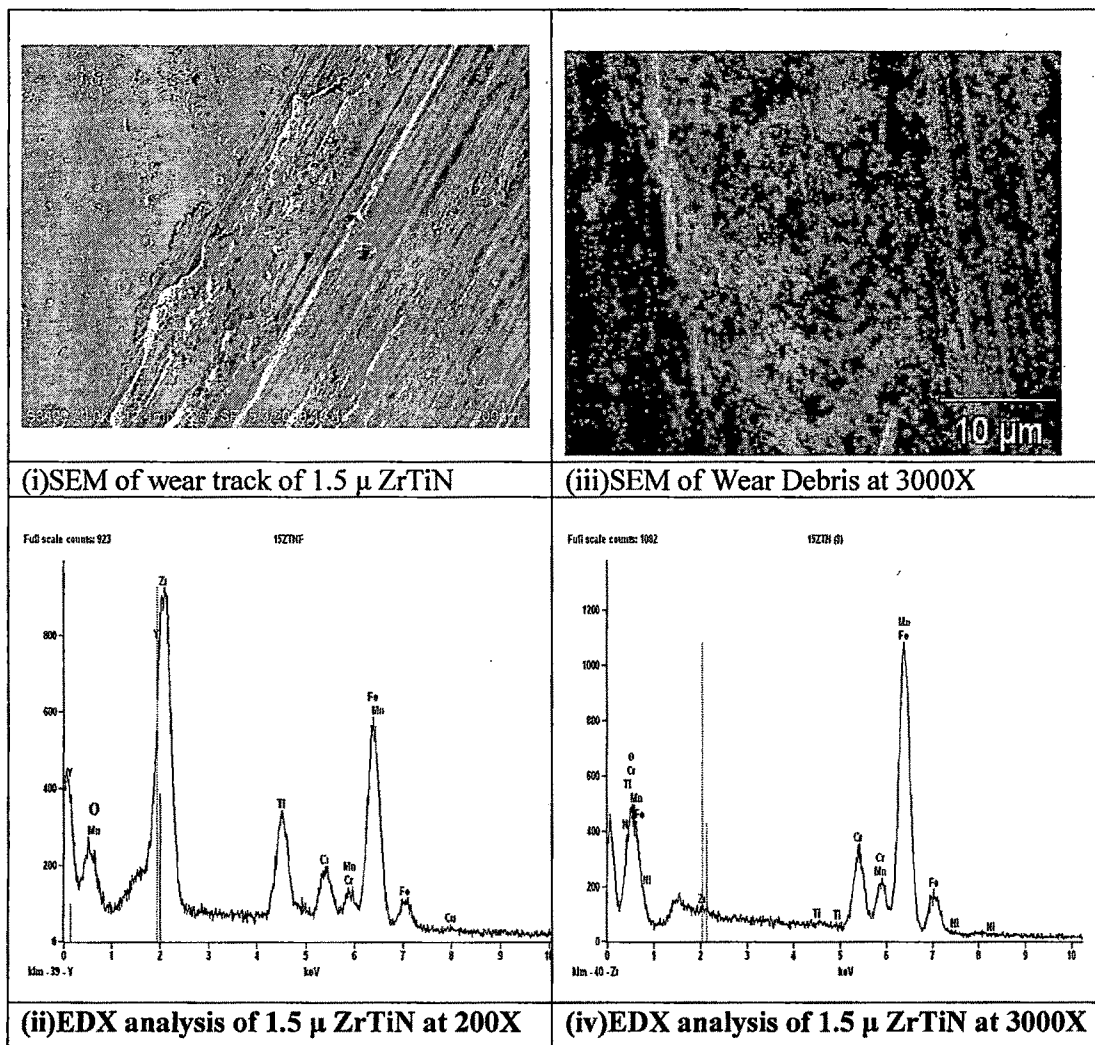


Fig 5.D.3.(a)(I)SEM(i& iii at 200X and 3000X) and EDX analysis(ii & iv at 200X & 3000X ) of  $1.5\mu$  ZrTiN

The Fig 5. D.3.(a)(I) show the typical profiles of the wear scars of the coatings after ball-on-disc wear test.. Fig 5. D.3(a)(I) (i) shows the deep ploughing grooves on the surface of specimen. The presence of this wear debris in the wear track resulted in a scratched appearance on the substrate, and also an increase of friction coefficient. [94] EDX analysis (ii) indicates the intense peak of Zr and less intense peak of iron and small peak of Ti and oxygen. The atomic concentration of Ti and Zr depended on the background pressure, though cathode currents were initially set to obtain equal fluxes of Ti and Zr ions. While at all pressures the concentration of Zr is higher, the dominance of Zr at higher pressure is even stronger. This behavior may possibly be explained by deflection of the ions. The lighter Ti ion is more affected by the background gas nitrogen pressure than the heavier Zr ion, resulting in a larger scattering of the Ti ions. [93] EDX analysis of as received  $1.5\mu$  ZrTiN indicates intense peak of Zr and less intense peak of Ti. (Fig 5.A.I.(iii)) Hence decrease in peak of Ti in Fig 5.D.3.(a)(ii) is not due to removal of Ti. SEM analysis at high magnification (iii) within the wear track shows flaky and very fine-grained submicron sized wear debris particles. Microgrooves are formed which are associated with crack nucleation on surface, subsequent crack propagation and finally loose particles are trapped and dragged along resulting in formation of macrogrooves.[70]Fine shaped particles are observed in wear debris indicative of ploughing wear followed by repeated loading and unloading fatigue as a result of nucleation and propagation of subsurface cracks or plastic shear in asperity contact.[74]EDX analysis at high magnification indicates the intense peak of iron and small peak of Zr /Ti i .e removal of coating has occurred. The absence of nitrogen in the debris indicated that the generated particles were thoroughly oxidized.

The damage pattern indicates that plastic deformation occurred to some extent via ploughing and wedge formation. The results are similar as obtained by [11].Irregular and fine wear debris are obtained within the wear track indicates detachment of transferred fragment in adhesive wear and brittle fracture and irregular shaped. [74]

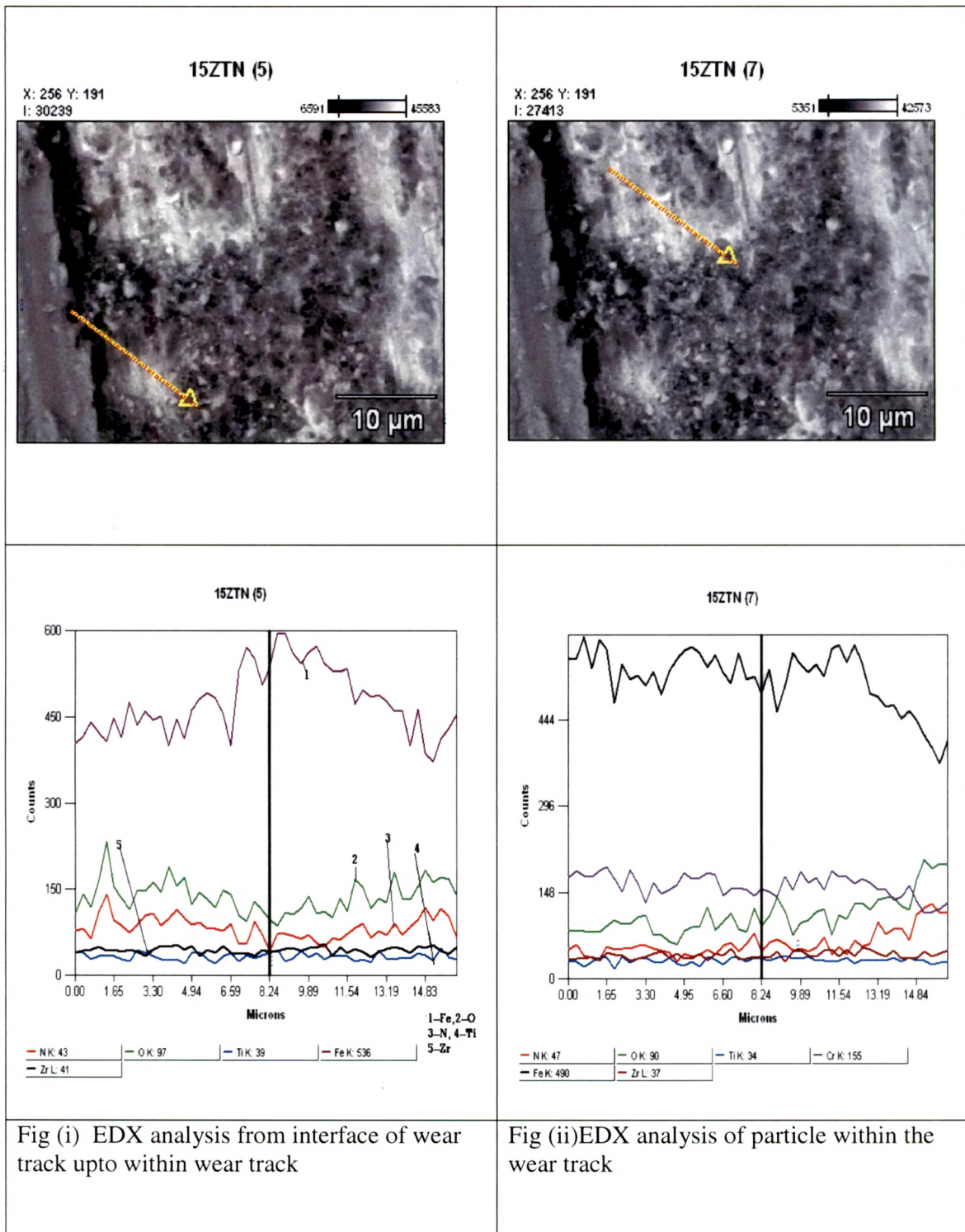


Fig 5.D.3.(a) (II) SEM and EDX analysis at (i) interface and (ii) within wear track of 1.5μ ZrTiN

The Fig 5.D.3.(a)(II) (i) indicates that at the interface intense peak of oxygen and nitrogen is obtained on further proceeding within the track intensity of Fe increases indicating its more amount, however intensity of oxygen decreases, further proceeding within the track intensity of iron decreases and intensity of oxygen, intensity of nitrogen increase. EDS analysis revealed formation of Fe, Cr and O rich islands (e.g. iron oxides) in the wear tracks of the examined coatings Fig 5.D.3.(a)(II) (i) indicating adhesive and oxidative damage on coating. These oxide islands may have formed due to mass transfer from steel ring during wear testing similar results were obtained by [86]

The Fig 5.D.3.(a)(II) (ii) EDX analysis of the particle within the wear track indicates at up to certain distance composition of particle is constant however later there is decrease in intensity of Fe and oxygen peak and increase in nitrogen peak hence oxy nitride of varying compositions may have formed. Further sophisticated instruments are required to determine exact composition of particles within wear track

As discussed earlier the temperature in wear track may be around 300<sup>0</sup>- 400<sup>0</sup> C and at this temperature oxynitride may have formed.

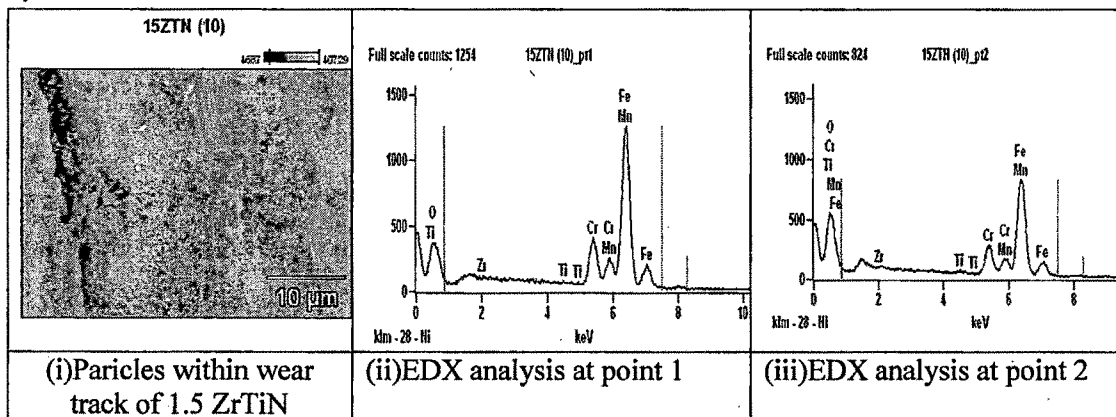


Fig 5.D.3(a)(III) EDX analysis of particles within the wear track of 1.5 μZrTiN thin film after wear testing.

As indicated in Fig 5.D.3(a)(II)(ii & iii), the wear debris obtained in the wear track consists mainly of Fe and oxygen with varying composition as depicted in the point analysis of two wear debris. Similar result were obtained by [4]

The friction coefficient values are different for the coatings depending on the time traveled. Fig 5.D.3(a)(IV) shows the friction coefficient of the 1.5  $\mu$  ZrTiN coatings with time when sliding against EN24 steel ring

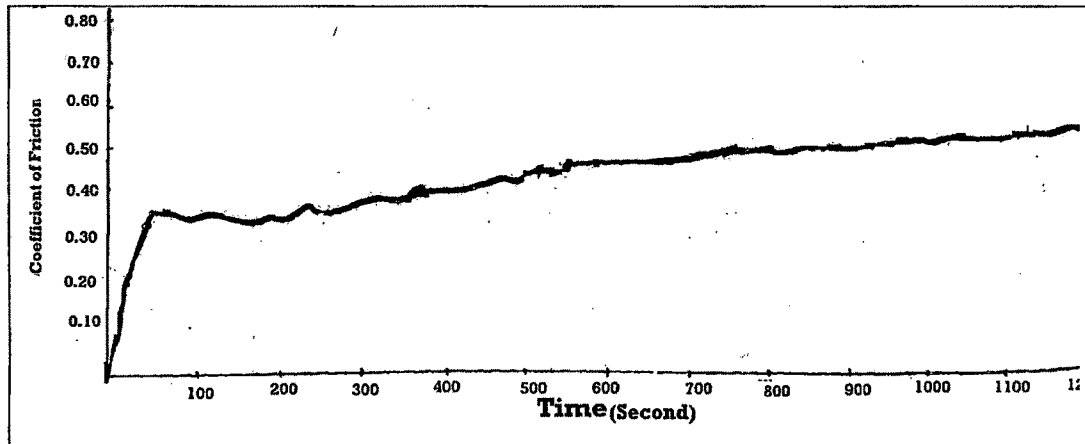


Fig 5.D.3 (a)(IV) Variation in COF(Coefficient of friction) with time for 1.5 $\mu$  ZrTiN

The COF of 1.5  $\mu$  ZrTiN coating is 0.440 As shown in Fig 5.D.3 (a)(IV) the increase in COF is associated with ploughing because of roughening and trapped wear particles[74].

### 5.D 3 (b)Wear Behaviour of 2.0 $\mu$ ZrTiN Thin Films

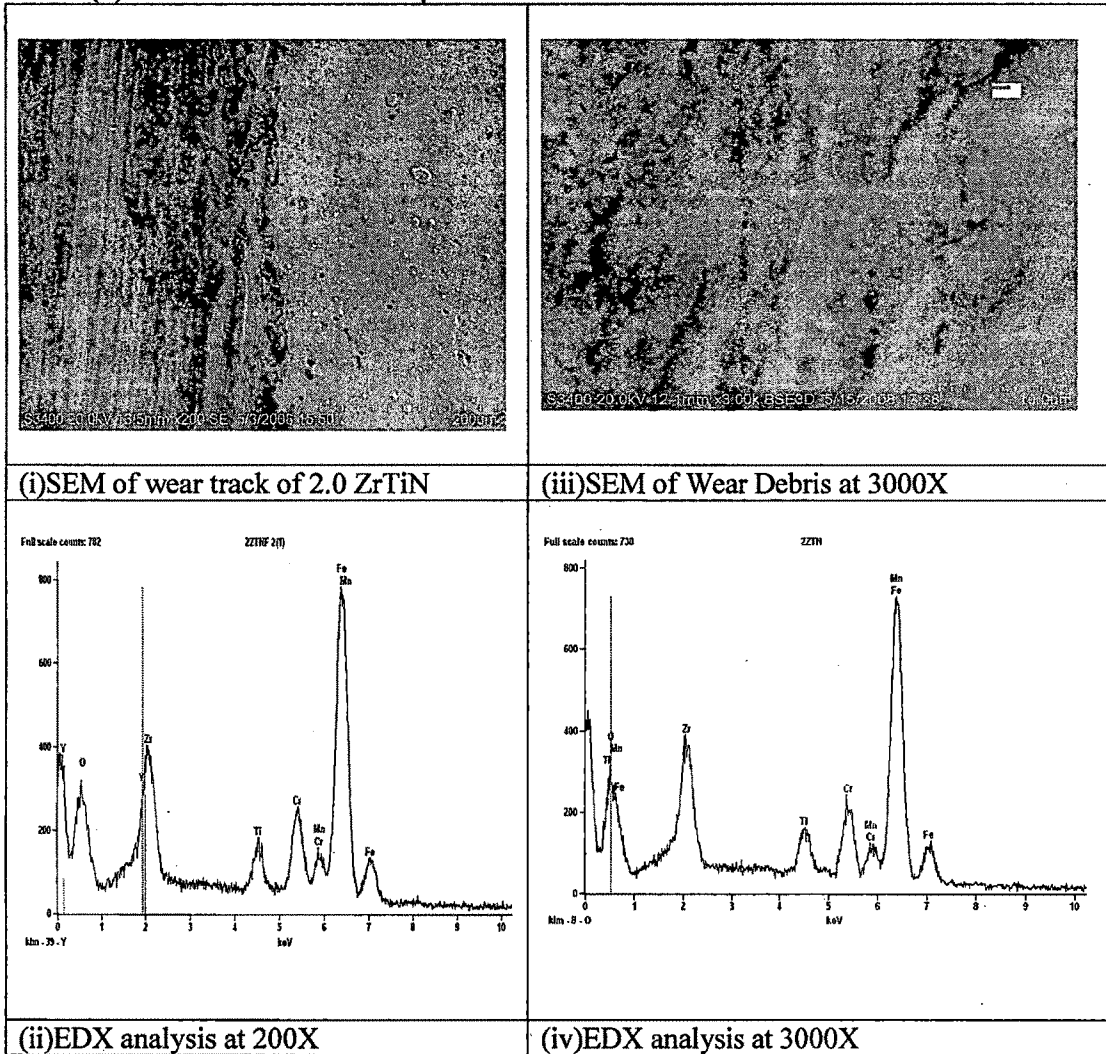


Fig 5.D.3.(b)(I)SEM(i& iii at 200X and 3000X) and EDX analysis(ii & iv at 200X & 3000X ) of 2.0 $\mu$  ZrTiN

Fig 5.D.3.(b)(I) show the typical profiles of the wear scars of the coatings after ball-on-disc wear test. Fig 5.D.1.(b)(I) (i) shows the deep ploughing grooves on the surface of specimen. Some region of wear track appears smooth due to the easy removing of debris particulates from the contact surface. The debris (tribo-chemical products) of the coating was ejected out and accumulated around the edge similar results were obtained by [94]

for AlCrN coating. SEM analysis at high magnification (iii) within the wear track shows flaky and very fine-grained submicron sized wear debris particles. Microgrooves are formed which are associated with crack nucleation on surface, subsequent crack propagation and finally loose particles are trapped and dragged along resulting in formation of macrogrooves.[70] Fine shaped particles are observed in wear debris indicative of ploughing wear followed nucleation and propagation of subsurface cracks or plastic shear in asperity contact.[71] The coating seems to be very brittle and delaminated completely, and the damage is of fractural nature. [95]EDX analysis at high magnification indicates the intense peak of iron and small peak of Zr/Ti i.e removal of coating has occurred. The absence of nitrogen in the debris indicated that the generated particles were thoroughly oxidized.

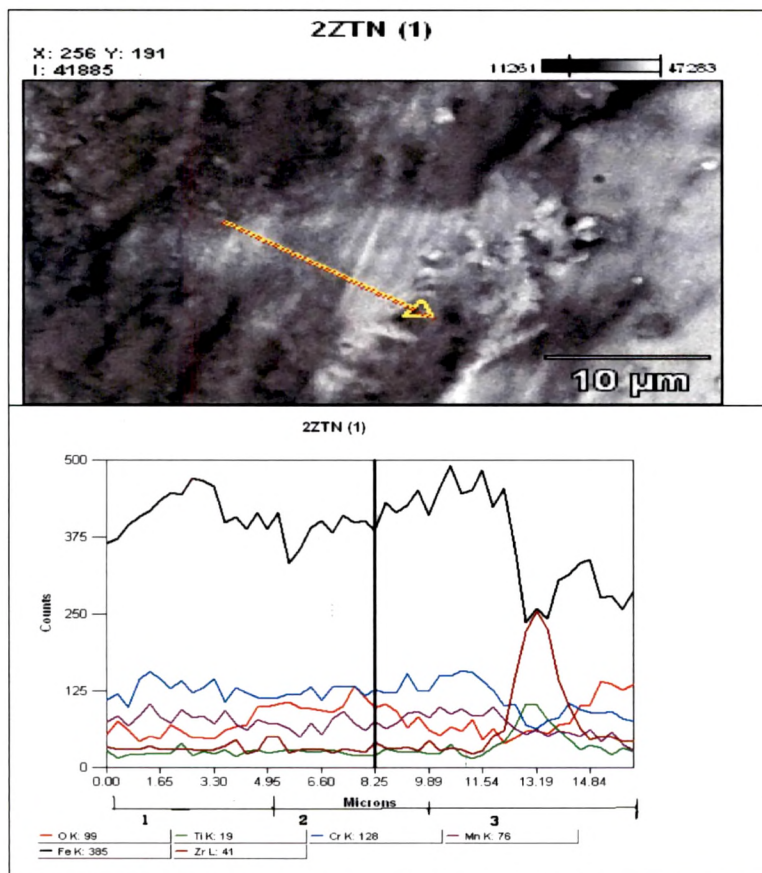


Fig 5.D.3 (b) (II) Composition of Particle within the wear track after wear testing of 2 μ ZrTiN at 3000X

As indicated in Fig 5.D.3(b)(II) the figure can be divided in three stages in the first stage there is high intensity of iron while intensity of oxygen remained constant, in the second stage there is slight increase in intensity of iron whereas in third stage there is prominent peak of Zr and Ti indicating that the complete removal of coating has not taken place and that the adhesion of  $2\mu$  ZrTiN may be better than  $1.5\mu$ ZrTiN.

Furthermore, the relative amount of Fe, Zr and Ti suggest a higher Fe content on the oxidized layer, from which it can be supposed the formation of an iron oxide titanium and zirconium oxide may have formed.

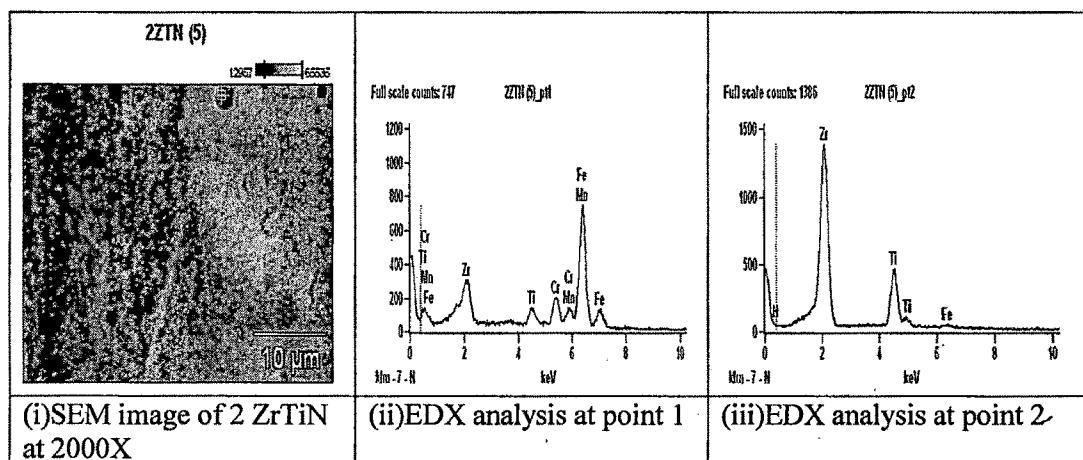


Fig 5.D.3(b)(III) (i)SEM image at 2000X (ii) & (iii) EDX analysis of  $2\mu$  ZrTiN at various points

The Fig 5.D.3(b)(II) indicates that at point (1) macroparticle is removed and the Fe peak is observed, although Zr and Ti is also present indicating that pore does not extent till the substrate (2) macroparticle consisting of Zr and Ti is intact hence no Fe peak is observed.

The friction coefficient values are different for the coatings depending on the time traveled. Fig 5.D.3(b)(IV) shows the friction coefficient of the 2  $\mu$  ZrTiN coatings with time when sliding against EN24 steel ring.

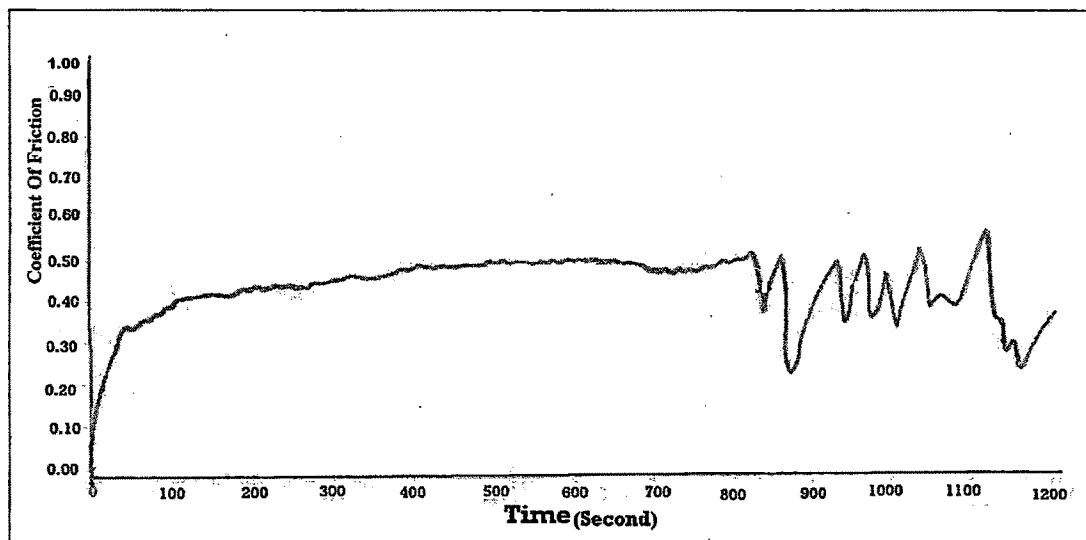


Fig 5.D.3 (b)(IV) Variation in COF(Coefficient of friction) with time for 2.0 $\mu$  ZrTiN after wear testing.

The COF of 2.0  $\mu$  ZrN coating is 0.442. As shown in Fig 5.D.3(b)(IV) The increase in COF is associated with ploughing because of roughening and trapped wear particles. Decrease in COF and fluctuation during the steady wear stage, is attributed to an accumulation of wear products (debris) in the contact zone[74]

### 5.D.3 (c)Wear Behaviour of 2.5 $\mu$ ZrTiN Thin Films

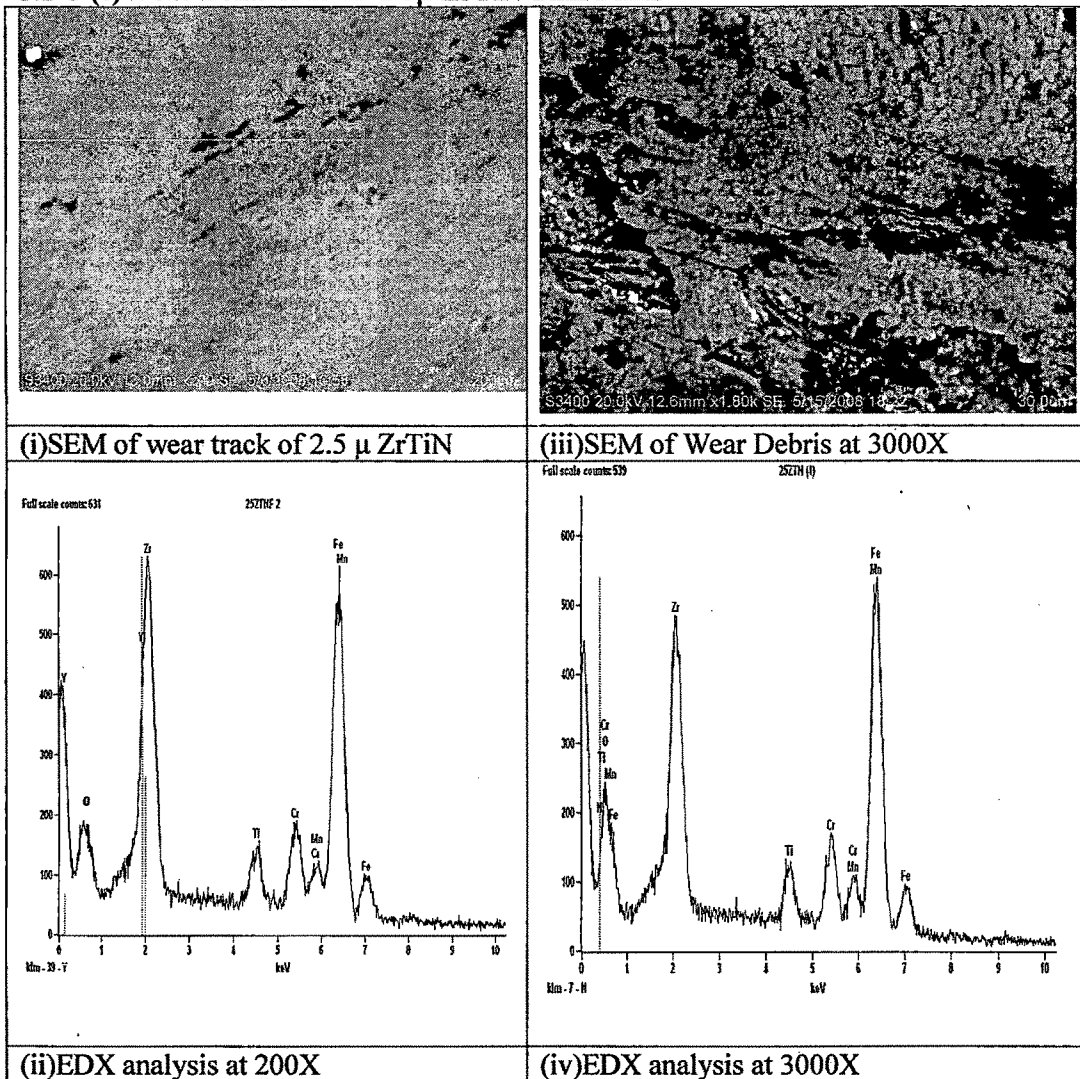


Fig 5. D.3.(c)(I)SEM(i& iii at 200X and 3000X) and EDX analysis(ii & iv at 200X & 3000X ) of 2.5  $\mu$  ZrTiN

The Fig 5.D.3.(c)(I) show the typical profiles of the wear scars of the coatings after ball-on-disc wear test.. Fig 5.D.1(c)(I) (i) shows smooth surface after the wear test. Some pores corresponding to removal of macroparticle were observed. No peeling of the ZrTiN coating was observed on the rubbed TiN coating surface. This suggests that the ZrTiN coating deposited by arc ion plating has a high adhesion to the substrate. Similar behaviour was observed by Fengqun Lang [2] when TiN coatings of 12  $\mu$  with the

thickness deposited by arc ion plating process on A3steel.EDX analysis (ii) indicates intense peak of Zr and Fe. SEM at higher magnification Fig (iii) indicates presence of very small irregular shaped debris. It seems that crack nucleation has occurred on the surface, subsequent crack propogation and finally loose particles are formed. EDX analysis at high magnification (iv) indicates decrease in peak intensity of Zr and Fe and increase in peak intensity of oxygen, confirming oxidation due to tribochemical reactions occurring during sliding tests.

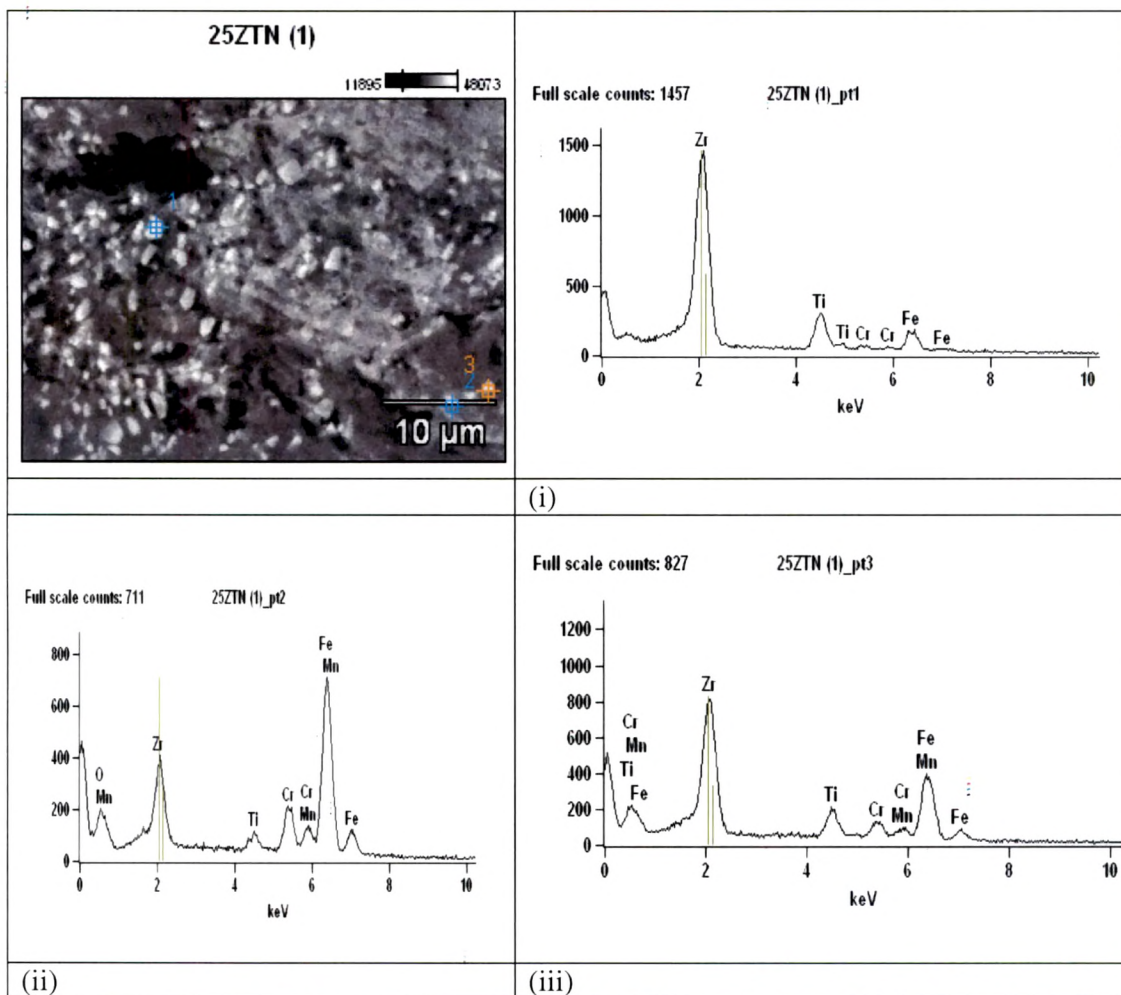


Fig 5.D.3.(c)(II) (i)SEM image at 2000X (ii) & (iii) EDX analysis of 2.5μ ZrTiN at various points

Fig 5.D.3(c)(II) indicates compositional analysis of particles observed within the wear track. At point (1) the debris is composed of Zr and Ti with very low Fe content indicating that it is a intact macroparticle. composition at point (2) is high intensity of Fe

and low intensity of Zr whereas composition at point (3) corresponds to high intensity of Zr and less intense Fe peaks. At point (2) along with Zr and Oxygen peak is observed indicating the oxidation of debris. Since intensity of iron peak is more it can be concluded that FeOx may be present.

The friction coefficient values are different for the coatings depending on the time traveled. Fig 5.D.3(c)(III) shows the friction coefficient of the 2.5  $\mu$  ZrTiN coatings with time when sliding against EN24 steel ring

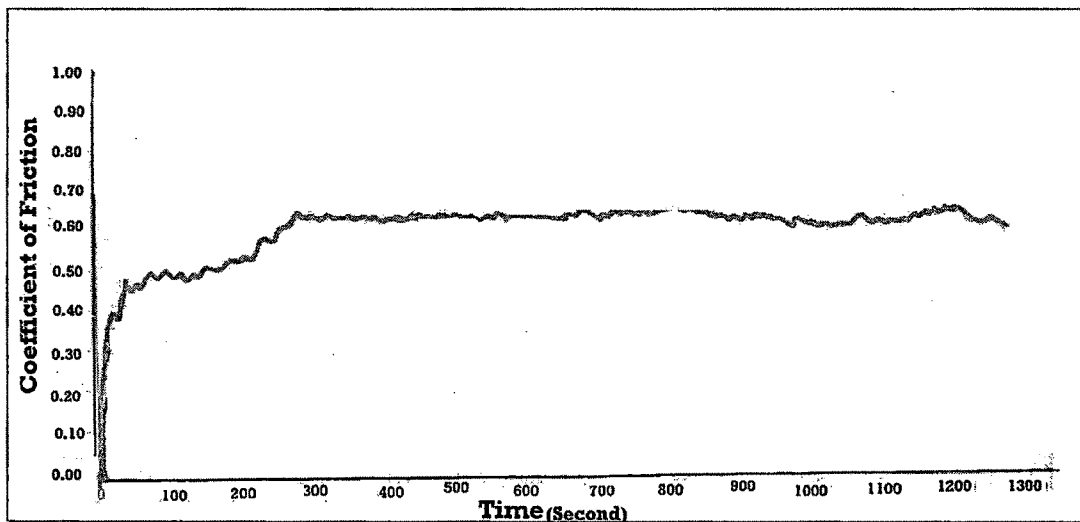


Fig 5.D.3.(c)(III) Variation in COF(Coefficient of friction) with time for 2.5 $\mu$  ZrTiN after wear testing.

The COF of 2.5  $\mu$  ZrN  $\mu$  coating is 0.464. As shown in Fig 5.D.3.(c)(III) The increase in COF is associated with ploughing because of roughening and trapped wear particles. Decrease in COF and fluctuation during the steady wear stage, is attributed to an accumulation of wear products (debris) in the contact zone.[74]

### 5.D.3 (d) Wear Behaviour of 3.0 $\mu$ ZrTiN Thin Films

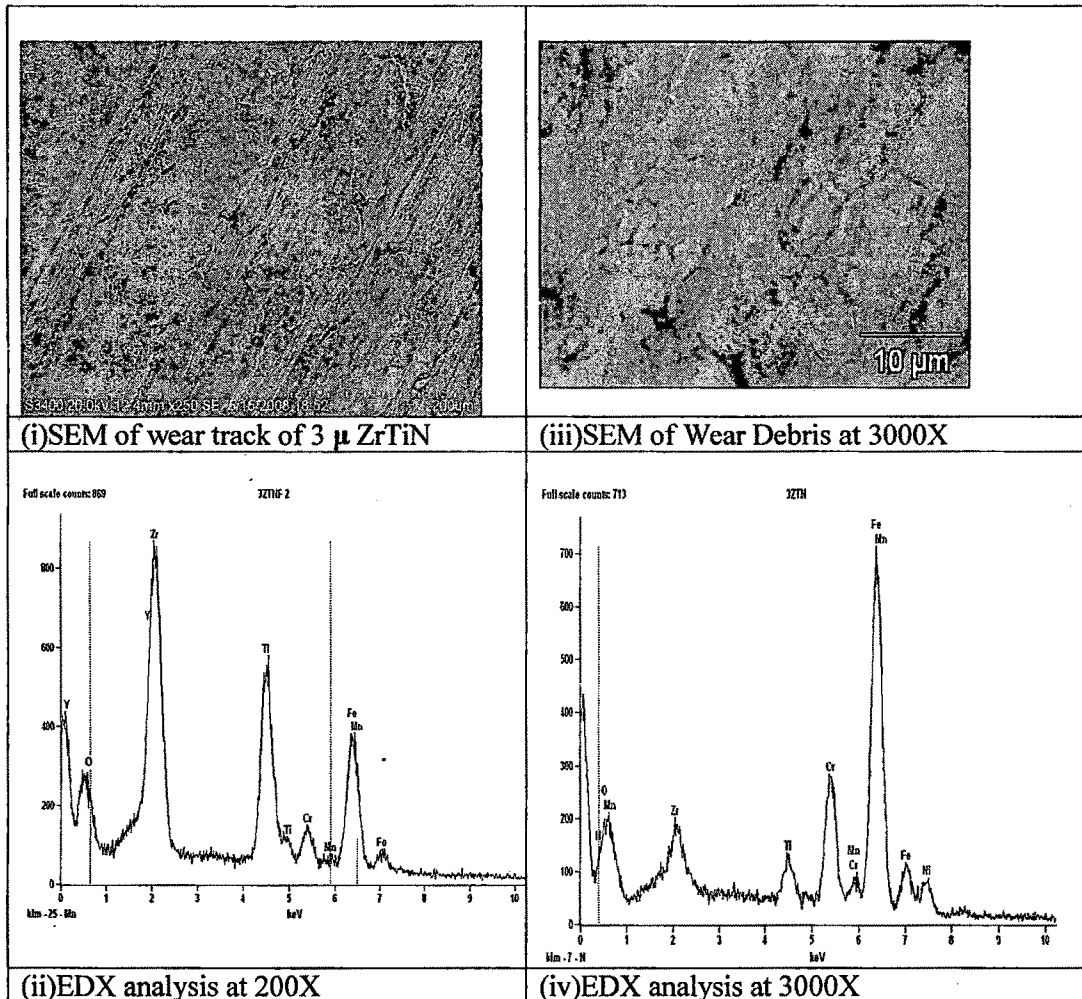


Fig 5. D.3(d) (I)SEM(i& iii at 200X and 3000X) and EDX analysis(ii & iv at 200X & 3000X ) of 3.0  $\mu$  ZrTiN

Fig 5.D.3(d)(I) (i) shows grooves and smooth surface after the wear test. Grain boundaries corresponding to substrate is observed at some places. EDX analysis (ii) indicates intense peak of Zr and Ti and less intense peak of Fe. Higher magnification Fig (iii) indicates presence of very small irregular shaped debris. Cracks perpendicular to sliding direction is observed. It seems that crack nucleation has occurred on the surface, subsequent crack propagation and finally loose particles are formed. EDX analysis at high magnification (iv) indicates decrease in peak intensity of Zr and Ti, increase in Fe peak intensity and

intensity of oxygen, remains almost same indicating oxidation of wear debris may not have occurred.

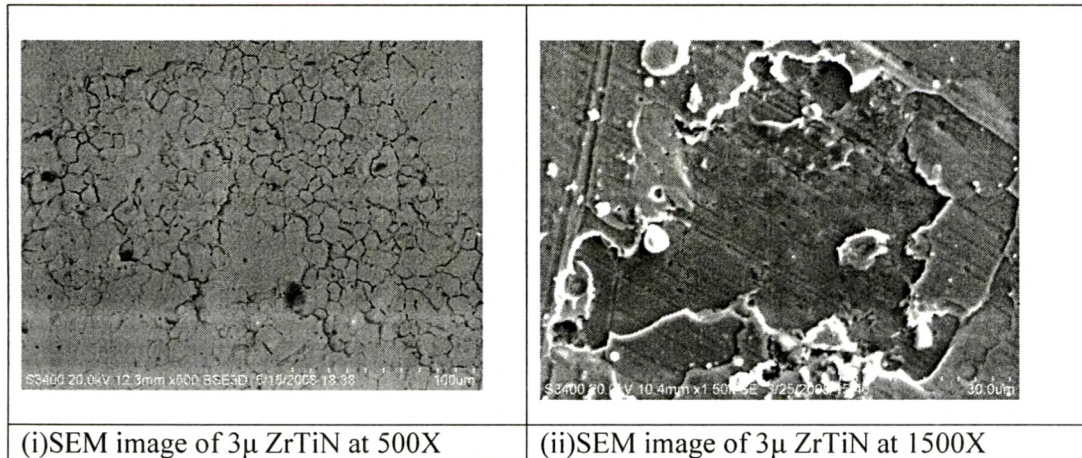


Fig 5.D.3(d)(II) SEM analysis of 3  $\mu$ ZrTiN within the wear track at (i) 500X and (ii) 1500X

Fig 5.D. 3(d) (II) (i) indicates intergranular fracture due to high amount of residual compressive stresses within the coating. In (ii) only a small area of the coating is removed at the pores of the coating. However, the remaining coating around the damaged area still adhered well to the substrate. This was reason for low friction even though part of the coating was removed. Similar results were obtained by K. Y. Lee R. Wei[93] where in DLC FILM by plasma immersion ion deposition PIID process alumina substrate with Si interlayer, Si derived from silane SiH<sub>4</sub> for the interlayer.

As per K.Y Lee [93], the coatings exhibiting delamination perform better than coatings in which brittle fracture occur. However as per M.D Bao [95] et al adhesion force or bonding strength is a resistance against loading stress, so it is stress governed behaviour. Nevertheless, the bonding strength between the coating layer and substrate competes with the cohesion strength of the layer itself. If the adhesion is very strong and can sustain the loading stress effectively, the layer will get damaged rather than being delaminated.

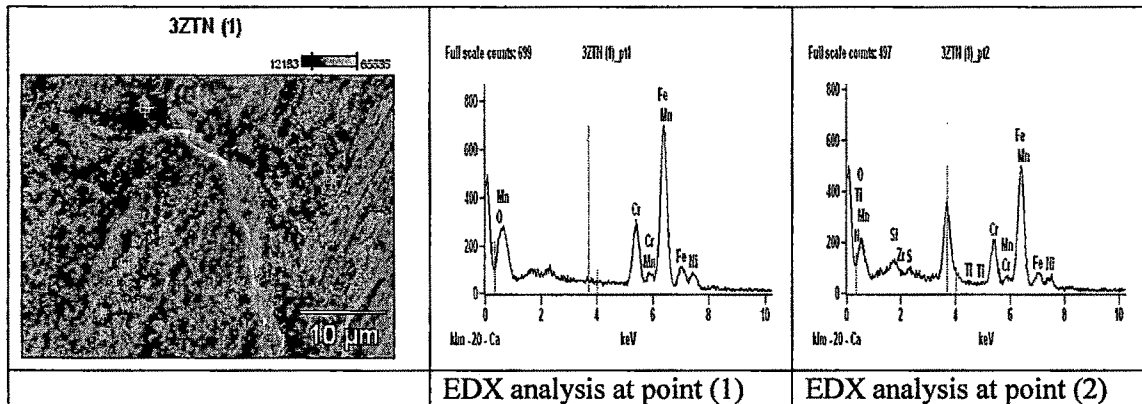


Fig 5.D.3(d)(III) (i)SEM image at 2000X (ii) & (iii) EDX analysis of 3.0  $\mu$  ZrTiN at various points

The Fig 5.D. 3(d)(III) indicates that at point (1) Particle composed of Fe and oxygen Point (2) is composed of Fe, O and Ti but intensity of iron peak is low, indicating oxides of Fe and Ti of varying compositions are formed.

The friction coefficient values are different for the coatings depending on the time traveled. Fig 5.D.1(d)(IV) shows the friction coefficient of the 3.0 $\mu$  ZrTiN coatings with the time when sliding against EN24 steel ring

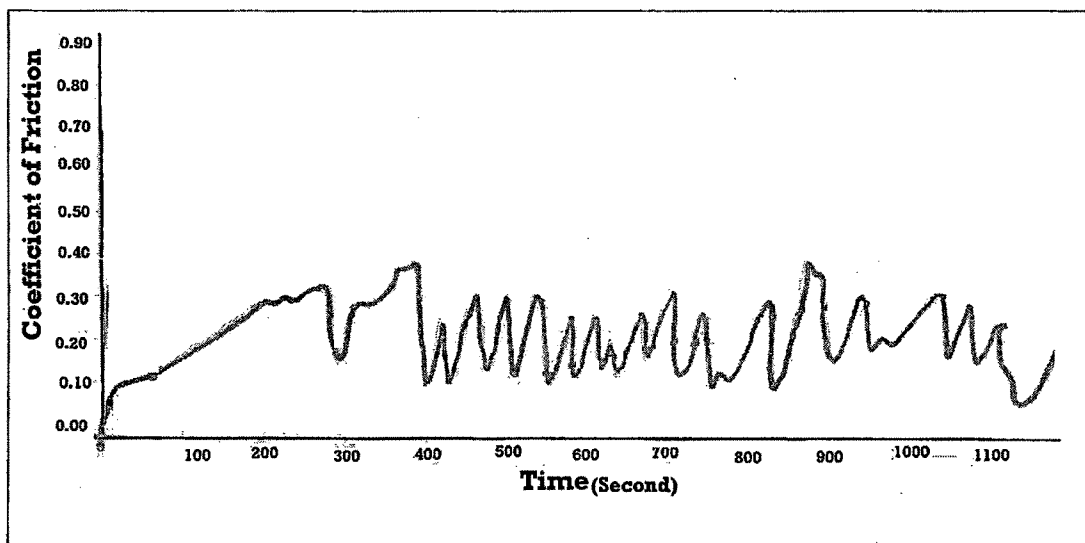


Fig 5.D.3 (d)(IV)Variation in COF(Coefficient of friction) with time for 3.0 ZrTiN after wear test.

The COF of 3.0  $\mu$  ZrTiN  $\mu$  coating is 0.246. As shown in Fig 5.D.3 (d)(IV) the oscillatory nature of the friction data for may be the indication that the coating was being removed however complete removal has not taken place due to high adhesion of coating with substrate. Hard debris delaminated from the coating layers or the oxides which were formed in the atmosphere are partly entrapped between rubbing surfaces. The three-body rolling wear process enables the friction coefficients in the wear process fluctuating with large amplitudes Since amount of debris formed is less increase in adhesive component is the main reason for such fluctuations.[96,97]

However Since amount of debris formed is less increase in adhesive component is the main reason for such fluctuations [65]

**Fig 5.D.3 Comparison of COF for all Thickness Of ZrTiN thin Films**

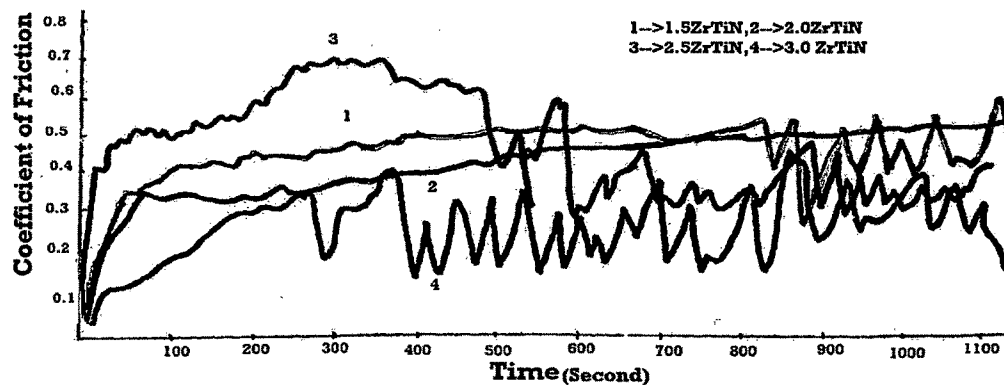


Fig 5.D.3.(abcd) indicates the variation in COF with time for ZrTiN of varying thickness during wear testing.

As indicated in the figure Fig 5.D.3(abcd) highest value of COF in the steady state friction is observed in 2.5  $\mu$  ZrTiN. Corresponding SEM micrograph at high magnification indicates formation of cracks. As indicated by Harish C. Barshilia et al [97] high temperature generated during sliding test, oxide is formed and the volume of

the film increases which induces stress in the film. This stress results in cracks, which provide easier path for oxygen transport.

Although COF of 3  $\mu$  ZrTiN is very low(0.246) the fluctuating nature of COF results in severe damage in the coatings.

The schiometric ZrTiN having single phase has been studied extensively by various workers,[33-38] however based on the literature survey carried out,ZrN-Ti<sub>2</sub>N coating has not being investigated yet. As discussed the wear performance is closely associated with the resistance of coating to the oxidation. Oxidation behaviour of schiometric ZrTiN was investigated by L Rebouta et al[98]

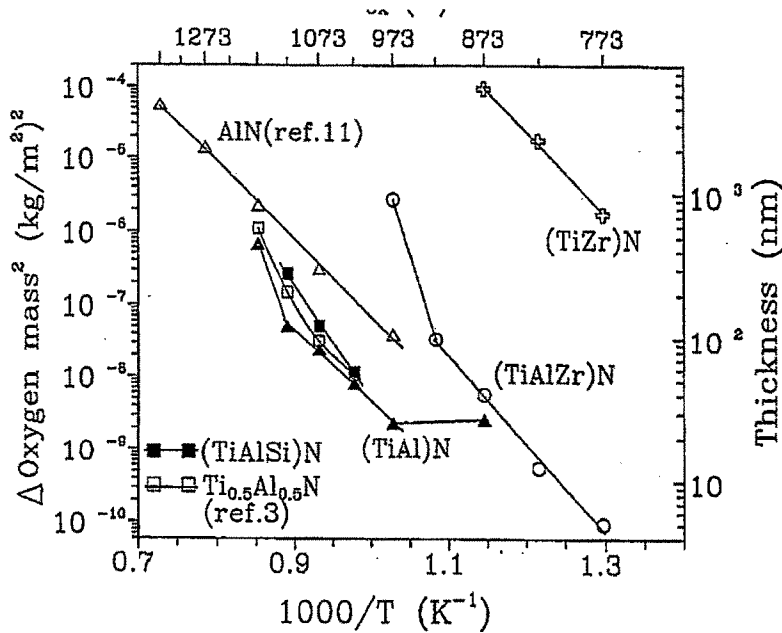


Fig 5.D.3 (I) Variation of oxygen gain with temperature for (Ti,Zr)N

As indicated in Fig 5.D.3 (I),the presence of Zr does not change significantly the oxidation of the coating when compared with the oxidation of TiN It generally develops a homogeneous oxide layer with a Zr to Ti atomic composition ratio similar to the ratio found in the as-deposited nitride. The Arrhenius plot of the mass square of incorporated oxygen for annealing temperatures between 500 and 600 °C is represented as a function of 1/T in Fig 5.D.3 (I) and indicates an activation energy of 219 kJ mol<sup>-1</sup>.

## References:

- [1] Zhongyuan Cheng , Min Wang , Jiyan Zou ,*Surface and Coatings Technology*, 92 (1997), 50-55
- [2] Fengqun Lang , Zhiming Yu, *Surface and Coatings Technology*, 145Z2001.80\_87
- [3] D.S. Rickerby, A.M. Jones, B.A. Bellamy, *Surf. Coat. Technol.* 37Z1989.111.,
- [4] D.M. Schneider, J. Maibach, E. Obermeier, D. Schneider, *J.Micromech. Microeng.* 5Z1995.121
- [5] Arias, Y.C. Arango[, A. Devia, *Applied Surface Science*, 253 (2006) 1683–1690
- [6] I. Grimberga , V.N. Zhitomirsky, R.L. Boxman, S. Goldsmithb, B.Z. Weissa, *Surface and Coatings Technology*, 108–109 (1998) 154–159
- [7] L.A. Donohue, J. Cawley, J.S. Brooks ,*Surface and Coatings Technology*,72 (1995) 128-138
- [8] Da-Yung Wang , Ko-weiweng , Chi-Lung Chang , Xien-Jien Guo, *Surface and Coatings Technology*, Volume 202, Issues 4-7, 15 December 2007, Pages 987-992
- [9] Philip C. Yashar, William D. Sproul, *Vacuum*, 55 (1999), 179-190
- [10] Erdem Atar, E. Sabri Kayali and Huseyin Cimenoglu, *Tribology International* Volume 39, Issue 4, April 2006, Pages 297-302
- [11] D. Nolan, S.W. Huang , V. Leskovsek , S. Braun, *Surface & Coatings Technology*, 200 (2006) 5698–5705
- [12] Henry J. Ramos, Nicomedes B. Valmoria ,*Vacuum*, 73 (2004) 549–554
- [13] G.L.N. Reddy, J.V. Ramana, Sanjiv Kumar, S. Vikram Kumar, V.S. Raju, *Applied Surface Science*, 253 (2007), 7230–7237
- [14] Oc-Nam Parka, Jong Hyun Parka, Seog-Young Yoona, Mi-Hye Leeb, Kwang Ho Kima ,*Surface and Coatings Technology*, 179 (2004), 83–88
- [15] L.A. Rocha , E. Ariza , J. Ferreir, bf. Vazb, E. Ribeirob, L. Reboutab, E. Alvesc, A.R. Ramosc, Ph. Goudeaud, J.P. Rivie`red ,*Surface and Coatings Technology* ,180–181 (2004) 158–163
- [16] S. Paldey, S.C. Deevi ,*Materials Science and Engineering*, A342 (2003) 58\_ 79
- [17] S. Logothetidis , I. Alexandrou, S. Kokkou, *Surface and Coatings Technology*, 80 (1996) 66-71
- [18] C. Quaeysaegen, M. Kerkhofs, L.M. Stals, M. Van Stappen, *Surface and Coatings Technology*, 80 (1996), 181-184
- [19] C. Friedrich, G. Berg, E. Broszeit, K.-H. Kloos, *Surface and Coatings Technology*, 74 75 (1995) 279-285
- [20] G. Berg, C. Friedrich, E. Broszeit, K.H. Kloos, *Surface and Coatings Technology*, 74 75 (1995), 135-142
- [21] E. Bemporad , M. Sebastiani, C. Pecchio, S. De Rossi ,*Surface & Coatings Technology*, 201 ,(2006,) 2155–2165
- [22] Hsyi-En Cheng, Min-Hsiung Hon, *Surface and Coatings Technology*, 81 (1996), 256-261, *Icmctf* 3
- [23] M. Herranen , U. Wiklund , J.-O. Carlsson S. Hogmark , *Surface and Coatings*

- Technology*, 99, (1998) 191-196
- [24] V.N. Zhitomirskya, I. Grimberg, L. Rapoport, N.A. Travitzky, R.L. Boxman, S. Goldsmith, A. Raihelc, I. Lapsker, B.Z. Weiss, *Thin Solid Films*, 326 (1998), 134-142
- [25] Eh. Hovsepianu, D.B. Lewis, W.-D. Münz, *Surface and Coatings Technology*, 133-134, 2000.166]175
- [26] K.L. Rutherford, P.W. Hatto, C. Davies, I.M. Hutchings, *Surface and Coatings Technology*, 86-87, (1996), 472-479
- [27] V.N. Zhitomirsky, I. Grimberg, R.L. Boxman, N.A. Travitzky, S. Goldsmith, B.Z. Weiss, *Surface and Coating Technology*, 94-95 (1997) 207-212
- [28] C. Mendibide, P. Steyer, J. Fontaine, P. Goudeau, *Surface & Coatings Technology*, 201 (2006), 4119-4124
- [29] H. Jiménez, E. Restrepo, A. Devia, *Surface & Coatings Technology*, 201, (2006) 1594-1601
- [30] J.V. Ramana, Sanjiv Kumar, Christopher David, A.K. Ray, V.S. Raju, *Materials Letters*, 43, 2000.73-76
- [31] M.M. Larijani, N. Tabrizia, Sh. Norouziana, A. Jafarib, S. Lahoutia, H. Haj Hosseini, N. Afshari, *Vacuum*, 81 (2006), 550-555
- [32] Cheng-Shi Chen, Chuan-Pu Liu, C.-Y.A. Tsao, Heng-Ghieh Yang, *Scripta Materialia*, 51 (2004) 715-719
- [33] R. L. Boxman, V. N. Zhitomirsky, I. Grimberg, L. Rapoport, S. Goldsmith and B. Z. Weiss, *Surface and Coatings Technology*, Volume 125, Issues 1-3, March 2000, Pages 257-262
- [34] E. Etchessahar, J.P. Bars, D. Ansel, *Journal of Alloys and Compounds*, 335 (2002) 126-131
- [35] P. Duwez, F. Odell, *J. Electrochem. Soc.*, 97 (1950) 299
- [36] R. Kieffer, H. Nowotny, P. Ettmayer, G. Dufek, *Metall. (Berlin)* 26. (1972) 701-708
- [37] O. Knotek, M. Böhm, T. Leyendecker, *J. Vac. Sci. Technol. A4*, 1975. (1986) 2695-2700
- [38] O. Knotek, M. Böhm, T. Leyendecker, F. Jungblut, *Mat. Sci. Eng. A* 105/106 (1988) 481
- [39] P.M. Perillo, *Corrosion*, vol.62, No2 pg 162-185
- [40] I. Miloslev and B. Navislek, *Surface and coating technology*, 63(1994) 173-180
- [41] Jia-Hong Huang, Fan-Yi Ouyang, Ge-Ping Yu, *Surface & Coatings Technology*, 201, (2007) 7043-7053
- [42] Wen-Jun Chou, Ge Ping Yu, Jiahong Huang, *Corrosion science*, 43(2001)2023-2035
- [43] Li Li, Erwu Niu, Guohua Lv, Xianhui Zhang, Huan Chen, Songhua Fan, Chizi Liu, Si-Ze Yang, *Applied Surface Science*, 253 (2007) 6811-6816
- [44] M.A.M. Ibrahim, S.F. Korablov, M. Yoshimura, *Corrosion science*, (2002) 815-822
- [45] B.F. Chen, W.L. Pan, G.P. Yu, J. Hwang, J.H. Huang, *Surface and Coatings Technology*, 111, (1999) 16-21
- [46] A. Shokouhy, M.M. Larijani, M. Ghoranneviss, S.H. Haji Hosseini, M. Yari, A.H. Sari, M. Gholipur Shahraki, *Thin Solid Films*, 515(2006), 571 - 575

- [47] Darja Kek Merl , Peter Panjan , Miha Čekada , Marijan Mac'ek ,*Electrochimica Acta*, 49 (2004) 1527–1533
- [48] M.L. Zheludkevich , K.A. Yasakau , A.C. Bastos , O.V. Karavai , M.G.S. Ferreira ,*Electrochemistry Communications* 9 (2007) 2622–2628
- [49] E. Ariza and L.A. Rocha, *Materials Science Forum*, Vols. 492-493 (2005) pp. 189-194
- [50] V.K. William Grips , Harish C. Barshilia , V. Ezhil Selvi , Kalavati , K.S. Rajam *Thin Solid Films*, 514, (2006) 204–211
- [51] Hong Liang, Furong mau, Xiaoyan Wang, Tonghe Zhang, Hong Zhu, Xianying Wu, Huixing Zhang ,*Surface and Coatings Technology*, 128]129\_2000.209]212
- [52] D.V. Tzaneva, V.I. Dimitrova, P.E Hovsepyan ,*Thin Solid Films*, 295 (1997) 178-184
- [53] Jia-Yang Chen, Ge-Ping Yu, Jia-Hong Huang ,*Materials Chemistry and Physics*, 65 (2000) 310–315
- [54] T. Savisalo , D.B. Lewis , Q. Luo , M. Bolton , P. Hovsepyan,*Surface & Coatings Technology*, 202 (2008) 1661–1667
- [55] M. Herranen , U. Wiklund , J.-O. Carlsson , Hogmark , *Surface and Coatings Technology*, 99 (1998) 191-196
- [56] Hikmet Altun, Hakan Sinici, *Materials haracterization*, doi:10.1016/j.matchar.2007.01.004
- [57] M. Flores, O. Blanco, S. Muhl, C. Piña and J. Heiras, *Surface and Coatings Technology*, Volumes 108-109, Issues 1-3, 10 October 1998, Pages 449-453
- [58] H.A. Jehn,,*Surface and Coatings Technology*, 125 (2000) 212–217
- [59] P. Eh. Hovsepyan, D. B. Lewis , W. D. Münz, S. B. Lyon and M.Tomlinson, *Surface and Coatings Technology* ,Volumes 120-121, November 1999, Pages 535-541
- [60] Hikmet Altun and Sadri Sen ,*Materials & Design*, Volume 27, Issue 10, 2006, Pages 1174-1179
- [61] W Precht, E Lunarska, b A Czyzniewski, M Pancielejko and W Walkowiak, *Vacuum*,/volume 47/pages 867 to 869 1996
- [62] K.A Pischow, A.S Korhonen and E.O Ristolainen STM and Sims analysis of the interfaces and intermedate layers of tin/Ti/Substrate system *Surface Engineering volume III process Technology and surface analysis edited by P.K Datta and J.S Gray Royal society of chemistry pg 193*
- [63] Guosong Wu , Xiaoqin Zeng, Wenbin Ding, Xingwu Guo, Shoushan Yao *Applied Surface Science*, 252 (2006) 7422–7429
- [64] Ellina Lunarska, N. Ageeva, J. Michalski,*Surface and Coatings technology*, Volume 85, Issue 3, 15 November 1996, Pages 125-130
- [65] I.Penttinen, J.M. Molarius & A.S. Korhonen, *J. Vac. Sci. Technol.* 6(3), May/Jun 1988 0734-201/88/032158-04\$01.00
- [66] H. Dong, Y. Sun and T. Bell, *Surface and Coatings technology*, 90 (1997), pp. 91–101
- [67] Frank Hollsteina, Renate Wiedemann, Jana Scholz, *Surface and Coatings Technology*, 162 (2003), 261–268
- [68] Tamilaelvi, R. Murugaraj and N. Rajendran, *Materials and Corrosion* 2007, 58, No2

- [69] Roberto Hubler Nuclear instrumentation and methods in *physical research B* 175-179 (2001) 630-638
- [70] J. Wagner , C. Mitterer, M. Penoy, C. Michotte, W. Wallgram and M. Kathrein *International Journal of Refractory Metals and Hard Materials Volume 26, Issue 2, March 2008, Pages 120-126*
- [71] Bharat Bhushan, *Introduction to tribology, John Wiley and sons inc,ISBN 0471-15893-3 pg 385*
- [72] J.L. Moa, M.H. Zhua, B. Leia, Y.X. Leng, N. Huang, *Wear* (2007), doi:10.1016/j.wear.2007.01.051
- [73] S.C Moulzolf, R.J Lad, P.J Blau, *Thin solid films, Volume 347,issue 1-2,22 june 1999 pages 220-225*
- [74] Bharat Bhushan, *Introduction to tribology, John Wiley and sons inc,ISBN 0471-15893-3 pg 234*
- [75] I. L. Singer, S. Fayeulle and P. D. Ebnitt ,*Wear, 149 (1991) 375-394 375*
- [76] Z.P. Huang, Y. Sun and T. Bell ,*Wear, 173 (1994) 13-20*
- [77] A. Chatterjee , S. Jayaraman , J.E. Gerbi , N. Kumar , J.R. Abelson ,P. Bellon , A.A. Polycarpou , J.P. Chevalier, *Surface & Coatings Technology, 201 (2006) 4317-4322*
- [78] Pranay Asthana Hong Liangl Metin Usta A. H. Ucisik ,*Journal of Tribology, JANUARY 2007, Vol. 129 / 1*
- [79] S. Wilson, A.T. Alpas, *Wear ,245 (2000) 223-229*
- [80] Ph. Steyer, A. Mege, D. Pech, C. Mendibide, J. Fontaine, J.-F. Pierson, C. Esnouf and P. Goudeau, *Surface and Coatings Technology, Volume 202, Issue 11, 25 February 2008, Pages 2268-2277*
- [81] C.B. Wei, X.B. Tian , Y. Yanga, S.Q. Yang , Ricky K.Y. Fu , Paul K. Chu, *Surface & Coatings Technology, 202 (2007) 189-193*
- [82] T. Savisalo, D.B. Lewis , Q. Luo , M. Bolton , P. Hovsepian ,*Surface & Coatings Technology, 202 (2008) 1661-1667*
- [83] H. Jiménez, E. Restrepo, A. Devia, *Surface & Coatings Technology, 201 (2006) 1594-1601*
- [84] S.J. Bulla, D.G Bhat, M.H. Staia ,*Surface and Coatings Technology, 163 -164 (2003) 507-514*
- [85] A. O" ztu" rka, K.V. Ezirmika, K. Kazmanlia, M. U" rgena, O.L. Eryilmazb, A. Erdemir ,*Tribology International ,41 (2008) 49-59*
- [86] D.V.Shtansky, E.A.Levashov, A.N.Sheveiko and J.J.Moore, *J. Mater. Synth. Process.,1998, vol.6, No.1, pp. 61.*
- [87] Avinash Kumar Agarwal , Ashish Garg , Dhananjay Kumar Srivastava , Mritunjay Kumar Shukla, *Surface & Coatings Technology, 201 (2007) 6182-6188*
- [88] Miloev , H.-H. Strehbtow , B. Navin~ek, *Thin Solid Films, 303 (1997) 246-254*
- [89] C. Friedrich, G. Berg, E. Broszeit, K.-H. Kloos,*Surface and Coatings Technology, 74 75 (1995) 279-285*
- [90] Hugues Wiame ,Paul Grange Miguel-Angel Centeno,t Sandra Picard, Philippe Bastians and *Journal of the European Ceramic Society, 18 (1998) 1293-1299 final*
- [91] Diego F. Arias, Diana M. Marulanda, Alejandra M. Baena, Alfonso Devia

- ,*Wear*, 261 (2006) 1232–1236
- [92] Hermann A. Jehn, *Surface and Coatings Technology*, Volume 131, Issues 1-3, 1 September 2000, Pages 433-440
- [93] [K. Y. Lee R. Wei, *Journal of Tribology*, OCTOBER 2006, Vol. 128 / 711
- [94] Deng Jianxin , Liu Jianhua, Zhao Jinlong, Song Wenlong, Niu Ming, *Wear*, (2007), doi:10.1016/j.wear.2007.03.014
- [95] M. D. Bao, X. D. Zhu and J. W. He ,*Surface Engineering*, 2006 VOL 22 NO 1 pg 11-14
- [96] Yeong Yan Guu , Jen Fin Lin , Chi-Fong Ai ,*Thin Solid Films*, 302 (1997) 193 200
- [97] Harish C. Barshilia, M. Surya Prakash, Anjana Jain, K.S. Rajam ,*Vacuum*, 77 (2005) 169–17
- [98] L. Rebouta,F.Vaz,M Andritschky,M.F da Silva, *Surface Engineering*, 76-77(1995)70-74